SANDIA REPORT

SAND2018-7002

Unlimited Release

Printed June 2018

Design Studies for Deep-Water Floating Offshore Vertical Axis Wind Turbines

D. Todd Griffith, M. Barone, J. Paquette, B. Owens, D. Bull, C. Simao-Ferriera, A. Goupee, and M. Fowler

Prepared by
Sandia National Laboratories
Albuquerque, New Mexico 87185 and Livermore, California 94550

Sandia National Laboratories is a multimission laboratory managed and operated by National Technology and Engineering Solutions of Sandia, LLC, a wholly owned subsidiary of Honeywell International, Inc., for the U.S. Department of Energy's National Nuclear Security Administration under contract DE-NA0003525.

Issued by Sandia National Laboratories, operated for the United States Department of Energy by National Technology and Engineering Solutions of Sandia, LLC.

Available to DOE and DOE contractors from
U.S. Department of Energy
Office of Scientific and Technical Information
P.O. Box 62
Oak Ridge, TN 37831

Telephone: (865) 576-8401
Facsimile: (865) 576-5728
E-Mail: reports@osti.gov
Online ordering: http://www.osti.gov/scitech

Available to the public from
U.S. Department of Commerce
National Technical Information Service
5301 Shawnee Rd
Alexandria, VA 22312

Telephone: (800) 553-6847
Facsimile: (703) 605-6900
E-Mail: orders@ntis.gov
Online order: http://www.ntis.gov/search

SAND2018-7002
Printed June 2018
Unlimited Release

Design Studies for Deep-Water Floating Offshore Vertical Axis Wind Turbines

D. Todd Griffith, M. Barone, J. Paquette, B. Owens, D. Bull
Wind Energy Technologies Department
Sandia National Laboratories
P. O. Box 5800
Albuquerque, New Mexico 87185-MS1124

C. Simao-Ferriera
Delft University of Technology
Delft, the Netherlands

A. Goupee, M. Fowler
University of Maine
Orono, Maine

Abstract

Deep-water offshore sites are an untapped opportunity to bring large-scale offshore wind energy to coastal population centers. The primary challenge has been the projected high costs for floating offshore wind systems. This work presents a comprehensive investigation of a new opportunity for deep-water offshore wind using large-scale vertical axis wind turbines. Owing to inherent features of this technology, there is a potential transformational opportunity to address the major cost drivers for floating wind using vertical axis wind turbines. The focus of this report is to evaluate the technical potential for this new technology. The approach to evaluating this potential was to perform system design studies focused on improving the understanding of technical performance parameters while looking for cost reduction opportunities. VAWT design codes were developed in order to perform these design studies. To gain a better understanding of the design space for floating VAWT systems, a comprehensive design study of multiple rotor configuration options was carried out. Floating platforms and moorings were then sized and evaluated for each of the candidate rotor configurations. Preliminary LCOE estimates and LCOE ranges were produced based on the design study results for each of the major turbine and system components. The major outcomes of this study are a comprehensive technology assessment of VAWT performance and preliminary LCOE estimates that demonstrate that floating VAWTs may have favorable performance and costs in comparison to conventional HAWTs in the deep-water offshore environment where floating systems are required, indicating that this new technology warrants further study.

ACKNOWLEDGMENTS

This report was prepared by Sandia National Laboratories for the US Department of Energy. The financial support of the US DOE Wind Energy Technology Office is greatly appreciated.

The authors would like to thank Professor John E. Hurtado of Texas A&M University (Department of Aerospace Engineering) for his support in the development of the OWENS code.

TABLE OF CONTENTS

FIGURES

TABLES

EXECUTIVE SUMMARY

Project Objectives and Major Accomplishments

PROJECT OBJECTIVES:

The over-arching objective of this project was to evaluate the feasibility of the Vertical-Axis Wind Turbine (VAWT) architecture for very large-scale deployment in the offshore environment.

Several of the inherent features of a deep-water VAWT system are illustrated in Figure 1. VAWTs offer the potential to reduce offshore project costs in several areas as noted in Figure 2.

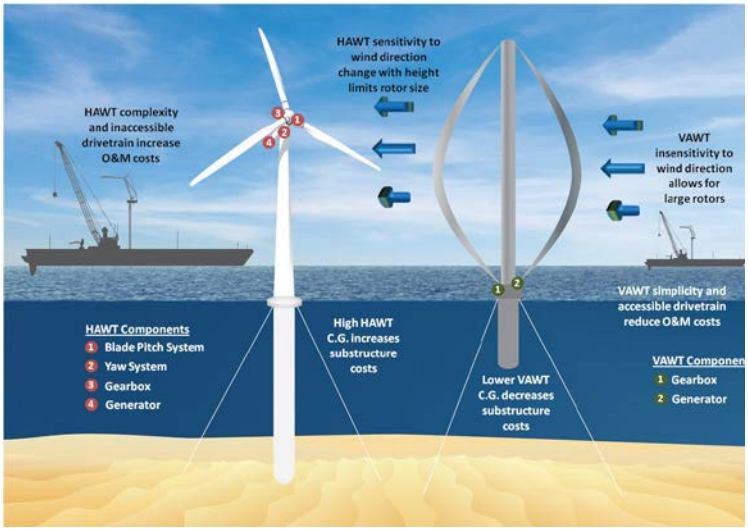

Figure 1. Comparison of HAWT and VAWT Machines for Offshore Deployment

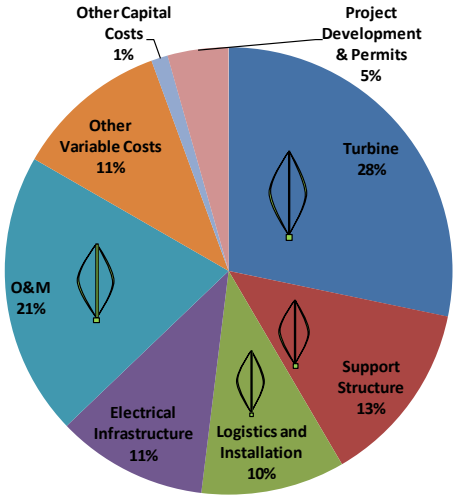

Figure 2. Estimated Life-Cycle Cost Breakdown for an Offshore Wind Project, and Areas that VAWTs could Improve

The proposed objectives were:

- Develop innovative VAWT rotor designs that enable reliable, cost-effective, and easily manufactured rotors for deep-water offshore machines at large-scale (5MW and greater);
- Demonstrate the potential for greater than 20% reduction in the levelized cost of energy (LCOE) COE for a deep-water, floating VAWT system compared to current shallow-water HAWT systems;
- Develop manufacturing techniques, certification test methods, and a commercialization plan for offshore VAWT rotors in order to accelerate deployment; and

This report documents the progress made in each of the these three areas.

The project was organized in three major tasks, which are as follows:

1) Task 1.0: Preliminary Design of Innovative Aero-elastic Rotor for Offshore VAWTs
2) Task 2.0: Deep-water Floating VAWT System Design and Cost Analysis
3) Task 3.0: Offshore VAWT Rotor Materials and Manufacturing Strategies.

This report details several main accomplishments, which can be summarized as follows:

1) Design codes development for floating offshore VAWT systems
2) Identification of wind and wave design conditions and standards
3) Design studies for floating VAWT design concepts
4) Innovations and analysis to mitigate barriers and design challenges, and
5) Preliminary cost analysis.

An overview of each area of accomplishment is provided here with more detail provided in the main body of the report.

Design Codes Development

VAWT design codes were developed and evaluated including the development of the OWENS Structural Dynamics code, the VAWTGen modeling code, and TU-Delft hybrid aerodynamics code. The existing SNL CACTUS code was evaluated to provide another option for aerodynamics calculations. An existing platform and mooring code was successfully adapted and coupled to the OWENS code for dynamics simulations. The highlights for each code are summarized here.

VAWT Modeling and Structural Dynamics Codes: VAWTGen and OWENS

With a relatively minimal set of inputs (as illustrated in Figure 3) a VAWT model of arbitrary configuration may be created using the VAWTGen code. Therefore, a separate tool is not required for the various types of configurations. VAWTGen requires data files be supplied to describe the geometry of the primary turbine components (blades, towers, and struts). The format of these data files is the same as the component files for NREL's FAST code. In addition, this allows existing design tools such as the Sandia National Laboratories Numerical Manufacturing and Design Tool (NuMAD) for wind turbine blades to be interfaced with the VAWT analysis tool without the need to consider new file formats. A mesh file is generated by VAWTGen that will be used by the analysis software (e.g. OWENS). VAWTGen is capable of modeling arbitrary VAWT configurations (Figure 4).

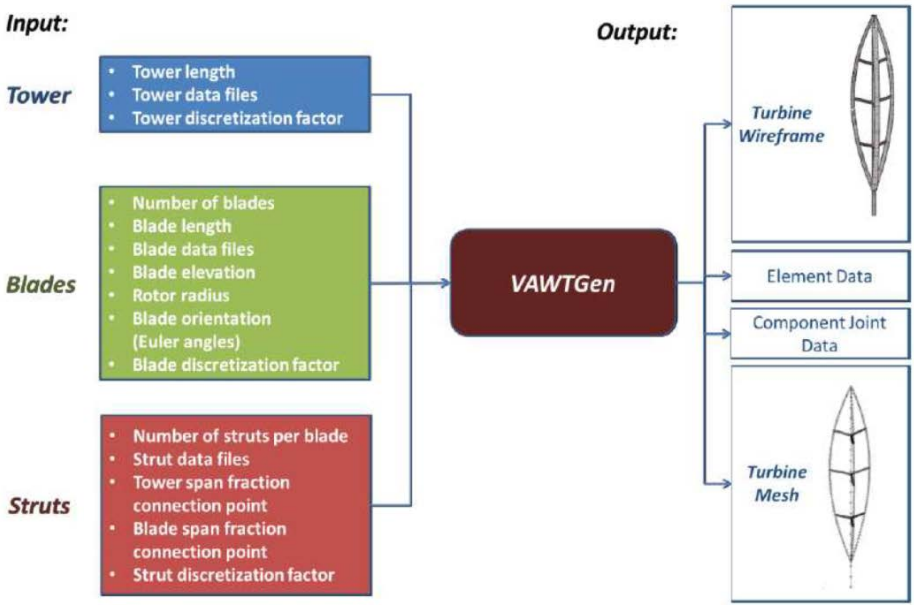

Figure 3. Flowchart of VAWTGen input and output

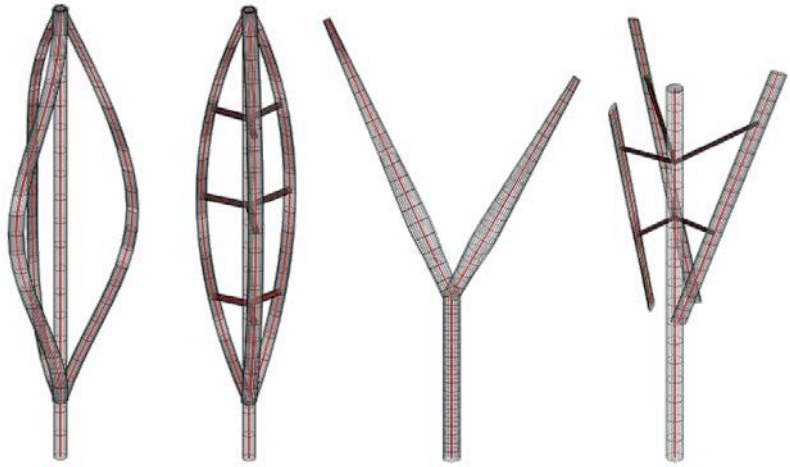

Figure 4. Wireframes of various VAWT configurations created with VAWTGen

The Offshore Wind ENergy Simulation (OWENS) toolkit is a custom design tool that has been developed to meet current and future needs for offshore VAWT design. Details of design tool features are presented in subsequent sections of this report. OWENS employs a finite element beam formulation to model the motion of rotating, flexible structural components of a VAWT, and allows for modal and transient structural dynamics analysis. The tool employs a modular analysis framework (shown in Figure 5) to allow for general interfaces to aerodynamic, hydrodynamic/platform, and generator/drivetrain modules. This allows for a high degree of flexibility in future development of analysis software. The OWENS structural dynamics model was verified with an analytical solution for a whirling (rotating) shaft and validated with test data

from structural dynamics experiments from the Sandia 34-meter testbed. The Campbell diagram of this validation exercise is shown in Figure 6.

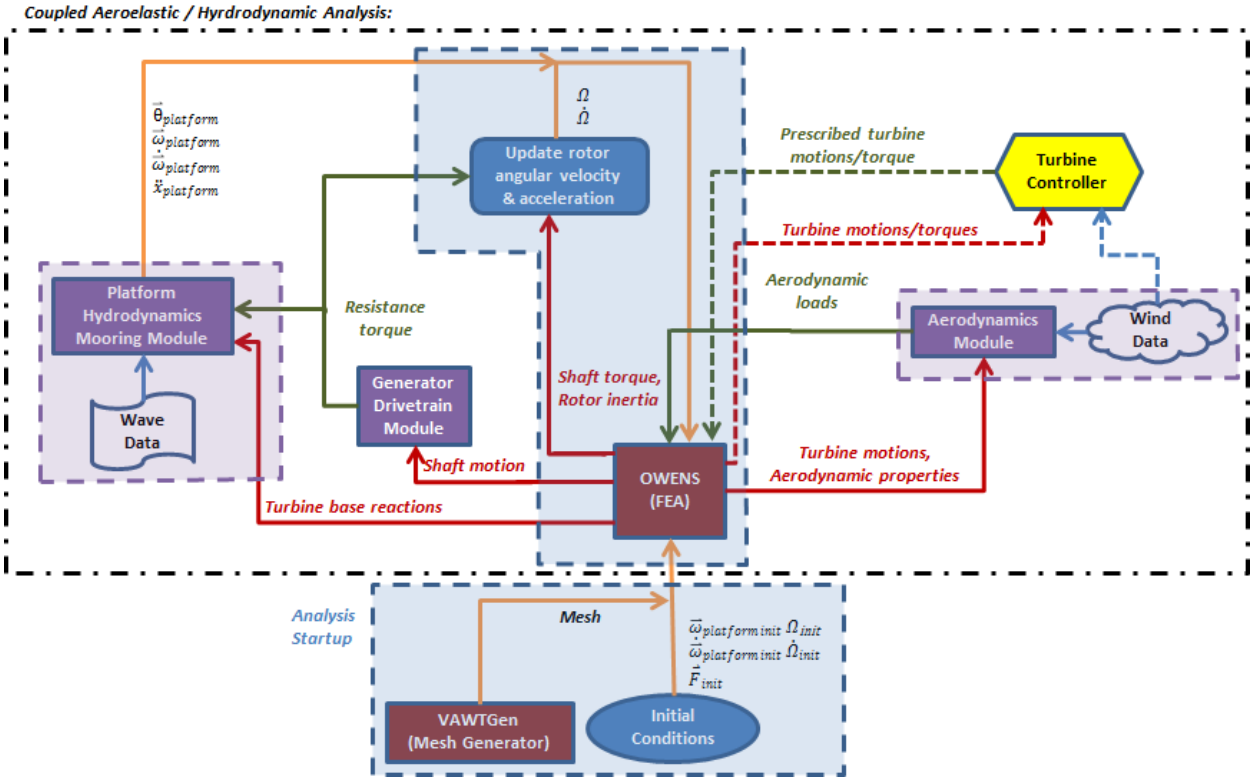

Figure 5. Analysis framework for the OWENS toolkit

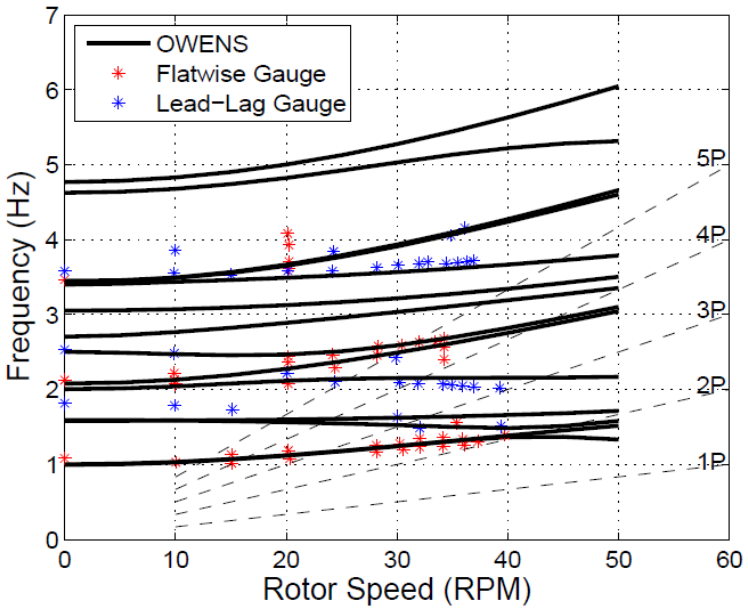

Figure 6. Campbell diagrams for 34-m VAWT (Predicted and Measured)

VAWT Aerodynamics: CACTUS and TU-Delft Hybrid Codes

The Code for Axial and Cross-flow TUrbine Simulation (CACTUS) is an aerodynamic design code capable of performing analysis of VAWT rotors of arbitrary geometry. Within CACTUS, the rotor blades are modeled as distributed line vortices, or "lifting lines," discretized into a number of blade elements. At each time step, the blade elements generate a vortex lattice system consisting of trailed and shed vortex line segments, shown in Figure 7. Blade loads are determined using airfoil look-up tables, modified by an unsteady aerodynamic model that includes dynamic stall effects when blade element angles of attack become large. A model for strut drag is also included; for "deep struts," where the strut extends to an appreciable fraction of the maximum rotor radius, strut drag can significantly reduce aerodynamic performance at high tip-speed ratios.

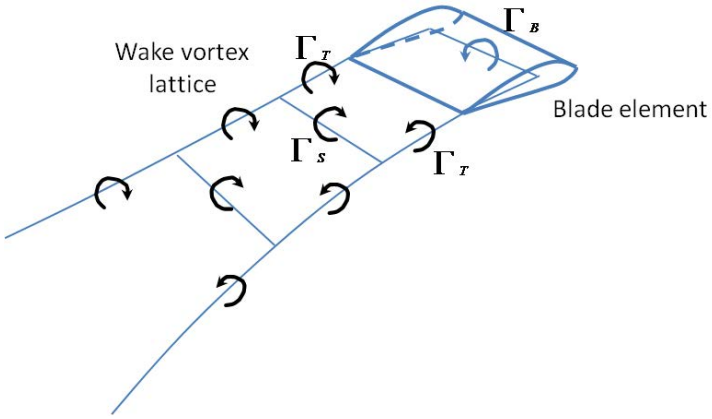

Figure 7. CACTUS blade element with associated vortex lattice system.

Most of the development of CACTUS was supported by the DOE Water Power Technologies Office, as axial crossflow turbines were under investigation. As part of that effort, a number of verification and validation calculations were performed, including models of legacy VAWT machines. Here, we present calculations that were carried out for the SNL 34 meter testbed machine (Figure 8). This was a 500 kW VAWT with a two-bladed, Darrieus rotor, for which power performance data were collected. Figure 9 shows comparisons of the measured and predicted power curves for three different rotational speeds (note: advance ratio is the inverse of the tip-speed ratio). The CACTUS predictions are in good agreement with the measured data; in particular, onset of rotor stall and maximum power are well-predicted, a challenging but important feature of stall-regulated VAWTs. The ability of CACTUS to predict performance of cantilevered-blade designs was also tested by performing calculations of the performance of the VAWT 850 rotor, a 500 kW H-VAWT that was developed in the UK. Good agreement was found between CACTUS predictions and published data for this machine at 13.6 RPM. In this case, including the model for strut drag is essential for obtaining good predictions of power.

Figure 8. The Sandia 34 meter VAWT Testbed.

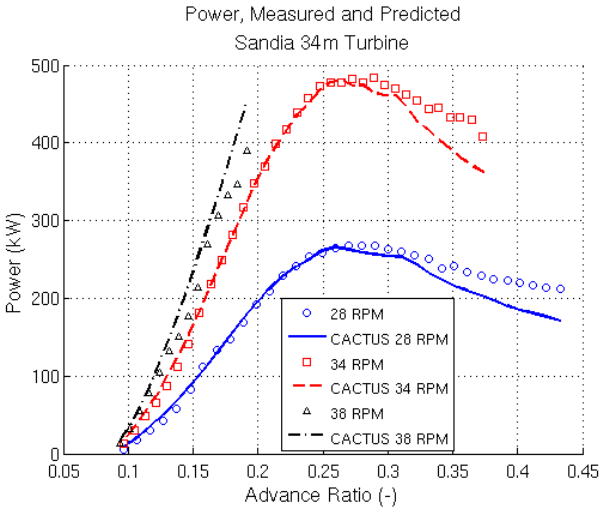

Figure 9. Measured and predicted power performance for the Sandia 34m Testbed VAWT.

The main idea behind the Hybrid solver being developed at TU-Delft is the following. In a region close to solid boundaries the flow is solved with a grid-based solver, where the full Navier-Stokes equations are solved (possibly with an arbitrary turbulence model or DNS, the limitations being the computational power and the physical properties of the flow). Outside of that region the flow is solved with a vortex particle method. See Figure 10 for a depiction of the Hybrid approach.

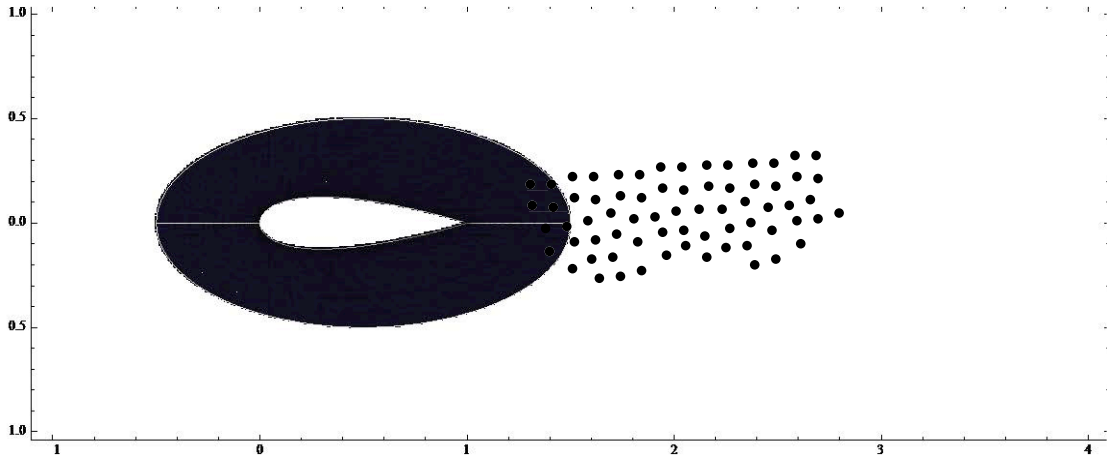

Figure 10. Conceptual diagram of hybrid method. Close to the solid boundaries a grid solver (Eulerian) is used. In the wake a vortex particle solver (Lagrangian) is used.

One of the successful test cases performed for the hybrid code was a circular cylinder (Figure 11).

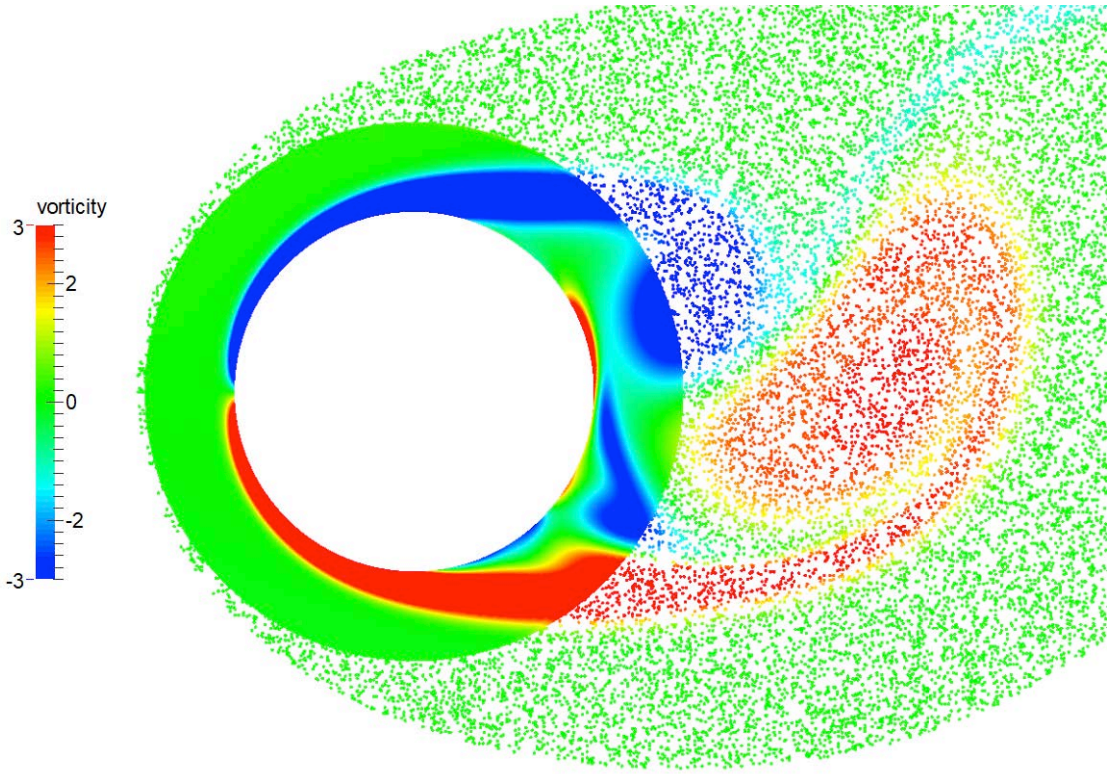

Figure 11. TU-Delft provided a hybrid aerodynamics code. The plot shows detail of the interface region between the Eulerian and the Lagrangian solvers. Some particles have been hidden to better visualize the particles.

Platform and Mooring Code: WavEC2Wire and OWENS coupling

For a floating VAWT, the overall system dynamics are significantly influenced by the interaction of the platform with the aquatic environment. To properly capture this interaction it is necessary to incorporate a hydrodynamic analysis code into the OWENS toolkit. With the goal being to develop an open-source and modular toolkit, WaveEC2Wire was used as the hydrodynamic module for this study. WaveEC2Wire is a MATLAB based numerical tool developed by Marco Alves at the Wave Energy Center for the analysis of wave energy converters (WECs). For initial verification, the topside was represented by a flexible tower structure as illustrated in Figure 12.

In one test case, the floating system was subjected to regular wave excitation with a period of 7 seconds (0.143 Hz) and wave height of 2 meters using the wave excitation functionality in WavEC2Wire. All six platform degrees of freedom were active in the simulation, as well as gravity, buoyancy, and damping. 1 minute of simulation time was considered. Figure 13 shows the time history and FFT of platform surge motion and tower tip displacement in the u1 direction. The regular wave frequency is evident as a peak in both the platform surge and tower top motion FFTs at approximately 0.14 Hz. This indicates that the regular wave excitation of the platform is manifesting itself in the structural motion of the attached flexible structure.

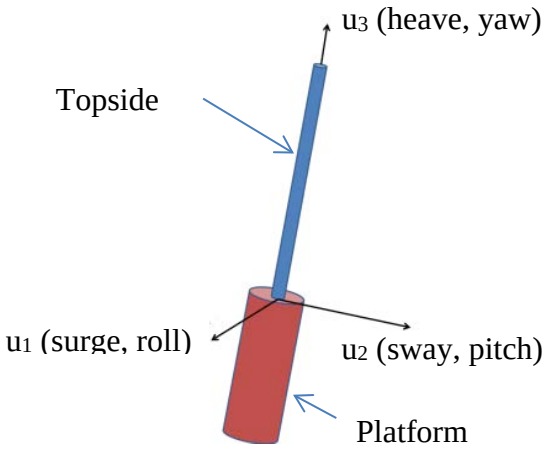

Figure 12. Representative system for verification procedures in WavEC2Wire Platform Code Coupling to OWENS rotor structural dynamics.

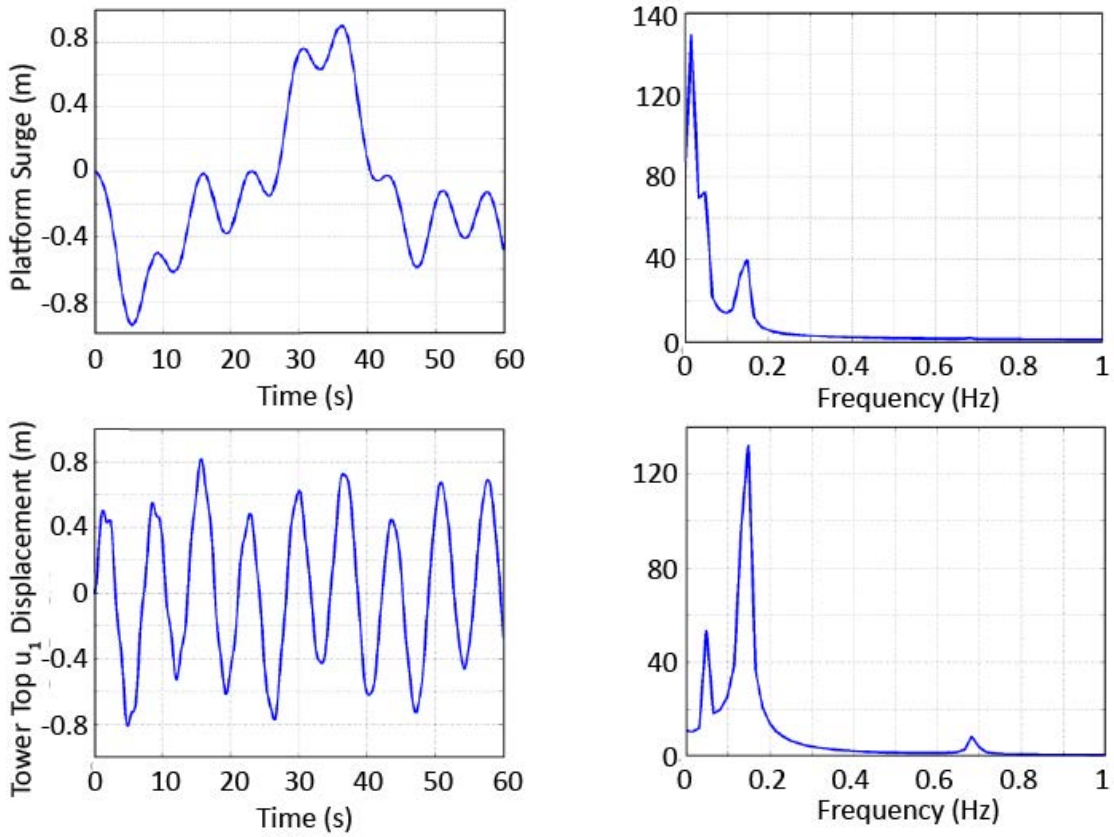

Figure 13. Wave excitation results.

Design Conditions: Extreme Conditions and Standards

IEC 61400-3 outlines the standard for offshore wind turbine design. While these standards are not specific to a certain machine configuration, they were developed primarily with HAWT rotors in mind. Two design load cases tend to drive most HAWT designs: DLC 1.4 (extreme coherent gust with direction change) and DLC 6.1a-b (extreme parked gust). HAWT designs are sensitive to quick changes in angle of attack on the blades like what would be experienced with DLC 1.4, as the blades can strike the tower. It is not anticipated that this would be as important to VAWT design as tower clearance would not be an issue. Also, in general, VAWTs should be less sensitive to load cases that contain direction changes due to their configuration.

However, VAWTs will likely be much more sensitive to cut-out load cases as they will likely be stall controlled, and thus unable to actively shed loads. The design load cases for VAWTs considered in this report are for aerodynamic loads at cut-out wind-speed under steady and uniform inflow. This is expected to provide an upper bound on aerodynamic loading under normal operation conditions.

The design standards and recommended practices of Det Norske Veritas (DNV) provided guidance in defining the extreme environmental conditions for the platform. The following environmental conditions are required:

- Combinations of significant wave heights and peak periods along the 100-year contour line for a specified location;
- 1 hour mean wind speed with a return period of 100 years;
- Surface and subsurface current speed with a return period of 10 years.

Data from the NDBC 44005 buoy was used to estimate the 100-year extreme wave return contour at the deployment site (Figure 14). This NDBC buoy is close to the hypothetical deployment site off the coast of Maine.

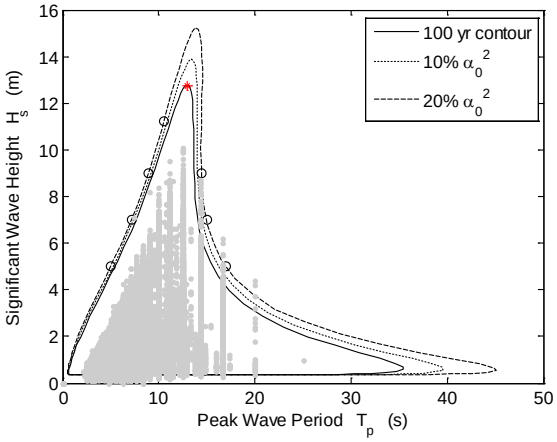

Figure 14. 100-year contour for spectral wave conditions from NBDC buoy 44005.

Design Studies and Concepts

Rotor Design Studies

Preliminary rotor design studies were performed with structural design for various design configurations including choice of rotor architecture, number of blades, tip chord length, material choice, tapering scheme, and curvature. The initial analysis includes stability of modes, static loadings at parked and operating conditions, and rotor cost modeling. A depiction of the 2- and 3-bladed Darrieus and V-VAWT models are shown in Figure 15.

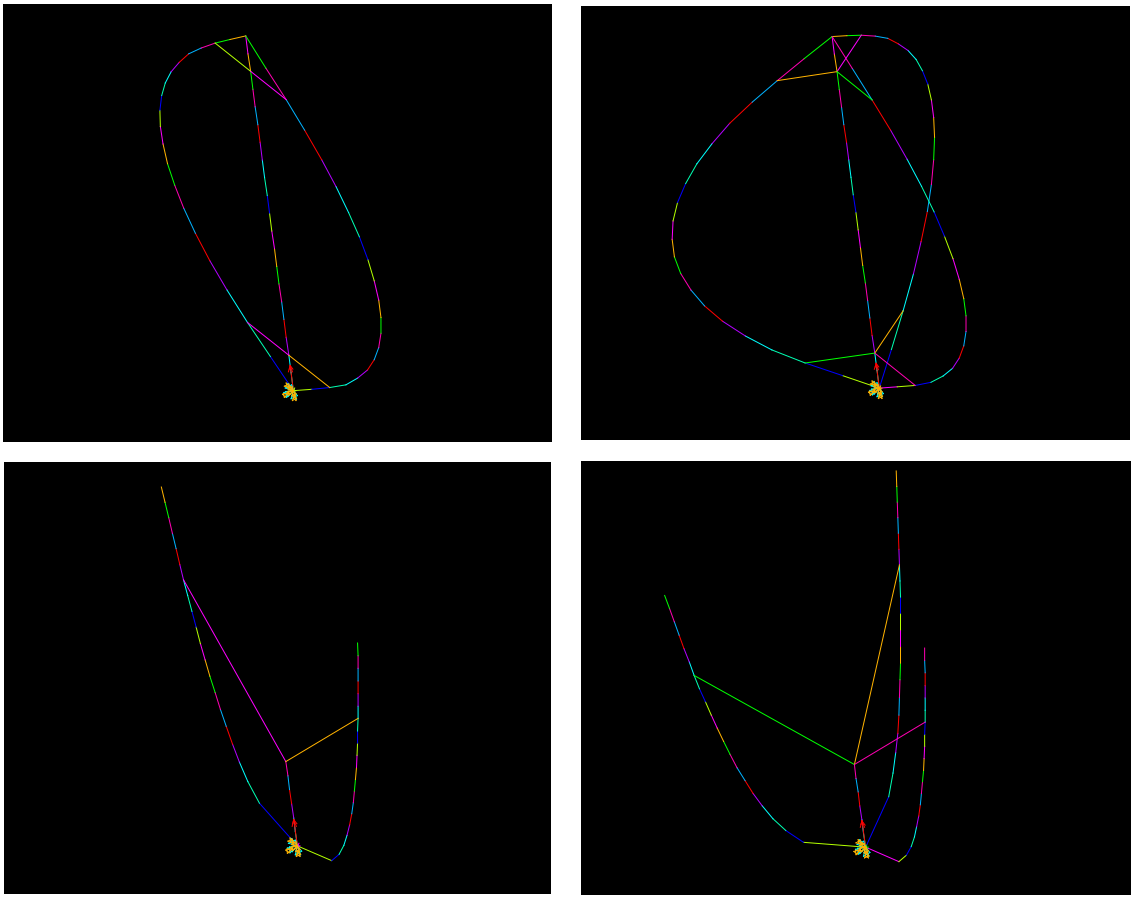

Figure 15. ANSYS finite element models of 2-bladed Darrieus (top left), 3-bladed Darrieus (top right), 2-bladed V (bottom left), and 3-bladed V (bottom right).

The vertical center of gravity (CG) location of the topside (rotor/tower) for all configurations analyzed is shown in Figure 16. For example, lowering of CG should lead to smaller underwater structure. The rotor material costs for the various VAWT designs are shown in Figure 17.

Twelve Darrieus rotor designs were analyzed, each design incorporating a unique combination of blade chord at maximum radius, number of blades, and choice of blade tapering (un-tapered, single-tapered, or double-tapered) as described in the previous section on rotor structural design.

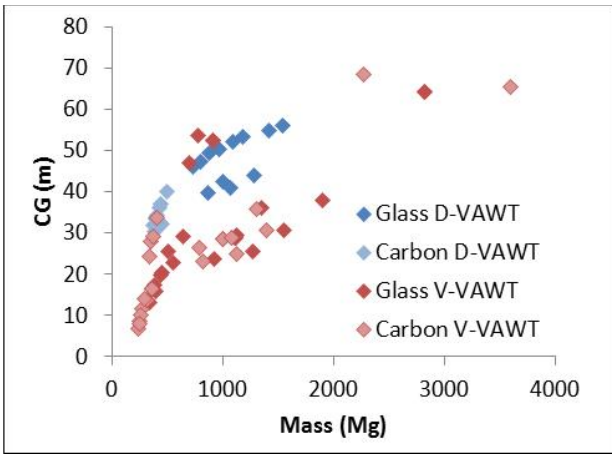

Figure 16. Rotor CG measured from water surface.

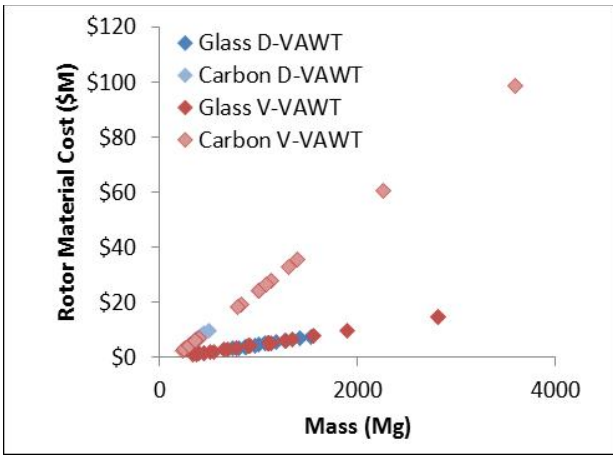

Figure 17. Rotor material costs for all designs.

The general trend is that the maximum rotor aerodynamic efficiency increases with rotor solidity. Solidity is increased by the addition of blade taper (in the present design study), by increasing the number of blades for a fixed blade chord, or by increasing the blade chord for a fixed number of blades. Increasing the solidity, however, comes at the price of lower maximum RPM as the lower RPM leads to higher torque, which increases the cost of the drive train.

As one example, Figure 18 shows the power curves for no blade taper, with varying number of blades and blade chord. The solidity of the two-bladed, large-chord design is the same as that of the three-bladed, small chord design, and the power curves for those two designs match prior to stall.

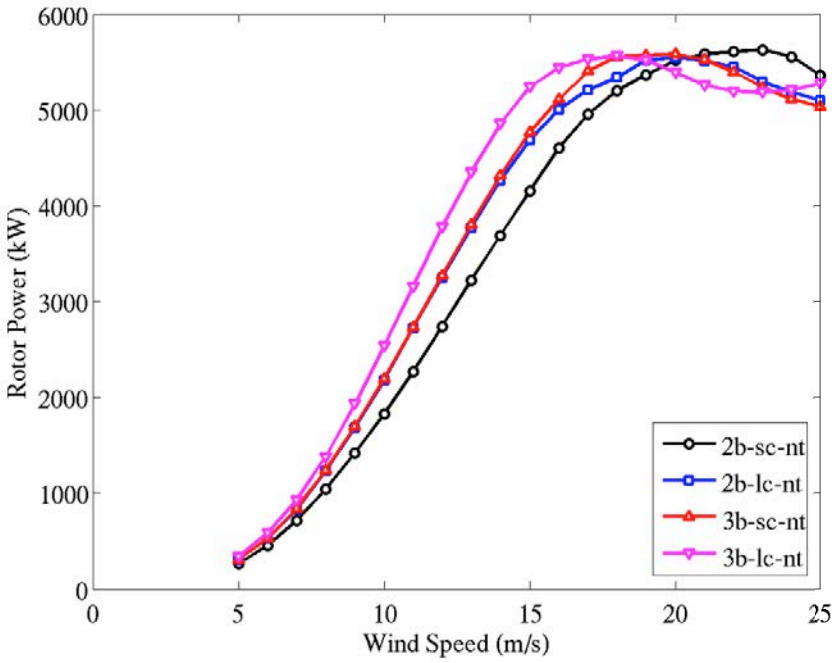

Figure 18. Power curves for Darrieus rotors, untapered designs.

Platform Design Studies

Platform design studies included an evaluation and comparison of spar and semi-submersible floating support structures. The approach in these platform design studies was to start with existing designs for both types of floating support structures, which had been developed previously for floating wind turbines, and then scale or re-size those designs based on the VAWT topside design conditions including topside mass, vertical CG, and wind thrust loading. A visual comparison of scaled platforms is shown in Figure 19 for three different design points. The design points were taken to represent the range of topsides properties from the rotor design studies. Details of hydrodynamic analysis of platform designs using WAMIT are discussed in Appendix A: Platform and Mooring Design Methodology.

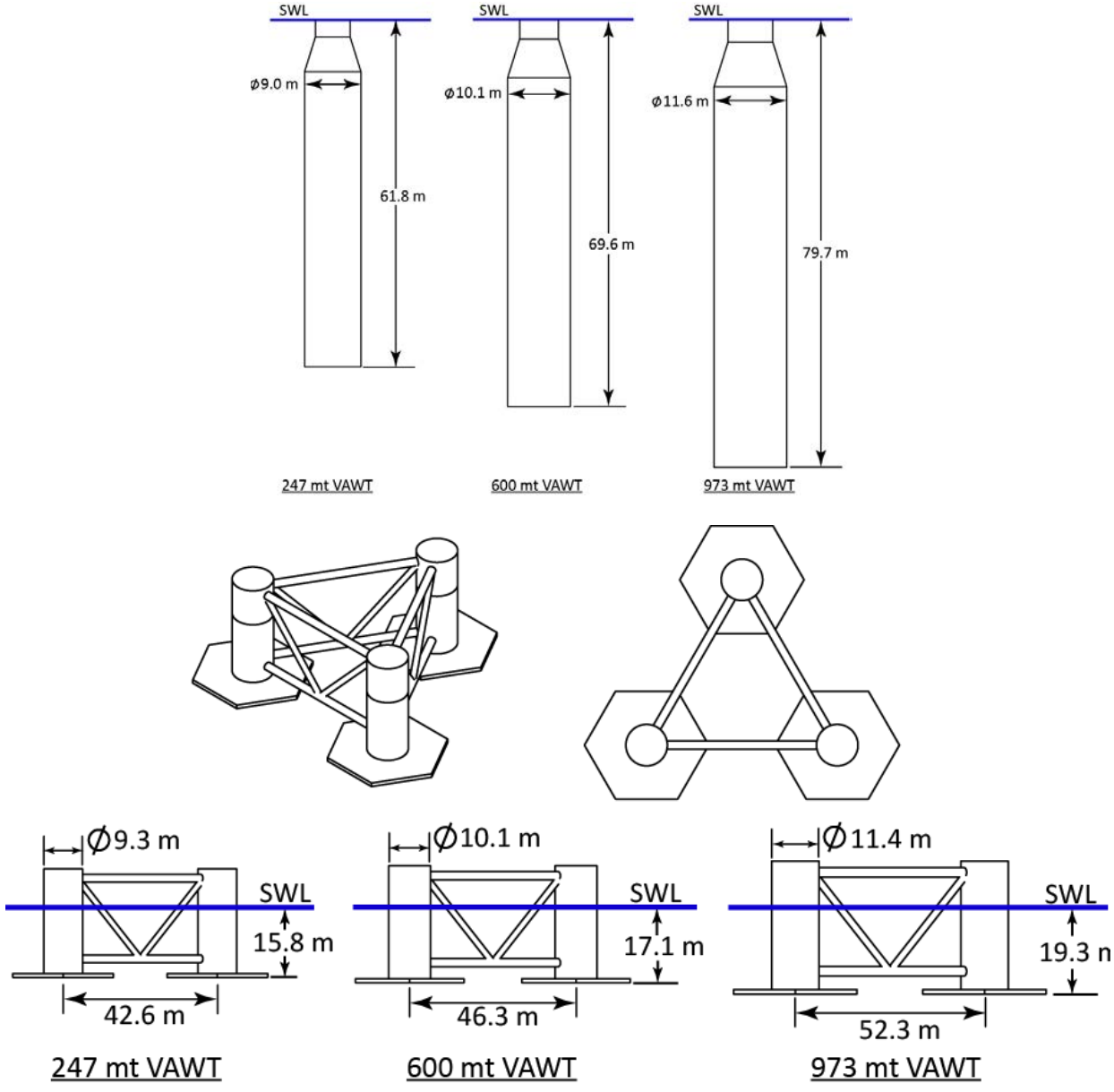

Figure 19. Spar and Semi size comparison over design range.

One result of the platform sizing study is presented for two VAWT rotor configurations and a comparable HAWT topside where estimates for the platform hull mass are provided for the semi-submersible and spar for each of the three 5MW rotor topside options. For each case, the platform was sized such that the platform pitch angle did not exceed a mean value of 5 degrees and the platform pitch period did not exceed 40 seconds. These constraints were applied for both the VAWT and HAWT designs in order to compare the platform sizing for the same design requirements, which provides a direct comparison for a 5MW HAWT versus a 5MW VAWT using the same sizing method and constraints.

Table 1. Platform mass comparison for similarly sized topsides

	Preliminary VAWT		HAWT (a lighter NREL 5MW topside)		VAWT of equal mass to HAWT	
	Spar	Semi-Sub	Spar	Semi-Sub	Spar	Semi-Sub
Topside Mass (kg)	973,000	973,000	600,000	600,000	600,000	600,000
Platform Steel Mass (kg)	1,500,000	2,370,000	2,000,000	2,900,000	1,045,000	1,708,000

Rotor/Platform Loads and Performance Analysis

Aero-elastic loads analysis for the rotor can be found in Section 3.4.

Loads analysis (wind and wave loading) for the platform can be found in Appendix A: Platform and Mooring Design Methodology.

Innovations and Analysis to Mitigate Barriers and Design Challenges

Novel VAWT Airfoils

Traditionally, symmetric NACA airfoil sections have often been used for vertical-axis wind turbine blades. Research at Sandia in the 1980s led to the development of natural-laminar flow airfoils with desirable drag and stall characteristics. However, little work has been done to date defining aerodynamically optimal airfoils for VAWTs. For a HAWT, airfoils with a large lift-to-drag ratio are generally good choices. It can be shown that the aerodynamic efficiency of the HAWT rotor under zero yaw and in a steady wind is a function of this lift-to-drag ratio. The aerodynamics of a VAWT, however, is fundamentally different from the aerodynamics of a HAWT. The power extraction process for a VAWT is inherently unsteady, with aerodynamic blade loadings changing radically during a single rotor revolution. It is not expected that airfoils optimized for a HAWT, assuming nominally steady aerodynamic conditions, will be optimal for a VAWT.

TU-Delft has devised a new method for design of VAWT airfoils that may lead to dramatically different blade designs with greatly improved aero-structural performance. The key insight is the formulation of a new aerodynamic objective function based not on the lift-to-drag ratio in steady

flow, but on the ratio of lift curve *slope* to drag coefficient integrated over a range of angles of attack. The lift curve slope is the slope of the curve resulting when the lift coefficient is plotted against the angle of attack. A promising aspect of this formulation is that it is possible to achieve large lift curve slopes by increasing airfoil thickness. If this benefit outweighs the increase in drag with thickness, then very thick airfoils with high aerodynamic efficiency are possible. Since thick airfoils are also structurally more efficient, it may be possible to avoid the usual tradeoff between aerodynamic efficiency and structural efficiency when designing airfoils for a VAWT.

A first generation of VAWT airfoils has been created using this new design approach. A genetic algorithm was used, along with the XFOIL viscous panel code, to create airfoils with various thickness-to-chord ratios that maximized the objective function described above. Two airfoils from this family of designs are shown in Figure 20. In general, these airfoils are not symmetric but are cambered, and the amount and direction of camber is a function of the thickness.

Figure 21 shows the calculated maximum power coefficient for a three-bladed, two-dimensional VAWT using various airfoils. Symmetric NACA foils are compared to the new family of VAWT airfoils for a range of thicknesses, and performance under both clean blade (free transition) and soiled blade (forced transition) conditions is included. The new family of thick foils outperforms the NACA foils, particularly at large thicknesses. The performance of the new foils at thicknesses above 35% is comparable to much thinner NACA foils.

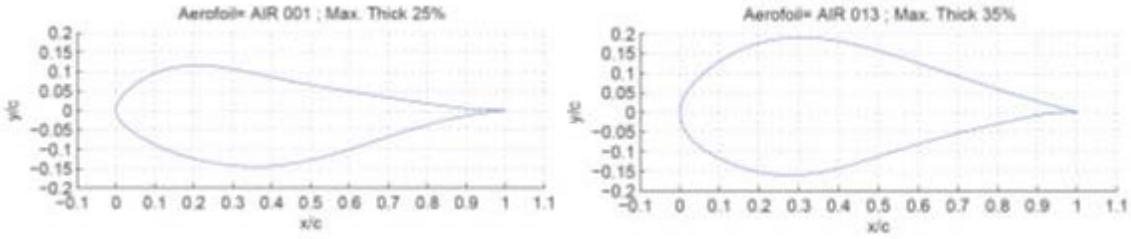

Figure 20. Two aerodynamically optimal thick VAWT airfoil designs.

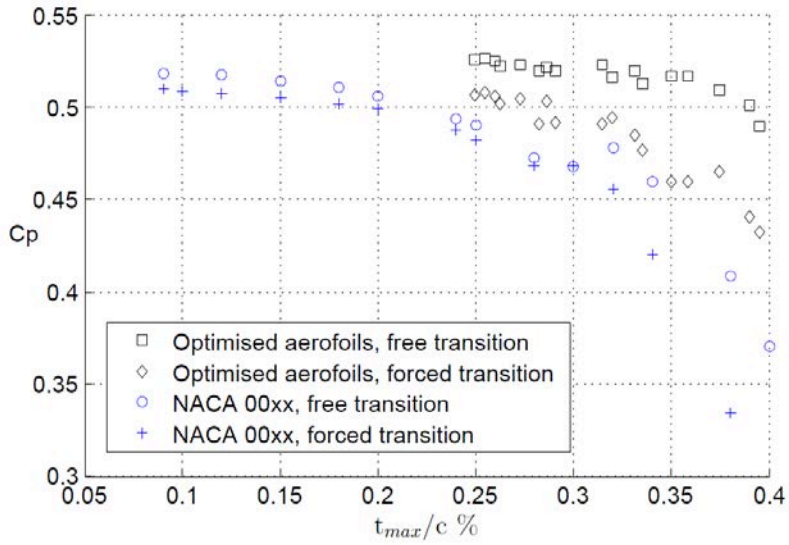

Figure 21. Two-dimensional rotor power coefficient for optimized airfoils, compared to NACA airfoils.

The new design approach appears to be very promising and opens up new opportunities in VAWT airfoil design. Verification of the airfoil designs through wind tunnel testing has commenced under a separate, parallel VAWT research project at TU-Delft.

Aero-elastic Stability

Dynamic aeroelastic instability or flutter can be a concern for lift-generating structures under aerodynamic loads. The coupling of aerodynamic forcing with a structure's natural modes can lead to large amplitude diverging motion. Recent studies have shown that flutter is a potential issue in very large HAWT wind turbine blades and may be a concern for very flexible multi-megawatt VAWT structures under large aerodynamic loads as well.

The six VAWT configurations considered for detailed structural dynamics analysis in Section 3.4 were examined for flutter instabilities. The aeroelastic formulation and automated procedures of the Sandia BLade Aeroelastic STability Tool (BLAST) for HAWT blades were implemented into the OWENS framework for considering the aeroelastic analysis of rotating VAWT structures.

Damping trends for the various configurations were observed and modes with negative aeroelastic damping were identified. Damping trends for these modes are shown in Figure 22 to illustrate the estimated RPM at which flutter may occur (when damping goes negative).

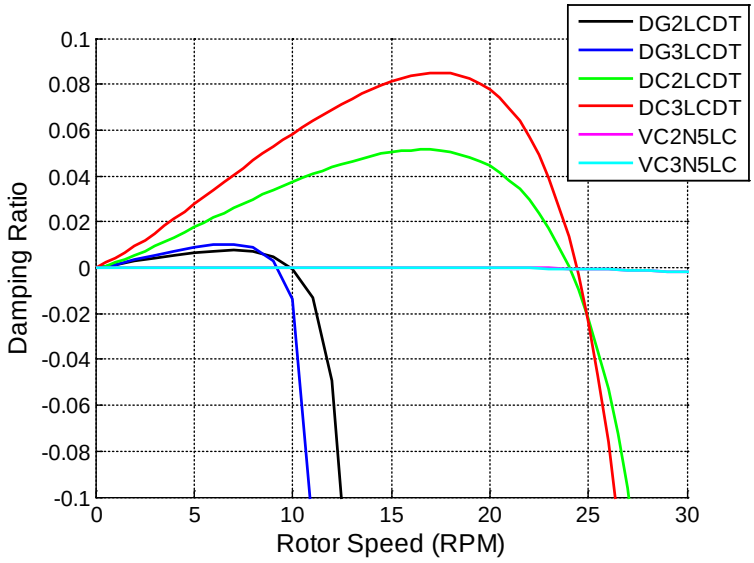

Figure 22. Damping trends of primary flutter modes for VAWT configurations.

This preliminary analysis indicates that while flutter instability is outside the operating RPM range in these designs, more attention should be placed on flutter analysis tools as the flutter margin is less than 1.5 for some design configurations. This flutter margin may drop to lower values with designs that are more lightweight and flexible including machines of larger size. Further, the current set of flutter analysis tools have not been validated with experimental data, and this should be done to understand the importance of flutter instability in VAWTs and how to mitigate it through design.

Rotor-Platform Coupled Dynamic Stability

Understanding the structural dynamic behavior of a system is useful for gaining insight into the fundamental behavior of a system before a large number of loading scenarios are considered. Furthermore, identification of potential instabilities at the initial design stage is critical for proactively mediating undesirable large dynamic response (structural resonance) of a system (e.g. that leads to increased fatigue loading and fatigue damage accumulation).

Floating support conditions on the 5 MW designs were also considered using the spar buoy and barge platforms described in the configurations section. Figure 23 and Figure 24 show the tower modes plotted in Campbell diagrams for the 3- and 2-bladed 5 MW VAWT designs respectively with land-based and floating support condition. There is a striking difference on the effect of platform support on tower modes for the spar and barge supports as the barge support shows the potential to significantly increase the frequency of tower mode. Of course, the topside rotor/tower is the same for each of the three support structures considered for the 2- and 3-bladed cases.

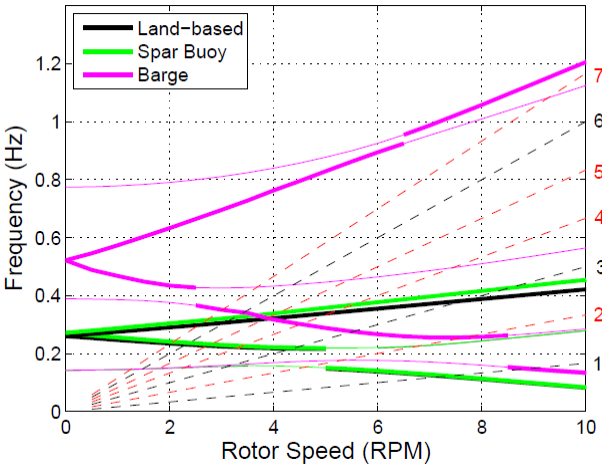

Figure 23. Tower mode Campbell diagram of 3 bladed 5 MW VAWT for land and floating support conditions.

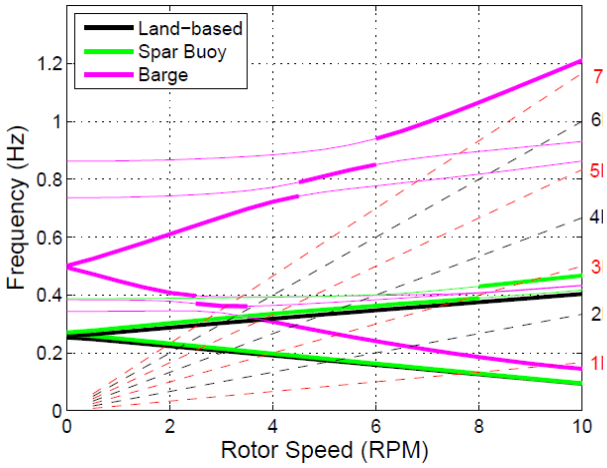

Figure 24. Tower mode Campbell diagram of 2 bladed 5 MW VAWT for land and floating support conditions.

The effect of the number of blades on aerodynamic forcing inputs was also analyzed in this research. Along with the support structure study, a generalized formula showing how the critical forcing frequencies (per-rev) excitations vary with number of blades was developed. This provided a new set of general guidelines for structural dynamics analysis in VAWT design that did not exist for previous design work.

Balance of Station Cost Reductions

As noted above in Table 1, based on a sizing study of existing wind turbine floating platforms, the platform hull masses are lower for a VAWT in comparison to HAWT of same power rating.

Further reduction in the platform costs could be found in innovative platform designs optimized for VAWTs. Offshore wind platforms have been typically designed within an envelope that is acceptable for HAWT rotor operation. The boundaries of the design envelope then enforce certain dynamic characteristics of the platform. Unique aspects of the VAWT rotor indicate that the design

envelope that has thus been applied to offshore floating platforms is not optimized. For instance, the VAWT rotor potentially exhibits increased aerodynamic efficiencies when it is moderately tilted to the incident wind.

An innovative floating platform initiative would systematically address the necessity of these design envelope conditions for a VAWT rotor. Since a moderate mean pitch angle increases aerodynamic efficiency, allowing the platform to react more to the operational environment potentially has the possibility of increasing power delivered. Further, a platform that reacts more to the operational environment will displace a smaller volume of water, and hence will require less steel to manufacture.

Storm Survival and Load Alleviation (Novel Operating Strategies)

Aeroelastic load alleviation has been explored at a conceptual level as an aerodynamic braking mechanism for VAWT rotors. This would take the form of either swept blades or laminate-induced twist-extension or twist-bend coupled blades depending on the application. Estimates of as little as 4° of twist in the equatorial region of the rotor could be enough to provide protection against overspeed in the event of an emergency. This amount of twist or greater has been proven in multiple HAWT experiments.

Preliminary Analysis of the Cost of Energy

The cost of an offshore wind farm can be decomposed into three main categories (as detailed in Figure 25): balance of system costs, turbine capital costs, and operations and operations and maintenance (O&M) costs. Balance of system costs can be further decomposed to include: transportation, installation, electrical interconnection, and other costs. Turbine capital cost can be further decomposed into: rotor cost, drive-train cost, support structure cost, control and monitoring system costs, and marinization cost.

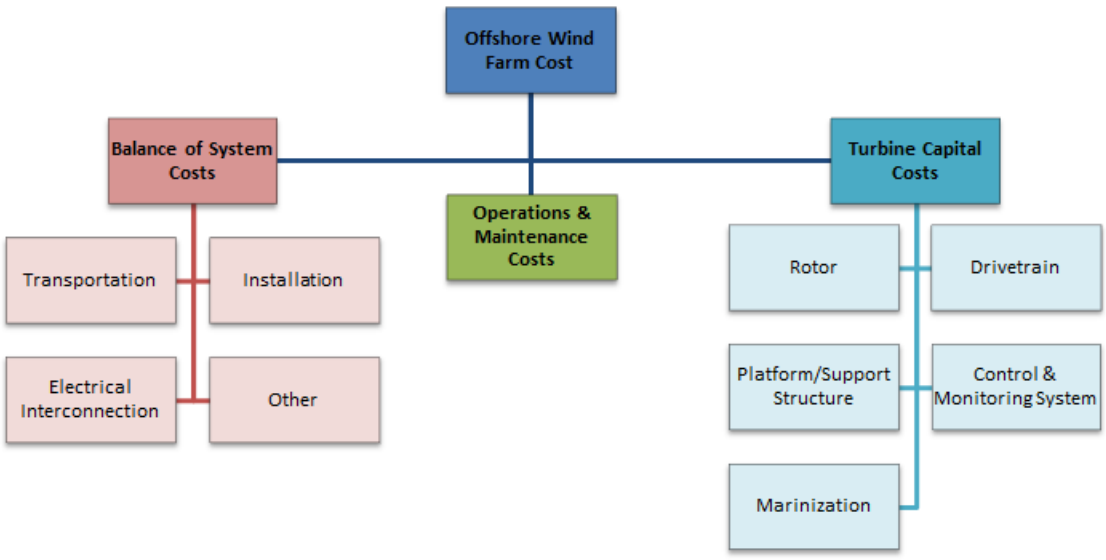

Figure 25. Offshore wind farm cost categories and sub components.

In total, results of cost of energy analysis are presented here for 31 offshore VAWT systems. Figure 26 shows the trends of LCOE versus rotor mass for these configurations. Investigations revealed that LCOE trends most noticeably with rotor mass as this is a critical parameter for both rotor cost and platform support costs. The effect of material choice is also evident in this figure, with carbon designs having LCOE trending with a higher slope than glass designs due to increased material cost relative to glass. Figure 26 shows that the Darrieus designs perform better from a cost perspective, while V-VAWT designs will likely require additional optimization or innovation to become cost competitive.

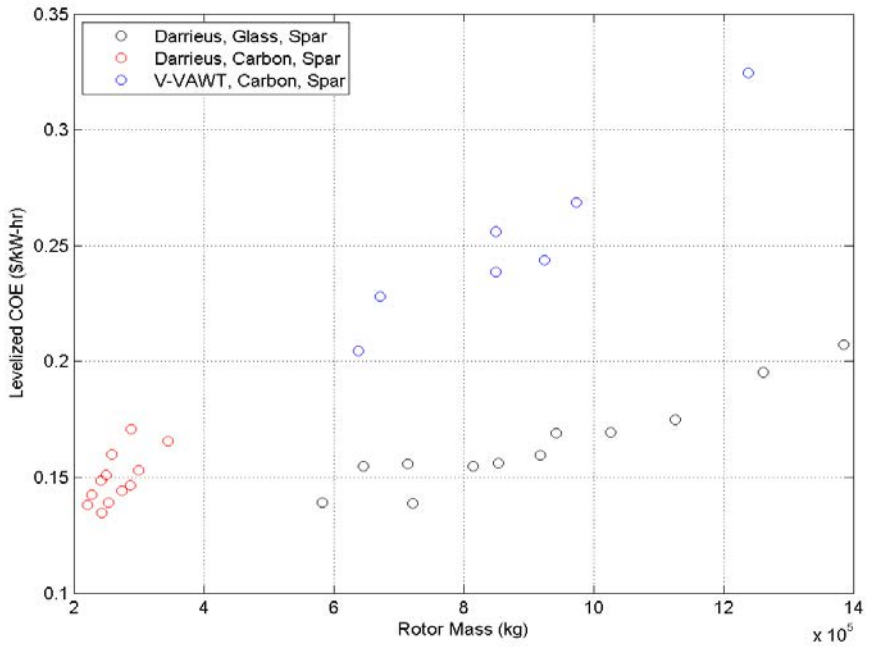

Figure 26. Preliminary Cost Analysis: LCOE vs. Rotor Mass.

In summary, for Darrieus designs, the minimum LCOE was determined to be 0.134 USD/kW-hr, the maximum LCOE was 0.207 USD/kW-hr, and the mean LCOE was 0.157 USD/kW-hr. V-VAWT designs had noticeably higher LCOE with minimum, maximum and mean of 0.205, 0.325, and 0.252 USD/kW-hr respectively.

1. INTRODUCTION AND PROJECT OVERVIEW

The offshore vertical-axis wind turbine project led by Sandia was performed to assess whether the trends and future development in the wind energy industry would be aided by considering this deviation from the traditional horizontal-axis wind turbines which dominate land-based installations. Both the continual move towards higher capacity machines and the anticipated development of deep-water, offshore sites which require floating platforms provide advantages for vertical-axis wind turbines, where platform costs represent the main single contributor to the total system costs. The goal of this project has been to produce better understanding of the technical and economic feasibility of the floating vertical-axis wind turbine technology solution for offshore wind. Floating vertical-axis wind turbines have many inherent advantages that show promise for reducing costs over floating wind systems using conventional horizontal-axis wind turbines. However, the technical and economic feasibility had been largely unexplored in a comprehensive manner, and it has been the purpose of this project to determine the challenges and opportunities for vertical-axis wind turbines at offshore sites where floating systems are required. The project was conducted in two phases, which are summarized by two reports. The first phase of study was conducting design studies using a variety of rotor architectures and platform types to assess the feasibility of the technology at this scale. The design studies, methodologies, and findings are described in the full report. Phase two of the project, which is the subject of a separate report, was performed to gain more confidence in the system cost analysis, with a focus on the platform design and cost estimate. The platform selection and design represents a large body of work from this study, which was performed in collaboration with a consultant from the oil and gas industry. The resulting system levelized cost of energy was then studied using the highest fidelity of sources available for each of the capital and operational expenses for the offshore wind plant with floating vertical-axis wind turbines.

1.1. Project Objectives

The over-arching objective of this project was to evaluate the feasibility of the Vertical-Axis Wind Turbine (VAWT) architecture for very large-scale deployment in the offshore environment. The most critical barrier to offshore wind, high Levelized Cost of Energy (LCOE), is specifically targeted with the overall goal of achieving a 20% reduction in COE through application of VAWT rotor technology. It was proposed to achieve this goal by:

- Developing innovative VAWT rotor designs that enable reliable, cost-effective, and easily manufactured rotors for deep-water offshore machines at large-scale (5MW and greater);
- Demonstrating the potential for greater than 20% reduction in COE for a deep-water, floating VAWT system compared to current shallow-water HAWT systems;
- Developing manufacturing techniques, certification test methods, and a commercialization plan for offshore VAWT rotors in order to accelerate deployment; and
- Testing, in a wind tunnel and combined wind-wave tank, of a proof-of-concept subscale, deep-water floating offshore wind turbine employing a VAWT rotor.

This report documents the progress toward each of the first three areas.

1.2. Project Organization: Task Structure

The project was structured in three primary tasks or work packages, as described in the following sections.

1.2.1. Task 1.0 Preliminary Design of Innovative Aero-elastic Rotor for Offshore VAWTs

In this project, we developed and compared several candidate rotor architecture concepts. We investigated curved-bladed Darrieus rotors as well as towerless V- or U-shaped rotors. We also investigated aerodynamic innovations, including a rotor optimized for increased energy capture, as well as airfoils specifically optimized for VAWTs. Underpinning this research effort was a design code development effort that resulted in a new tool for VAWT structural dynamics analysis, as well as new capabilities to synthesize aerodynamic and structural dynamic codes to create an aero-hydro-elastic design tool for VAWTs. In future work, we plan to investigate rotor concepts that incorporate novel VAWT load-alleviation and braking strategies. In addition, we will develop a blade shape optimizer for the new aero-elastic design code, and apply it to identify the main rotor design drivers and optimize rotor designs for low COE.

In the deep-water floating-platform configuration, the coupled dynamics of the rotor and floating platform will be essential to accurate prediction of full-system loads and stability. We coupled the aforementioned rotor aero-elastic model to an existing floating-platform dynamics model. We initially validated the aero-elastic simulation models developed during this project against existing data for VAWTs.

We used the simulation tools to perform design trade-off studies to compare several candidate rotor designs. These studies incorporated constraints developed under the design for manufacturability task described in Task 3.0. This will result in high-performance designs that have built-in manufacturability from the outset. At the end of the project, we have down-selected to a set of candidate rotor designs for more detailed investigation and optimization in the future.

1.2.2. Task 2.0 Deep-Water Floating VAWT System Design and Cost Analysis

Our objective for this task was to enable offshore VAWT system designs that are optimized with respect to LCOE. This first required us to develop an offshore VAWT system LCOE model. We performed preliminary system design studies to determine how capital costs and LCOE scale with rotor architecture and material selection as well as with floating platform type. A range of LCOE estimates for both Darrieus and V-VAWTs were produced based on rotor and platform design studies.

1.2.3. Task 3.0 Offshore VAWT Rotor Materials and Manufacturing Strategies

The optimal VAWT rotor design requires consideration for manufacturing. Given the complexity and scale of a 10-20 MW VAWT blade structure, along with significant differences in blade loading, alternative manufacturing methods may be needed compared to what is employed in modern HAWT blade production. We applied the research team's experience in blade design to concurrently consider manufacturability and reliability during the initial design phases. The team identified the principal material drivers for VAWT rotors along with applicable material, coating, and manufacturing options. The screening was open to multiple fiber and resin types—including

glass, carbon, and aramid fibers, as well as thermoset and thermoplastic resins—for compatibility and resistance to combined mechanical and environmental loads. We then used the output of the dynamic models developed and applied in Tasks 1.0 and 2.0 to develop and analyze FEA models, including design loads analysis, of selected rotor concepts. Through this analysis, we evaluated material and manufacturing concepts for large-scale VAWT blades.

1.3. Major Technical Barriers this Project Aimed to Address

This project aimed to address the following major technical barriers to performance, reliability, and cost reduction for offshore wind technology.

1.3.1. Large O&M Costs Associated with System Architecture

O&M costs are estimated to comprise between 20% and 30% of the total life-cycle cost for offshore wind projects. Current strategies for reducing O&M costs rely on incremental improvements on HAWT technology. The HAWT configuration, including location of the drivetrain, active blade pitch, and yaw systems within a relatively inaccessible, tower-top nacelle, leads to inherently large O&M costs for offshore deployment. Replacement and overhaul operations for these drivetrain components are also expensive, involving large, specialized vessels and requiring calm sea conditions, which can significantly affect turbine availability and energy production. These preliminary design studies indicate the feasibility of the floating VAWT concept and indicate that the inherent ability to reduce O&M costs is possible.

1.3.2. Large Support Structure Costs of Offshore Systems

Deep-water deployment offers potential for access to a very large wind resource, especially off the New England and Mid-Atlantic coast, within the Great Lakes, and off the Pacific coast— all regions with large electrical loads and relatively small amounts of current renewable energy production. For floating deep-water systems, static and dynamic system stability depends critically on the unit's center of gravity. A large mass located on the top of the tower, as in the drivetrain/generator set in the nacelle of a HAWT configuration, requires a relatively large support structure to ensure stability. On the other hand, a VAWT rotor configuration offers a fundamental advantage as demonstrated in these preliminary design studies.

1.3.3. Scaling to Large Rotor Sizes

Balance of station costs for offshore turbines favor large turbine sizes. However, two issues make scaling HAWT architectures to very large sizes challenging: (1) the gravitational fatigue loads become a severe design constraint; and (2) the variability of wind direction across the rotor becomes more pronounced, making it increasingly difficult to point the turbine into the wind direction.

1.3.4. Storm Survivability

Offshore wind turbines must operate in a very severe marine environment, which may include hurricane wind and sea states. Innovative methods for ensuring survivability under such conditions are needed to enable penetration of offshore wind into markets in the mid-Atlantic and Gulf of Mexico. Detailed studies of load alleviation and storm survivability will be needed in the future, and the current study provides initial design models and insights into load alleviation and storm survival.

1.3.5. Lack of Suitable Design Codes for Rotor Aero-elastics and Platform/Mooring Hydrodynamics

Design codes were needed to perform the preliminary design studies for VAWT rotor designs as well as platform and mooring systems. The design codes developed, coupled, and validated in this project are documented in this report.

1.4. Offshore VAWT Technical Innovations and Their Impact on Addressing Technical Barriers, Improving Performance, and Reducing Costs

In developing this project, we proposed a pathway to overcome the barriers described above by maximizing the inherent advantages of the VAWT architecture over that of a HAWT (Figure 27), as well as by introducing breakthrough innovations in the VAWT rotor's system performance. Several specific technology innovations have underpinned our approach in design for overcoming barriers to cost reduction and performance. These specific technical areas are described below in greater detail.

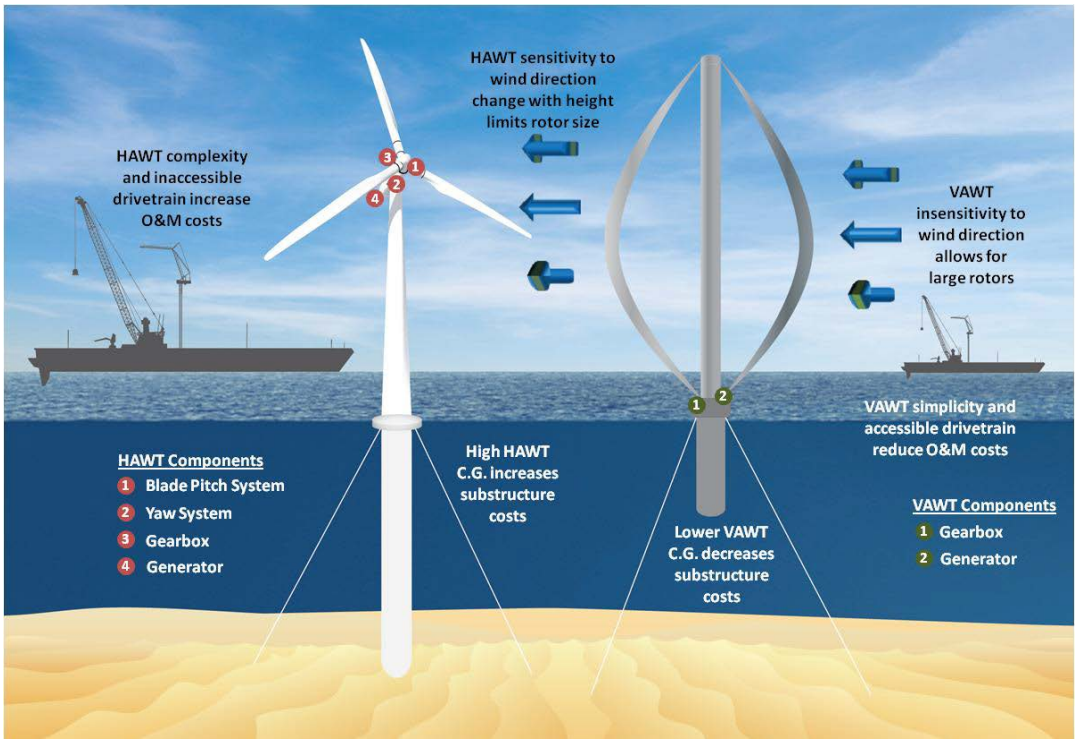

Figure 27. Comparison of HAWT and VAWT Machines for Offshore Deployment.

1.4.1. Reduce System Complexity and Ease Access to Major Components (Addresses O&M and Support Structure Barriers)

Unlike the HAWT architecture, VAWTs do not require blade pitch or yaw systems. This greatly reduces system complexity and associated O&M costs. In addition, VAWT drivetrains are located at water level, resulting in lower cost for repair and replacement of parts. To further reduce both O&M and support-structure costs, we explored rotor designs that employ passive load-alleviation technology and the possible elimination of the central tower.

1.4.2. Reduce Tower-Top Mass (Addresses Support Structure Barrier)

The drivetrain for a VAWT is located at the base of the machine, which substantially lowers the center of gravity and increases system stability, thereby reducing the size and cost of the required support structure. This will be especially advantageous for deep-water floating systems, enabling access to the Pacific coast and deep-water wind resource located along the Atlantic coast and in the Great Lakes.

1.4.3. Enable Large-Scale, High-Performance Rotors (Addresses Scaling Barrier)

In contrast to a HAWT rotor, a large VAWT rotor is ***not*** constrained by operating cyclical gravity loads, but rather by a combination of centrifugal and aerodynamic loadings. Thus, VAWT blade weight does not limit the achievable rotor size. VAWTs are also naturally insensitive to variability in wind direction across the rotor, making very large rotors feasible, and the lower shear in the offshore wind profile enables VAWT rotors that extend close to the sea surface. Additionally, due to recent developments in VAWT aerodynamics research, the aerodynamic performance of the VAWT can potentially meet or exceed that of a HAWT, as demonstrated below. This research aims to improve the aerodynamic efficiency of the VAWT through both design and manufacturing improvements.

1.4.4. Manufacturing Strategies for Large-Scale VAWT Blades (Addresses O&M and Scaling Barriers)

We applied optimal structural design, manufacturing processes, and quality-assurance methods to generate VAWT blade designs that are reliable and cost effective both in initial manufacturing and future O&M costs. With manufacturing processes that have greater precision and repeatability, designs with the same aerodynamic performance can be made lighter and cheaper. We evaluated advanced manufacturing methods—including large-section composite pultrusions, automated fiber placement, and segmented blades—to reduce defects and minimize weight and cost.

1.4.5. Survivable VAWT Designs (Addresses Storm Survival Barrier)

We outlined concepts for addressing both extreme storm loadings on an offshore VAWT, as well as concepts for effective aerodynamic braking of the machine. The VAWT architecture lends itself to several active control arrangements, enabling increased system stability for floating systems and decreased rotor loads under hurricane conditions. Aero-elastic coupling methods provide a mechanism for over-speed limitation. These concepts could lead to increased reliability of VAWT systems and enhanced probability for survival in the hurricane conditions that will be encountered in the mid-Atlantic and Gulf of Mexico.

1.4.6. Passive Load Alleviation and Speed Control for VAWT Rotors

VAWT aerodynamics are very different than HAWT aerodynamics, leading to different aerodynamic load characteristics for the two machine types. In a steady, uniform wind, VAWT blade loads and rotor torque change with rotor azimuth, leading to a cyclical variation in loads and torque. The cyclical blade and torque loads are sources of blade fatigue and drivetrain fatigue, respectively. Additionally, extreme wind events can lead to large blade loads, especially for the cantilevered VAWT blades used in the H-VAWT or V-VAWT configurations. Rotor and drivetrain weight and cost can be decreased if these cyclical and extreme loads can be reduced. Additionally, unlike HAWTs, VAWTs have not typically employed an active blade pitch system,

which provides VAWTs an advantage in simplicity. However, VAWT rotors still need braking in case of rotor overspeed. Reliance solely on a mechanical brake leads to a heavy and expensive brake system, as well as severe shutdown loads on the turbine. Aerodynamic braking, achieved by an increase of the rotor drag, is more benign and potentially much more cost-effective than mechanical braking. To date, no one has achieved a reliable aerodynamic braking system for VAWTs. This represents a technology barrier for realization of cost-effective VAWT machines.

In this work, we addressed both the unsteady aerodynamic loading and the braking issues through the innovative application of passive aero-elastic tailoring. In this approach, the blades respond to increases in loading by twisting. The resulting torsional deflection leads to increased drag, reduced rotor speed, and/or reduced blade loads. Passive twist offers a potential means for achieving performance benefits without introducing a mechanically complex pitch actuation and control system. It has been investigated and applied to HAWT rotors (1) (2) for some time, but, to our knowledge, has not been systematically investigated for application to VAWT rotors. In addition to load and speed limitation, we also considered aero-elastic tailoring for optimizing blade twist variation to improve aerodynamic efficiency.

In this work we took full advantage of the reliability advantage given by the relative simplicity of the VAWT system. However, it is unknown if the passive concepts described above will ultimately have enough authority to provide for both load alleviation *and* effective aerodynamic braking. Thus, we also considered actively controlled Darrieus concepts.

1.4.7. Design for Simultaneous Optimization of Loads and Performance

Recent advances in VAWT aerodynamics at TU-Delft have demonstrated that, due to the unsteady and cyclic behavior of the VAWT, it is possible to design a VAWT with the instantaneous rotor loading decoupled from the average power generation (3). This new design process separates the optimization of blade design parameters that govern loading (blade pitch, twist, camber, etc.) from the optimization for power conversion. The practical consequence of this process is a shift of the range of aerodynamic operation of the blade, avoiding lift losses due to flow separation and high drag; instead, it is now possible to design blades that will operate at maximum lift range and with low aerodynamic drag, while keeping a high cross-sectional thickness (above 27% for cantilevered blades), which will allow stiffer and lighter blades. Recent design analysis work demonstrated the potential of design for aerodynamic power coefficients of C_p>0.5, above what is currently achieved by HAWTs. We will use this innovative design process for VAWT rotors, in conjunction with the load-alleviation strategies described in the previous section, to develop lightweight and efficient VAWT rotor designs.

1.4.8. Floating Platform VAWT System

The VAWT machine configuration naturally leads to a lower center of gravity than for the HAWT configuration. This lower center of gravity will reduce support structure costs regardless of the type of support structure, but this cost reduction will be largest for floating platforms. Floating platforms enable deployment in deep waters (> 60 m depth), where the wind resource is often greater than in shallow water and public acceptance is greater. The excellent wind resource of many deep-water sites offers further reductions in COE due to increased energy capture. Preliminary studies at the University of Maine have shown that the energy generated from a turbine located 30 nm offshore is 20% and 33% higher as compared to a turbine located in shallow water and onshore locations, respectively.

Our proposed work will exploit this potential synergy by studying the system cost benefits in coupling VAWTs with deep-water deployment on floating platforms. Our preliminary design efforts and full coupled system dynamics modeling will examine the feasibility of this concept. We will consider different floating platforms (tension leg platform, spar buoy, barge), along with mooring designs that will enable resistance to yawing moments caused by rotor torque. Additionally, we will explore the potential for using the underwater structure to add damping to the system. These studies will heavily leverage ongoing and future projects at the U. of Maine in modeling and experimentation with floating platforms for HAWTs.

1.4.9. Design for Manufacturability and Innovative Manufacturing Techniques

To address the cost, performance, and reliability barriers in manufacturing offshore turbines, we evaluated rotor designs using fundamental design principles that will make them more readily manufacturable, the processes more automatable, and rotors having consistent quality.

2. DESIGN CODE DEVELOPMENT

To facilitate the development of VAWT technology, robust design tools must be developed to assess innovative design concepts for off-shore wind energy technology. In this project, a suite of design tools were developed based on a modular analysis framework with a finite element structural dynamics implementation for flexible, rotating structures at its core. The framework is capable of interfacing with external modules to consider aerodynamic loadings, platform dynamics, and generator/drive-train dynamics. We developed a general mesh generator, capable of considering arbitrary VAWT architectures and allowing a large degree of flexibility in the VAWT configurations that may be considered in design studies. Aerodynamic design tools for VAWTs with varying degrees of fidelity, ranging from vortex lifting line methods to hybrid Lagrangian/Eulerian computational fluid dynamics (CFD) methods, were also developed. Furthermore, platform dynamic/ hydrodynamic/mooring design tools were developed to assess platform designs and the response of a flexible VAWT configuration deployed in a deepwater environment. The following sections present overviews of design tool development efforts for offshore VAWTs.

2.1. SNL OWENS and VAWTGen

This section presents the analysis framework for the Offshore Wind Energy Simulation (OWENS) toolkit and VAWTGen for vertical-axis wind turbines, which provide structural analysis and geometry generation. First, the desired features for the analysis tool are identified. These features are necessary to consider preliminary design studies of innovative VAWT configurations, as well as ensure the tool will be extensible to future needs of the wind energy community. Fundamentals of the model formulation are discussed, and a modular framework for interfacing a core structural dynamics solver with various external modules is presented. The concept of a "loose" coupling strategy is presented, and the practical implementation of data flow between a core analysis framework and external modules using network sockets is also discussed. A robust mesh generator has been developed that is capable of considering arbitrary VAWT configurations and the design and features of this mesh generator are discussed. An overview of the finite beam element that is central in the development of the analysis tool is given.

2.1.1. OWENS Features

The OWENS analysis tool has been designed according to the envisioned needs of modeling efforts for large offshore vertical-axis wind turbines. This tool has been developed with the goal of maintaining a general framework for analyzing VAWTs of an arbitrary blade and strut configuration. Furthermore, the formulation seeks to provide flexibility for future analysis needs. In particular the following features are central in the design and development of the analysis tool.

- The analysis tool can model the structural dynamics of a collection of beam structures in an arbitrarily prescribed path in space that rotates around a central, vertical axis. Potential VAWT configurations will include Darrieus rotors, H-rotors, and V-rotors. Blades may be affixed to the tower directly or through the use of struts, and rotor blades can be swept toward or against the direction of travel.
- The analysis tool can integrate the equations of motions in the time-domain as well as consider frequency domain analysis. Transient analysis is necessary to consider structural response under transient conditions such as start-up, shut down, and irregular wave and

wind loadings. A frequency domain analysis is desirable to facilitate stability analysis of a VAWT configuration and identify potential resonance issues.

- The analysis tool has a streamlined, modular framework that can account for various fidelities of structural dynamics analysis models. These models include linear beam representations with geometric nonlinearities, efficient reduced order structural models, and future development could include geometric nonlinearities due to large deformation of components.
- The structural model can account for passive aeroelastic coupling mechanisms, including bend-twist, extension twist, and sweep-twist couplings. Thus, the structural elements have a torsional degree of freedom.
- The structural formulation can accommodate jointed blade structures. This includes the ability to specify concentrated mass and stiffness terms.
- The boundary conditions for the blade connections as well as the platform/turbine base are general and can include fixed, free, and pinned conditions.
- The analysis tool enables general coupling with available VAWT aerodynamic models.
- The analysis tool enables general coupling to floating support structure, and mooring system hydrodynamic models.
- The code will interface with a turbulent wind field file, allowing simulation of VAWT response under turbulent wind conditions. Initial development may assume steady wind fields.
- The analysis tool enables a general interface to a model for drive-train mass and dynamics.
- The analysis tool design considers the interface of a turbine control algorithm, as well as prescribed motion of the blades and tower, and prescribed braking torque on the tower.
- The analysis tool considers ease of interface with existing wind turbine design tools.

The following sections present a formulation for the aeroelastic modeling of offshore VAWTs while satisfying these desired features.

2.1.2. Geometry and Mesh Generation

A VAWT rotor primarily consists of a tower and blade components. The blades may be affixed to the tower at their ends as in the Darrieus and V-VAWT configurations or via struts (H-VAWT). Struts may also provide a connection between the tower and blades at any position along the tower and blade spans. Accordingly, a mesh generator called VAWTGen has been created that is capable of generating VAWTs of arbitrary geometry, including H-type, V-type, and Darrieus configurations shown in Figure 29. The VAWT configuration will be discretized from continuous structural components into a finite number of beam elements. Elements span between discrete points in the mesh, known as nodes. Finite element analysis will examine the motion of nodes as dictated by the deformation of the beam elements under prescribed boundary conditions. This collection of nodes and elements forms the mesh of the VAWT configuration.

VAWTGen accepts data files containing the basic geometry of tower, blade, and strut components. Other crucial configuration information is specified, such as the elevation of the blade root from the tower root, as well as the radial distance the blade root is positioned from the tower. An

arbitrary number of blades may be specified for the configuration. VAWTGen positions the blade roots in equal angular increments about the tower axis. The blades may be rotated into an arbitrary orientation per a sequence of Euler angles input by the user. If required, struts may be inserted between the tower and a blade by specifying a fraction of the tower span and the blade span the strut will span. VAWTGen will insert a straight strut of the appropriate length between the tower and blade components. The geometry of the strut component is specified by a file containing geometric data. The strut may be oriented at a certain pitch angle as described by user input.

With these relatively minimal set of inputs (as illustrated in Figure 28) a VAWT of arbitrary configuration may be created. Therefore, a separate tool is not required for the various types of configurations. VAWTGen provides a convenient means to visualize the VAWT turbine as a wireframe (Figure 29). This serves as a quick check for the user to ensure the VAWT has been constructed as intended, and shows the actual turbine configuration that the mesh of beam elements represents. VAWTGen also visualizes the finite element mesh (Figure 30) to allow the user to visually inspect the refinement of the mesh. VAWTGen identifies points of intersection between the various components and inserts nodes accordingly. These node pairs at points of intersection (i.e. strut to tower, blade to strut, blade to tower) are recorded so appropriate constraint conditions at these joints may be imposed. Details of imposing constraints are discussed in (4). A mesh file is generated that will be used by the analysis software. An elemental data file is also created, containing the structural and aerodynamic properties of the element, as well as the Euler angles representing the orientation of the element. By default, the mesh is discretized in the same manner as the geometric description of components. The user may further subdivide the mesh by specifying an integer factor to further refine the geometric data into smaller elements.

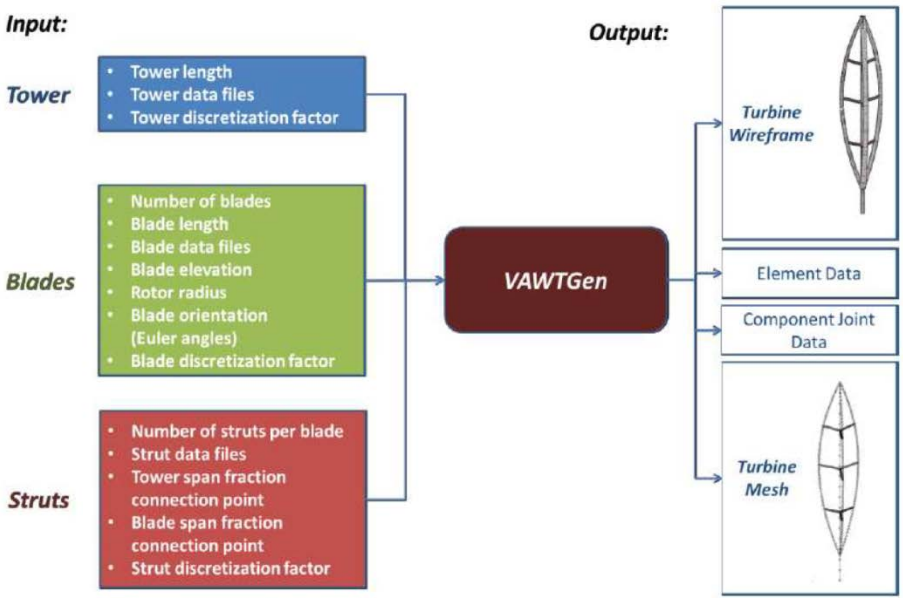

Figure 28. Flowchart of VAWTGen input and output.

VAWTGen requires data files be supplied to describe the geometry of the primary turbine components (blades, towers, and struts). The format of these data files is the same as the component files for NREL's FAST code (4). These files describe the geometry and aerodynamic properties of general turbine components, and there is nothing that restricts their use to HAWTs specifically. For example, even though a Darrieus blade is not likely be installed on a HAWT, it

is easily described by the NREL blade geometry file format. This allows existing design tools such as the Sandia National Laboratories Numerical Manufacturing and Design Tool (NuMAD) for wind turbine blades (5) to be interfaced with the VAWT analysis tool without the need to consider new file formats. The NREL file format separates geometrical/structural properties of a blade and aerodynamic properties of a blade into two files. This potentially allows one to segment structural dynamics analysis from aeroelastic analysis, depending on the design of the mesh generation and analysis tools. Also, a separation of information more readily facilitates parametric studies. If a user would like to change aerodynamic properties of a blade under the assumption that structural properties do not change significantly, there is no need to create two files with duplicate information (which is inherently prone to introducing errors in analysis files).

Next, the mesh generation capabilities of the VAWTGen software are demonstrated in Figure 29. From left to right: a Darrieus type configuration with swept blades is considered, a strutted Darrieus configuration with un-swept blades, a two bladed V-VAWT configuration, and a three bladed H-VAWT with multiple strut connections is considered (the blades are oriented at an arbitrary orientation, and two strut connections per blade are specified). Note that the blades may be positioned at any orientation. The blades and tower/strut components may share a common point and can be joined together via a constraint that appropriately models the joint. Details regarding joint constraints are available in (6).

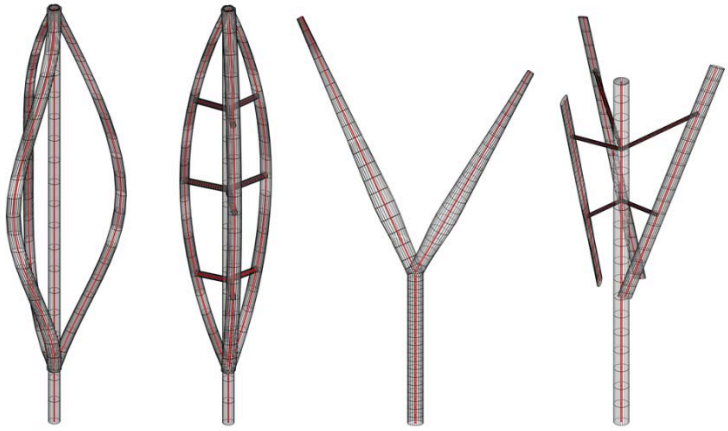

Figure 29. Wireframes of various VAWT configurations created with VAWTGen.

Figure 30. Finite element mesh visualization of a VAWT configuration created with VAWTGen.

2.1.3. Model Formulation

The fundamental requirements of the aeroelastic analysis tool for offshore VAWTs necessitates a flexible framework capable of considering arbitrary configuration geometries, arbitrary loading scenarios, and the ability to interface with various modules that account for the interaction of the environment and power generation hardware with the turbine structure. The finite element method

provides a means to satisfy these general requirements. If a sufficiently robust element is developed, a mesh (collection of elements) of an arbitrary VAWT configuration may be constructed via a mesh generator. The ability to capture various couplings and provide an accurate representation of turbine behavior will depend on the robustness of the element formulation.

The finite element method requires boundary conditions to be imposed on the elements by specifying loads or displacements at discrete points (nodes) in the mesh. These boundary conditions provide a clear interface between aerodynamic and hydrodynamic modules that impart forces on the turbine. With boundary conditions specified, unspecified displacements and loads may be calculated. Next, displacement motions of the turbine and/or internal reaction forces may be provided to aerodynamic and hydrodynamic modules to calculate loads on the turbine. This gives rise to mutual causation because in reality loads and displacements are intricately connected. Iterative procedures and coupling methods that will be discussed in this chapter, however, allow for convergence to be reached, eliminating this issue for all practical purposes.

The subsections that follow will present basic formulation concepts including the equations of motion and considerations for modal and transient analysis. Subsequent sections will present a modular analysis framework, along with coupling strategies. Details of a mesh generator for VAWTs, and necessary features of a finite beam element formulation are also discussed.

2.1.4. Basic Formulation Concepts

Basic formulation concepts will be discussed before describing components of the proposed formulation in detail. As stated earlier, the finite element method will be employed for its robustness and flexibility. A robust element formulation will become the foundation of the aeroelastic analysis tool. Analysis of the dynamic response of the turbine is challenging because of rotating components. Because almost all structural components of the turbine will be rotating at some rotor speed (Ω), it is convenient to perform the formulation in a rotating reference frame. Such a frame is capable of capturing rotational effects, including centrifugal stiffening/softening and Coriolis effects in a straightforward manner.

2.1.5. Equations of Motion

Equations of motion for the platform are developed by treating the platform as a rigid body, whereas the turbine is treated as a rotating deformable body. Motions of discrete points on the turbine can be expressed as the sum of the turbine motion (deformation and rigid rotor rotation) and the platform motion (rigid). Expressions for the velocities of the platform and for an arbitrary point on the turbine are shown below:

$$\vec{V}_{platform} = \frac{^{(N)}d\vec{R}_{P/N}}{dt} = \dot{U}_1\hat{p}_1 + \dot{U}_2\hat{p}_2 + \dot{U}_3\hat{p}_3 \tag{1}$$

$$\vec{\omega}_{platform} = \omega_1\hat{p}_1 + \omega_2\hat{p}_2 + \omega_3\hat{p}_3 \tag{2}$$

$$\vec{v} = \vec{V}_{platform} + [(\vec{\omega}_{platform} + \Omega\hat{h}_3) \times \vec{r}] + \frac{^{(H)}d}{dt}\vec{r} \tag{3}$$

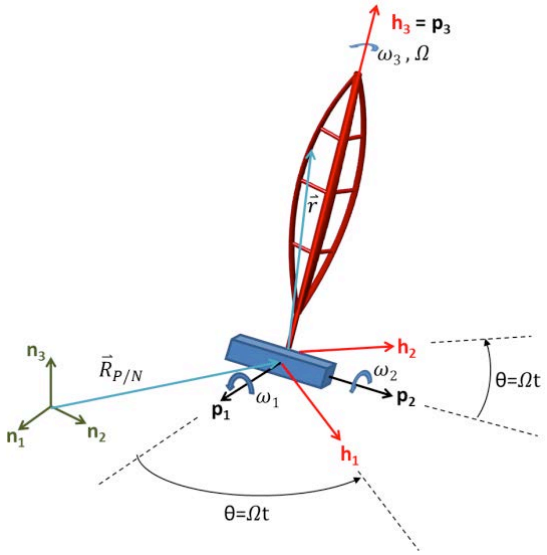

Figure 31. Illustration of frames, position vectors, and angular velocities.

Figure 31 presents an illustration of the frames, angular velocities, and positions vectors that will be described. Here, U_i represents the displacement components of the platform center of mass, and ω_i represents the angular velocity of the platform. The inertial frame is represented by the $\hat{n}_i$ coordinate axes, the platform frame is represented by the $\hat{p}_i$coordinate axes, and the rotating hub frame is represented by the $\hat{h}_i$ coordinate axes. The operators $\frac{^{(N)}d}{dt}$ and $\frac{^{(H)}d}{dt}$ define derivatives with respect to the inertial and hub frames respectively. The vector r_i defines the position of an arbitrary point on the turbine with respect to the hub frame origin. The expression for velocity of a particle in this floating frame is arrived at through use of the Transport Theorem (7). An offset between the platform frame origin and the hub-frame origin may be introduced through the vector $\vec{R}_{offset}$.The rigid nature of the platform enforces that $\dot{\vec{R}}_{offset}$.=0. Here an overdot represents the explicit time derivative of a quantity. Angular acceleration $\dot{\Omega}$ and $\dot{\omega}_i$ will become apparent when these velocities are used in conjunction with Hamilton's extended principle to formulate finite element equations of motion, but these details will not be elaborated on in this section. Hamilton's principle relates the variation of kinetic energy T and potential energy V, and virtual work of non-conservative forces W_{np} to formulate equations of motion. Hamilton's extended principle is written simply as:

$$\delta \int_{t_1}^{t_2} [T(t) - V(t)]dt + \int_{t_1}^{t_2} \delta W_{np} = 0 \tag{4}$$

The kinetic energy of the system may be written compactly as:

$$T_{system} = T_{platform} + T_{turbine} \tag{5}$$

$$T_{platform} = \frac{1}{2} M_{platform} \vec{V}_{platform}^{T} \vec{V}_{platform} + \frac{1}{2} \vec{\omega}_{platform}^{T} [J_{platform}] \vec{\omega}_{platform} \tag{6}$$

$$T_{turbine} = \frac{1}{2}\int_V \rho \vec{v} \cdot \vec{v}\, dV \tag{7}$$

The platform kinetic energy is decomposed into two parts, translational kinetic energy and rotational kinetic energy (where $M_{platform}$ and $[J_{platform}]$ are the platform mass and the moment of inertia tensor for the platform). The turbine (which will be represented by a collection of finite elements) kinetic energy is expressed in terms of the volume integral of the structural component density(ρ) at infinitesimal points and the velocity of the infinitesimal points in the turbine (as developed earlier).

Note that the quantities described above may be represented or ``coordinatized" in any frame. Indeed, some vectors were expressed in the inertial ($\hat{n}_i$) frame, and others in the rotating hub ($\hat{h}_i$) frame. Because the rotating turbine represents the bulk of the modeling effort, the implementation of the equations of motion will be coordinatized in the hub frame. Platform motions and forces, however, are likely to be described in the inertial frame. Therefore, transformations between the inertial and hub frame are performed where necessary.

The resulting equations of motion for a floating turbine structure will be of the following form (hyperbolic):

$$[M]\{\ddot{q}\} + [C]\{\dot{q}\} + [K]\{q\} = \{Q\} \tag{8}$$

$$\begin{bmatrix} M_{TT} & M_{TP} \\ M_{PT} & M_{PP} \end{bmatrix} \begin{Bmatrix} \ddot{q}_T \\ \ddot{q}_P \end{Bmatrix} + \begin{bmatrix} C_{TT} & C_{TP} \\ C_{PT} & C_{PP} \end{bmatrix} \begin{Bmatrix} \dot{q}_T \\ \dot{q}_P \end{Bmatrix} + \begin{bmatrix} K_{TT} & K_{TP} \\ K_{PT} & K_{PP} \end{bmatrix} \begin{Bmatrix} q_T \\ q_P \end{Bmatrix} = \begin{Bmatrix} Q_T \\ Q_P \end{Bmatrix} \tag{9}$$

Such that $M, C,$ and K represent the system mass, damping, and stiffness matrices respectively. The terms q_T and q_P denote the generalized displacements of the turbine and platform respectively. The terms Q_T and Q_P denote the generalized forces acting on the turbine and platform respectively. Terms with subscript “TT” denote influence of the turbine forces on the turbine response. Whereas, terms with subscript “TP” denote influence of turbine forces on the platform response, and terms with subscript “PT” denote influence of the platform forces on the turbine response. Finally, terms with subscript “PP” denote the influence of platform forces on the platform response. Although not explicitly shown here, the rotor angular velocity/acceleration and platform angular velocity/acceleration are incorporated in the turbine damping and stiffness matrices through gyroscopic effects. Effects related to translational acceleration of the hub-frame (due to platform rigid body motion) are manifested in the turbine force vector through body forces. These details are elaborated on in the finite element formulation presented in (6).

2.1.6. Finite Element Formulation and Implementation

To facilitate the aeroelastic analysis of a vertical axis wind turbine via a finite element approach, a three-dimensional Timoshenko beam element has been formulated. The beam is “three-dimensional” in the sense that it allows for deformations of the beam in all physical dimensions. Each node of the beam has three translational degrees of freedom and three rotational degrees of freedom. Retaining a torsional degree of freedom in the element allows passive aeroelastic tailoring concepts to be explored. Furthermore, the constitutive relations of the beam element have been developed in a manner that allows for coupling terms to be introduced for bend-twist and

extension-twist couplings that may arise due to cross-sectional geometry or composite material usage. The equations of motion are developed for a beam element of arbitrary orientation in a co-rotating (hub) frame. Thus, rotational effects of Coriolis and spin softening phenomenon are included in the formulation. This reference frame is allowed to translate to account for platform or foundation effects. These considerations allow for formulations with couplings between platform and element motions. The various reference frames used to describe the motion of a point in the structure are shown in Figure 31.

The ability for the element to have arbitrary orientation in the hub frame allows for complex VAWT configurations to be constructed using the VAWTGen mesh generator (discussed in a subsequent section). This also allows the investigation of passive aeroelastic couplings through swept configurations. Inherent in the beam formulation is that deformations of the elastic axis are being modeled. For proper dynamics modeling, mass center offsets from the elastic axis at each cross-section are introduced. The beam formulation also accounts for the ability to model concentrated masses and stiffness at any point along the element. Imposing concentrated masses allows for one to account for unsmooth mass distributions in the turbine, due to joints at tower/strut/blade connections or other hardware. Concentrated masses can also be used to model internal joints in a turbine blade that result in unsmooth mass distributions. Concentrated stiffness can model stiffness at component joints, or even at internal blade joints.

The beam formulation utilizes numerical integration to construct the element system matrices that will be assembled into a global system of equations. This allows flexibility in the shape functions that are used to describe the variation of a displacement along the length of an element. Simple linear shape functions can be used for piecewise representation of a structural component from many beam elements. Alternatively, more advanced shape functions can represent a structural component with a single beam element (comparable to an assumed modes approach, as utilized by National Renewable Energy Laboratory FAST dynamics code for HAWTs (4)). If one can construct mode shapes for the predominant motions of structural components (perhaps by performing finite element dynamics analysis on structural components with various boundary conditions), these mode shapes can be provided to the software implementation with relatively minimal changes to the core analysis framework. Alternatively, modal analysis may be utilized to create a custom, configuration specific reduced order structural model composed of a selected subset of system modes.

Geometric nonlinearities have been included in the beam element formulation to include von Kármán strains (8). Nonlinear strain relationships introduce a coupling between bending and extension of a beam and may be considered for small to moderate rotations. Future formulations of the beam element may consider large deformations of structures which may significantly alter load-displacement relationships. If necessary, more robust geometric nonlinearities can be included via a total or updated Lagrangian formulation (8) or using more advanced formulations such as Geometrically Exact Beam Theory (GEBT).

2.1.7. Modal and Transient Analysis

Modal analysis may be performed on the above turbine system of equations to examine the stability of the turbine configuration. The framework supports pre-stressed modal analysis by including stress stiffening effects (9). Such effects model the stiffening that occurs in a structure under load. Stress stiffening can be critical in the modal analysis of rotating structures to obtain appropriate predictions of system frequencies for a structure under rotational loads. Whereas understanding

the stability of a turbine to avoid potential resonance issues is critical, transient conditions such as rotor start-up, turbulent/unsteady winds, and unsteady waves require a transient analysis capability. Explicit time integration of the ordinary differential equations (ODEs) is convenient due to its simplicity and the availability of commercial ODE integrators. Unfortunately, explicit time integration typically requires the time domain to be highly discretized (small time steps). This concern is exacerbated by the high frequencies that can be present in the finite element representation of the turbine configuration. Therefore, implicit time integration methods have been considered for their ability to reduce time step restriction and maintain efficiency. The Newmark-β (10) method has been employed in the analysis framework. An energy-preserving implicit integration method for *Gyric* systems was also developed as part of this work (6).

2.1.8. Analysis Framework

The proposed analysis framework will allow a convenient coupling of the structural dynamics finite element analysis to aerodynamic, hydrodynamic/mooring/platform dynamics, and generator modules. Figure 32 shows an illustration for the framework of the Offshore Wind Energy Numerical Simulation (OWENS) toolkit indicating data flow among the analysis tool and various modules. In this figure, analysis components surrounded in the purple boxes are independent modules that will interface with the VAWT simulation tool. The proposed analysis tool will provide and receive data to and from these modules. The implementation of these modules, however, are “as is" and cannot be modified by the developer. Components outlined in the blue boxes are components of the analysis tool that are under direct development by the developer. Data flow is illustrated by various colored arrows. Orange arrows denote an internal data flow from one segment of OWENS analysis components to another. Red arrows denote flow of information from the core analysis tool to external modules. Green arrows represent flow of information from external modules to the core analysis tool components. Blue arrows denote the flow of information from one external module to another or external data to an external module.

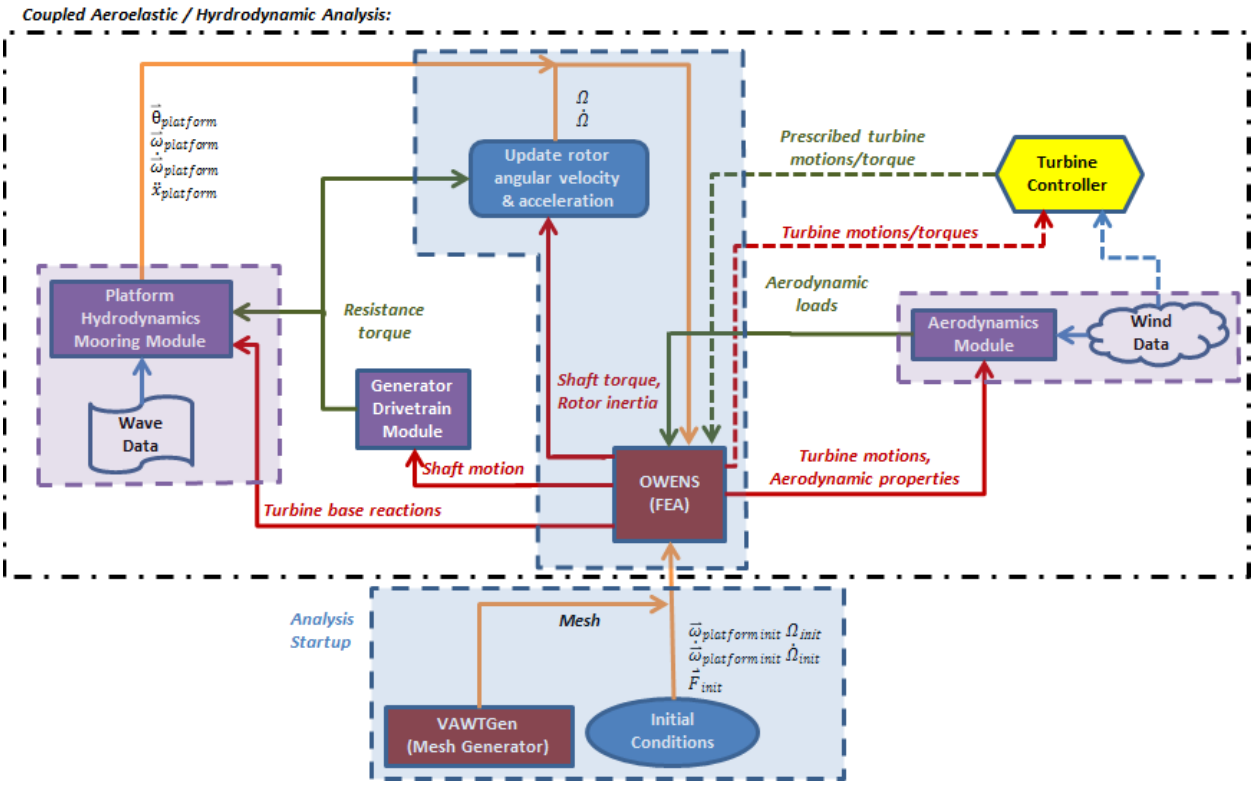

Figure 32. Analysis framework for the OWENS toolkit.

The proposed framework begins with start-up procedures. These include the creation of the VAWT configuration mesh using the mesh generator VAWTGen, and specification of initial conditions. VAWTGen produces a finite element mesh (a collection of beam elements and concentrated masses/springs) representative of the VAWT turbine. Initial conditions such as the initial forces acting on the turbine/platform, initial rotor angular velocity/acceleration, and initial platform angular velocity/acceleration must be provided. With these specifications complete, the coupled aeroelastic/hydrodynamic analysis begins, involving the components outlined in the black box.

The mesh and initial conditions are provided to the OWENS toolkit. By performing a transient analysis via the aforementioned time integration procedures, turbine and platform motions are calculated. The turbine motions along with aerodynamic properties of the turbine are provided to an aerodynamics module. Wind field data is also considered along with the motions to calculate aerodynamic loads on the turbine. The aerodynamic loads are provided back to the OWENS toolkit as boundary conditions for the next timestep or iteration.

The motion of the turbine shaft is provided to a generator/drive-train model, which considers the relative motions of the shaft and generator to calculate a resistance torque provided by the generator. By considering the resistance torque along with the shaft torque and rotor inertia, an updated rotor angular velocity/acceleration may be calculated.

Turbine base reactions are provided to the hydrodynamics/mooring/platform dynamics module. This serves as external forcing on the platform in addition to wave excitation and hydrodynamic/mooring restoring forces. Within the platform module, a dynamics solver predicts the rigid body motion (translation and rotation) of the floating platform and the rigid body motion

is returned to the structural dynamics solver. Translational acceleration, angular acceleration, and angular velocity of the platform are used to apply body forces to the flexible structure as well as update the rotational effects that are inherent in the finite element formulation system matrices. The attitude description of the platform is also used to perform coordinate transformations between the platform an inertial frames. This along with the transforms related to the rotor azimuth ensures that effects coordinatized in the inertial frame (such as gravity) are correctly applied to the rotating structure that is represented in the hub frame.

The above description fully outlines the proposed analysis framework and interface of the core analysis tool with various modules. In the development of this framework, a one-way coupling is inherent in that motions are typically provided to a module and loads are calculated and supplied back to the analysis tool. In reality such a clear flow of information does not exist, and the coupling is more complex with loads influencing motions in addition to the motions influencing loads. Therefore, at any given time step an iterative procedure will likely be considered to reach a convergence among the actual two-way coupling between the turbine structural dynamics and aerodynamics, hydrodynamics/platform dynamics, and generator dynamics. The framework can also account for a turbine controller algorithm, such as an applied breaking torque to control rotor speed.

As illustrated in Figure 32, the turbine controller accepts turbine motions, rotor speed/torque, or wind data and provides prescribed motions or braking torques. Details of the controller will be addressed in future development; however, consideration for a controller algorithm interface has been made in the development of the proposed framework. Details of various “internal modules” implemented into the analysis tool including rotor speed update, generator, and drive-shaft modules are discussed in Reference (6).

2.1.9. Coupling Strategies

The OWENS toolkit has been designed with ability to interface with arbitrary modules that provide forcing during a structural dynamics simulation. There are a number of ways to consider incorporating external forcing in the analysis framework. One approach, which has been termed “monolithic” (11) incorporates the solution for both the external loads and the structural responses into a single system of equations to be solved at each time step. Whereas this potentially allows for structural dynamics and loading calculations to be performed simultaneously, the modularity of the framework is severely limited. This approach requires all details of loading calculations be implemented alongside the structural dynamics code under a single framework. Furthermore, this approach potentially requires more overhead in code management and limits the ease of collaboration. A monolithic code not only requires developers to understand the details and implementation of particular external loading calculations, but also requires understanding the intricacies of the monolithic framework design and implementation. This can potentially limit code development and collaboration efforts. Therefore, a monolithic framework has not been considered for the OWENS toolkit.

Another approach considers “loose” coupling of modules and provides a greater degree of flexibility and modularity in the framework. The framework is no longer monolithic and knowledge of the details of the external modules is not required by the core analysis framework. Instead, only the data flow between the module and core analysis framework must be defined. This approach has been illustrated in Figure 32 for the OWENS toolkit. A specific example is that reaction force at the base of a turbine will be provided to a platform/hydrodynamics module that

calculates the rigid body motions (translational and rotational) of a floating platform under the influence of an attached, flexible turbine structure. The core analysis has no knowledge of the hydrodynamics calculations being performed and only requires the rigid body motions of the platform system to perform the coupled simulation.

The drawback of the loosely coupled approach is that analysis occurs in a staggered manner with motions/forces at previous time steps being utilized to calculate solutions at a current time step (see Figure 33). This can lead to potential stability concerns in the coupling procedure, and critical time step sizes must be considered to maintain a stable solution procedure. The stability limits of this approach are understood (12) and consequences of the inherent approximations in this approach can be eliminated for most partitioned systems with sufficiently small time steps.

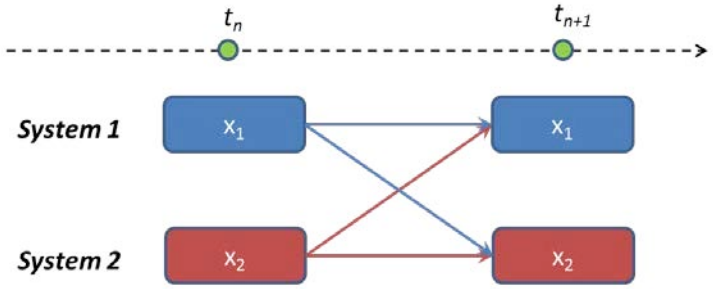

Figure 33. Illustration of the loose coupling approach.

An improvement over the loose coupling procedure considers an iteration at each time step, using a "predictor-corrector" approach. A popular approach is the Gauss-Seidel method (13). This approach is illustrated in Figure 34, in which a coupling of two sub-systems is considered. First, information from solutions established at a previous time is used to predict the solution of system 1. This is the "predictor" step of the method. Second, a substitution of the predicted system 1 solution is used to obtain a solution prediction for system 2. Third, a correction to the solution of system 1 is obtained by using the most current estimates. The second and third steps may be iterated until some convergence criterion between current predictions and previous predictions is met. Although this simple discussion considered only two systems, the Gauss-Seidel iterative method is applicable to a modular framework composed of an arbitrary number of systems, such as that in the OWENS analysis framework.

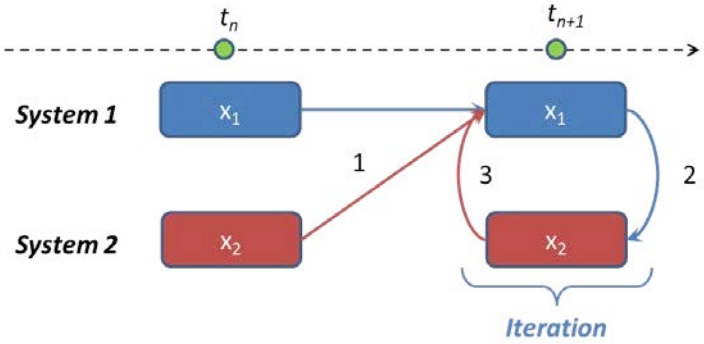

Figure 34. Illustration of Gauss-Seidel iterative coupling approach.

A drawback of the Gauss-Seidel iterative approach is that it requires more evaluations per time step. For k iterations, the approach will require $1 + nk$ sub-system evaluations where n is the number of sub-systems in the modular framework. Thus, the iterative approach comes at greater computational cost per time step compared to a loose coupled approach. Nevertheless, stability and accuracy concerns can exist for a loose coupled methodology. As will be shown, the Gauss-Seidel approach can relax stability concerns (allowing a larger time step size) and can allow for a more accurate solution. Such benefits can outweigh the increased computational cost per time step associated with the Gauss-Seidel approach. These concepts are demonstrated with a simple 2-degrees-of-freedom, partitioned system analogous to a turbine on a floating platform in Reference (6).

To facilitate data flow between software modules, network sockets have been employed in the aforementioned analysis framework. This approach allows data packets to be sent across a network connection between a server and client. These data packets are constructed by a server, sent via a socket connection, and received by a client for processing. Although originally intended to provide a means of data flow between two computers on a network (e.g. to permit collaboration in code coupling among partners in this project), this approach can also be used internally on a single computer (e.g. for analysis and development). The ports on a computer's network card allow clients and servers to be initialized between various applications. This allows for convenient and efficient data flow between various applications such as the core analysis capability and external modules. Indeed, the analysis framework is treated as a network with the core analysis application and external modules being equivalent to servers and clients on a network.

An external module is truly treated as a “black box” in this approach just as the details of a computer on a network need not be known to send and receive information. The defined input and output between these modules is accounted for in the format of the data packets being sent across the network. Thus, only the data packet format needs to be defined as well as a general framework for the interaction of an external module with the core analysis capability. With these defined, development of the core analysis framework and external modules may be made at the discretion of the independent developers. Figure 35 shows this proposed framework for providing a general socket interface between a core analysis software and an external module.

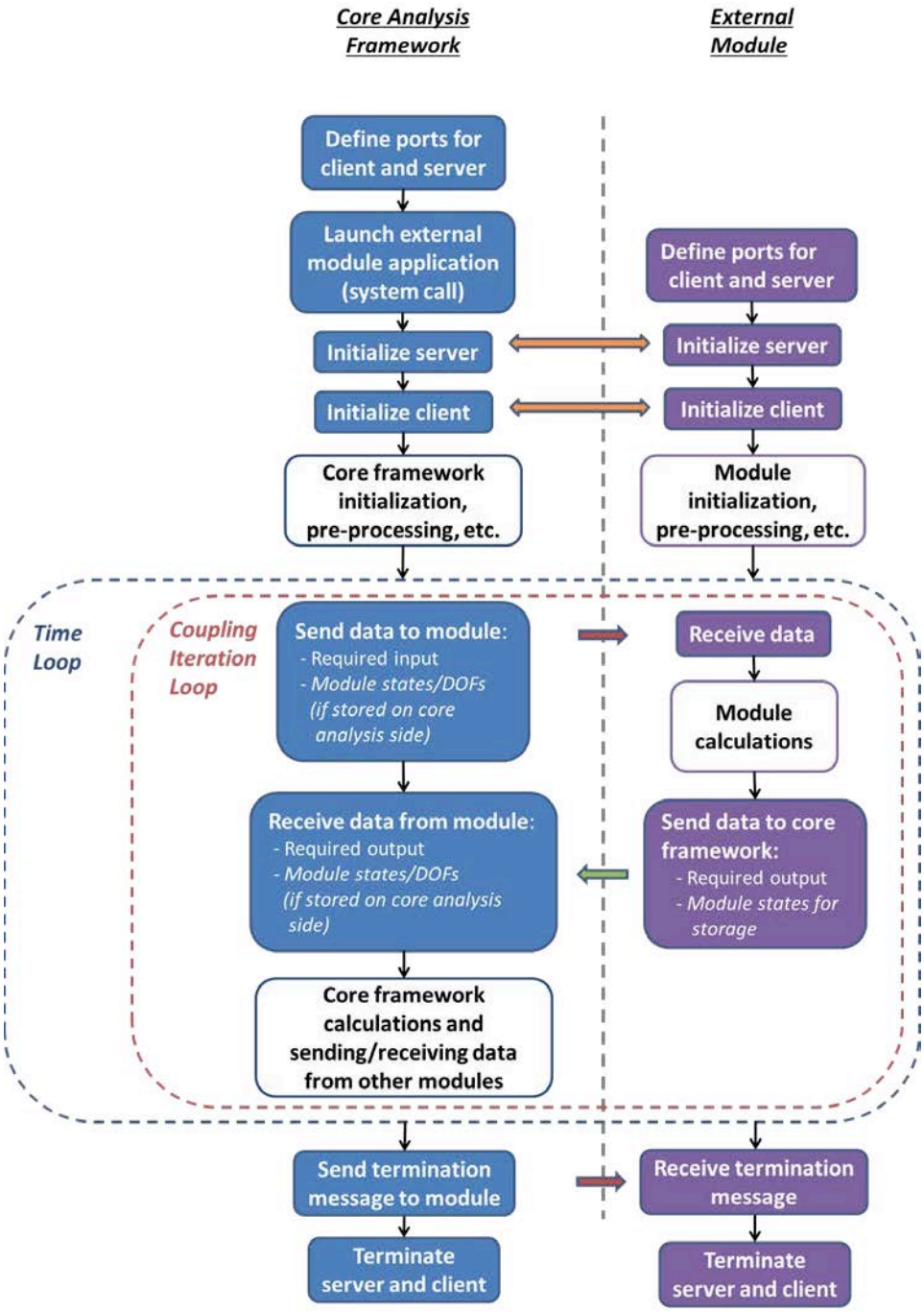

Figure 35. General framework for network socket interface of core analysis code to an external module.

The core analysis framework begins by defining ports for the client and server on the core analysis side. These port numbers will correspond to the server and client on the external module software and may be specified by an input file for each software application. The core analysis software can then launch the external module software application using a system call. After which, server and client initialization occurs within the core analysis software as well as within the external module software. At this point, a connection is created between the two applications, allowing a two-way

flow of data as required by the modular analysis framework. After connections are made, each software application can perform any required initialization, pre-processing, or start-up procedures. Next, the time step loop begins in the core analysis software. Required input is sent to the module, the module receives this data, and performs calculations before sending the required output back to the core analysis framework. The core analysis framework can then perform calculations or send/receive data to/from other modules as necessary. As discussed in the previous section, at each time step an iteration to converge the coupling between the two modules may occur. The segments of the framework shown in Figure 35 contained in the red dashed box may be repeated until convergence is reached. After this, the next time step may be considered performing the steps contained in the blue dashed box. At the end of the time step loop the coupled analysis is completed, and the core analysis module sends a termination message to the external module that prompts the end of analysis and termination of the external module client and server. The core analysis software client and server are also terminated.

2.1.10. Potential Future Development

The OWENS toolkit and VAWTGen have been developed with a great degree of flexibility to meet the desired features of an offshore VAWT design tool and to be adaptable to future analysis needs. The structural dynamics formulation and finite element implementation have been verified via a number of verification procedures and validated using experimental data from the Sandia 34-meter VAWT (see Figure 36). Structural dynamics verification and validation exercises are detailed in Reference (6). Further verification and validation can be examined as future verification/validation datasets are identified. Future enhancements to the structural dynamics formulation may be performed as necessary to meet future analysis needs. Although the existing structural dynamics formulation in OWENS are believed to be adequate for initial design studies, more advanced structural theories such as Geometrically Exact Beam Theory (GEBT) may be considered if required in future development work.

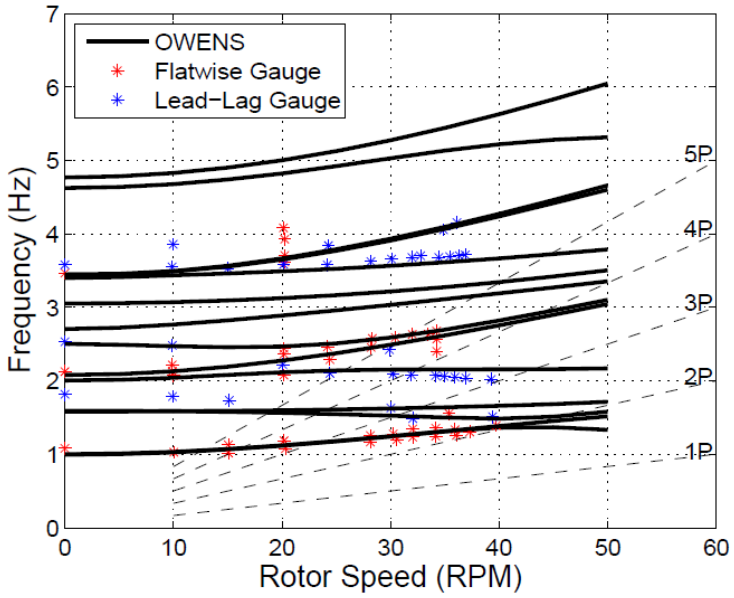

Figure 36. Campbell diagrams for 34-m VAWT (Predicted and Measured).

The analysis framework and coupling schemes described in this section provide a general means of coupling to external modules such as aerodynamics, and hydrodynamics/platform dynamics software. Practical implementation of the interface between the structural dynamics analysis capability and external modules has been accomplished via network sockets. The modular framework, coupling schemes, and software interfaces have been exercised successfully between OWENS and a platform dynamics module described in the next section. Baseline verification procedures for this coupling are also presented in a subsequent section and described in Reference (6). A one-way coupling of the CACTUS aerodynamics software has been implemented, and future work could extend to a two-way coupling between OWENS and CACTUS. Interfaces to general drivetrain and generator modules have also been developed and are presented in Reference (6). The envisioned VAWT designs do not currently make use of prescribed motion of VAWT components. The flexibility of the analysis framework, however, can support this capability in future development efforts. Similarly, although turbine controller algorithms have not been considered for the current VAWT designs, the flexibility of the analysis framework can support future development of this capability.

The mesh generator VAWTGen has been developed with a high level of generality with the capability to model arbitrary VAWT configurations. The software has performed well with a high degree of flexibility in considering various VAWT configuration geometries. VAWTGen can be developed on an "as-needed" basis if limitations are identified as future VAWT configurations are considered.

2.2. SNL CACTUS Aerodynamics Software

The Code for Axial and Cross-flow TUrbine Simulation (CACTUS) is an aerodynamic design code capable of performing analysis of VAWT rotors of arbitrary geometry. Within CACTUS, the rotor blades are modeled as distributed line vortices, or "lifting lines," discretized into a number of blade elements. At each time step, the blade elements generate a vortex lattice system consisting of trailed and shed vortex line segments, shown in Figure 37. The strength of the vortex elements in the wake is determined by the loading on the blade elements. The vortex elements are free to convect under the influence of the free-stream wind velocity and the velocity field induced by the vortex elements themselves. Blade loads are determined using airfoil look-up tables, modified by an unsteady aerodynamic model that includes dynamic stall effects when blade element angles of attack become large. A model for strut drag is also included; for "deep struts," where the strut extends to an appreciable fraction of the maximum rotor radius, strut drag can significantly reduce aerodynamic performance at high tip-speed ratios. More details on the CACTUS code can be found in (14).

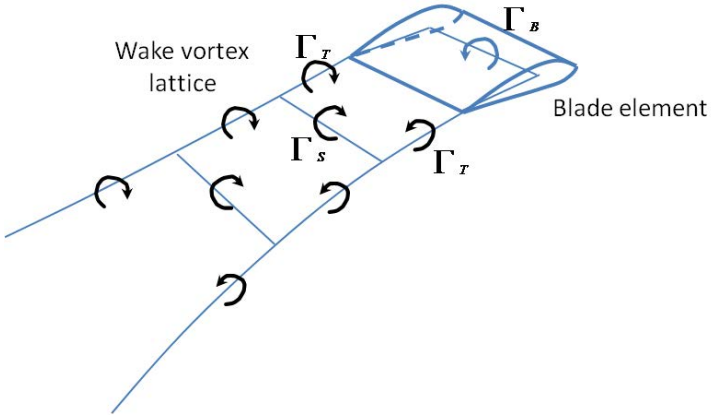

Figure 37. CACTUS blade element with associated vortex lattice system.

Within CACTUS, the influence of each vortex element on every other vortex element must be calculated in order to update the vortex field. This operation can become computationally demanding as the simulation progresses, since more vortex elements are generated at each time step. This has traditionally limited the application of free-wake codes in a design setting. However, we have found that a single CACTUS run executes within seconds to several minutes on a workstation, depending on the tip-speed-ratio specified in the calculation. We have also been able to execute simultaneous CACTUS runs on many compute cores using Sandia's high-performance computing clusters. This has enabled the use of CACTUS in a design setting for the present project.

Most of the development of CACTUS was supported by the DOE Water Power Program. As part of that effort, a number of verification and validation calculations were performed, including models of legacy VAWT machines. Here, we present calculations that were carried out for the SNL 34 meter testbed machine (Figure 38). This was a 500 kW VAWT with a two-bladed, Darrieus rotor, for which power performance data were collected. Figure 39 shows comparisons of the measured and predicted power curves for three different rotational speeds (note: advance ratio is the inverse of the tip-speed ratio). The CACTUS predictions are in good agreement with the measured data; in particular, onset of rotor stall and maximum power are well-predicted, a challenging but important feature of stall-regulated VAWTs. The ability of CACTUS to predict performance of cantilevered-blade designs was tested by performing calculations of the performance of the VAWT 850 rotor, a 500 kW H-VAWT that was developed in the UK (Figure 40). Figure 41 shows good agreement between CACTUS predictions and published data for this machine at 13.6 RPM. In this case, including the model for strut drag is essential for obtaining good predictions of power.

Figure 38. The Sandia 34 meter VAWT Testbed.

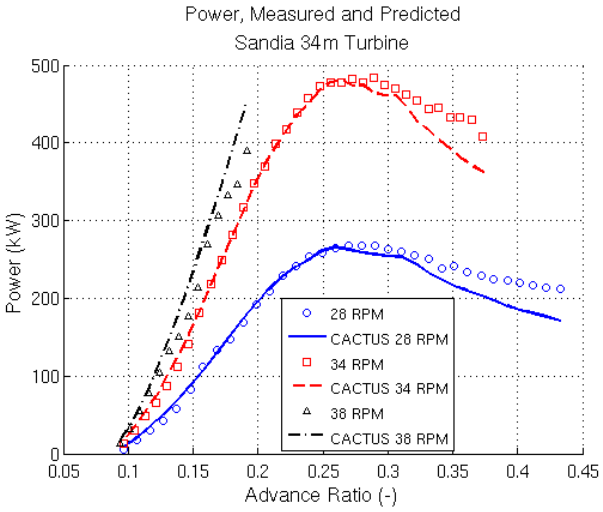

Figure 39. Measured and predicted power performance for the Sandia 34m Testbed VAWT.

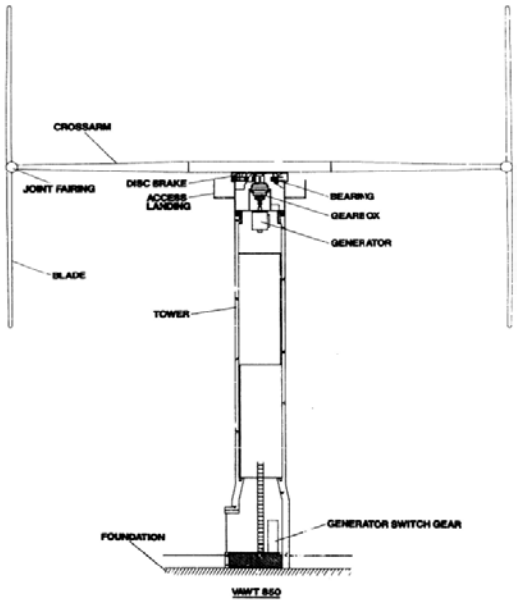

Figure 40. Schematic of the VAWT 850 Turbine.

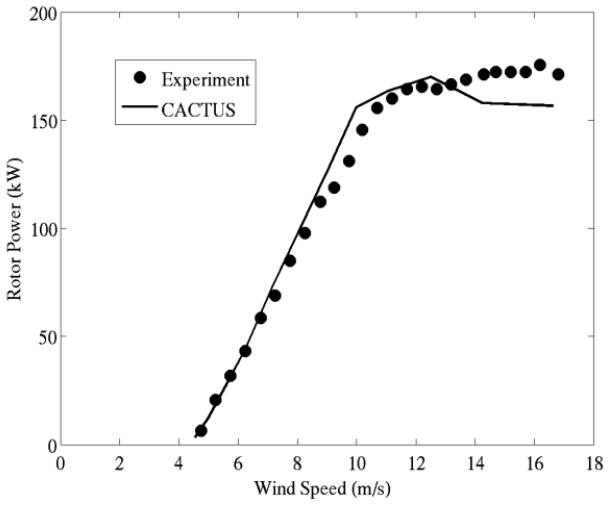

Figure 41. Measured and predicted power curve for the VAWT 850.

2.3. TU-Delft Hybrid Aerodynamics Software

The aerodynamics of vertical-axis wind turbines are governed by complex fluid mechanical phenomena that are difficult to model. These include two-dimensional and three-dimensional dynamic stall, blade-vortex interaction, and instability and mixing of an unsteady, turbulent wake. Inability to accurately predict the details of aerodynamic loading in VAWTs was often highlighted as a fundamental issue that limited development of the technology (15). Without accurate unsteady aerodynamic models, rotor loads, energy capture, and prediction of stall-regulation of power will not be well predicted leading to large uncertainties in aero-structural performance and levelized cost-of-energy.

Currently available aerodynamic design tools, such as CACTUS, are able to reasonably predict energy capture and blade loads. However, for novel designs and certain operating conditions, these predictions can be uncertain, with little information available to reduce the uncertainty. There is, therefore, a need for a higher-fidelity aerodynamic analysis tool that provides accurate aerodynamic predictions involving fewer modeling assumptions. Such a code would then be used for several purposes: to validate the lower-fidelity design codes; to perform point simulations of new designs to understand the aerodynamic phenomena governing their performance; and to provide data for model calibration and improvement within the lower-fidelity design codes. An analysis code based on a Computational Fluid Dynamics (CFD) approach would provide such a capability. There is an additional requirement, however, that the high-fidelity analysis tool be computationally efficient, providing useful turnaround times measured in hours and not in days.

Currently, traditional Eulerian CFD solvers[*] are very efficient in accurately resolving the flow near solid boundaries. On the other hand, Eulerian solvers tend to be diffusive and dampen high-intensity vortical structures, such as VAWT wake vortices, after a short distance away from the boundary. The use of high order numerical methods and fine grids, although alleviating this problem, gives rise to large systems of equations that are expensive to solve.

Lagrangian solvers, for instance vortex particle methods, have been shown to eliminate (in practice) the diffusion in the wake. As a drawback, the modeling of solid boundaries is less accurate and much more complex and costly than with Eulerian solvers (due to the isotropy of the Lagrangian computational elements and the strong anisotropy of the flow).

Given the drawbacks and advantages of both the Eulerian and Lagrangian solvers the combination of both methods, giving rise to a hybrid CFD solver, is advantageous.

The main idea behind the hybrid solver being developed is the following. In a region close to solid boundaries the flow is solved with a grid-based solver, where the full Navier-Stokes equations are solved (possibly with an arbitrary turbulence model or DNS, the limitations being the computational power and the physical properties of the flow). Outside of that region the flow is solved with a vortex particle method. See Figure 42 for a depiction of the hybrid approach.

[*] An Eulerian solver solves the governing equations on a grid that is fixed in space, while a Lagrangian solver utilizes computational elements that move with the flow.

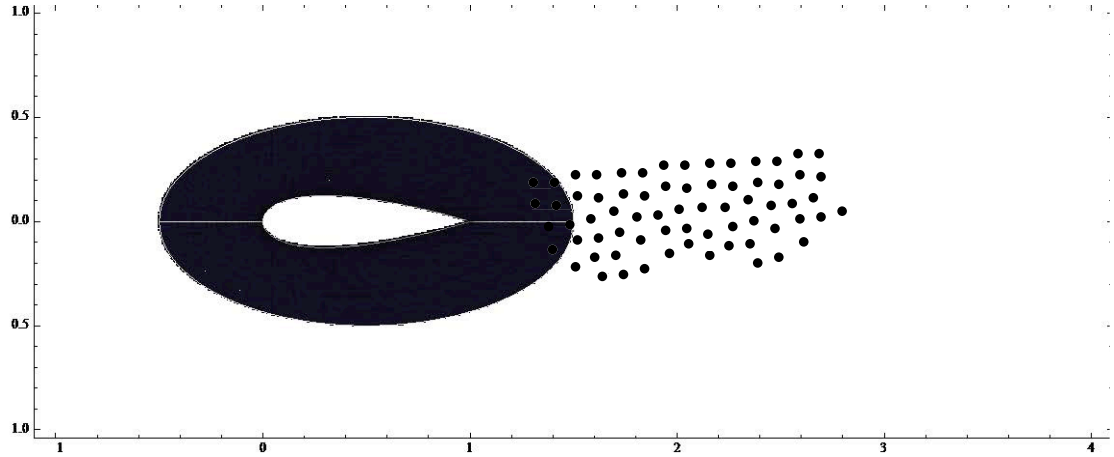

Figure 42. Conceptual diagram of the hybrid method. Close to the solid boundaries a grid solver (Eulerian) is used. In the wake a vortex particle solver (Lagrangian) is used.

The main focus of the coupling between the Eulerian and the Lagrangian solvers, as in any domain decomposition approach lies in:

1) Ensuring consistent boundary conditions in each subdomain;
2) Accurately transferring information between each subdomain.

Two main approaches exist to couple the two subdomains. One (not followed here) is presented in (16) and is based on classical domain decomposition techniques for partially overlapping subdomains, the Schwarz alternating method, where the boundary conditions of each subdomain are iterated. The second (followed here) is based upon the work of Daeninck (17). In this approach, instead of iterating the solutions, the Eulerian solution is used to correct the circulation of the particles that overlap the Eulerian subdomain. In this way, a gain in speed is attained since successive iterative solves of both methods are avoided. The Eulerian solver functions as a correction for the unresolved vortex particle solver close to the solid boundary.

2.3.1. Vortex Particle Solver (Lagrangian solver)

The vortex particle method currently being developed is a regularized vortex particle method, which means that particles have a finite size and the vorticity distribution associated to each particle is bounded. This implies that the particles need to cover the support of the vorticity. The distribution of particles is then used to compute induced velocities at the center of the particles in order to advance them in time. To ensure that the particles always cover the support of the vorticity, the particles need to be redistributed onto a regular grid. This is done with standard M'4 interpolation kernels (smooth 4th order interpolation, kernel of 4 particles for 1d, 16 particles for 2d and 64 particles for 3d). For viscous effects, the method presented in (18) is used. This method is faster than standard Particle Strength Exchange (PSE) methods since we can accomplish both re-gridding and diffusion in one step.

For the computation of the induced velocities, a fast multipole (FMM) solver optimized for Graphical Processing Units (GPUs) is being used. This approach reduces the computational cost of the problem from $O(N^2)$ to $O(N \log(N))$, where N is the number of particles, enabling the computation of simulations with several millions of particles. Future efforts will be focused on the extension of the implementation of this algorithm to a Message Passing Interface (MPI)

architecture, allowing for the computation with several GPUs. This will largely increase the computational capabilities of the solver.

2.3.2. Grid Solver (Eulerian solver)

As discussed previously, for the solution of the flow close to solid boundaries a grid solver where the Navier-Stokes equations are to be solved is employed. One of the main concerns is to implement this solver in such a way that changing the actual solver should not imply a restructuring of the whole hybrid code. Different Navier-Stokes grid solvers should be usable, the only requirements resting on the inputs and outputs of the solver.

Currently we have opted to use the FEniCS project, (19), which is a package for the automated solution of systems of partial differential equations by arbitrary order finite element methods. This project is currently being developed by Simula Research Laboratory, University of Cambridge, University of Chicago, Baylor University, KTH Royal Institute of Technology with contributions from Chalmers University of Technology, Argonne National Laboratory and Delft University of Technology. This package has several Navier-Stokes implementations including a G2 (General Galerkin) adaptive stabilized finite element discretization.

The current choice of Eulerian solver is not restrictive. One of the main design objectives of the hybrid solver is modularity. Therefore exchanging one module by another one is possible without much work, the only requirement being the construction of the interface classes. Currently, work is being done to also use OpenFoam in order to compare both grid solvers, since one is based on finite elements and the other on finite volumes.

2.3.3. Test Cases

In order to assess the performance of the hybrid solver implemented, a set of test cases has been performed and their comparison to a single Eulerian solver solution has been made. The test cases presented are:

1) Vortex dipole without solid boundaries
2) Vortex dipole with solid boundaries
3) Circular cylinder

2.3.3.1. Vortex dipole without solid boundaries

The first test case that has been simulated was the advection of a dipole without solid boundaries. This test case was run using a pure Eulerian simulation and compared to the results reported in the literature, showing a perfect agreement with them. These results are considered the benchmark results and the ones to which all other results are compared to.

The same case has been run for a pure Lagrangian simulation (for the four cases of 150 and 300 vortex blobs per unit length and 0.5 and 1.0 of overlap ratio). The same case has been run for a Hybrid simulation (for the four cases of 150 and 300 vortex blobs per unit length and 0.5 and 1.0 of overlap ratio). For the Hybrid case, a small Eulerian domain has been placed in the trajectory of the dipole, as in Figure 43, in order to study the transfer of information from the Lagrangian to the Eulerian domain and vice-versa.

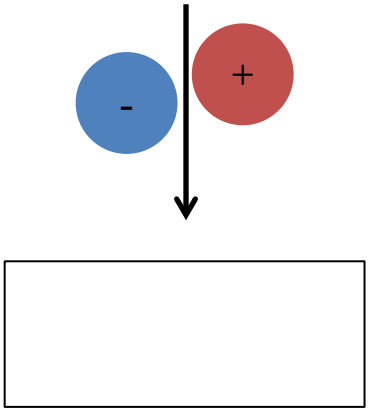

Figure 43. Schematics representing the passage of the dipole vortex by the Eulerian domain in the Hybrid method.

The results of all simulations have been compared. In Figure 44, the contour plots for the simulations with the pure Eulerian method, pure Lagrangian method and Hybrid method are shown after the dipole has completely crossed the Eulerian domain. As can be seen, the resolution of the Lagrangian domain, although not playing such an important role in the pure Lagrangian case, is fundamental in the Hybrid case. When the resolution between the Eulerian and the Lagrangian domains is matched, the Hybrid code gives very close results to both pure solvers. In Figure 45 and Figure 46, the L2 norm of the solution errors for both the velocity field and the vorticity are presented as a function of time. Once more it is possible to see that in the Hybrid case the resolution of the Lagrangian domain plays a fundamental role in the minimization of the error.

As can be seen, the pure Lagrangian simulation requires a smaller density of particles than the Hybrid simulation to achieve a comparable result to the pure Eulerian one. This poses a restriction on the density of particles on the overlap region between the Eulerian and the Lagrangian domains and increases the computational cost of the Lagrangian solver. For this reason it is fundamental to implement an adaptive Lagrangian solver where different densities of particles are used in different regions of the domain. This is one of the current focuses of the research.

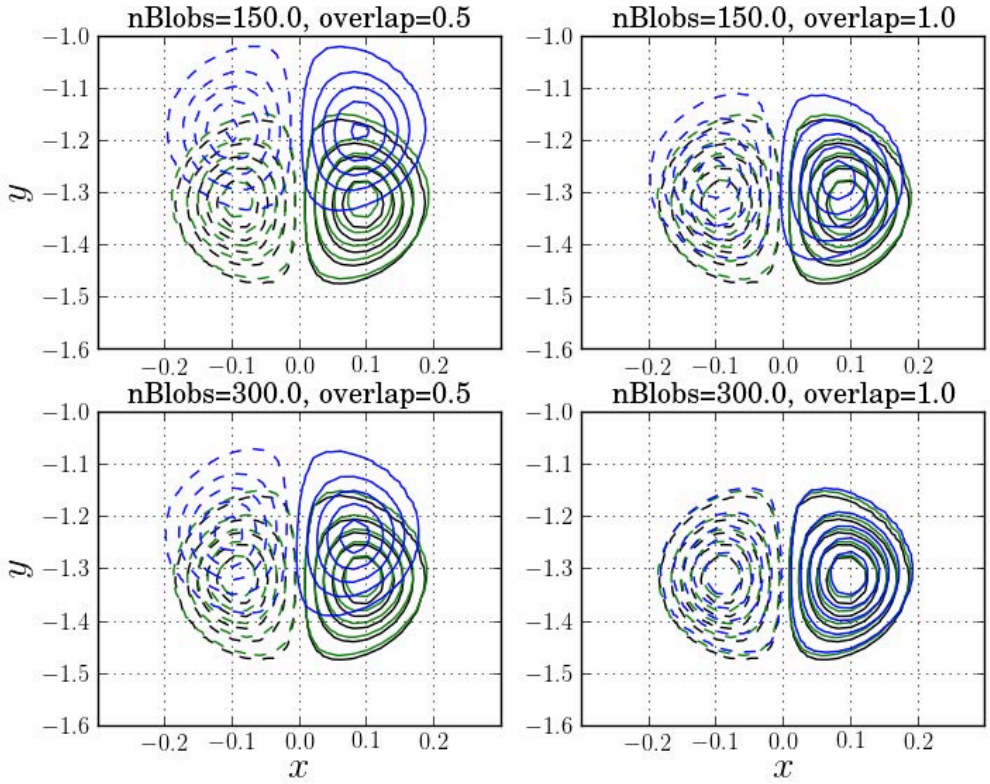

Figure 44. Comparison of vorticity contours for the pure Eulerian solution (black), pure Lagrangian solution (green) and Hybrid solution (blue), for different number of blobs and overlap ratios.

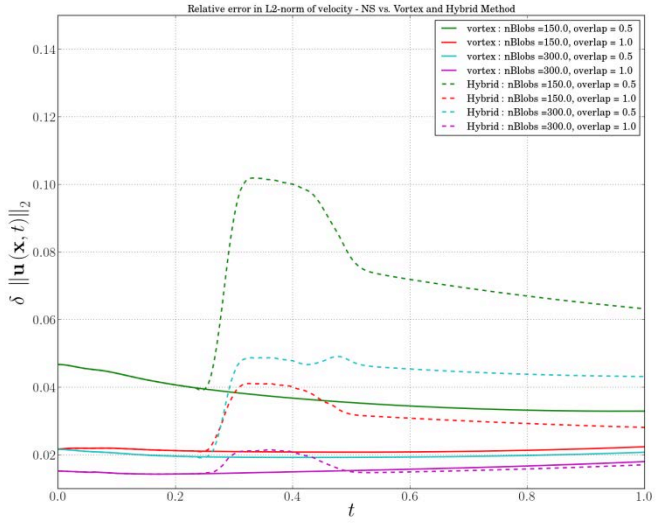

Figure 45. L2 norm error of the velocity between the pure Eulerian solution and the Hybrid solution for different number of blobs and overlap ratios.

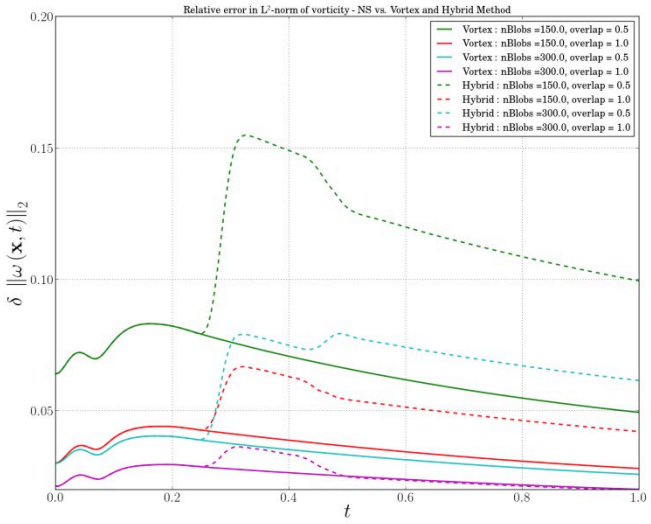

Figure 46. L2 norm error of the vorticity between the pure Eulerian solution and the Hybrid solution for different number of blobs and overlap ratios.

2.3.3.2. Vortex dipole with solid boundaries

The second test case that has been simulated with the Hybrid code was the advection of a dipole with solid boundaries. This test case was run using a pure Eulerian simulation and compared to the results reported in the literature, showing a perfect agreement with them. These results are considered the benchmark results and the ones to which all other results are compared to.

The same case has been run for the Hybrid case (with 300 vortex blobs per unit length and an overlap of 1.0). In this case, as intended, a thin domain surrounding the solid boundaries is meshed with an Eulerian domain, as in Figure 47, in order to study the transfer of information from the Lagrangian to the Eulerian domain and vice-versa.

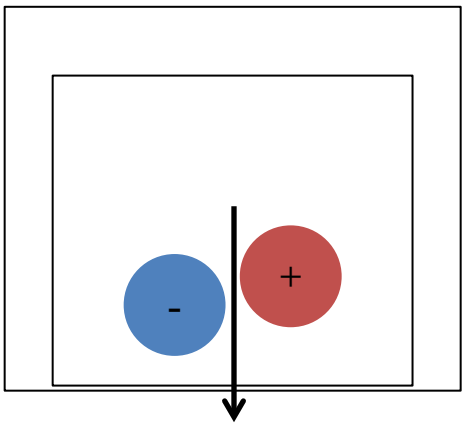

Figure 47. Schematics representing the passage of the dipole vortex by the Eulerian domain in the Hybrid method.

The results of all simulations have been compared. In Figure 48 it is possible to see the superposition of the contour plots of the pure Eulerian solution and the Hybrid solution. As can be seen, the two solutions are in good agreement.

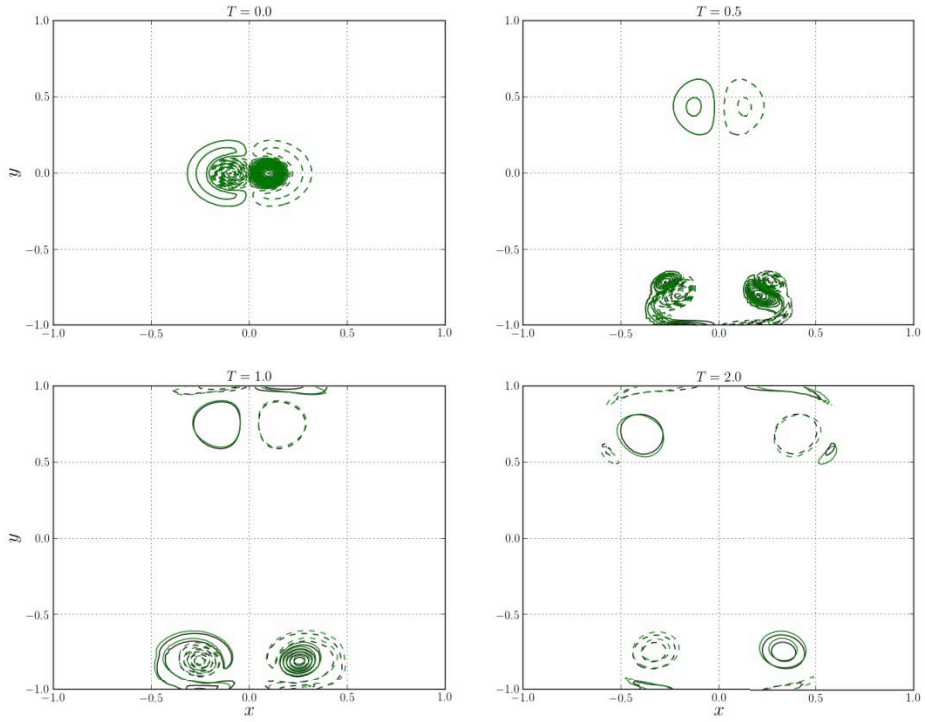

Figure 48. Comparison of vorticity contours for the pure Eulerian solution (black) and Hybrid solution (green), for different time instants (before and after the collision with the wall).

2.3.3.3. Circular cylinder

The final test case performed was the circular cylinder one. In this standard test case, we simulate the flow around a circular cylinder at a Reynolds number of 500.

As can be seen from Figure 49, Figure 50 and Figure 51, the flow solutions in both domains match very well and there is a smooth transition between both domains. Moreover it is possible to observe one of the properties of the Lagrangian solver which is of great advantage: automatic adaptivity. Particles exist where flow structures occur, improving the performance of the solver when compared to the pure Eulerian method.

Nevertheless, as was reported previously, due to the restrictions on the density of particles in the overlap region, the number of particles quickly grows in time, leading to unmanageable numbers of particles (above six million). A solution to this is to implement an adaptive Lagrangian solver where smaller particles (larger density of particles) are placed in the overlap region whereas larger particles (smaller density of particles) are placed in the wake. This is currently being implemented and it will greatly improve the efficiency of the solver.

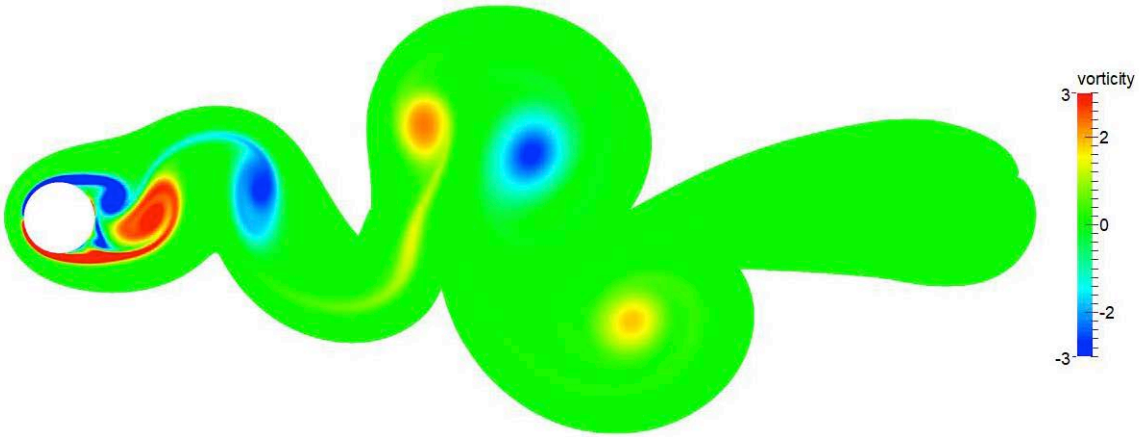

Figure 49. Snapshot of the pure Eulerian solution.

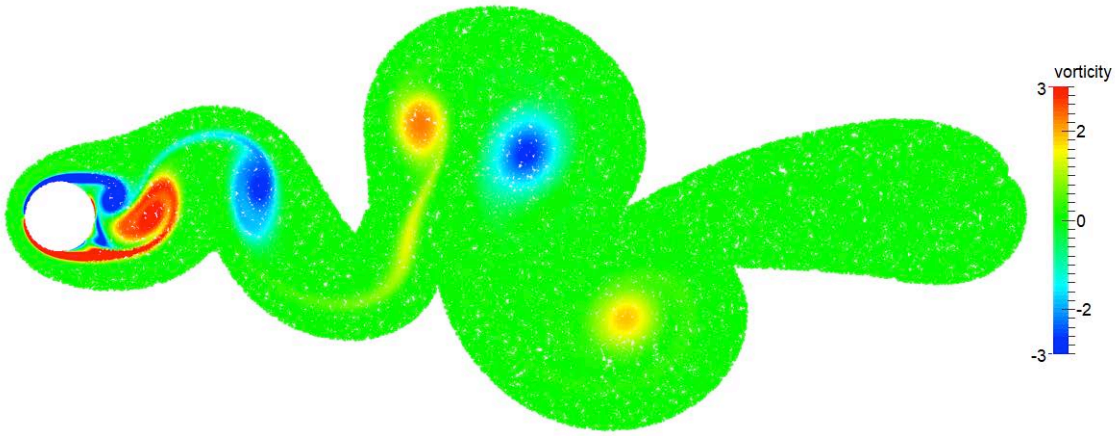

Figure 50. Snapshot of solution of the Hybrid solver with Eulerian solution in the vicinity of the cylinder and vortex particles in the wake (several particles have been hidden in order to better visualize the two regions).

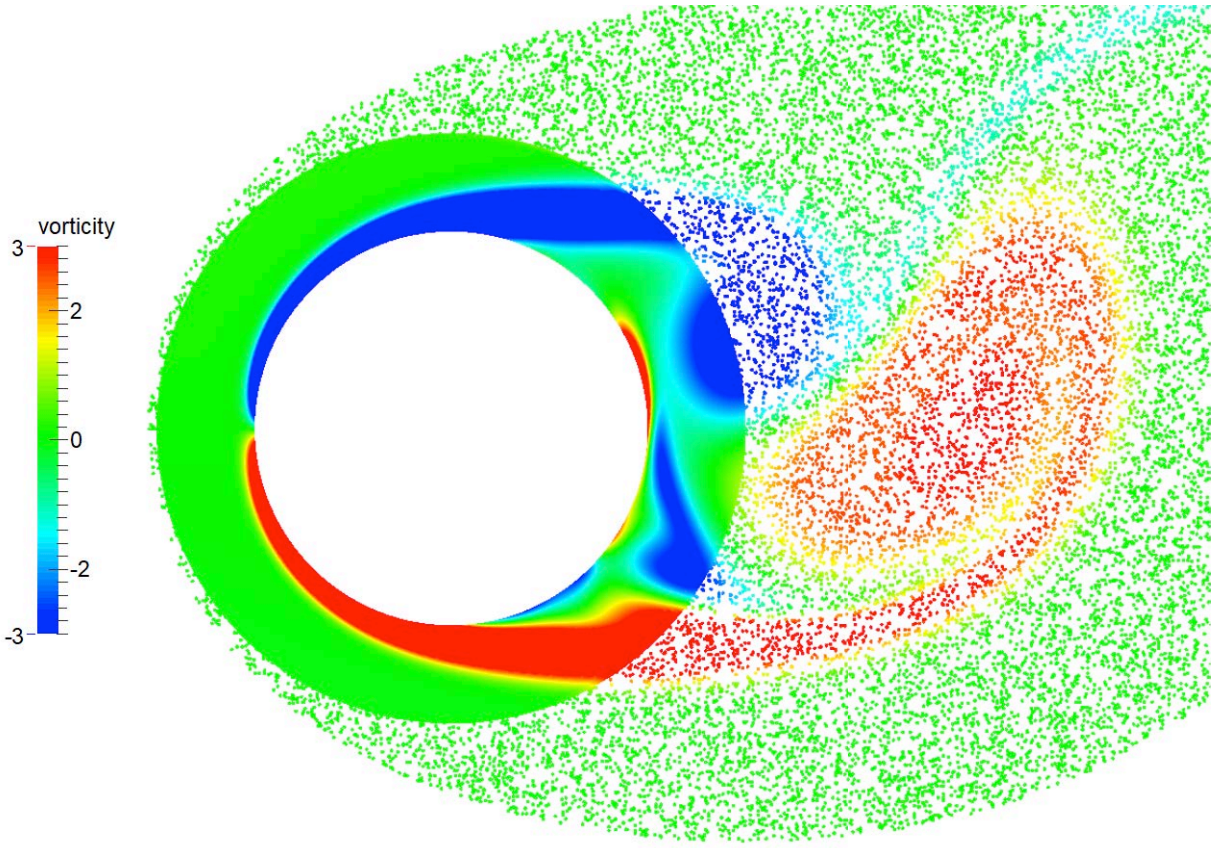

Figure 51. Detail of the interface region between the Eulerian and the Lagrangian solvers. Some particles have been hidden to better visualize the particles.

2.3.4. Summary of Hybrid Aerodynamics Software

A hybrid CFD/vortex particle method has been formulated and the initial implementation and verification studies are complete and have been presented here. A key issue that affects computational performance is the required density of the particles. It has been found that an adaptive Lagrangian solver is necessary to fully realize the benefits of the hybrid approach. Current work includes implementing the adaptive approach as well as testing and validation on a two-dimensional airfoil problem. Following successful completion of this effort, the hybrid code will be ready to apply to VAWT geometries as a high-fidelity aerodynamic analysis code.

2.4. Coupling to WavEC Hydrodynamic and Platform Dynamics

This section presents an overview of the theory of the WavEC hydrodynamics and platform dynamics software as well as a demonstration of coupling between OWENS and WavEC.

2.4.1. WavEC Hydrodynamics and Platform Dynamics Software

For a floating VAWT, the overall system dynamics are significantly influenced by the interaction of the platform with the aquatic environment. To properly capture this interaction it is necessary to incorporate a hydrodynamic analysis code into the OWENS toolkit. With the goal to develop an open-source and modular toolkit, WaveEC2Wire was used as the hydrodynamic module for this study. WaveEC2Wire is a MATLAB-based numerical tool developed by Marco Alves at the Wave Energy Center for the analysis of wave energy converters (WECs) (20). In order to interface with OWENS, WaveEC2Wire has been modified and restructured such that it functions as the platform hydrodynamics/mooring module shown in Figure 32. Additionally, to use WaveEC2Wire, results from a 3D radiation-diffraction analysis are required for many of the analysis steps. In this study WAMIT was used but any capable analysis code is acceptable.

As the hydrodynamic module of OWENS, WavEC2Wire calculates the platform dynamics of the floating VAWT. This is done by applying Newton's second law and equating the body inertial force with the forces acting on the device (Eq. (10)).

$$M\ddot{\xi} = F_{pe}(t) + F_{pto}(t) + F_m(t) + F_f(t) + F_{app}(t) \tag{10}$$

where M is the platform inertia matrix, $\ddot{\xi}$ the platform accelerations, F_{pe} are forces due to pressure differences on the rigid body platform (i.e. purely wave-structure interaction forces), F_{pto} are forces from the power take-off conversion chain (PTO) which interact with the structure to produce electrical power, F_m are mooring forces, F_f are friction forces, and F_{app} are user defined applied forces. For use with OWENS, the PTO terms are removed and F_{app} is defined as the VAWT tower reaction forces which are provided from OWENS through the coupling interface. WaveEC2Wire implements a rigid body assumption for the platform and retains only DOF relating to rigid body motion. This is consistent with other analysis codes (21) and considered adequate as the turbine tower is significantly more flexible than the platform, rendering platform deformations negligible. The user defines the active DOF (e.g. surge, sway, heave, roll, pitch, yaw) to be considered in the analysis.

WaveEC2Wire utilizes a fully linear approach to determine the wave-structure interaction forces. For offshore platforms in operating conditions, meaning non-storm sea states with low- to medium-amplitude waves, the linear assumption holds true and is consistent with other platform analysis codes (21). Utilizing the linear assumption, the complex amplitudes of the hydrodynamic diffraction (wave excitation) and radiation forces are determined due to a unitary amplitude incident wave as a function of frequency using a 3D radiation-diffraction solver (WAMIT (22)). The excitation complex amplitude is then applied to the wave time history for the desired incident environment to obtain the excitation force time history. WaveEC2Wire can calculate wave time histories for definitions of regular waves, JONSWAP or Pierson-Moskowitz spectrums (directional or non-directional), and sea wave measurements.

The radiation force is calculated using a state-space approach and is represented by a small number of first order linear differential equations with constant coefficients. This approach uses the

frequency dependent added mass and damping coefficients as well as the infinite added mass computed from WAMIT to calculate the frequency dependent radiation transfer function K(ω), (Eq. (11)).

$$K(\omega) = \frac{2}{\pi}\int_0^\infty K(t)e^{-i\omega t}dt = B(\omega) + i\omega[A(\omega) - A_\infty] \tag{11}$$

Then, a parametric model of the transfer function is calculated using the least squares method. This model is computed in the frequency domain to eliminate additional errors introduced in calculation of the impulse response functions. For each convolution in the convolution integral, a state-space representation is created using Eq. (12). These states are used in the global state space system defined later.

$$y = \int_0^t K(t-\tau)\dot{\xi}(\tau)dt \cong \begin{vmatrix} \dot{x} = Ax(t) + B\dot{\xi}(t) \\ y = Cx(t) \end{vmatrix} \tag{12}$$

The buoyancy force is calculated through the use of the hydrostatic coefficients which are provided by a 3D radiation diffraction code (WAMIT). The inertia matrix is defined as shown in Eq. (13) below and can be either calculated by WAMIT or input by the user.

$$M = \begin{bmatrix} m & 0 & 0 & 0 & mz_g & -my_g \\ 0 & m & 0 & -mz_g & 0 & mx_g \\ 0 & 0 & m & my_g & -mx_g & 0 \\ 0 & -mz_g & my_g & I_{11} & I_{12} & I_{13} \\ mz_g & 0 & -mx_g & I_{21} & I_{22} & I_{23} \\ -my_g & mx_g & 0 & I_{31} & I_{32} & I_{33} \end{bmatrix} \tag{13}$$

Where m is the mass of the platform; x_g, y_g, and z_g coordinates of the platform CG, and $I_{\#\#}$ the moments of inertia of the platform. All quantities are calculated for the platform only and contributions from the attached VAWT and tower are introduced through the coupling interface.

Other force terms consist of forces imposed by the PTO equipment, mooring system, and friction/drag. As mentioned earlier, the PTO system is deactivated and will not be discussed here. Mooring forces and drag forces are calculated using user defined polynomial functions of platform position and velocity. For this study, simple linear springs were used to simulate the mooring stiffness as a function of platform displacement and drag was neglected. The mooring and drag force calculations are currently an area of improvement and more robust modules are being developed, as discussed in Section 6.2.

To solve the equation of motion, a global state-space model is created. The size of the model depends on the number of convolution states and the number of active DOF in the solution as shown below (Eq.(14)).

$$M'\dot{X}(t) = AX(t) + BF_{app}(t) \tag{14}$$

$$y(t) = CX(t)$$

$$X(t) = \left[[x_{r1}] \dots [x_{rn}] \ [\xi] \ [\dot{\xi}]\right]^T$$

Where $x_{r1\text{-}rn}$ are the convolution states, ξ and $\dot{\xi}$ are the displacement and velocity vectors respectively and F_{app} are applied forces. M' is the mass matrix (Eq. (15)).

$$M' = \begin{bmatrix} 1 & 0 & \dots & 0 & 0 \\ 0 & \ddots & \vdots & \vdots & \vdots \\ \vdots & & 1 & 0 & 0 \\ 0 & \dots & 0 & 1 & 0 \\ 0 & 0 & 0 & 0 & [M + A_\infty] \end{bmatrix} \tag{15}$$

where M is the mass matrix defined in Eq. 4 and A_∞ is the infinite added mass from WAMIT. A, B, and C are the state-space coefficient matrices (Eq. (16)).

$$A = \begin{bmatrix} [A_{r1}] & 0 & \dots & 0 & [B_{r1}] \\ 0 & \ddots & \vdots & \vdots & \vdots \\ \vdots & & [A_{rn}] & 0 & [B_{rn}] \\ 0 & \dots & 0 & 0 & [1] \\ [C_{r1}] & 0 & [C_{rn}] & [f_f(\xi) + f_m(\xi)] & [f_m(\dot{\xi})] \end{bmatrix}, \tag{16}$$

$$B = \begin{bmatrix} 0 \\ \vdots \\ 0 \\ [-1] \end{bmatrix}, \; C = \begin{bmatrix} 0 \\ \vdots \\ 0 \\ [1] \end{bmatrix}^T$$

where f_f and f_m are the coefficients for the friction drag and mooring forces respectively. The system of ODEs represented in Eq. (14) is then solved using the MATLAB explicit ODE45 Runge-Kutta ODE solver with initial conditions and time steps defined by OWENS. The solution contains state-space terms, as well as platform position, velocity, and acceleration which are output from the WaveEC2Wire module to OWENS. All results are calculated in the platform body coordinate system and transformed to the tower base in order to send to OWENS. Similarly, the external force from OWENS is transformed from the tower base to the platform center of gravity (CG) for inclusion in the platform equation of motion. As the transformation capability was under development at the time of this study, it was chosen to attach the tower to the platform CG, thus requiring no transformation. This was adequate to demonstrate the coupling between codes and a finalized transformation routine has been developed for future work. Results for each time step are computed and sent to OWENS according to the coupling methodology, described in the next section.

2.4.2. Coupling of OWENS and WavEC

The aforementioned framework and coupling procedures were employed to couple the WavEC platform dynamics/hydrodynamics software to the structural dynamics analysis capability in the OWENS framework. Verification procedures considered the isolated motion of individual platform surge, sway, heave, roll, pitch, and yaw rigid body degrees of freedom. First, step relaxations of each platform mode were considered and the influence of platform motion on the response of the flexible structure attached to the platform was observed. Next, an excitation force was applied to the flexible structure, and the response of the platform was observed. Fast Fourier Transforms (FFTs) of the platform and structural response were observed in each case and the frequency content of platform and structure were checked for consistency. Furthermore, all

damping mechanisms were deactivated from the platform module (radiation damping, drag, etc.) and no structural damping was applied to the flexible structure. This verified energy was not being dissipated by the numerical time integration schemes or the coupling procedure. The Gauss-Seidel iterative method was employed to couple the two simulations together, and a convergence criterion of 1e-8 was enforced at each time step for iterations of the coupled structural dynamics and platform analysis. Gravity was deactivated in these initial verification procedures.

Additional tests were conducted that examined the combined sway/roll (surge/pitch) response of the coupled platform and structural dynamics analysis. Buoyancy effects were verified by examining a coupled platform/structural dynamics analysis under gravity and buoyant loads to confirm the platform design behaved as intended under self-weight and weight of the attached structure. Finally, a full six-degree of freedom platform analysis was also considered with wave loading active. This exercise sought to verify the effect of hydrodynamic forcing on the platform was also evident in the tower motion. Selected results are shown in the next sections.

The topside is represented by a flexible tower structure with the rigid body properties described in Table 2 and illustrated in Figure 52. Platform properties are specified in Table 3. For simplicity, the tower is assumed to be mounted at the center of mass of the platform via a fixed/clamped connection. The flexibility of the tower will also influence the natural periods of the system. In particular, the pitch/roll period will shorten slightly, as demonstrated in the following sections.

A Newmark-Beta implicit time integration method was considered in the structural dynamics simulation with a time step size of 0.1 seconds. To expedite the analysis, nonlinear effects were deactivated in the structural dynamics simulation. Furthermore, a reduced order model was employed in the structural dynamics simulation which included only the first 10 flexible modes of the tower structure. Although, the linear nature and reduced order of this structural model introduce certain approximations, the goal of this exercise is to verify coupling between a structural dynamics module and platform hydrodynamics module regardless of the fidelity of the individual modules.

Table 2. Topside VAWT Properties

Property	Value
Mass	973 mt
Center of gravity (CG)	54.9 m above still water line
Roll/Pitch moment of inertia about CG	1.35e9 kg-m^2
Thrust load	550.0 kN
Center of pressure	67.0 m

Table 3. Spar-buoy Properties

Property	Value
Mass (with ballast)	9050 mt
Draft	80 m
Major/Minor Diameter	8.0/13.0 m
Center of gravity (CG) below still water level	63.5 m
Roll/Pitch moment of inertia about CG	3.4e9 kg-m2
Yaw inertia about CG	2.0e8 kg-m2

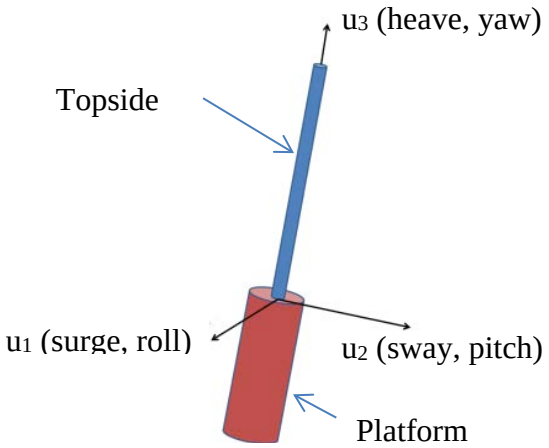

Figure 52. Representative system for verification procedures.

2.4.3. Isolated Roll/Pitch

The roll and pitch motions of the platform were isolated and all other rigid body motions of the turbine were constrained. Due to the axisymmetric nature of the platform and attached representative topside, roll and pitch verification tests are identical. First, the platform step relaxation in roll/pitch was considered. Second, an excitation force was applied in the sway/surge direction (u_2/u_1) to the tower top for a configuration with an initially stationary platform. The platform and structural motions were inspected for consistency in frequency content as well as periodicity, indicating energy was not being spuriously dissipated during the coupling scheme.

To perform the step relaxation, the platform was displaced at a roll angle of 0.1 radians with all other rigid body modes of the platform deactivated. The attached flexible turbine structure was initially at rest. At *t=0* the platform was released and hydrodynamic restoring/mooring forces resulted in harmonic motion of the platform as well as the attached tower structure. The response

of the simulation was simulated for two minutes. Figure 53 shows the time history and FFT of platform roll motion and tower tip displacement in the u_2 direction.

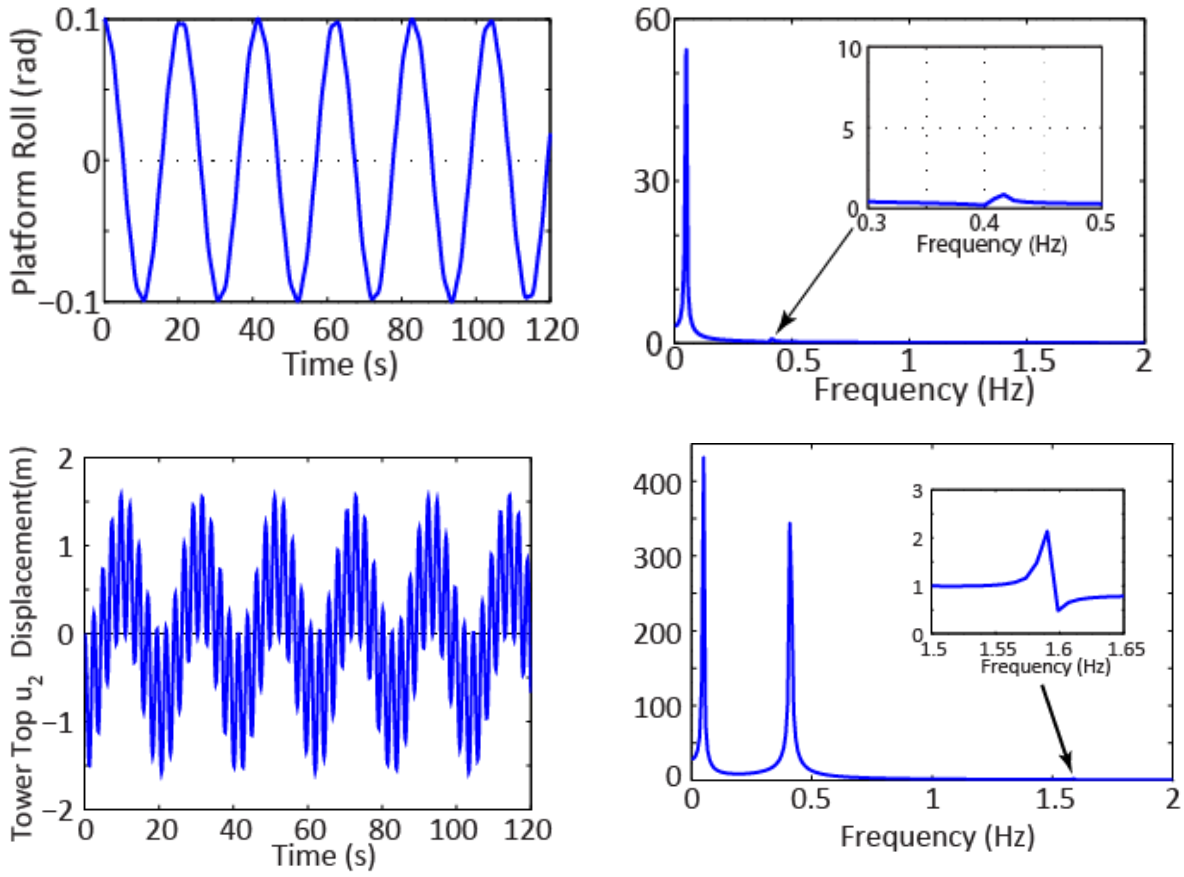

Figure 53. Roll/pitch Step Relaxation Results.

Periodicity of the platform motion as well as the tower motion is observed, indicating the coupling scheme and numerical integration schemes are working properly and not spuriously dissipating energy. Frequencies of 0.050 and 0.41 Hz are observed in the tower motion, the former being representative of the low frequency platform motion and the latter being representative of the tower structural vibration. Furthermore, a frequency of the 0.050 Hz is observed in the platform motion. Closer inspection of the FFT of platform motion reveals a small irregularity in the smooth FFT distribution around 0.41 and 1.59 Hz. This suggests there is some impact of the structural motion on the frequency content of the tower although the forcing as a result of structural vibration is minimal compared to restoring forces acting on the platform.

For the second test, the tower structure was excited by applying a force of 1e7 N for one second to the tower top in the sway direction to excite a roll rotation of the platform. The platform was initially stationary in this verification exercise. After one second, the excitation force was removed and the natural response of the system was observed. Figure 54 shows the time history and FFT of platform roll motion and tower tip displacement in the u_2 direction.

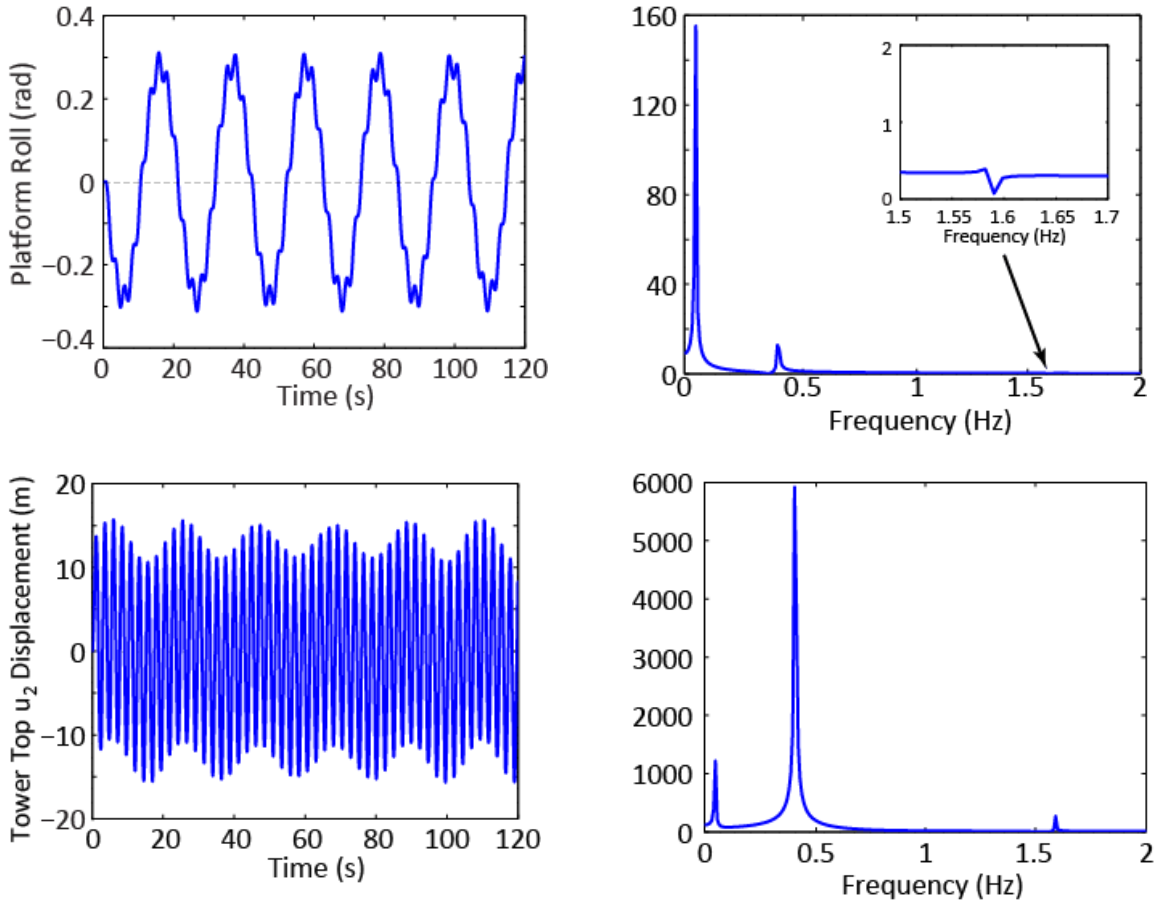

Figure 54. Roll/pitch tower forcing results.

As before, periodicity of the platform motion and tower deformation is observed, indicating the coupling scheme and numerical integration schemes are not spuriously dissipating energy. Furthermore, the frequency content of the platform and flexible structure reflected the rigid body and deformable modes of the floating system.

2.4.4. Combined Sway and Roll

The combined sway/roll and surge/pitch motions of the platform were isolated and all other rigid body motions of the turbine were constrained. First, a platform step relaxation in sway was considered. Second, an excitation force being applied in the sway/surge direction (u_2/u_1) to the tower top for a configuration with an initially stationary platform.

The platform was displaced in sway/surge a distance of one meter with all other rigid body modes of the platform constrained to zero. The attached flexible tower was initially at rest. At $t=0$ the platform was released and hydrodynamic restoring/mooring forces resulted in harmonic motion of the platform sway and roll (surge and pitch) as well as the attached tower structure. The simulation was run for two minutes. Figure 55 shows the time history and FFT of platform sway and roll motion as well as the tower tip displacement in the u_2 direction.

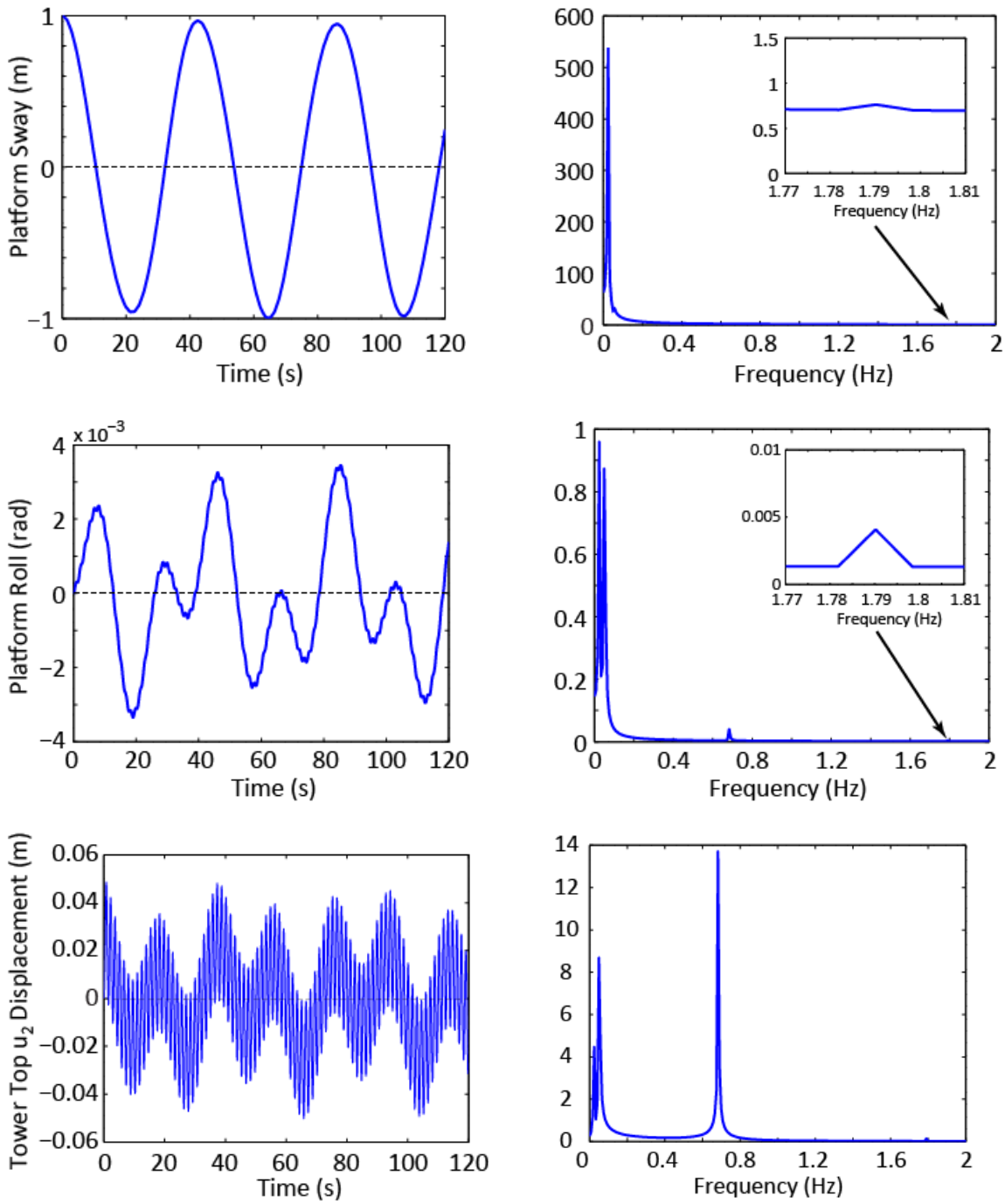

Figure 55. Combined sway and roll results.

Frequencies of 0.025, 0.05, 0.68, and 1.79 Hz are observed in the tower motion, the lowest two being representative of the low frequency platform motion and the higher two being representative of the tower structural vibration. Furthermore, a frequency of the 0.025 Hz is observed in the platform sway motion. Frequencies of 0.025, 0.05, and 0.68 Hz are apparent in the platform roll motion. Closer inspection of the FFTs of platform motion reveals small irregularities in the smooth FFT distribution around 0.05, 0.68, and 1.79 Hz for sway and 1.79 Hz for roll. This suggests there

is some impact of the structural vibration on the frequency content of the tower although the forcing as a result of structural vibration is minimal compared to restoring forces acting on the platform.

2.4.5. Wave Excitation

The floating system was subjected to regular wave excitation with a period of seven seconds (0.143 Hz) and wave height of two meters using the wave excitation functionality in WavEC2Wire. All six platform degrees of freedom were active in the simulation, as well as gravity, buoyancy, and damping. One minute of simulation time was considered. Figure 56 shows the time history and FFT of platform surge motion and tower tip displacement in the u_1 direction. The regular wave frequency is evident as a peak in both the platform surge and tower top motion FFTs at approximately 0.14 Hz. This indicates that the regular wave excitation of the platform is manifesting itself in the structural motion of the attached flexible structure.

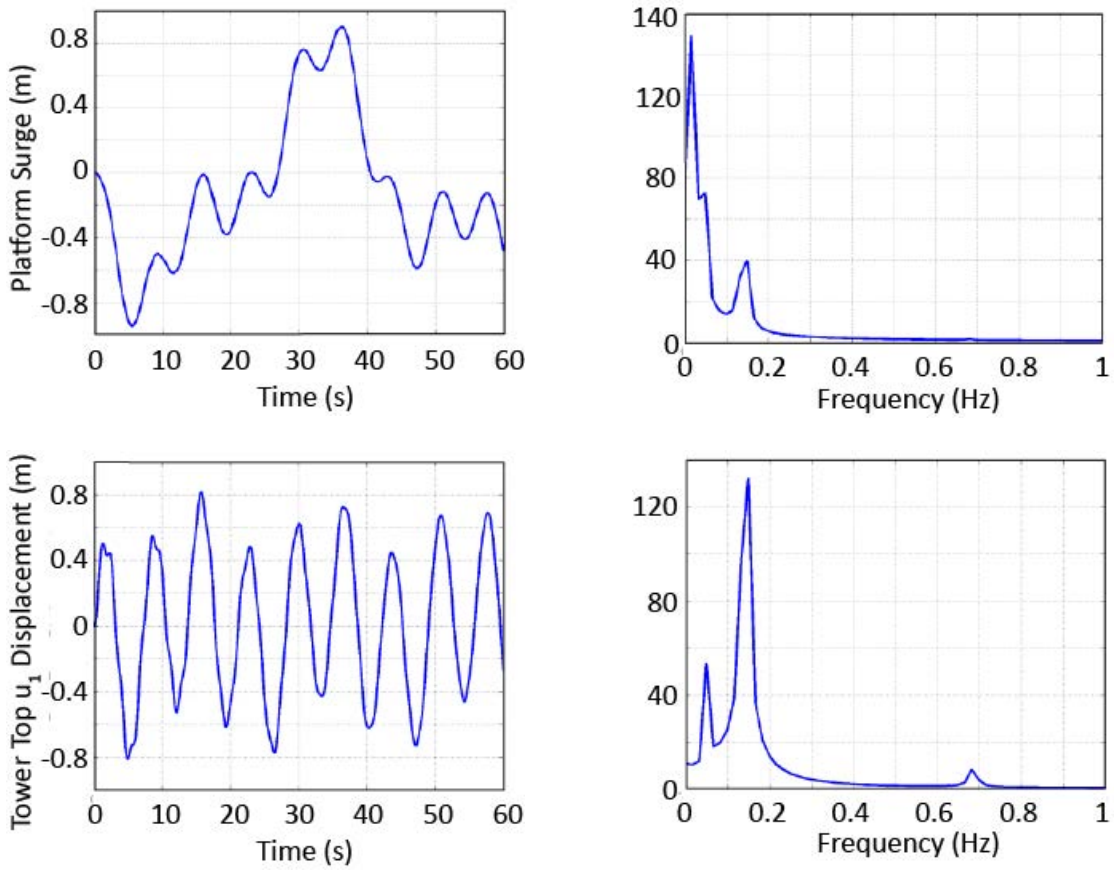

Figure 56. Wave excitation results.

2.4.6. Buoyancy Effects

This exercise seeks to verify correct buoyancy behavior in the analysis. When coupled with OWENS, the weight of the topside is accounted for in the reaction force passed through the coupling interaction and balances the buoyant force calculated by WavEC2Wire based on the platform position. For this test, the topside mass was reduced slightly in OWENS, resulting in a

positive vertical force as the system was initially defined in equilibrium. Figure 57 shows the heave displacement of the platform as the system seeks the new equilibrium point. After ten minutes of simulation, the platform approaches a steady state value of approximately 0.1 meters. This heave displacement results in the correct buoyant force for static equilibrium and is consistent with the desired behavior of the platform under self-weight and a reduced weight of the attached structure.

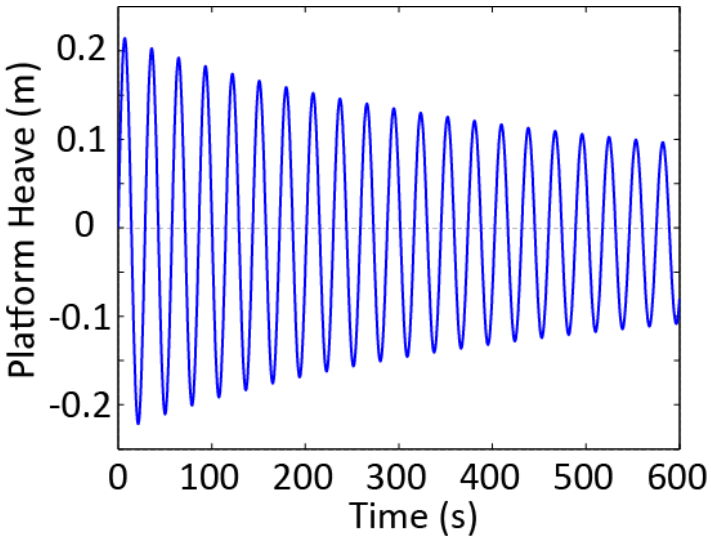

Figure 57. Heave displacement results.

3. LARGE-SCALE FLOATING VAWT SYSTEM DESIGN STUDIES

This section presents design studies performed using design tools mentioned in the previous section. First, the section discusses design load cases, and the availability and applicability of design standards. This is followed by design studies for the rotor structural design, rotor aerodynamic design, rotor structural dynamics/aeroelasticity, and the platform design.

3.1. Design Load Cases and Standards Availability/Applicability for Offshore VAWTs

IEC 61400-3 outlines the standard for offshore wind turbine design. While these standards are not specific to a certain machine configuration, they were developed primarily with HAWT rotors in mind. It is worthwhile to discuss which standards would likely play major versus minor roles in VAWT rotor design as opposed to HAWT rotor design.

Two design load cases tend to drive most HAWT designs: DLC 1.4 (extreme coherent gust with direction change) and DLC 6.1a-b (extreme parked gust). HAWT designs are sensitive to quick changes in angle of attack on the blades such as what would be experienced with DLC 1.4, as the blades can strike the tower. It is not anticipated that this would be as important to VAWT design as tower clearance would not be an issue. Also, in general, VAWTs should be less sensitive to load cases that contain direction changes due to their configuration. VAWTs should also be less sensitive to vertical wind shear as they assimilate those changes along the height of the rotor. It may be true that vertical shear is actually advantageous to VAWTs as it would have the effect of spreading out the torque pulse over a wider azimuth range. VAWTs are sensitive to parked gust cases, just like HAWTs. They may be more impacted as the total blades solidity will likely be higher. Finally, VAWTs will likely be much more sensitive to cut-out load cases as they will likely be stall controlled, and thus unable to actively shed loads.

The design load cases for VAWTs considered in this report are for aerodynamic loads at cut-out wind-speed under steady and uniform inflow. This is expected to provide an upper bound on aerodynamic loading under normal operation conditions.

Design and cost-of-energy calculations are carried out using a hypothetical deployment site in deep water off the coast of Maine. The site average wind speed at 90 meters height above the water is assumed to be 9.2 m/s, and the wind speed is assumed to follow a Weibull distribution with k=2. The water depth is 206 meters.

Table 4. IEC 61400-3 Design Load Cases.

Design situation	DLC	Wind condition	Waves	Wind and wave directionality	Sea currents	Water level	Other conditions	Type of analysis	Partial safety factor
1) Power production	1.1a	NTM $V_{in} < V_{hub} < V_{out}$ RNA	NSS $H_s=E[H_s \mid V_{hub}]$	COD, UNI	NCM	MSL	For extrapolation of extreme loads on the RNA	U	N (1,25)
	1.1b	NTM $V_{in} < V_{hub} < V_{out}$ Support structure	NSS Joint prob. distribution of H_s, T_p, V_{hub}	COD, UNI	NCM	NWLR	For extrapolation of extreme loads on the support structure	U	N (1,25)
	1.2	NTM $V_{in} < V_{hub} < V_{out}$	NSS Joint prob. distribution of H_s, T_p, V_{hub}	COD, MUL	No currents	NWLR or ≥ MSL		F	*
	1.3	ETM $V_{in} < V_{hub} < V_{out}$	NSS $H_s=E[H_s \mid V_{hub}]$	COD, UNI	NCM	MSL		U	N
	1.4	ECD $V_{hub} = V_r - 2$ m/s, V_r, $V_r + 2$ m/s	NSS (or NWH) $H_s=E[H_s \mid V_{hub}]$	MIS, wind direction change	NCM	MSL		U	N
	1.5	EWS $V_{in} < V_{hub} < V_{out}$	NSS (or NWH) $H_s=E[H_s \mid V_{hub}]$	COD, UNI	NCM	MSL		U	N
	1.6a	NTM $V_{in} < V_{hub} < V_{out}$	SSS $H_s= H_{s,SSS}$	COD, UNI	NCM	NWLR		U	N
	1.6b	NTM $V_{in} < V_{hub} < V_{out}$	SWH $H = H_{SWH}$	COD, UNI	NCM	NWLR		U	N

Table 5. IEC 61400-3 Design Load Cases (continued).

Design situation	DLC	Wind condition	Waves	Wind and wave directionality	Sea currents	Water level	Other conditions	Type of analysis	Partial safety factor
2) Power production plus occurrence of fault	2.1	NTM $V_{in} < V_{hub} < V_{out}$	NSS $H_s=E[H_s \mid V_{hub}]$	COD, UNI	NCM	MSL	Control system fault or loss of electrical network	U	N
	2.2	NTM $V_{in} < V_{hub} < V_{out}$	NSS $H_s=E[H_s \mid V_{hub}]$	COD, UNI	NCM	MSL	Protection system or preceding internal electrical fault	U	A
	2.3	— EOG — $V_{hub} = V_r \pm 2$m/s & V_{out}	NSS (or NWH) $H_s=E[H_s \mid V_{hub}]$	COD, UNI	NCM	MSL	External or internal electrical fault including loss of electrical network	U	A
	2.4	NTM $V_{in} < V_{hub} < V_{out}$	NSS $H_s=E[H_s \mid V_{hub}]$	COD, UNI	No currents	NWLR or ≥ MSL	Control, protection, or electrical system faults including loss of electrical network	F	*
3) Start up	3.1	NWP $V_{in} < V_{hub} < V_{out}$	NSS (or NWH) $H_s=E[H_s \mid V_{hub}]$	COD, UNI	No currents	NWLR or ≥ MSL		F	*
	3.2	— EOG $V_{hub} = V_{in}, V_r \pm 2$m/s — and V_{out}	NSS (or NWH) $H_s=E[H_s \mid V_{hub}]$	COD, UNI	NCM	MSL		U	N
	3.3	EDC_1 $V_{hub} = V_{in}, V_r \pm 2$m/s and V_{out}	NSS (or NWH) $H_s=E[H_s \mid V_{hub}]$	MIS, wind direction change	NCM	MSL		U	N

Design situation	DLC	Wind condition	Waves	Wind and wave directionality	Sea currents	Water level	Other conditions	Type of analysis	Partial safety factor
4) Normal shut down	4.1	NWP $V_{in} < V_{hub} < V_{out}$	NSS (or NWH) $H_s=E[H_s \mid V_{hub}]$	COD, UNI	No currents	NWLR or ≥ MSL		F	*
	4.2	— EOG — $V_{hub} = V_r \pm 2m/s$ & V_{out}	NSS (or NWH) $H_s=E[H_s \mid V_{hub}]$	COD, UNI	NCM	MSL		U	N
5) Emergency shut down	5.1	NTM $V_{hub} = V_r \pm 2m/s$ & V_{out}	NSS $H_s= E[H_s \mid V_{hub}]$	COD, UNI	NCM	MSL		U	N
6) Parked (standing still or idling)	6.1a	EWM Turb. wind model $V_{hub} = 0,95\ V_{ref}$	ESS $H_s = 1,09\ H_{s50}$	MIS, MUL	ECM	EWLR		U	N
	6.1b	EWM Steady wind model $V(z_{hub}) = V_{e50}$	RWH $H = H_{red50}$	MIS, MUL	ECM	EWLR		U	N
	6.1c	RWM Steady wind model $V(z_{hub}) = V_{red50}$	EWH $H = H_{50}$	MIS, MUL	ECM	EWLR		U	N
	6.2a	EWM Turb. wind model $V_{hub} = 0,95\ V_{ref}$	ESS $H_s = 1,09\ H_{s50}$	MIS, MUL	ECM	EWLR	Loss of electrical network	U	A
	6.2b	EWM Steady wind model $V(z_{hub}) = V_{e50}$	RWH $H = H_{red50}$	MIS, MUL	ECM	EWLR	Loss of electrical network	U	A
	6.3a	EWM Turb. wind model $V_{hub} = 0,95\ V_1$	ESS $H_s = 1,09\ H_{s1}$	MIS, MUL	ECM	NWLR	Extreme yaw misalignment	U	N
	6.3b	EWM Steady wind model $V(z_{hub}) = V_{e1}$	RWH $H = H_{red1}$	MIS, MUL	ECM	NWLR	Extreme yaw misalignment	U	N
	6.4	NTM $V_{hub} < 0,7\ V_{ref}$	NSS Joint prob. distribution of H_s, T_p, V_{hub}	COD, MUL	No currents	NWLR or ≥ MSL		F	*

Table 6. IEC 61400-3 Design Load Cases (continued).

Design situation	DLC	Wind condition	Waves	Wind and wave directionality	Sea currents	Water level	Other conditions	Type of analysis	Partial safety factor
7) Parked and fault conditions	7.1a	EWM Turb. wind model $V_{hub} = 0,95\ V_1$	ESS $H_s = 1,09\ H_{s1}$	MIS, MUL	ECM	NWLR		U	A
	7.1b	EWM Steady wind model $V(z_{hub}) = V_{e1}$	RWH $H = H_{red1}$	MIS, MUL	ECM	NWLR		U	A
	7.1c	RWM Steady wind model $V(z_{hub}) = V_{red1}$	EWH $H = H_1$	MIS, MUL	ECM	NWLR		U	A
	7.2	NTM $V_{hub} < 0,7\ V_{ref}$	NSS Joint prob. distribution of H_s, T_p, V_{hub}	COD, MUL	No currents	NWLR or ≥ MSL		F	*
8) Transport, assembly, maintenance and repair	8.1	To be stated by the manufacturer						U	T
	8.2a	EWM Steady wind model $V_{hub} = V_{e1}$	RWH $H = H_{red1}$	COD, UNI	ECM	NWLR		U	A
	8.2b	RWM Steady wind model $V(z_{hub}) = V_{red1}$	EWH $H = H_1$	COD, UNI	ECM	NWLR		U	A
	8.3	NTM $V_{hub} < 0,7\ V_{ref}$	NSS Joint prob. distribution of H_s, T_p, V_{hub}	COD, MUL	No currents	NWLR or ≥ MSL	No grid during installation period	F	*

The design standards and recommended practices of Det Norske Veritas (DNV) provided guidance in defining the extreme environmental conditions for the platform. The offshore standard on position mooring (23) includes a list of required design documentation for device certification. Among the items listed, the following environmental conditions are required:

- Combinations of significant wave heights and peak periods along the 100-year contour line for a specified location;
- One hour mean wind speed with a return period of 100 years;
- Surface and subsurface current speed with a return period of 10 years.

Data from the NDBC 44005 buoy was used to estimate the 100-year extreme wave return contour at the deployment site according to the methodology presented in (24), see Figure 58. This NDBC buoy is close to the hypothetical deployment site off the coast of Maine. The wind, wave and current conditions for these cases are shown in Table 7. However, instead of using the 100 year wind event, an extreme 50 m/s event was applied to the parked VAWT rotor (25).

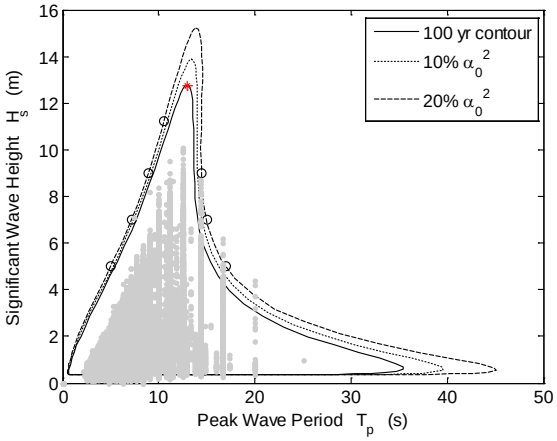

Figure 58. 100-year contour for spectral wave conditions from NBDC buoy 44005.

Table 7. Environmental conditions for 100-year storm event.

Extreme Case	
Water Depth	206 m
Regular Wave Height Equivalent	24.24 m
Period	12.97 s
Wind Speed	50 m/s
Ocean Current Speed	0.88 m/s

The wind loads are provided based on drag of the topsides in an extreme event wind case. They are considered independent of the platform type or size. For all VAWT designs, the wind load is given as 3,140 kN. This value is based on a CACTUS analysis and represents the form drag of a

parked VAWT and tower subject to the Gulf of Maine extreme mean wind speed of 50 m/s (25). The calculated value is for what was considered the worst case VAWT design for area and drag and should be conservative.

3.2. Rotor Structural Design

This section presents rotor structural design, including design configurations, structural analysis procedures and analysis results. Design configurations include choice of architecture, number of blades, tip chord length, material choice, tapering scheme, and curvature. Initial analysis includes stability of modes, static loadings at parked and operating conditions, and rotor cost modeling.

3.2.1. Design Configurations

Reduction of parameter space was essential at the early stages of the design process. It was deemed important to study the overall architecture of the rotor, the number of blades, the chord length, the material the rotor was made out of, and blade tapering and curving schemes. Also, for all designs in this initial conceptual design study, the following assumptions were made:

- For tapered blade designs, the blade chord was assumed to vary inversely with radius, up to a maximum dimension, which was set at the tower diameter of 6m.
- Skin thickness was constant around the circumference of the airfoil at a given location. Thus, spar areas were the same thickness as leading and trailing edge reinforcements, and panel regions.
- Spar and leading edge reinforcement areas were assumed to be made of mostly unidirectional material. A small amount of bi-axial material was used on the interior and exterior of the blade skins.

The major parameters of architecture, number of blades, chord length, material, tapering, and curvature scheme are now discussed.

3.2.2. Architecture

Two major configurations were analyzed, a Darrieus design and a “U” or “V” shaped machine. The Darrieus design is advantageous in that the blades are typically in tension during operation which should allow for lighter blade designs as tension loads are much easier to resist than bending loads. Additionally, Darrieus machines do not have blade tips and thus do not experience aerodynamic tip losses. V/U-VAWTs, which will be referred to as V-VAWTs from hereon, may offer the advantage of a lower center of gravity, lower center of aerodynamic thrust load and associated overturning moment, and elimination of tower weight realized through a partial height tower.

H-VAWTS were not considered in this design study as they share much in common with V-VAWTS in terms of aerodynamic efficiency and loading, and thus were not seen as unique or outside the design envelope of the Darrieus and V-VAWT study.

For all Darrieus designs, the shape of the 34-m Sandia VAWT was used. There is a body of research on the effect of different aspect ratios (i.e. height over diameter) for Darrieus machines. This was not examined as a parameter in this study, but it is possible that the optimal shapes that have been found for smaller land-based machines may not be the same for large offshore rotors.

3.2.3. Number of Blades

Historically, VAWTs have been produced having blade numbers ranging from two to six or more. Two-bladed designs have the advantage of lower rotor cost and higher rotational speed which lowers drivetrain costs. The disadvantages of two-bladed designs are that they have different in-plane and out-of-plane moments of inertia and that they have a relatively strong torque pulse as each blade is aerodynamically loaded as it rotates about the axis. Machines with higher numbers of blades tend to cost more but alleviate some of the aforementioned design issues. Previous work at Sandia has shown that three-bladed designs successfully mitigate torque pulses. Thus, in this study, only two- and three-bladed designs were examined.

3.2.4. Tip Chord Length

Chord length is another important parameter to study. Larger chord machines rotate slower in operation and thus, increase drivetrain costs. However, they offer improved structural efficiency as bending resistance is proportional with the cube of chord length for a given airfoil. To understand this effect while keeping the parameter space small, two chord lengths were examined for the equatorial or largest radius position: a scaled up SNL 34-m chord of 3m (large chord or LC), and a smaller chord of 2m (small chord or SC). A 2m chord was selected as it would be the chord length that would be used for a three-bladed, scaled up version of the 34m machine with the same operating rotational speed as a two-bladed rotor with 3m chord.

3.2.5. Composite Material

For this study it was important to examine the extremes of what would be possible given likely material candidates. In the wind industry, glass and carbon composites are used to manufacture blades. Carbon has three to four times the specific stiffness of glass and up to 10 times the specific strength. However, carbon comes at about 7-10 times the cost. This has led to carbon being difficult to economically integrate into blade designs. While carbon is used, it is used selectively in highly loaded parts of the blade. So-called hybrid designs are becoming common-place in the industry as the added cost of the carbon is offset by increased rotor sizes and resulting increased energy capture. For offshore rotors, where under-water structure costs are high and driven by above-water mass, a lightweight carbon rotor may prove to be cost-effective. Thus, in this study, designs with all glass and all carbon were investigated. However, some intermediate, hybrid design may still prove to be the optimal choice.

3.2.6. Tapering Scheme

VAWT blade shapes have tended to come in two tapering schemes in past designs: tapered from tower to equator and constant chord or non-tapered. Tapering offers blade designs that are structurally and aerodynamically optimized while more costly to manufacture. Non-tapered designs give up some aerodynamic performance near the tower, but are cheap to produce and can employ pultrusion as a manufacturing method. These two options were considered in this study, along with a hybrid version for Darrieus designs where tapering was employed on the bottom half of the rotor only. Thus, the tapering schemes investigated were double-tapered (DT), single-tapered (ST), and non-tapered (NT).

3.2.7. Curvature

To examine V-VAWT designs, a power law blade geometry was used where

$$\frac{h}{H} = \left(\frac{r}{R}\right)^n \tag{17}$$

For a power law blade shape, the swept area of the rotor is the integration of (1) from 0 to R, and is

$$A = HR[1 - (n+1)^{-1}] \tag{18}$$

The center of area (C_A) for power-law V-VAWT rotors is then

$$C_A = \left(\frac{1+n^{-1}}{2+n^{-1}}\right) H \tag{19}$$

V-VAWT designs with the same maximum radius and swept area as the Darrieus shape are shown for n=1 through n=5 in Figure 59.

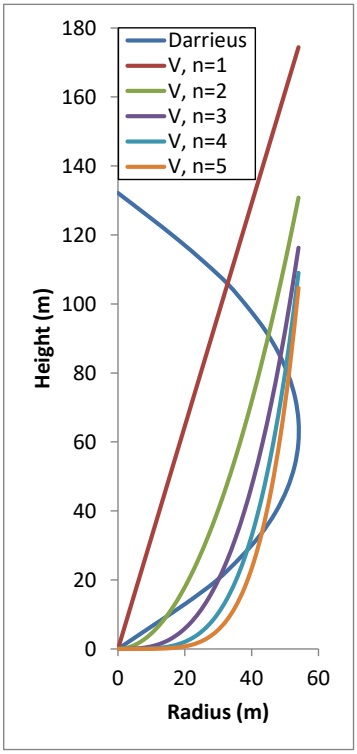

Figure 59. Comparison of V-VAWT shapes to baseline Darrieus geometry for same diameter and swept area.

Keeping the rotor radius and swept area the same as for the 5MW Darrieus design, the effect of increasing power law exponent on blade tip height and rotor area center can be seen in Figure 60. This shows a relatively large decrease for both quantities from n=1 to n=3, and smaller decreases beyond n=3. For power law shape of n=1, straight blades would be employed, likely leading to lower manufacturing cost through a more simple design. Higher n values would lead to more of the blade rotating at the maximum radius. Thus a clear tradeoff between rotor cost and performance exists for this configuration.

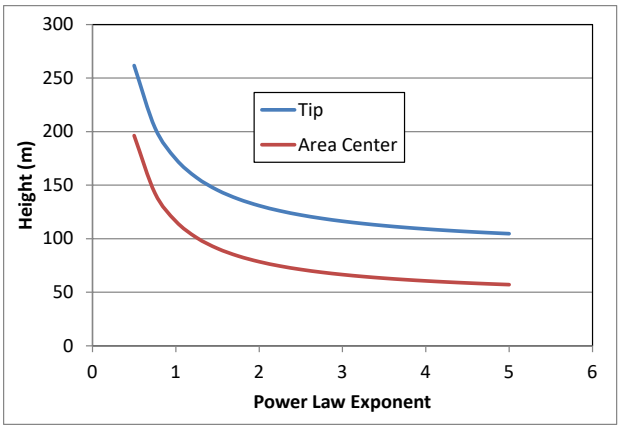

Figure 60. Effect of blade shape on rotor height and area center for V-VAWT.

To summarize, the studied design configuration parameters were the following:

- Architecture: Darrieus, V
- Number of Blades: 2, 3
- Tip Chord Length: 4m, 6m
- Composite Material: Glass/Epoxy, Carbon Epoxy
- Tapering Scheme (Darrieus): No Taper, Single Taper, Double Taper
- Curvature or Power Law Exponent (V): n=1, n=3, n=5

3.2.8. Analysis Procedure

As a complete, coupled aero analysis code was not available during the conceptual design stages of this project, an alternative design procedure was used. A simplification of design constraints was employed, whereby, initially, designs were based off of inertial loads. Four criteria were used to evaluate the designs:

- Stability of modes within the operating envelope
- Parked, gravity-caused strains
- Blade axial strains at the maximum operating RPM
- Blade bending strains at the maximum operating RPM

All initial analyses were performed in ANSYS using BEAM188 elements. Input files were created using a custom MATLAB script. Designs were first specified using Sandia NuMAD software. An analysis of mass and stiffness properties was then performed using NREL's PreComp code. The mass and stiffness properties were then returned to the NuMAD design spreadsheet. From there, ANSYS input files were written which created the geometry, nodes, elements, element structural properties, and boundary conditions. All designs featured 20 blade elements, with Darrieus designs having 20 tower elements and V-VAWT designs having six tower elements as they had shorter towers. The bottom of the rotor was fixed in all degrees of freedom. It is known that this boundary condition is not appropriate for floating designs, but as it predominately serves to lower the frequency of the tower mode, it serves as a conservative assumption. A depiction of the two- and three-bladed Darrieus and V-VAWT models are shown in Figure 61.

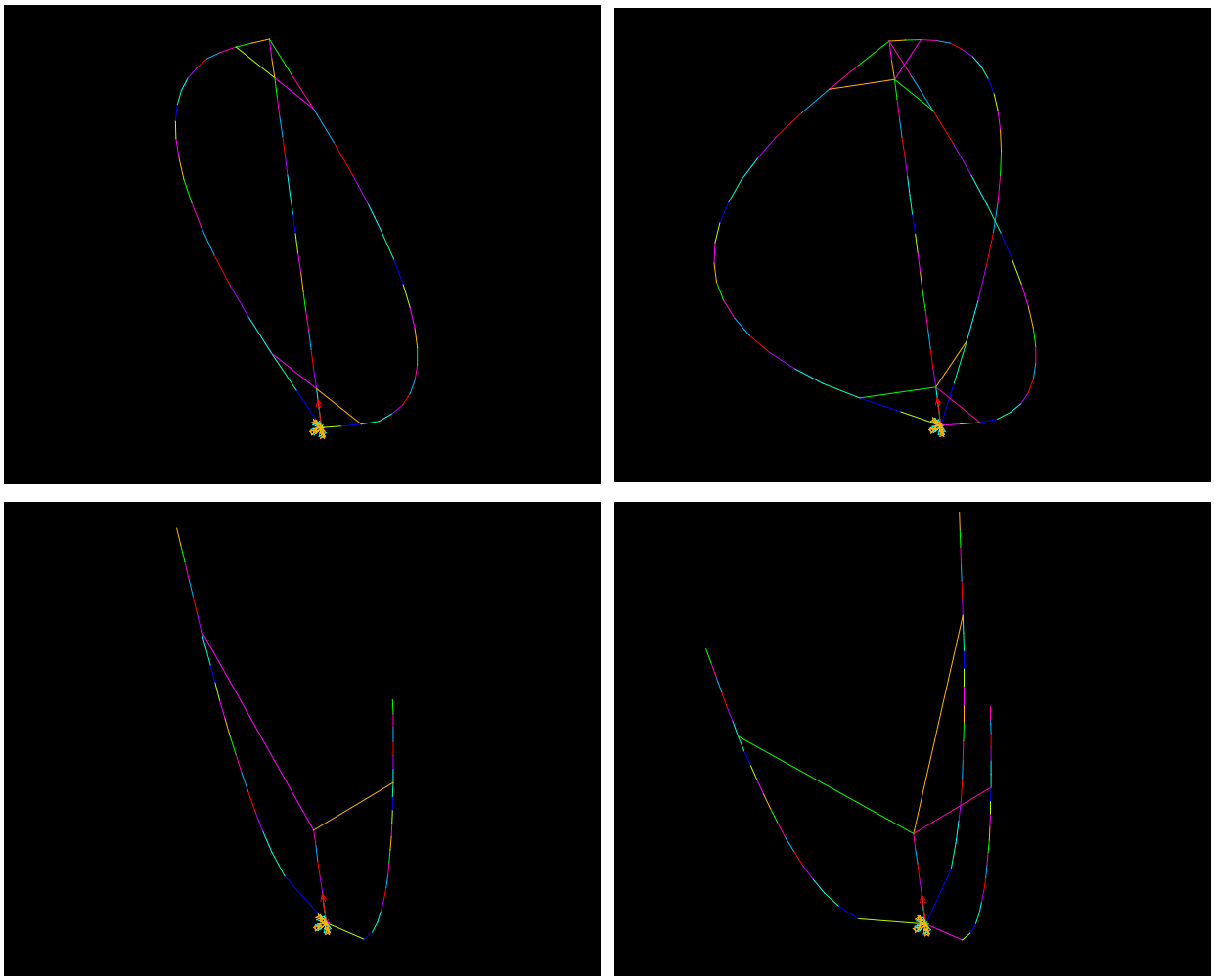

Figure 61. ANSYS finite element models of 2-bladed Darrieus (top left), 3-bladed Darrieus (top right), 2-bladed V (bottom left), and 3-bladed V (bottom right).

For each configuration, a series of analyses were performed. First, mass properties were obtained, including total mass, center of gravity (CG), mass moment of inertia about the rotor bottom in the rotational (IRO) and pitching (IPO), and mass moment of inertia about the CG in the rotational (IRC) and pitching (IPC). Next, a modal analysis was performed on a pre-stressed structure at 2-rpm increments from 0 to 20 rpm. The results of these analyses were collected together in the form of a Campbell plot using the PLCAMP command within ANSYS, as well as an APDL code to retrieve the results for further processing in MATLAB. Then, a nonlinear analysis was performed of the structure at rest to determine blade bending strains from displacements caused by gravity. Finally, an analysis with prescribed rotor velocity was performed to determine axial and bending strains in the blades under rotational effects.

3.2.9. Results

3.2.9.1. Mass Properties

The mass properties for all configurations analyzed are shown in Figure 62 through Figure 64.

Figure 62 shows the center of gravity (CG), as measured from the water surface as a function of total rotor mass. It is evident that V configurations may offer a potential reduction in CG over Darrieus designs, although there is overlap in some cases. Lowering of CG should lead to smaller underwater structure.

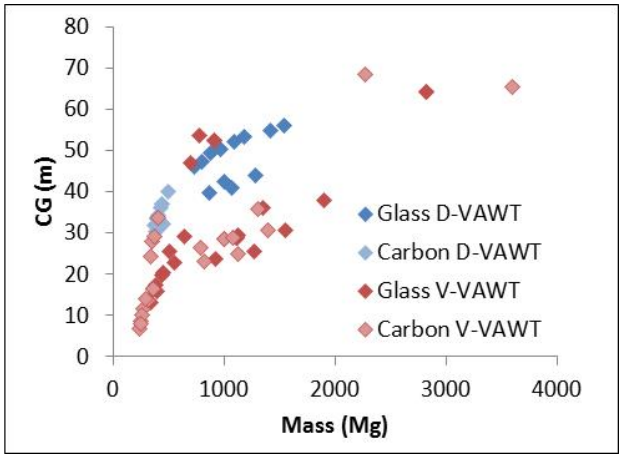

Figure 62. Rotor CG measured from water surface.

Figure 63 shows pitching and rotational mass moments of inertia (MOI) about the water surface. V designs can be seen to have a lower MOI than Darrieus designs, which shows potential for smaller underwater structure to resist pitching motion. Figure 64 shows a similar effect when these quantities are calculated about the CG.

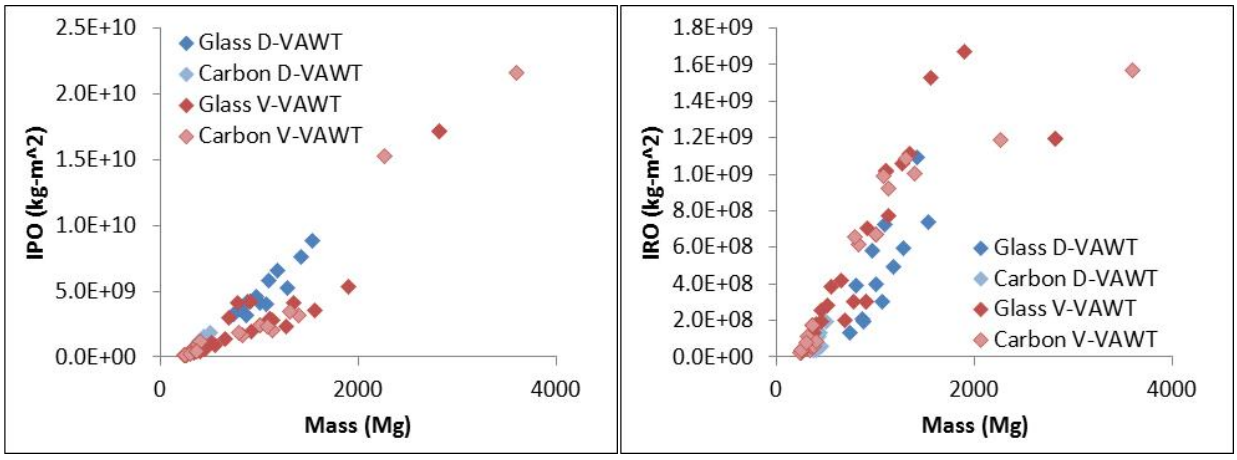

Figure 63. Rotor pitch (left) and rotational (right) mass moments of inertia measured about bottom of rotor.

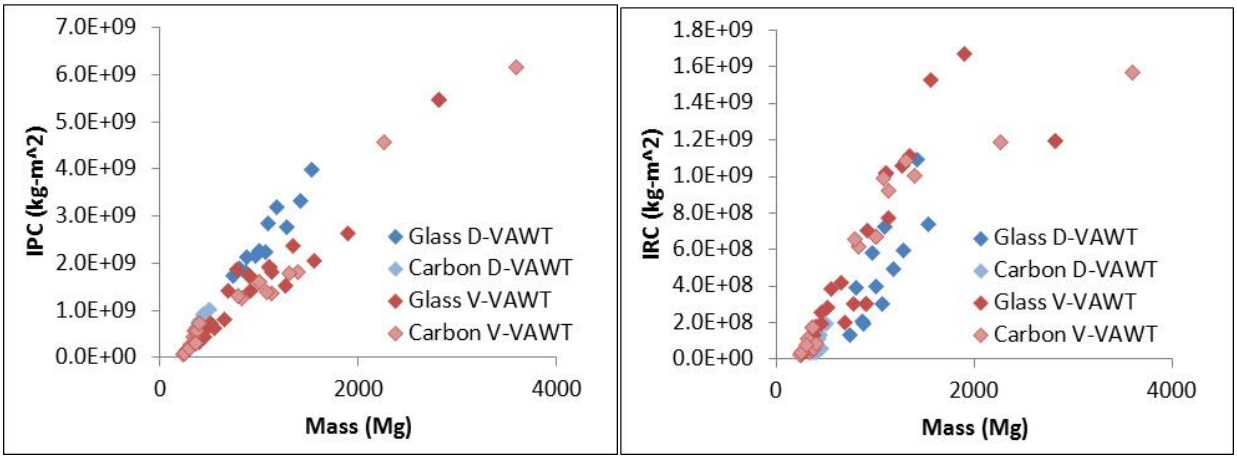

Figure 64. Rotor pitch (left) and rotational (right) mass moments of inertia measured about the rotor CG.

3.2.9.2. Blade Strains

Parked blade strains due to inertial forces are shown in Figure 65. A group of both Darrieus and V designs made both of glass and carbon are under 0.3% strain, and a few others are under 0.6% strain. This indicates that these designs should be acceptable under this criterion. Without getting into a detailed discussion of specific glass and carbon allowable ultimate and loading-dependent fatigue strains, 0.3% is usually an acceptable level of fatigue strain for both materials using lower quality manufacturing methods, while 0.6% can be used with higher-quality methods. Ultimate strains for as-built glass and carbon structures can be as high as 2.5% and 1.5%, respectively, but structural instabilities are often encountered at lower load levels.

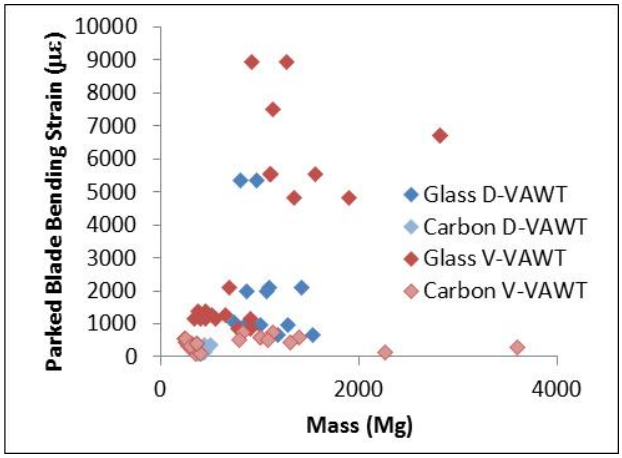

Figure 65. Parked blade bending strain.

The blade axial strains from rotation only at 15 rpm are shown in Figure 66. Again there are a large number of Darrieus and V, glass and carbon designs that fall within reasonable limits for strain.

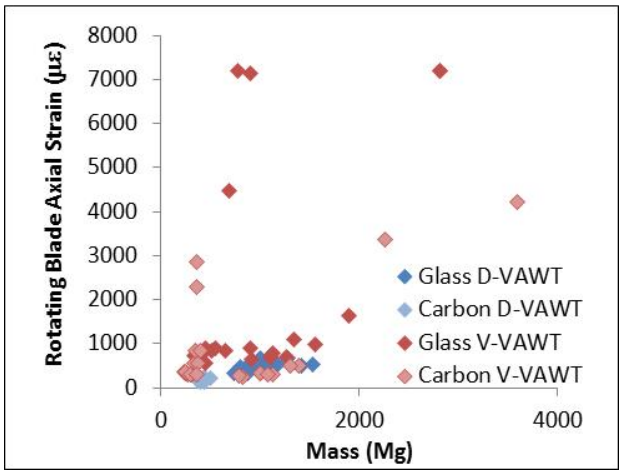

Figure 66. Rotating (15 rpm) blade axial strain.

Finally, the bending strains from rotation at 15 rpm are shown in Figure 67. For this case, there is a significant difference between Darrieus and V designs, with the V designs mostly having larger strains and all glass V designs being well beyond acceptable limits. Both glass and carbon Darrieus designs are within acceptable limits, with carbon designs having very low strains.

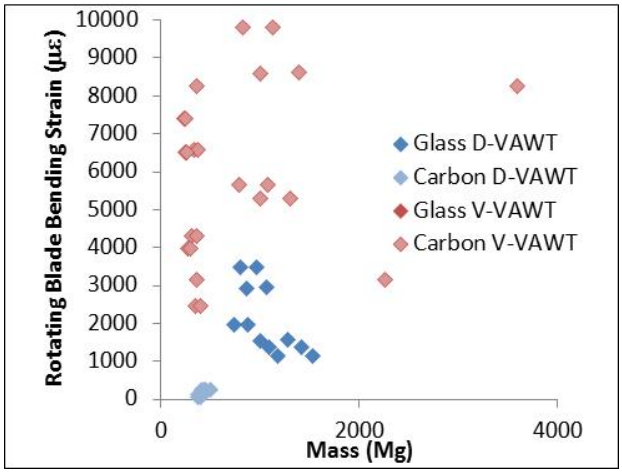

Figure 67. Rotating (15 rpm) blade bending strain.

3.2.9.3. Rotor Material Cost

The rotor material costs for the various VAWT designs are shown in Figure 68. Composite material costs were computed under the cost assumptions shown in Table 8. This clearly shows the increased cost incurred by considering carbon composite designs relative to glass composite designs. Glass composite Darrieus designs ranged from $3.2M to $7.6M with an average rotor material cost of $5.0M. Carbon composite Darrieus designs ranged from $6.3M to $9.9M with an average rotor material cost of $7.6M. Glass composite V-VAWT designs ranged from $1.0M to $14.7M with an average rotor material cost of $4.9M. Carbon composite V-VAWT designs ranged from $2.5M to $98.5M with an average rotor material cost of $18.1M.

Table 8. Material costs.

Material System	Unit Cost ($/lb)
Glass composite	2.0
Carbon composite	13.0

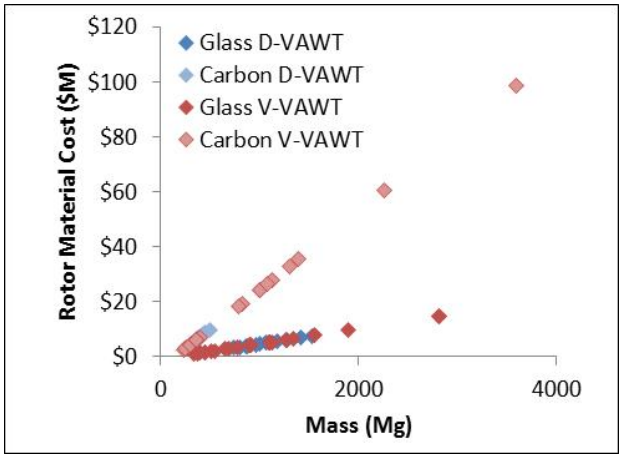

Figure 68. Rotor material costs for all designs.

3.3. Rotor Aerodynamic Analysis and Design

3.3.1. Assumptions and Procedure

In order to evaluate the relative cost of candidate rotor designs, annual energy production must be estimated. Further, aerodynamic loads are required for iterative design of the rotor and foundation structures. Estimates for these quantities are obtained from CACTUS (Code for Axial and Cross-flow TUrbine Simulation), a rigid body aerodynamic performance analysis code. This code has been successfully validated for power performance predictions by detailed comparisons to legacy test data from the Sandia 34m test-bed campaign.

For the purposes of this study, the VAWT machines are assumed to be stall-regulated, with no active power or loads control. They are also assumed to operate with a simple variable-speed controller to optimize energy capture in region two of the power curve. Cut-in and cut-out wind speeds of 5 m/s and 25 m/s, respectively, are imposed. The performance data presented here are generated assuming zero wind shear; only small quantitative differences are expected when shear is introduced, and these are not expected to impact the resulting trends in performance with design changes. For aerodynamic modeling purposes, all rotor designs employ NACA-0021 airfoils for all modeled blade sections. In future work, we plan to incorporate more advanced VAWT airfoils into the aerodynamic designs; the present results allow for baseline aerodynamic predictions to which we will compare these future results.

The starting point for the aerodynamic performance analysis is a fixed-rotor geometry definition that is taken as given. A three-step process is followed to generate a power curve. In the first step, a Cp curve is generated (power coefficient (Cp) versus tip-speed-ratio). During this step, the rotor RPM is held constant at a fixed value that is a reasonable estimate of the rotational speed at rated

power. Two pieces of information are extracted from the Cp curve: the optimal tip speed ratio for maximum Cp, and the tip speed ratio at which a rotor stall occurs (see Figure 69). These two parameters are input for the second stage of the process. The second stage consists of performing a sweep in rotational speed at the stall tip speed ratio. This sweep identifies the rotor RPM for which the desired rated power is achieved at stall. The desired rotor power is set to 5500 kW for the present study, assuming a drive train efficiency of 0.91 and resulting generator power of 5 MW.

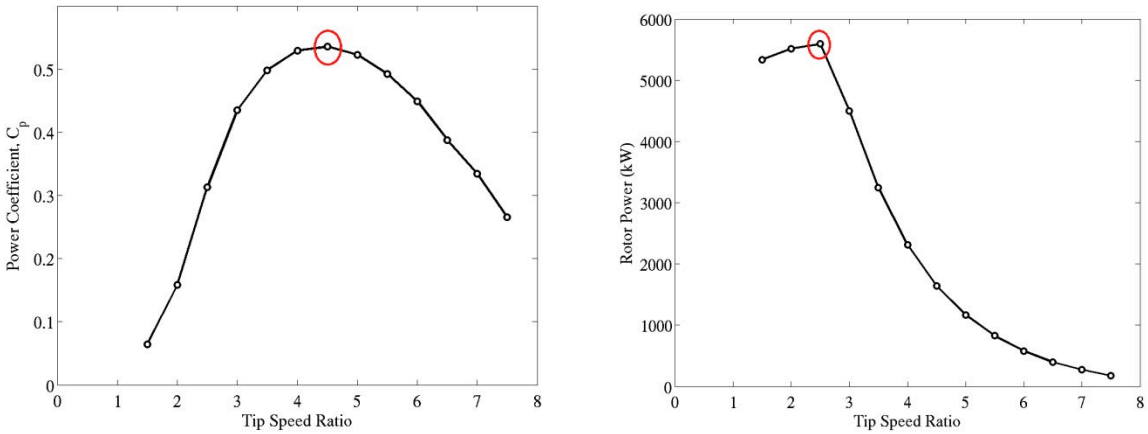

Figure 69. Examples of a Cp curve and Power vs. Tip Speed Ratio curve used for stage one of the analysis. The maximum Cp and the stall point are indicated by red circles.

Now the rotor RPM schedule is completely defined as a function of wind speed. The RPM is set to the minimum of the RPM giving the optimal tip speed ratio (TSR) for a given wind speed, and the RPM for rated power at stall. This defines a simple variable speed control schedule that provides for optimal energy capture under the constraint that the required RPM to maintain rated power is never exceeded. An example of an RPM schedule and resulting operating TSR range is shown in Figure 70.

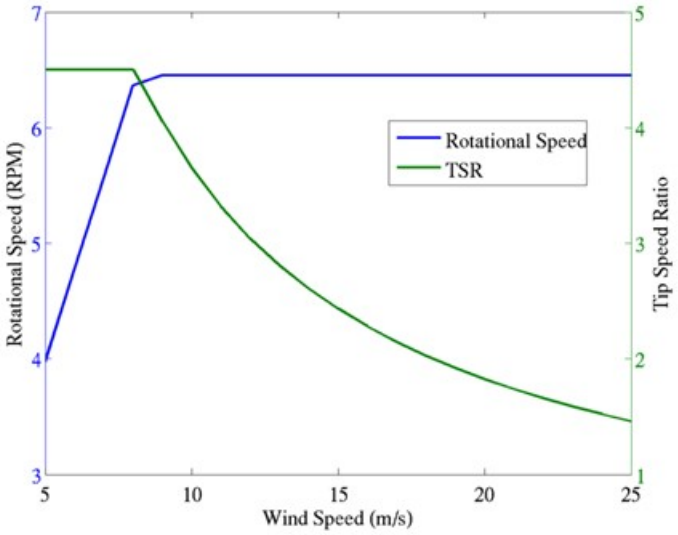

Figure 70. Example of a rotor speed schedule and resulting tip speed ratio variation with wind speed.

3.3.2. Darrieus Rotor Performance

Twelve Darrieus rotor designs were analyzed, each design incorporating a unique combination of blade chord at maximum radius, number of blades, and choice of blade tapering (un-tapered, single-tapered, or double-tapered) as described in the previous section on rotor structural design.

Power coefficient versus tip speed ratio curves were generated for each rotor design, and were used to estimate a maximum rotor Cp. These results are presented in Table 9 for the Darrieus rotor designs. The general trend is that maximum rotor aerodynamic efficiency increases with rotor solidity. Solidity is increased by the addition of blade taper (in the present design study), by increasing the number of blades for a fixed blade chord, or by increasing the blade chord for a fixed number of blades. Increasing the solidity, however, comes at the price of lower maximum RPM, as shown in Table 10. Lower RPM leads to higher torque, which increases the cost of the drive train.

Darrieus rotor power curves are presented in Figure 71 through Figure 74. Figure 71 shows the effect of blade chord taper on the power curve. Tapering increases the aerodynamic efficiency in region two, primarily because the manner in which tapering was applied increased the rotor solidity. Figure 72 shows the power curves for no blade taper, with varying number of blades and blade chord. Performance is again shown to be a function primarily of blade solidity. The solidity of the two-bladed, large-chord design is the same as that of the three-bladed, small chord design, and the power curves for those two designs match prior to stall. Similar trends are evident in the power curves for single- and double-tapered rotor designs.

Table 9. Maximum rotor power coefficient for the Darrieus rotor designs.

	2B, SC	2B, LC	3B, SC	3B, LC
No Taper	0.36	0.42	0.42	0.47
Single Tapered	0.39	0.45	0.46	0.49
Double-Tapered	0.43	0.48	0.50	0.52

Table 10. Maximum rotor RPM for the Darrieus rotor designs.

	2B, SC	2B, LC	3B, SC	3B, LC
No Taper	8.95	7.70	7.80	6.75
Single Tapered	8.55	7.45	7.50	6.50
Double-Tapered	8.25	7.20	7.20	6.30

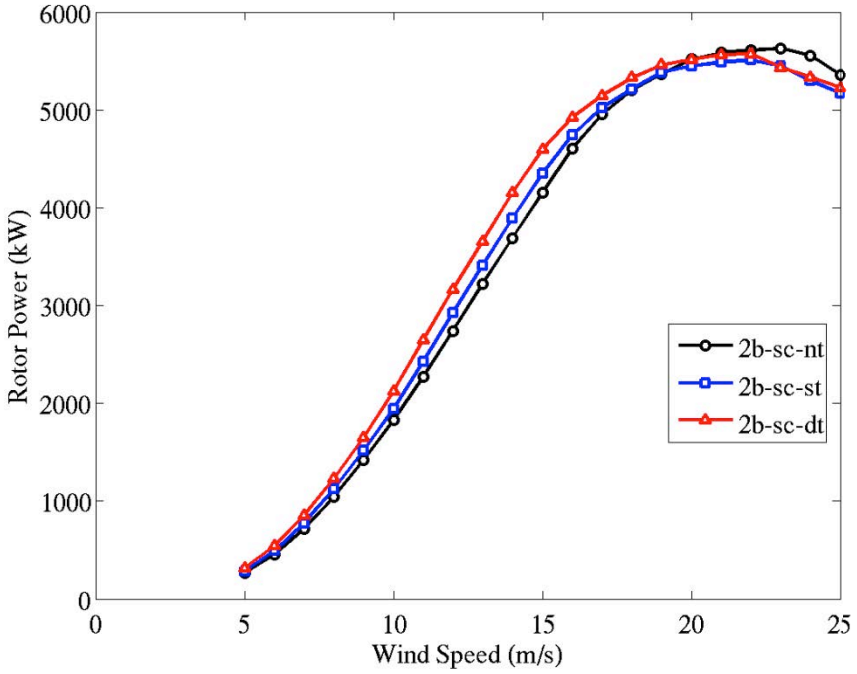

Figure 71. Power curves for Darrieus rotors, two-bladed, small-chord designs.

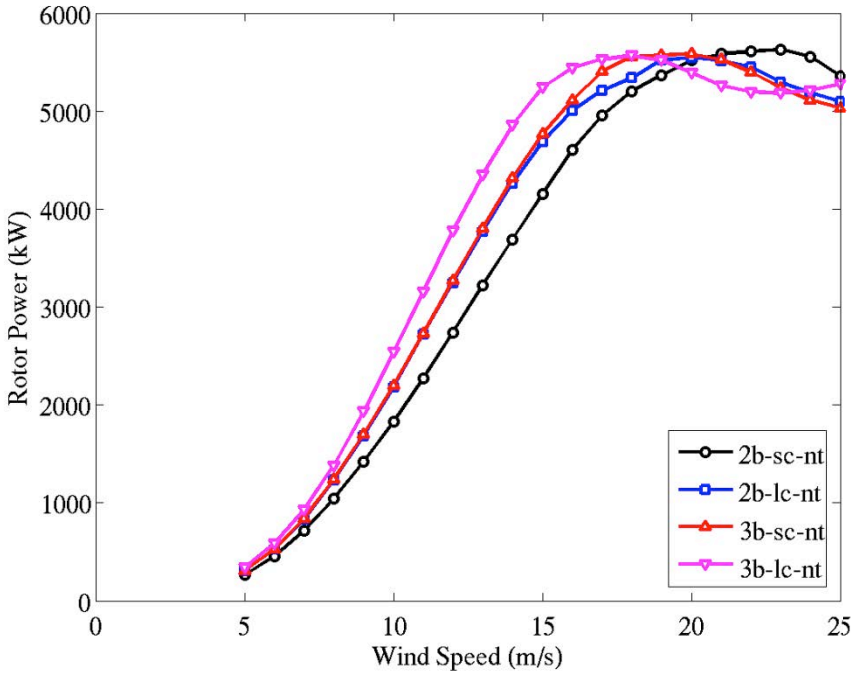

Figure 72. Power curves for Darrieus rotors, untapered designs.

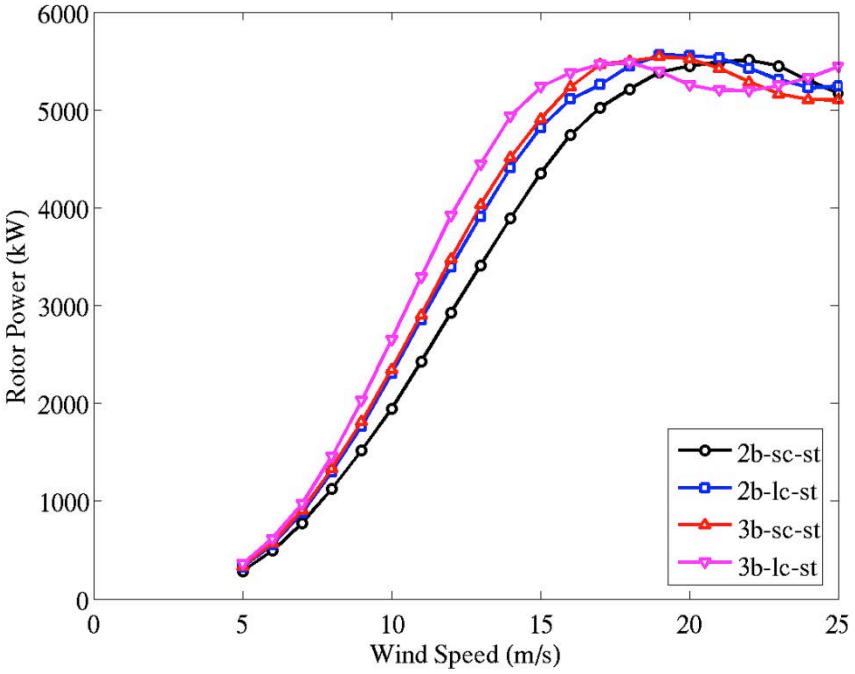

Figure 73. Power curves for Darrieus rotors, single-tapered designs.

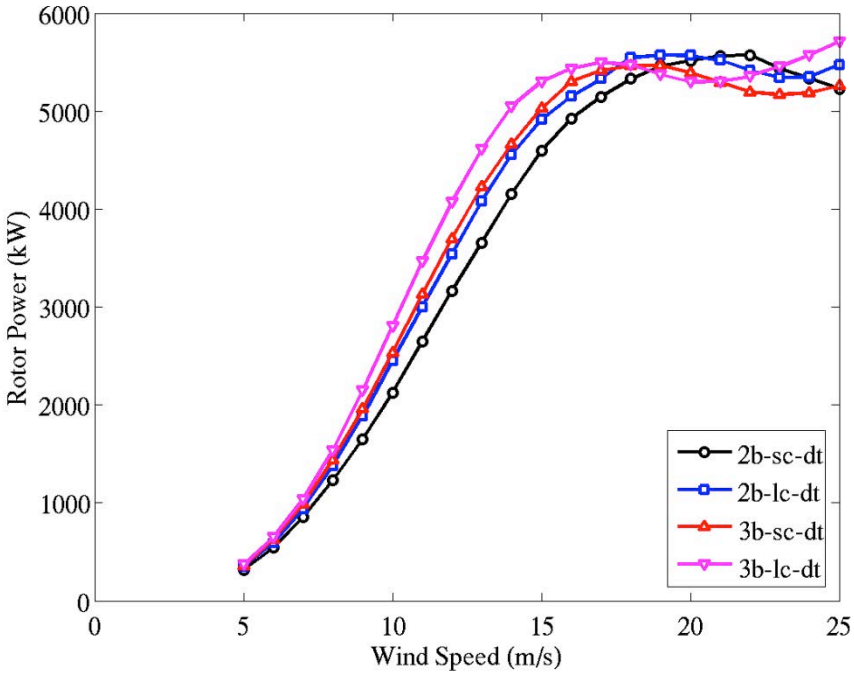

5

Figure 74. Power curves for Darrieus rotors, double-tapered designs.

3.3.3. V-VAWT Rotor Performance

Twelve V-VAWT rotors were analyzed, each design comprised of a unique combination of blade chord, number of blades, and blade power law shape exponent, n.

Table 11 shows the maximum power coefficient for the V-rotor designs. There is no discernable trend of max Cp with blade shape exponent, n. For the lowest solidity designs (two-bladed, small chord), the max Cp decreases with increasing n, while for the highest solidity designs (three-bladed, large chord), the max Cp increases with increasing n. For intermediate solidity, there is no clear variation with n, keeping in mind that there is an uncertainty of +/0.01 in these max Cp values due to a limited number of calculation points from which the maximum is estimated. The overall range of max Cp values for the V-rotors is 0.42 – 0.54. This is compared to the range of max Cp values for the Darrieus designs of 0.36 – 0.52. This suggests the V-rotor configuration has a small advantage in aerodynamic efficiency. This advantage is not large enough to eliminate one configuration in favor of the other; rather, it is much more likely that other design considerations, such as structural, dynamical, and/or platform costs will determine the most economical rotor configuration.

Table 11. Maximum rotor power coefficient for the V-rotor designs.

	2B, SC	2B, LC	3B, SC	3B, LC
n=1	0.46	0.47	0.50	0.49
n=3	0.44	0.49	0.51	0.53
n=5	0.42	0.48	0.49	0.54

Table 12 gives the maximum rotor RPM for the V-rotor designs. The trend of increasing maximum RPM with decreasing solidity is again evident. The maximum RPM range for the V-rotor designs is very similar to that of the Darrieus designs.

Table 12. Maximum rotor RPM for the V-rotor designs.

	2B, SC	2B, LC	3B, SC	3B, LC
n=1	8.80	7.65	7.70	6.70
n=3	8.65	7.50	7.50	6.55
n=5	8.50	7.40	7.40	6.45

Figure 75 shows the power curves for the V-rotor designs with smaller value of blade chord. The increased aerodynamic efficiency in region two for smaller n is seen here, although as noted in the discussion of Table 11 this trend is reversed for higher-solidities. The n=1 design has a more gradual stall characteristic than the other two designs, although too much should not be read into this given the uncertainties associated with modeling of dynamic stall for VAWTs. Figure 76 through Figure 78 show the power curves for the V-rotors, grouped by shape exponent. Again, like the Darrieus rotors, higher-solidity rotors are able to extract more power in region two.

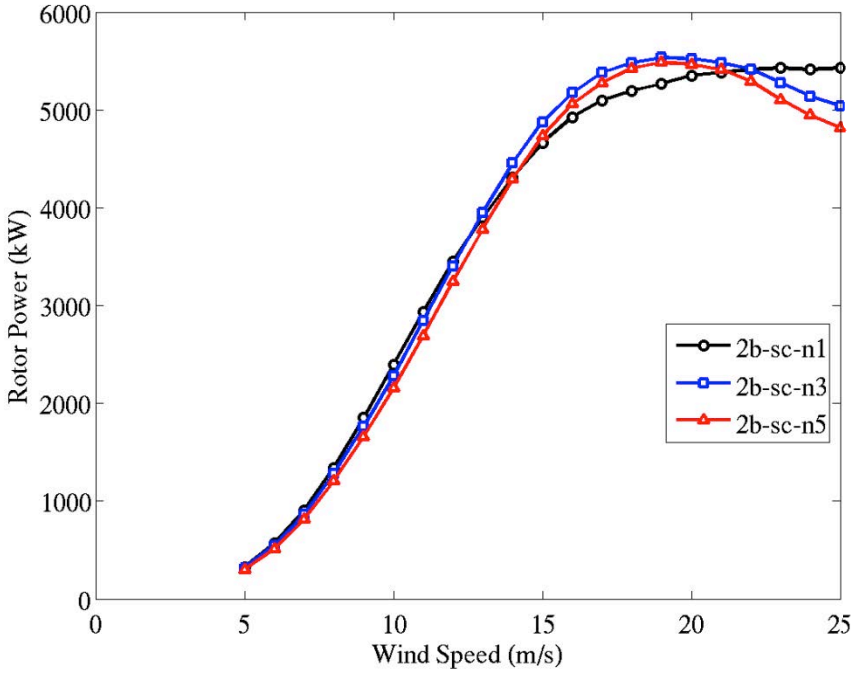

Figure 75. Power curves for V-rotors, two-bladed, small chord designs.

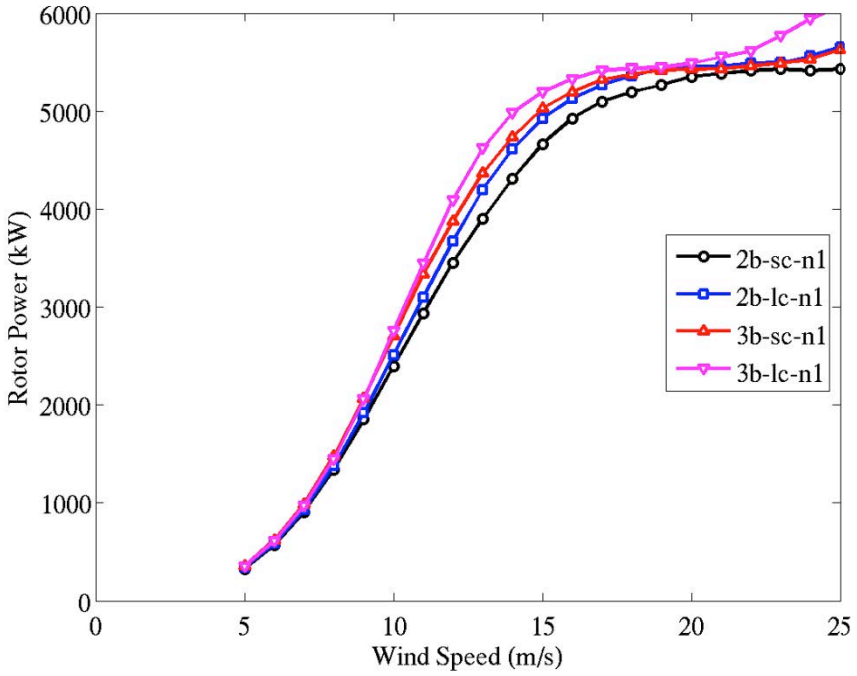

Figure 76. Power curves for V-rotors, n=1 designs.

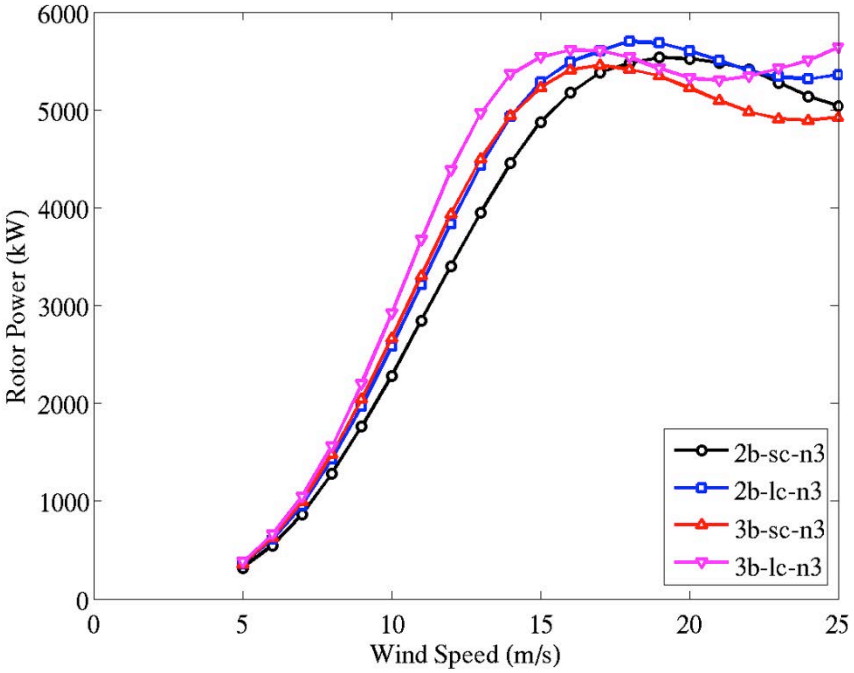

Figure 77. Power curves for V-rotors, n=3 designs.

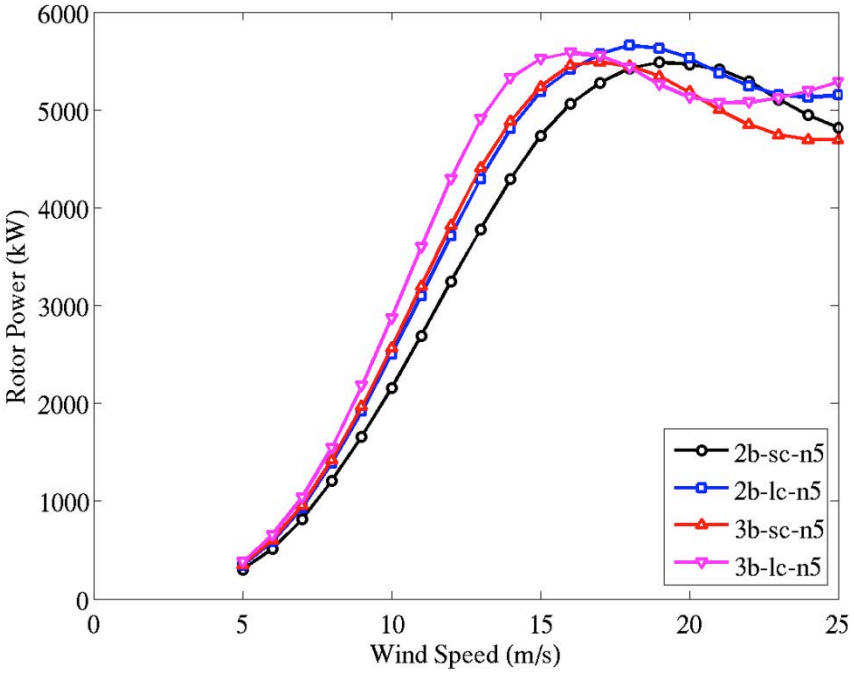

Figure 78. Power curves for V-rotors, n=5 designs.

3.4. Structural Dynamics/Aeroelastic Analysis

After the initial scoping of designs, detailed aeroelastic analysis of a subset of configurations was considered. For the Darrieus designs, up-scaled versions of the Sandia 34-meter VAWT were selected. In particular, the following Darrieus configurations were chosen for detailed aeroelastic analysis:

- Carbon 2-bladed large chord, double taper Darrieus (DC2LCDT)
- Carbon 3-bladed large chord, double taper Darrieus (DC3LCDT)
- Glass 2-bladed large chord, double taper Darrieus (DG2LCDT)
- Glass 3-bladed large chord, double taper Darrieus (DG3LCDT)

These configurations employed tower-to-blade struts that were located at 10% and 90% of the blade span.

Many of the V-VAWT designs proved to be at a structural disadvantage compared to the Darrieus designs. The large scale of the machine, lengthy strut components, and lack of blade-to-tower connection at the top of the machine (such as that of the Darrieus design) resulted in configurations with a high degree of flexibility. This along with increased centrifugal body loads due to increased machine radius, made structural design of feasible configurations challenging. Nevertheless, two of the more promising V-VAWT configurations were selected for detailed aeroelastic analysis:

- Carbon 2-bladed large chord, n=5 power law blade profile V-VAWT (VC2N5LC)
- Carbon 3-bladed large chord, n=5 power law blade profile V-VAWT(VC3N5LC)

These configurations employed tower-to-blade struts that were located at 50% (tower connection) and 70% (blade connection) blade span respectively.

3.4.1. Aerodynamic Loads

Previous aerodynamic analysis of VAWT configurations at cut-out (25 m/s uniform, steady wind speed) was considered in aeroelastic analysis. The rotor speed at cut-out is related to rotor solidity and operating rotor speeds for the VAWT configuration were prescribed to be consistent with those specified in Table 10 and Table 12. The aerodynamic loads experienced at cut-out are expected to be the largest under normal operating conditions. Future aeroelastic analysis can consider irregular conditions such as gust and turbulent winds.

The aerodynamic loads calculated via the CACTUS aerodynamics code were mapped from the aeroelastic domain to the structural domain as generalized forces to be applied to the structural dynamic model in OWENS. This provided a one-way aeroelastic coupling in which aerodynamic loads cause structural motion. Future analysis can consider two-way coupling as analysis capabilities are enhanced.

3.4.2. Structural Displacements of Selected Configurations at Cut-Out Operating Condition

Aeroelastic analysis was performed on the selected configurations using a coupling between the OWENS structural dynamics software and CACTUS aerodynamics software. Body forces such as gravitational and centrifugal effects were also included in the analysis and modal damping of 2%

was employed. The implicit Newmark-Beta time integration (constant averaged acceleration scheme) was utilized with a time step of 0.05 seconds. This time step is adequate for design studies given the low frequency structural motion and low frequency aerodynamic forcing observed in this analysis.

Results of structural dynamics analysis of the selected configurations at cut-out under aerodynamic loads are presented below. In particular, the tower top motion and blade displacements are considered. For Darrieus designs the blade mid-span is examined, and for V-VAWT designs the blade tip is examined. These areas typically have the largest displacements for the VAWT configurations considered in this study.

Table 13 shows maximum displacement values for the six VAWT configurations considered for aeroelastic analysis. Given the scale of the designs, all displacements are relatively small and Table 14 presents the percent deflection of the tower top relative to the tower height and percent deflection of the blade mid-span relative to the half span for the Darrieus designs and relative to the full blade span for the V-VAWT designs. The time histories of tower top and blade mid-span displacements of the Darrieus designs are shown in Figure 79 and Figure 80 respectively. Time histories of tower top and blade mid-span displacements of the V-VAWT designs are shown in Figure 81 and Figure 82 respectively.

Overall, the Darrieus designs perform well in minimizing structural deflections under aerodynamic loads at cut-out conditions. The lowest performing configuration was the glass, two-bladed large chord design (DG2LCDT) with a maximum tower displacement of 7.5m and maximum blade mid-span displacements of 4.4 meters. These were deflections (as shown in Table 14) of 5.7% and 6.7% respectively. The remaining Darrieus configurations performed well with tower top deflections of 2% or less and blade mid-span deflections of 3.6% or less. The two V-VAWT configurations considered also performed well with very minimal tower top displacements (0.2m) due to the lower tower length (52m) of these designs. Blade end deflections were also minimal with deflections of 1.9% or less.

Table 13. Maximum displacement of selected configurations

Configuration	Max Tower Top Displacement (m)	Max Blade Total Displacement (m)	Max Blade Radial Displacement (m)	Max Blade Edgewise Displacement (m)
DC2LCDT	2.14	2.05	1.33	1.69
DC3LCDT	2.68	2.35	1.36	2.11
DG2LCDT	7.53	4.41	3.78	2.60
DG3LCDT	1.26	0.95	0.72	0.60
VC2N5LC	0.23	1.92	1.43	1.33
VC3N5LC	0.23	1.66	1.22	0.96

Table 14. Percent deflections of selected configurations

Configuration	% Deflection of tower top	%Deflection of blade mid-span
DC2LCDT	1.6	3.1
DC3LCDT	2.0	3.6
DG2LCDT	5.7	6.7
DG3LCDT	1.0	1.4
VC2N5LC	0.4	1.9
VC3N5LC	0.4	1.6

These trends are shown in greater detail in Figure 79 through Figure 82. The time scale in these plots is normalized by the rotor period since the operating speed for each configuration is different. In these figures some initial transients due to the starting of the simulation are visible. These initial transients are damped out within the first few rotor revolutions and a period solution is observed due to the steady, uniform winds and development of the wake in the aerodynamic simulation.

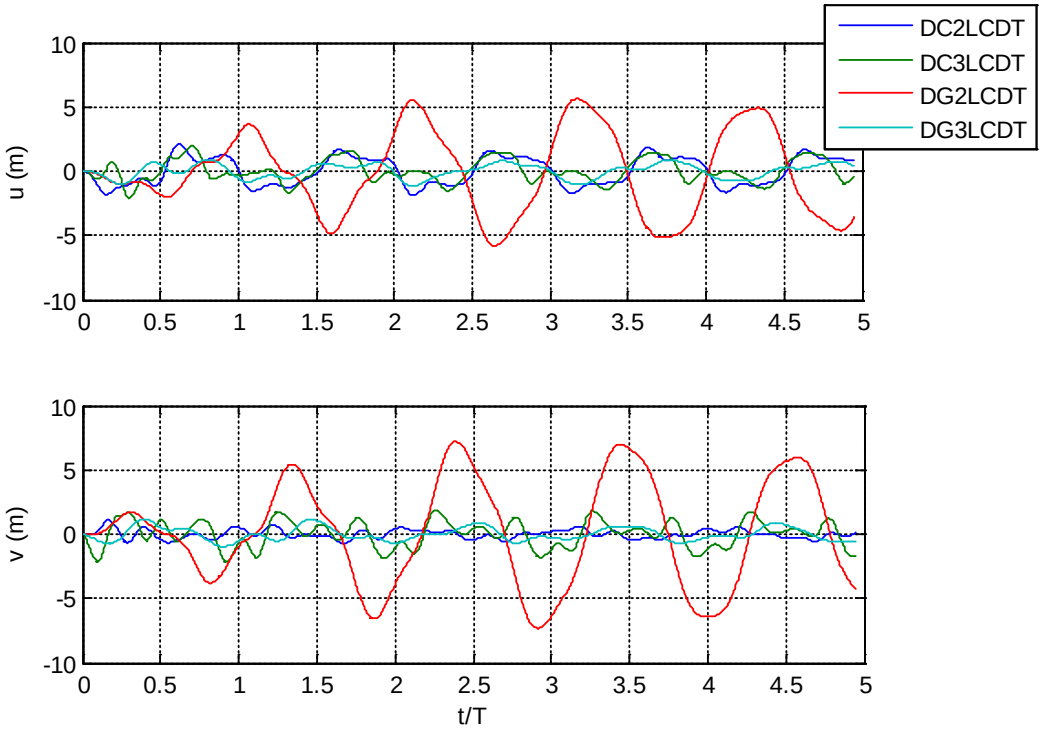

Figure 79. Tower top displacements for selected Darrieus designs.

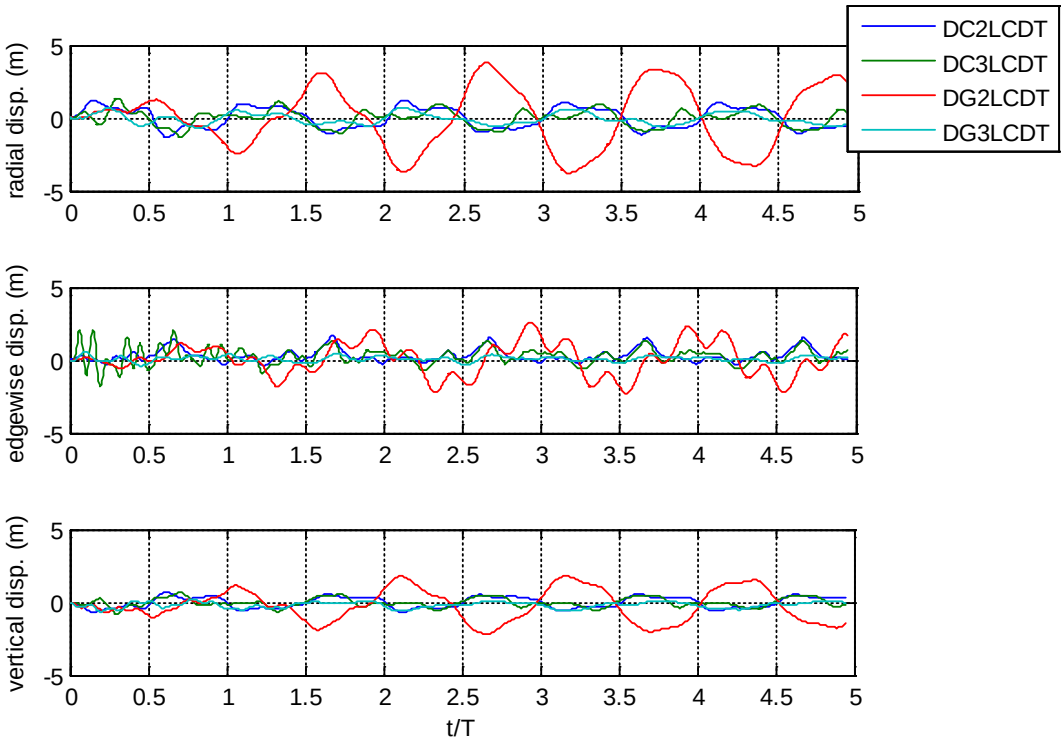

Figure 80. Blade mid-span displacements for selected Darrieus designs.

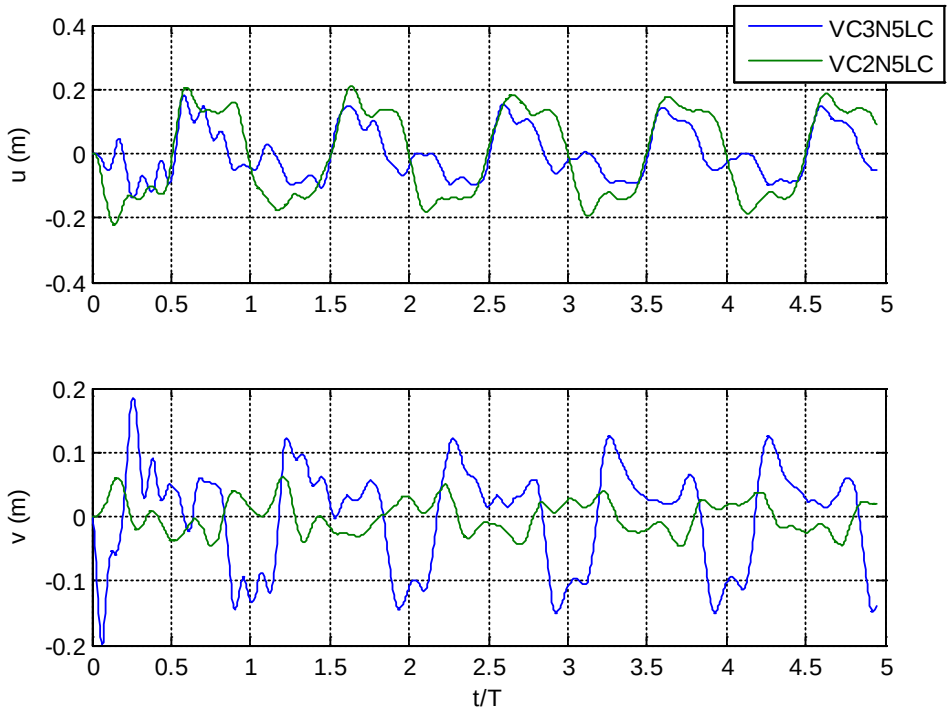

Figure 81. Tower top displacements for selected V-VAWT designs.

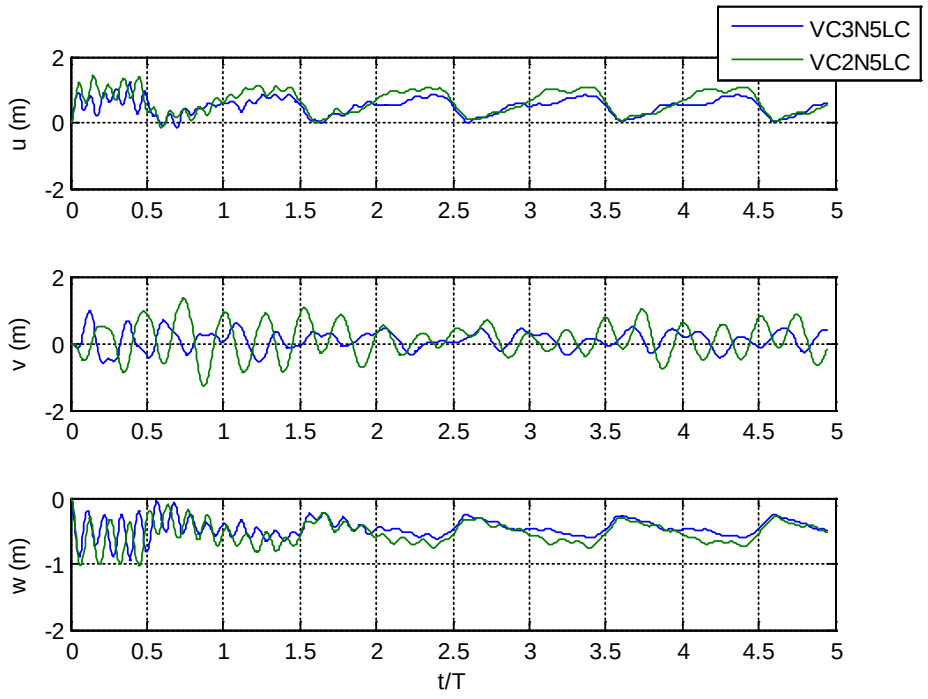

Figure 82. Blade mid-span displacements for selected V-VAWT designs.

3.4.3. Structural Strain of Selected Configurations at Cut-Out Operating Condition

The selected configurations were then examined for maximum strain under aerodynamic loads at cut-out. As with the previous study on structural displacement, strain is a temporally and spatially varying quantity. To succinctly characterize performance with respect to strain, the maximum tensile and compressive strains were examined at a select number of cross-sectional locations depicted in Figure 83. Namely, trailing edge (CS-A), the upper surface (CS-B), leading edge (CS-C), and lower surface (CS-D) of the blade cross-sections were considered. Using these four cross-sectional locations, the maximum and minimum axial strain was examined throughout the simulated time history. This allowed the locations at which maximum strains occur to be identified for each configuration. Strain time histories were generated throughout the model at cross-sectional coordinates CS-A, CS-B, CS-C, and CS-D and maximum compressive and tensile strains are reported in Table 15. This table present maximum strains after two rotor revolutions to allow the structural response to reach a periodic state (i.e. initial transients have damped out). Cross-sectional CS-A had the largest strains due to edgewise bending and maximum strains from flapwise bending could occur at either CS-B or CS-D. For the Darrieus configurations the maximum compressive strain at CS-A typically occurred around the blade mid-span and maximum tensile strain at CS-A typically occurred above the lower strut connection on a blade. Maximum compressive strain at CS-B and CS-D typically occurred near the blade mid-span and maximum tensile strain typically occurred in the vicinity of strut connections on blades. For V-VAWT configurations the maximum strain due to edgewise bending typically occurred at CS-A in the vicinity of a blade to strut connection and maximum strain due to flapwise bending typically occurred at CS-D at the blade root.

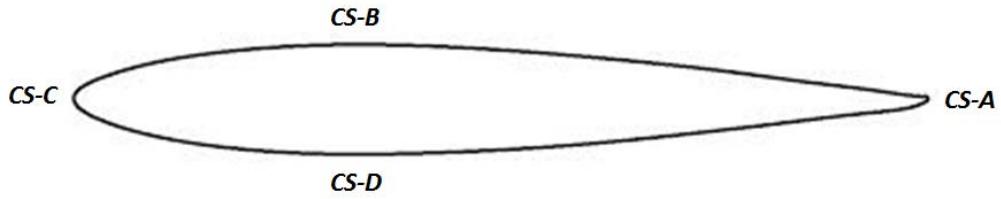

Figure 83. Cross-sectional locations examined for strain extrema.

Table 15. Maximum axial strains of selected configurations at selected cross-sectional coordinates (microstrains)

Configuration	CS-A		CS-B		CS-C		CS-D	
	Max Comp.	Max Tensile	Max Comp.	Max Tensile	Max Comp.	Max Tensile	Max Comp.	Max Tensile
DC2LCDT	-2800	2500	-570	500	-100	660	-540	480
DC3LCDT	-2500	2400	-560	450	-930	610	-540	510
DG2LCDT	-4300	4900	-1800	2000	-1600	1500	-1900	2000
DG3LCDT	-653	720	-750	970	-200	300	-900	830
VC2N5LC	-430	530	-750	680	-210	150	-550	720
VC3N5LC	-250	230	-620	350	-110	50	-415	630

Inspection of Table 15 shows that for Darrieus configurations, the maximum tensile strain due to edgewise bending is 2500 microstrain or less except for the two-bladed glass design which has a maximum tensile strain of 4900 microstrain (See Section 3.2.9.2 for a discussion on strain allowables). Similar trends are observed for maximum edgewise compressive strains. Maximum tensile strain due to flapwise bending is below 970 microstrain for all Darrieus configurations except for the 2-bladed glass design which has a maximum flapwise bending tensile strain of 2000 microstrain. Again, similar trends are seen for maximum compressive strain from flapwise strain. Overall, the selected designs maintain minimal levels of strain under aerodynamic and body loads at the cut-out operating condition. Figure 84 and Figure 85 show the strain histories for the maximum tensile strains in the selected Darrieus designs at cross-sectional locations CS-A and CS-B/CS-D respectively.

Inspection of Table 15 also shows that the selected V-VAWT designs maintain minimal strain levels at cut-out conditions. For these configurations maximum tensile strains due to edgewise bending were at or below 530 microstrain and similar trends were observed for compressive strains. Maximum tensile strains due to flapwise bending were at or below 720 microstrain with similar trends observed for compressive strains. Figure 86 and Figure 87 show the strain histories for the maximum tensile strains in the selected Darrieus designs at cross-sectional locations CS-A and CS-D respectively.

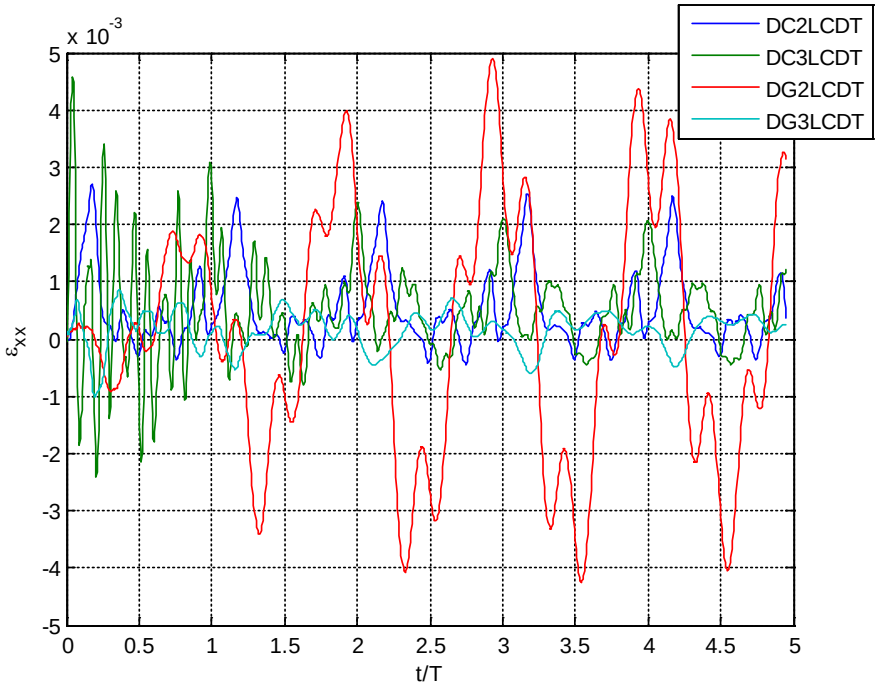

Figure 84. Axial strain at location of maximum tensile strain (CS-A) for selected Darrieus designs.

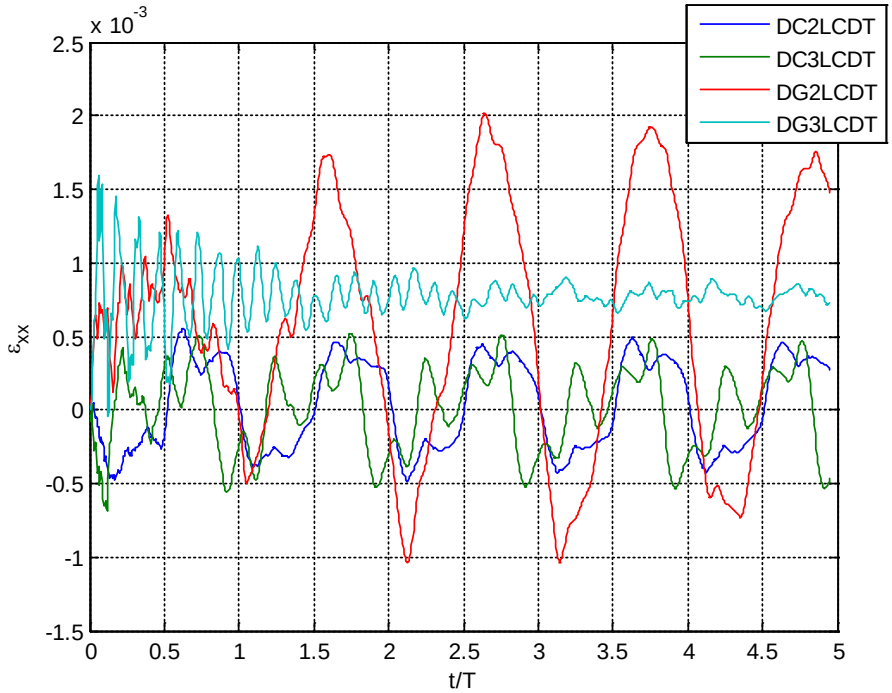

Figure 85. Axial strain at location of maximum tensile strain (CS-B or CS-D) for selected Darrieus designs.

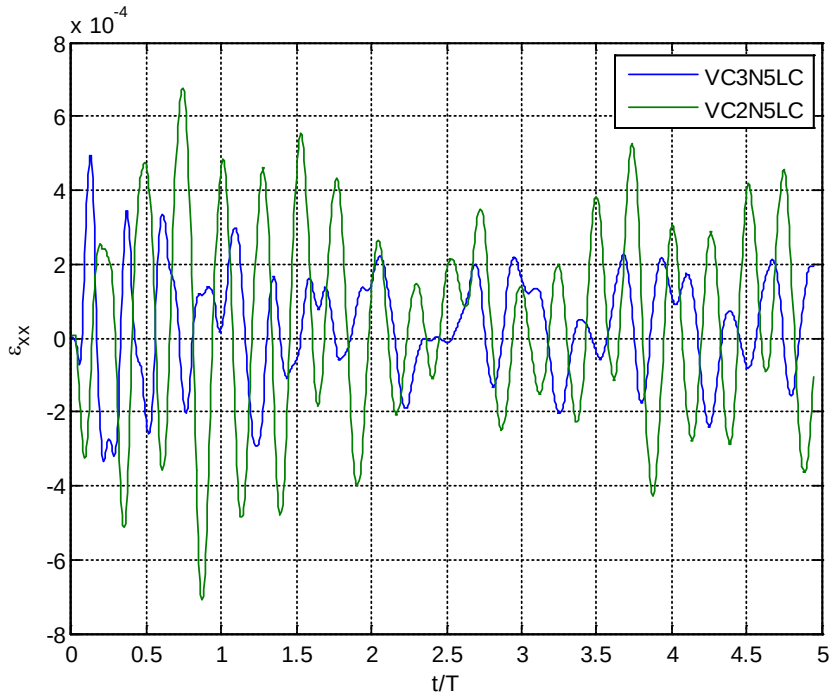

Figure 86. Axial strain at location of maximum tensile strain (CS-A) for selected V-VAWT designs.

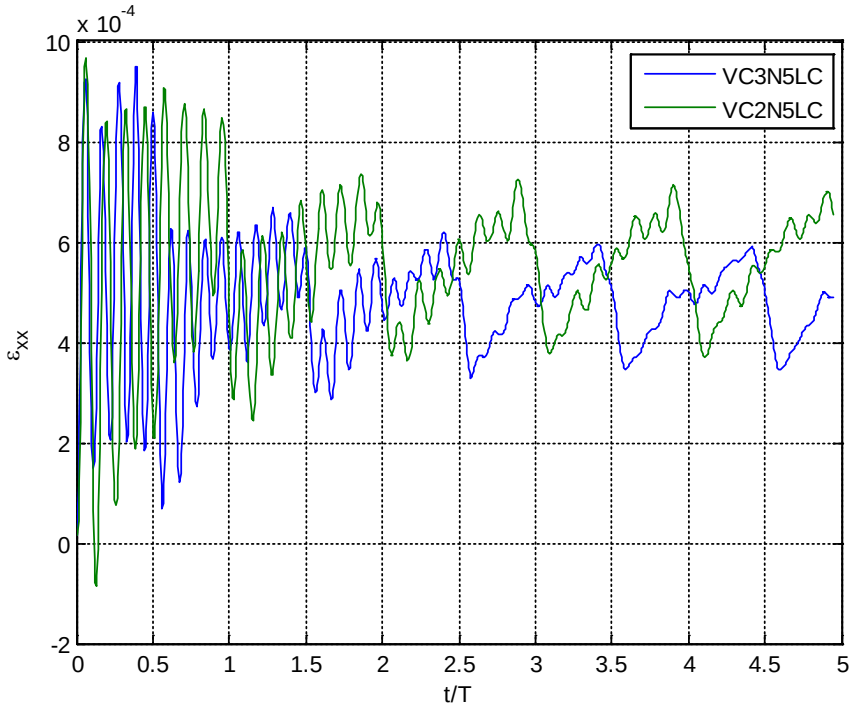

Figure 87. Axial strain at location of maximum tensile strain (CS-D) for selected V-VAWT designs.

3.5. Platform Design Study

As with any new technology, the cost of developing a floating offshore wind turbine is high. Not only is the cost of the substructure significant, but the nature of the deep water offshore environment means that installation, operations, and maintenance costs are also higher than land-based counterparts. The most significant capital cost associated with an offshore wind turbine farm is the balance of station (BOS). An assessment by NREL estimates that while a land-based wind farm may have 23% of the total cost allocated to BOS, an offshore wind farm is closer to 52% (Figure 88 and Figure 89) (26). Methods of reducing these expenditures could greatly reduce the levelized cost of energy (LCOE) for an offshore wind project. Sandia National Laboratories (SNL) and its partners believe that vertical axis wind turbines (VAWTs) offer multiple advantages over other rotor configurations for reducing the BOS for offshore wind turbines. Figure 90 shows potential substructure configurations for offshore turbines. The unique arrangement of a VAWT allows the heavy generator and related components to be located at the base of the tower as opposed to the top, as is typical of a horizontal axis wind turbine (HAWT). This configuration lowers the topside vertical center of gravity, which may reduce the size and cost of the floating platform. Additionally this configuration locates high maintenance systems close to the ocean surface thus increasing maintainability to potentially reduce LCOE.

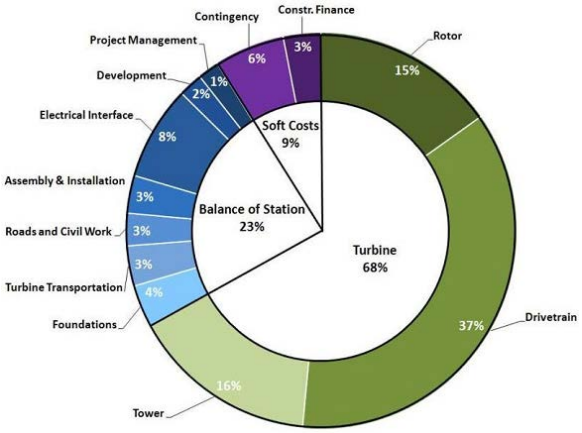

Figure 88. Land-based wind farm, installed capital costs. (26)

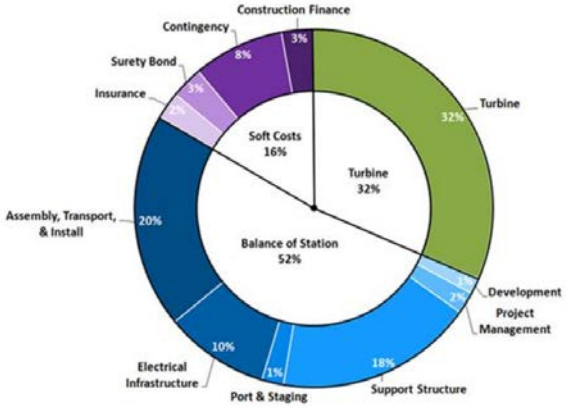

Figure 89. Offshore wind farm, installed capital costs. (26)

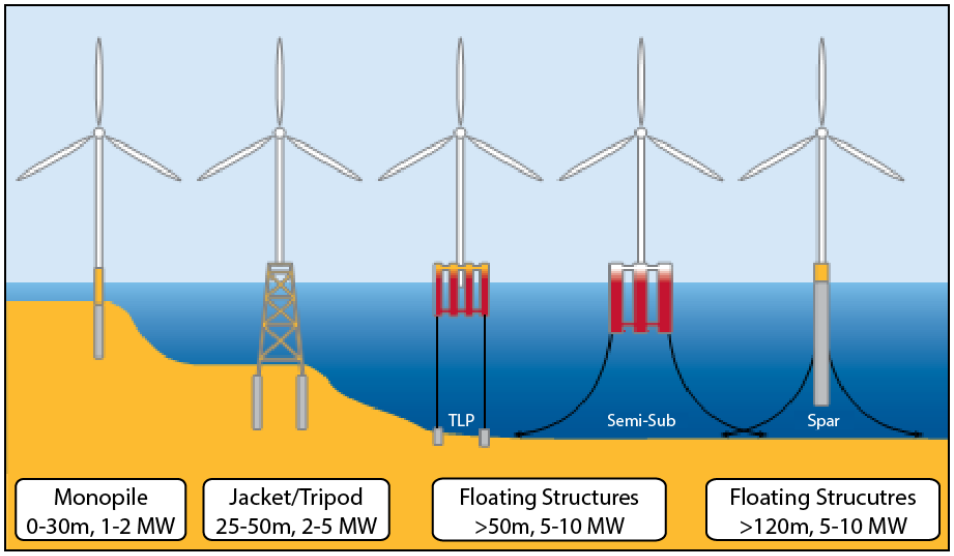

Figure 90. Wind turbine substructure classes. (27)

The goal of this study is to explore the costs of a 5 MW floating offshore VAWT and investigate potential BOS cost savings. To this end, a range of 5 MW VAWT topsides was determined based on Darrieus and V-VAWT designs (as detailed in previous sections) utilizing a variety of geometries, blade materials, and strut arrangements as described in the previous sections. Various conceptual VAWT designs are shown in Figure 29.

For this platform design study, the topside design space is parameterized by the topside mass and pertinent design characteristics are defined as functions of the topside mass where possible. Two types of floating support platforms are considered, one being a spar design similar to the OC3 Hywind spar and the other a semi-submersible similar to the WindFloat semi-submersible. For each topside in the design space, a spar and a semi-submersible platform is designed using a sizing spreadsheet that scales these existing proven platform concepts. These designs are then used to determine the mass and cost of the platform, focusing on the most significant BOS cost categories of support structure construction, mooring, system assembly, transportation, and installation. A comparable 5 MW HAWT design is also included for comparison.

3.5.1. Rotor Topsides for the Platform Design Study

3.5.1.1. HAWT Topside

The topside for the HAWT comparison is based on the NREL 5 MW HAWT (28). The HAWT topside has a mass of 600,000 kg with a CG of 70.4 m above the still water line (SWL). Note that the 600,000 kg topside mass used here is lower than the 697,500 kg specified in (28). This is because the original turbine was designed utilizing land-based turbines and uses a heavier tower. For an offshore application, the tower will likely be lightened and comparable to the OC3 Hywind tower. Therefore, for the HAWT topside in this study, a tower similar to the OC3 Hywind is used, resulting in a lower mass of 600,000 kg for the turbine and tower combined (29). The primary moments of inertia in pitch and roll about the topside CG are 5.8e8 kg-m2. The aerodynamic thrust load is 825.0 kN with a center of pressure of 90.0m above the SWL.

Table 16. HAWT topside configuration

Mass (kg)	CG (m) above SWL	Roll Inertia (kg-m^2) about CG	Pitch Inertia (kg-m^2) about CG	Aerodynamic Thrust Load (kN)	Center of Pressure (m)
600,000	70.4	5.8 x 10^8	5.8 x 10^8	825.0	90.0

3.5.1.2. Preliminary VAWT Topside

Early on in the study, characteristics of a VAWT designed for a 5 MW application were determined by scaling an existing Darrieus design. This rotor topside wasn't optimized for use on a floating platform, but was used as a starting point for the initial platform design studies. For reference, this topside is referred to as the "preliminary VAWT" configuration and specifics are shown in Table 17 below. This configuration is also highlighted in the overall design envelope shown in Figure 91 and Figure 92.

Table 17. Preliminary VAWT Configuration

Mass (kg)	CG (m) above SWL	Roll Inertia (kg-m^2) about CG	Pitch Inertia (kg-m^2) about CG	Aerodynamic Thrust Load (kN)	Center of Pressure (m)
973,000	54.9	3.77 x 10^8	2.32 x 10^9	550.0	67.0

3.5.1.3. VAWT Topside Design Envelope

Once the preliminary sizing had been completed, the design envelope for the VAWT topsides was then defined by Sandia National Laboratories (30) and used to define the range of topsides considered in this study. The design power for the turbine was chosen to be 5 MW and all design variations maintain this power generation capacity. While there are currently two VAWT topside architectures being considered, a Darrieus (D-VAWT) and a V-VAWT, the D-VAWT design is encompassed by the V-VAWT design space in terms of the parameterizations of interest for this study (Figure 91). As such, the V-VAWT design space is used to parameterize both styles of VAWT. Based on earlier work, the key parameters that influence the floating platform design are the topside mass, center of gravity, aerodynamic load, and center of pressure. For the range of topsides considered here, the assumption is that the aerodynamic load and center of pressure remain constant over the range, but the mass, center of gravity, and primary moments of inertia about the topside CG (IPC=pitch and IRC=roll) will vary depending on the VAWT design. To parameterize the design space, the center of gravity and moments of inertia are treated as a function of the topside mass using a linear best fit (Figure 91). This allows the full range of VAWT topsides to be characterized using the topside mass as the independent variable (Figure 92). The circular markers on the graphs highlight the preliminary VAWT configuration. As the topside design matures, additional data on how the aerodynamic load and center of pressure vary with topside

mass could be used to parameterize these quantities in a similar manner. Additionally, more refined functional forms of the relationship between the design parameters could be established. Future work will consider a more rigorous definition of the topside design envelope utilizing more robust functional forms.

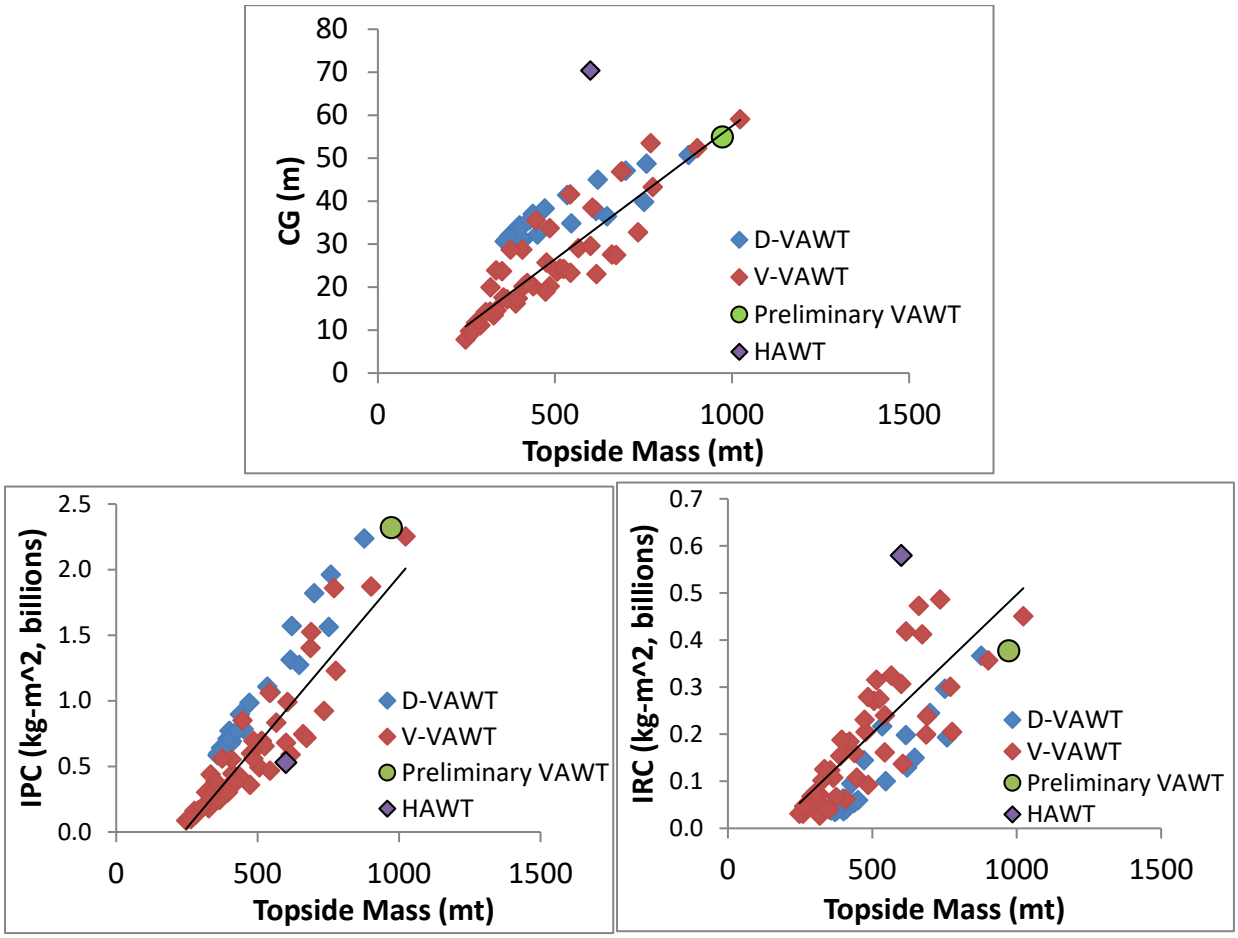

Figure 91. Topside CG, Pitch Moment of Inertia about CG (IPC) and Roll Moment of Inertia about CG (IRC) vs Topside Mass.

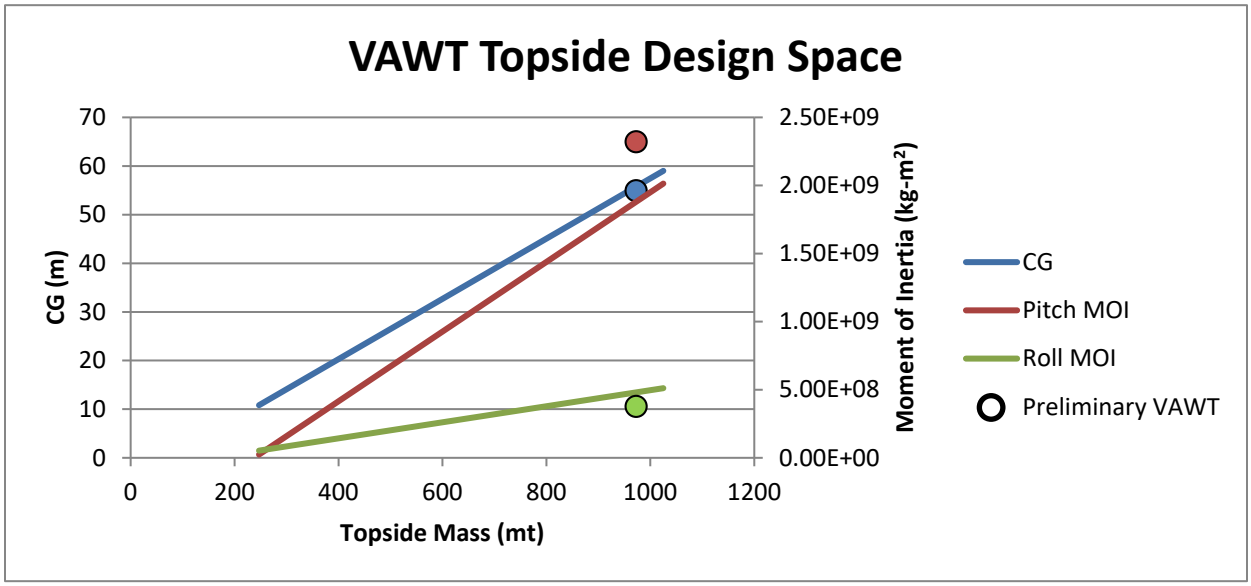

Figure 92. VAWT design space as a function of topside mass.

3.5.2. Platform Design Description

3.5.2.1. Overview

Designing the floating platform for an offshore wind turbine is a complicated process. As an emerging field, there is little to no historical data on floating offshore wind projects to leverage and few currently deployed systems. While experience with floating platforms designed for offshore oil and gas is applicable, the design conditions and operational requirements for a floating wind turbine are different than a floating oil production facility.

To facilitate this cost of energy analysis, two existing floating wind turbine platforms are utilized and adapted to meet the criteria of the VAWT. The baseline platform parameters are determined using a Froude number scaling approach based on achieving the desired system performance over the topside design space. The baseline platform designs are derived from existing floating platforms developed for horizontal axis wind turbines, namely the spar platform designed for use with the Offshore Code Comparison Collaboration (OC3) and DeepCwind programs and the WindFloat semi-submersible. These baseline designs are presented briefly and the scaling methods used are described. Using the topside design envelope defined above, a range of platforms are designed and the results presented. Both a spar and a semi-submersible type platform are designed for use with the VAWT topside and compared with comparable platforms designed for a HAWT.

3.5.2.2. Baseline Platform Designs

Again, two types of floating platform are considered, a semi-submersible and a spar. For the semi-submersible platform, a scaled 5 MW version of Principle Power's WindFloat platform was used as the baseline design. The original WindFloat is a three column semi-submersible with a draft of 23 m and displacement of 7,105,000 kg (31). The spar is based on the OC3 Hywind spar used in the OC3 study (29). The original OC3 Hywind spar is based on Statoil's Hywind spar, which is a demonstration floating offshore horizontal axis wind turbine on a spar and was deployed in 2009.

The OC3 Hywind spar is modified from the original, due to the heavier 5 MW topside, which results in a 120 m draft spar buoy with a total platform mass (including ballast) of 7,466,330 kg (29). While both of these platforms were designed for a HAWT, they provide an appropriate initial design for a VAWT of similar capacity (in this case all rotors having rated power of 5-MW). Both platforms are shown in Figure 93 below.

3.5.2.3. Platform Design Methodology

The approach for designing platforms covering the range of VAWT topsides is to apply Froude-scaling relationships to the baseline configurations described in the previous section. Additionally, the draft of the OC3 Hywind baseline is modified from 120 m to 80 m due to the 100 m deployment water depth of the chosen deployment site. As the end goal of this analysis is to determine the system cost, each platform is characterized by the mass of fabricated steel required as this represents the primary construction cost for the floating platform. The required mass of fabricated steel is proportional to the overall size of the platform and provides a reasonable parameter for the cost analysis. With the Froude-scaled approach, the geometry of the platform scales as the ratio of platform steel mass of the scaled design relative to the platform steel mass of the baseline design. This scaling relationship applies equally to each of the gross platform design parameters (draft, column diameter, etc.) and has been coded into an excel spreadsheet for use in this study.

a) b)

Figure 93. a) WindFloat Semi-Submersible (31) and b) Hywind Spar (32).

As described earlier, the topside design envelope was defined as a function of the topside mass. To create data for use in the sizing spreadsheet, this function was discretized at intervals of 1,000 kg of topside mass, starting at the lightest topside of 247,000 kg and ending with the heaviest at 1,025,000 kg. This resulted in 779 design points, each with a unique center of gravity and moments

of inertia based on their mass. To adequately cover the design envelope, the sizing spreadsheet was used to design a scaled platform for each of these topside data points. This process was performed for both the spar and semi-submersible platform type. For the initial study, platforms were designed for the preliminary VAWT topside. These platform designs served as the initial platform sizing and are referred to as the preliminary platform designs. For the HAWT design there is only a single topside data point, so only a single spar and semi-submersible platform was designed.

As described earlier, the design parameter for each platform is the required mass of fabricated steel. Due to the Froude-scaled nature of the design process, this mass is related to the design parameters of the platform as well as the dynamic and static stiffnesses of the system. By manipulating the platform fabricated steel mass, the performance of the system can be adjusted to meet the performance characteristics specified. For floating offshore wind turbines, two of the most important performance characteristics are the mean heel angle due to the design wind load and the dynamics of the platform motion. For an operating turbine, the mean heel angle is limited to 5° to prevent loss of power generation capacity due to an excessive reduction in turbine frontal area. To control the platform dynamics, the natural frequencies of the system need to be outside of the primary wave energy range. In this case, the pitch and roll periods are ideally between 30-40 seconds. Using these design conditions, an appropriately sized platform is determined for each topside in the design envelope using the scaling relationships in the sizing tool.

3.5.2.4. Platform Design Results

The results of the platform design are presented below. As can be seen in the graphs of Figure 94 and Figure 95, for the largest topsides the controlling parameter is limiting the pitch period to fewer than 40 seconds. However, as the topside mass decreases, the controlling parameter begins to shift towards keeping the mean pitch angle fewer than 5 degrees. As the topside keeps decreasing in mass, the pitch period keeps decreasing while maintaining a constant pitch angle. After a certain point, depending on the platform type, the pitch period drops below 30 seconds. At this point, there is no more design work that can be accomplished with the scaling relationships in sizing spreadsheet as decreasing the platform steel mass will lower both the pitch angle and the pitch period. Therefore, both parameters can't be satisfied once the topside becomes too light. It was chosen to maintain the pitch angle and let the pitch period continue to fall, to demonstrate the trend as shown in the regions where the pitch period drops below 30 seconds and the 5 degree pitch angle is maintained. For these light-weight topsides it is recommended that a more specialized platform design be considered instead of scaling a baseline design. Results for the preliminary VAWT design are shown with circular marks and the HAWT design is shown as diamond marks on each graphs.

Additionally, the 600-mt refined HAWT platform was designed to have the same performance as the VAWT design in an effort to provide a similar basis for comparison. As a result of applying the same performance constraints on pitch angle and pitch period to the VAWT and the refined 600-mt HAWT topside having a higher CG, larger aerodynamic load and higher center of pressure than the VAWT, the size of the platform for the refined HAWT must increase to provide a similar level of performance. This is shown in the figures below by comparing the diamond markers for the refined HAWT design with the design curves for the VAWT design at 600-mt topside mass.

Table 18 shows results for a few of the platform designs with comparison of the platform masses for 3 rotor topsides (again with the same rating of 5-MW). These rotor topsides include the

preliminary 973mt VAWT, a 600mt HAWT (which, as discussed above, is a lighter offshore version of the NREL 5MW HAWT), and a 600mt VAWT. Even though the topside mass is higher for the 973mt VAWT, the required platform mass for the HAWT is significantly higher due to its higher vertical CG and larger aerodynamic overturning moment. Additionally, it can be noted that when the rotor topside mass of the VAWT is reduced (from 973 to 600mt) the platform steel mass is significantly reduced. Additional details regarding the platform study and system-level design trade-offs can be found in (33) (34).

A visual comparison of the scaled platforms is shown in Figure 96 for three different design points. The design points were taken to represent the range of topsides and include the 973-mt Preliminary VAWT at the upper end, a 600-mt VAWT which matches the HAWT topside mass, and a 273-mt VAWT which is the lightest VAWT topside considered. Basic dimensions are shown to illustrate the scaling relationship. Details of hydrodynamic analysis of platform designs using WAMIT are discussed in Appendix A.

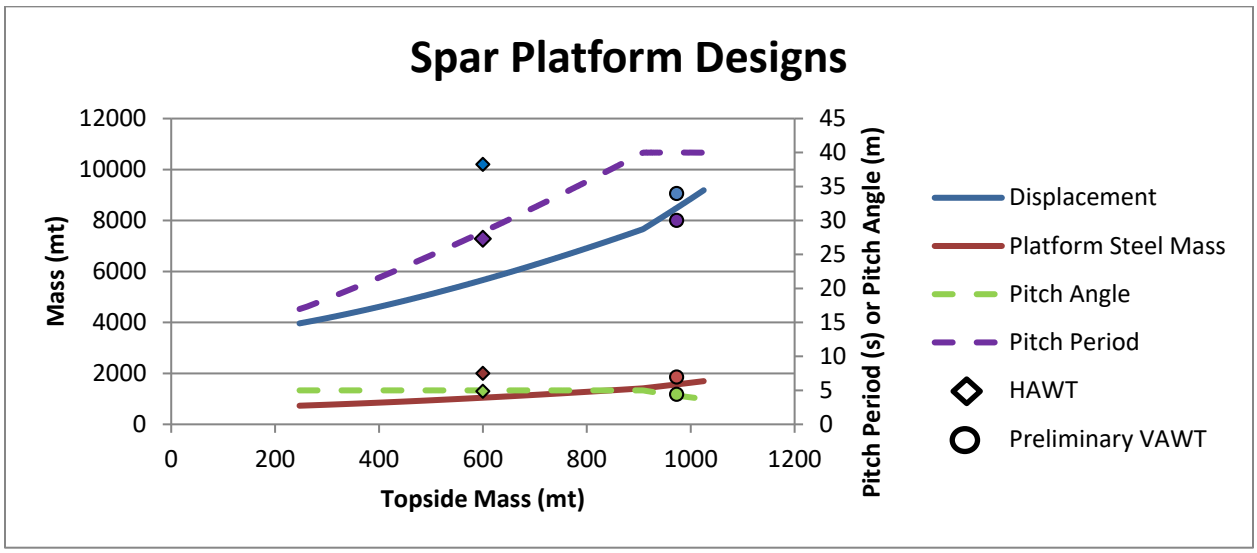

Figure 94. Spar platform design results.

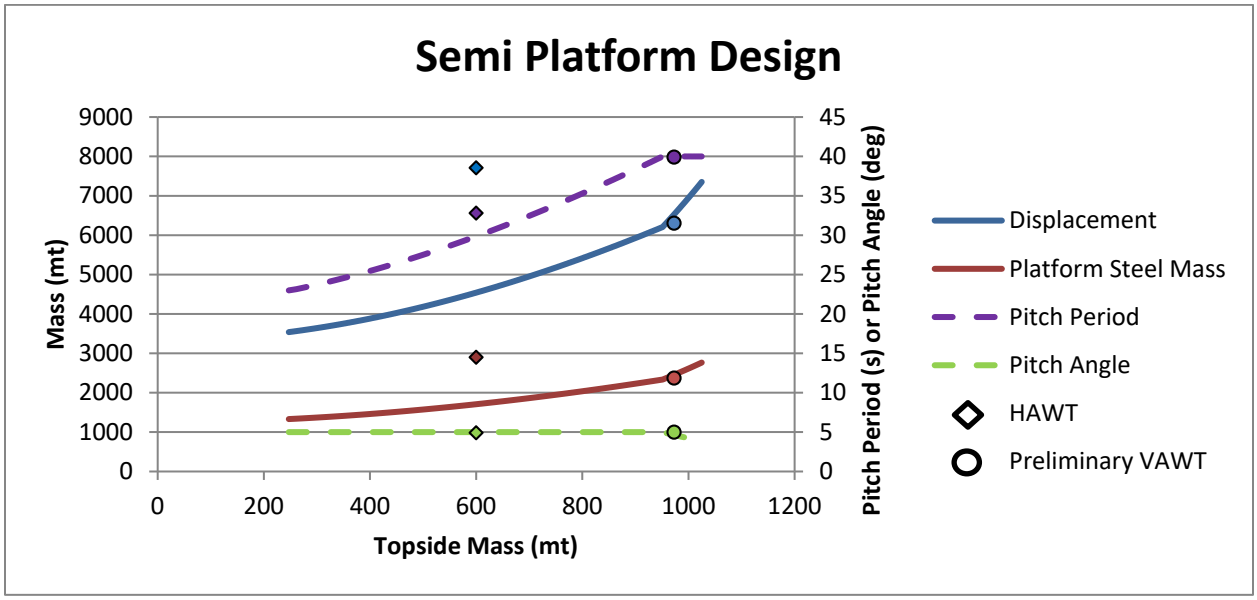

Figure 95. Semi-submersible platform design results.

Table 18. Platform mass comparison for three 5MW rotor topsides

	Preliminary VAWT		HAWT (a lighter NREL 5MW topside)		VAWT of equal mass to HAWT	
	Spar	Semi-Sub	Spar	Semi-Sub	Spar	Semi-Sub
Topside Mass (kg)	973,000	973,000	600,000	600,000	600,000	600,000
Platform Steel Mass (kg)	1,500,000	2,370,000	2,000,000	2,900,000	1,045,000	1,708,000

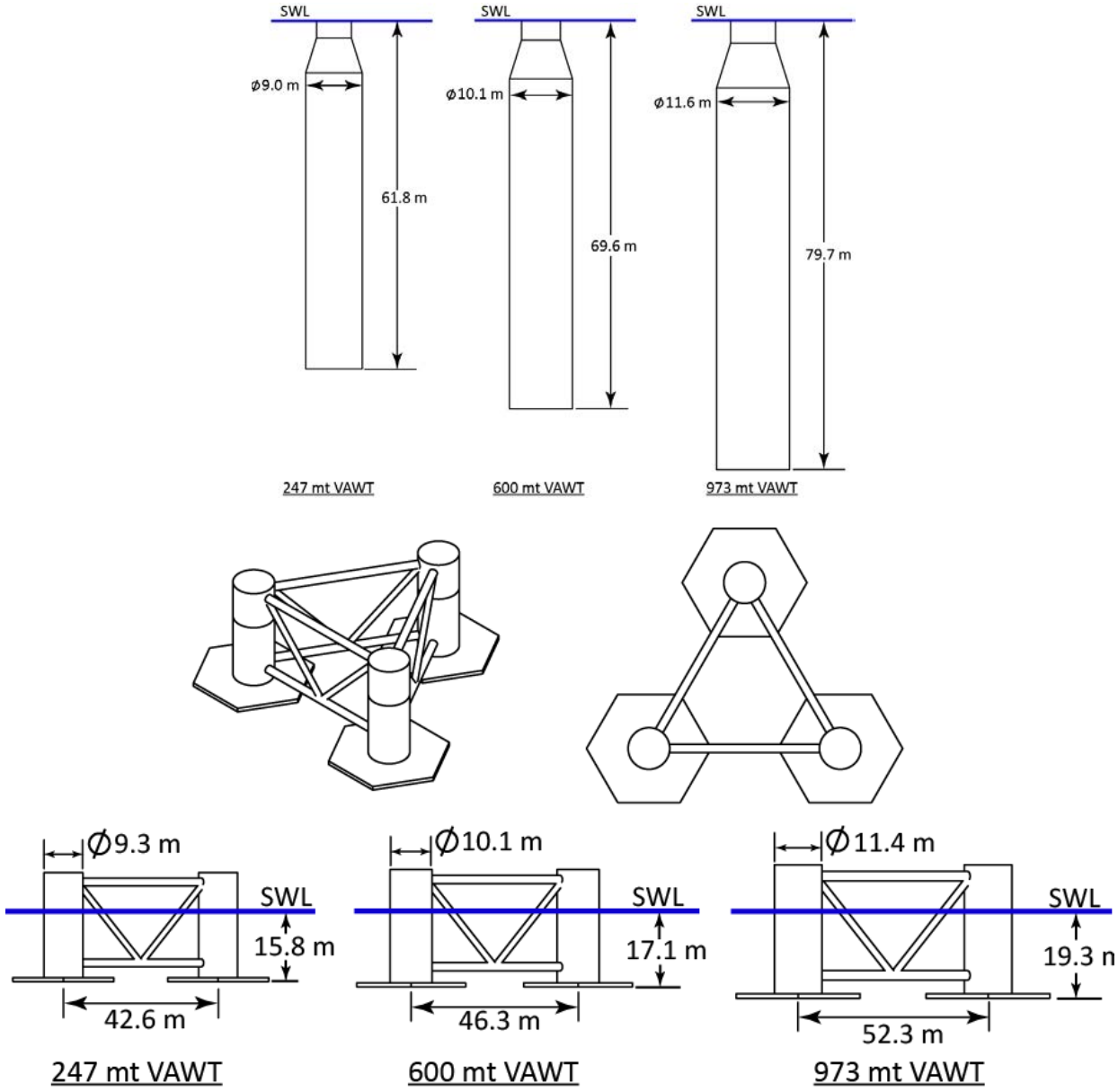

Figure 96. Spar and Semi size comparison over design range.

3.5.2.5. Concluding Remarks on Platform Design Studies

This study presents an analysis of floating offshore platforms designed to support a range of VAWT topside configurations, and supports the cost analysis of utilizing a VAWT topside for a floating offshore application. Results of the study show that for the chosen range of 5 MW VAWT topsides, savings can be realized through reducing the construction costs of the platform. When compared with the costs of a comparable platform designed for a HAWT topside, this study found

that the lower mass, vertical CG, thrust load and center of pressure of the VAWT allows for a reduction in platform size, resulting in significant reduction in both the construction cost of the platform. This provides motivation for further study of the VAWT design as a potentially cost effective option for floating offshore wind turbine applications. Future VAWT designs should focus on reducing the mass and CG of the topside, as well as lowering the aerodynamic load and center of pressure to maximize the possible reductions in platform stability requirements and cost. Additionally, methods of mitigating the wind loads during extreme events would be beneficial in reducing the loads on the mooring system, allowing for more efficient designs.

Future work includes further development of the topside design envelope enabling platforms to be designed and analyzed for more mature topsides. In particular, the mooring system design will benefit from updated load inputs. Additionally, once the topside design envelope undergoes a down-selection process, more advanced mooring and platform analyses will be carried out with the improved inputs from the more mature topside designs. With an initial cost of energy analysis completed, future work should include determining an appropriate topside and platform design to pursue for development of model scale testing and more advanced analyses.

It should be noted that an advantage of this platform design approach is that the platform design study started with two concepts (one spar and one semi-submersible) that were already proven concepts for offshore wind energy systems. These designs were publicly available and have been extensively analyzed in previous studies. As a result, both the sizing and cost bases (or cost factors) have already been established for these spar and semi-submersible concepts, and this sizing study was able to take advantage of that to develop preliminary design sizings based on existing, proven concepts.

However, a limitation of this design approach is that other floating concepts (such as barges or tension leg platforms), which may offer better technical and cost performance for a VAWT, were not analyzed. The previously developed concepts utilized in this study, although mature for floating HAWTs, were not systematically reconfigured or tailored for the unique floating VAWT characteristics that include lower vertical center of gravity and VAWT periodic dynamic loading of the rotor (i.e. dynamic rotor torque, and pitch/roll moments). Starting from scratch with a new platform design tailored to the VAWT was outside the scope of this initial system design study; however, considering new platform design concepts tailored for this application should be considered in future work.

4. CHALLENGES AND OPPORTUNITIES FOR FLOATING VAWTS

This section presents challenges and opportunities associated with multi-MW offshore VAWTs. In this work, we explored several opportunities to improve VAWT technology or mitigate design barriers, which include the design of novel airfoils, innovative structural and platform design, and design and analysis for aeroelastic instability (or flutter). Studies on coupled rotor/platform structural dynamics, and novel operating strategies are also discussed.

4.1. Novel VAWT Airfoils

Traditionally, symmetric NACA airfoil sections have often been used for vertical-axis wind turbine blades. Research at Sandia in the 1980s led to development of natural-laminar flow airfoils with desirable drag and stall characteristics. However, little work has been done to date on defining aerodynamically optimal airfoils for VAWTs. For a HAWT, airfoils with a large lift-to-drag ratio are generally good choices. It can be shown that the aerodynamic efficiency of the HAWT rotor under zero yaw and in a steady wind is a function of this lift-to-drag ratio. The aerodynamics of a VAWT, however, is fundamentally different from the aerodynamics of a HAWT. The power extraction process for a VAWT is inherently unsteady, with aerodynamic blade loadings changing radically during a single rotor revolution. It is not expected that airfoils optimized for a HAWT, assuming nominally steady aerodynamic conditions, will be optimal for a VAWT.

TU-Delft has devised a new method for the design of VAWT airfoils that may lead to dramatically different blade designs with greatly improved aero-structural performance (33). The key insight is the formulation of a new aerodynamic objective function based not on the lift-to-drag ratio in steady flow, but on the ratio of lift curve slope to drag coefficient integrated over a range of angles of attack. The lift curve slope is the slope of the curve resulting when lift coefficient is plotted against angle of attack. A promising aspect of this formulation is that it is possible to achieve large lift curve slopes by increasing the airfoil thickness. If this benefit outweighs the increase in drag with thickness, then very thick airfoils with high aerodynamic efficiency are possible. Since thick airfoils are also structurally more efficient, it may be possible to avoid the usual tradeoff between aerodynamic efficiency and structural efficiency when designing airfoils for a VAWT.

A first generation of VAWT airfoils has been created using this new design approach. A genetic algorithm was used, along with the XFOIL viscous panel code, to create airfoils with various thickness-to-chord ratios that maximized the objective function described above. Two airfoils from this family of designs are shown in Figure 98. In general, these airfoils are not symmetric but are cambered, and the amount and direction of camber is a function of the thickness.

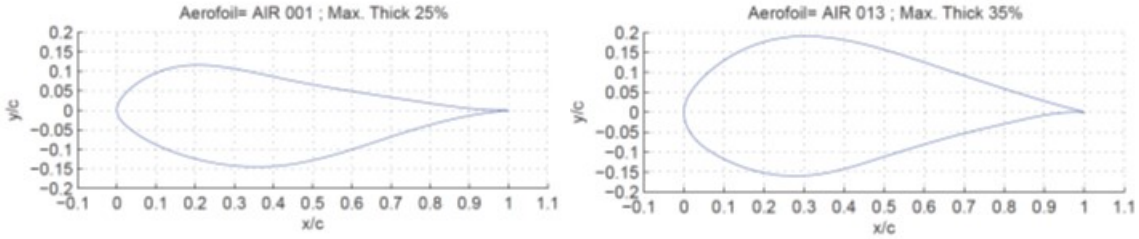

Figure 97. Two aerodynamically optimal thick VAWT airfoil designs.

Figure 98 shows the calculated maximum power coefficient for a three-bladed, two-dimensional VAWT using various airfoils. Symmetric NACA foils are compared to the new family of VAWT

airfoils for a range of thicknesses, and performance under both clean blade (free transition) and soiled blade (forced transition) conditions is included. The new family of thick foils outperforms the NACA foils, particularly at large thicknesses. The performance of the new foils at thicknesses above 35% is comparable to much thinner NACA foils.

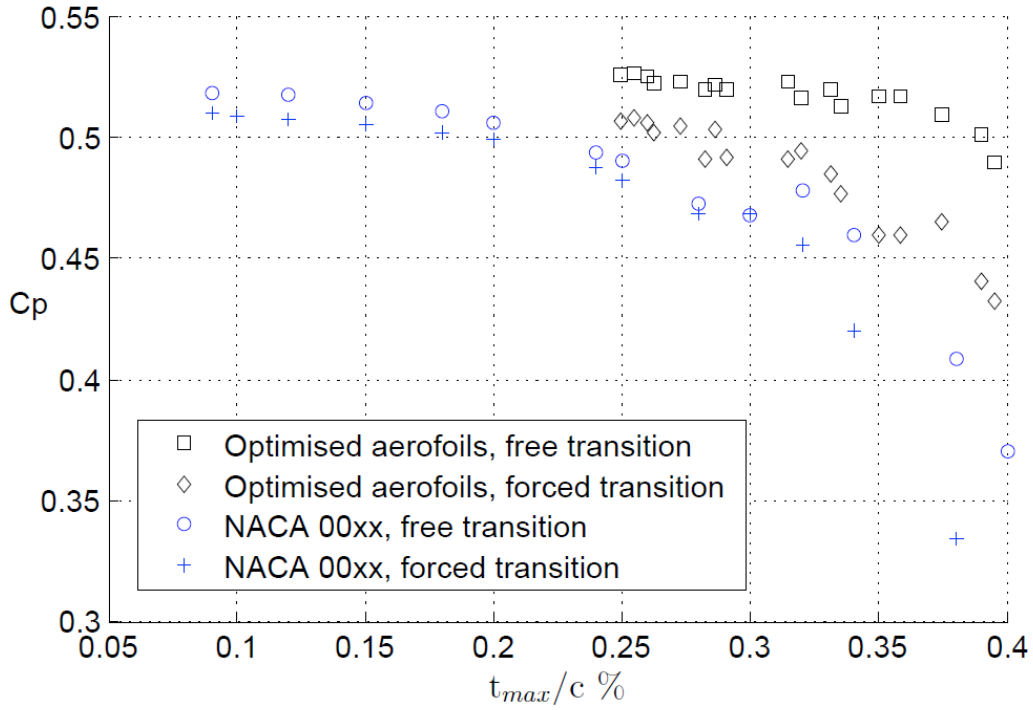

Figure 98. Two-dimensional rotor power coefficient for optimized airfoils, compared to NACA airfoils.

The new design approach appears to be very promising and opens up new opportunities in VAWT airfoil design. Verification of the airfoil designs through wind tunnel testing has commenced under a separate, parallel VAWT research project at TU-Delft (34). So far, only aerodynamic performance has been considered in the design objective. Current research is directed towards including constraints related to effective stall regulation of power. This was a major factor in determining the design of the earlier Sandia natural laminar flow airfoils, for example. Future work will consider including structural objectives in the overall design process. For example, although increased thickness is desirable from a structural point of view, the thickness distribution along the chord may also be important in order to accommodate desired internal structural members such as spars. We expect these new design approaches to offer significant improvements in blade section aero-structural performance, resulting in higher aerodynamic efficiency, lower blade weight, lower rotor costs and increased energy capture.

4.2. Aeroelastic Stability: Flutter Analysis

Dynamic aeroelastic instability or flutter can be a concern for lift-generating structures under aerodynamic loads. The coupling of aerodynamic forcing with a structure's natural modes can lead

to a large amplitude diverging motion. Recent studies have shown that flutter is a potential issue in very large HAWT wind turbine blades (35) (36) (37) (38) and may be a concern for very flexible multi-megawatt VAWT structures under large aerodynamic loads as well. Flutter has been observed in smaller-scale VAWT designs (39), but this issue has not been explored for large-scale VAWT systems. For an equivalent power rating, a VAWT design must have much larger (and likely more flexible) blades than a HAWT design. Indeed, the risk of flutter increases with increased tip speed ratios, low frequency flapwise and torsional modes, and the positioning of a blade cross-section mass center aft of the aerodynamic center. All of which are characteristic of large VAWT blades.

Analysis and design to avoid aeroelastic instabilities is a key issue addressed in initial design studies. The design requirements and analysis techniques are well established for the conventional 3-bladed HAWT, but these issues are not well-addressed for the range of VAWT configurations. This section presents an initial design study on the aeroelastic stability of large, multi-MW VAWT configuration. Design parameters such as the number of blades, rotor material selection, and fundamental VAWT configuration are examined within the context of aeroelastic stability.

The six VAWT configurations considered for detailed structural dynamics analysis in Section 3.4 were examined for flutter instabilities. The aeroelastic formulation and automated procedures of the BLade Aeroelastic STability Tool (BLAST) for HAWT blades were implemented into the OWENS framework for considering the aeroelastic analysis of rotating VAWT structures. Details of BLAST and the implementation into OWENS are given in References (36) and (6) respectively and will not be elaborated on in this report. Pre-stressed modal analysis and iterative procedures were employed to conduct aeroelastic stability analysis at a number of specified rotor speeds. Frequency and damping trends were examined and potential aeroelastic stabilities were identified for each VAWT configuration. Figure 99 shows representative frequency and damping trends with respect to rotor speed for the DC2LCDT turbine. Frequency changes are apparent due to rotational, stress stiffening, and aeroelastic effects as rotor speed increases. Damping trends are dependent on aeroelastic damping. Some modes are minimally affected, while others have noticeable increases in damping. Finally, certain modes of the aeroelastic system cross from being positively to negatively damped. The cross-over point is considered the flutter speed at which the onset of aeroelastic instability occurs.

Damping trends for the various configurations were observed and modes with negative aeroelastic damping were identified. Damping trends for these modes are shown in Figure 100. “Hard” flutter modes are observed for the Darrieus VAWTs while very “soft” flutter modes are observed for the V-VAWTs. No modal damping was assumed in the analysis, and these soft flutter modes are likely to be mediated by small amounts of damping in the structure. Inspection of the mode shapes at the onset of aeroelastic instability are shown in Figure 101 and Figure 102 for the two- and three-bladed glass composite Darrieus designs. The mode shape reveals that the flutter mode shape is primarily that of a first tower mode. Similar flutter mode shapes were seen for the carbon composite Darrieus designs.

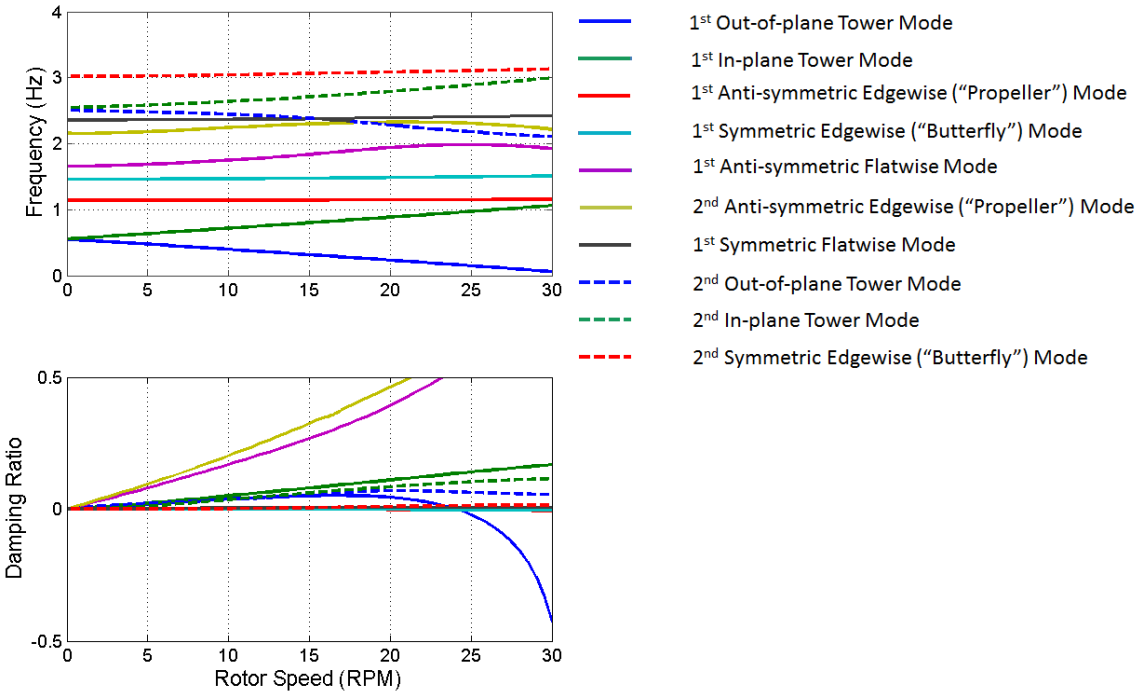

Figure 99. Frequency and damping vs. rotor speed for the DC2LCDT turbine.

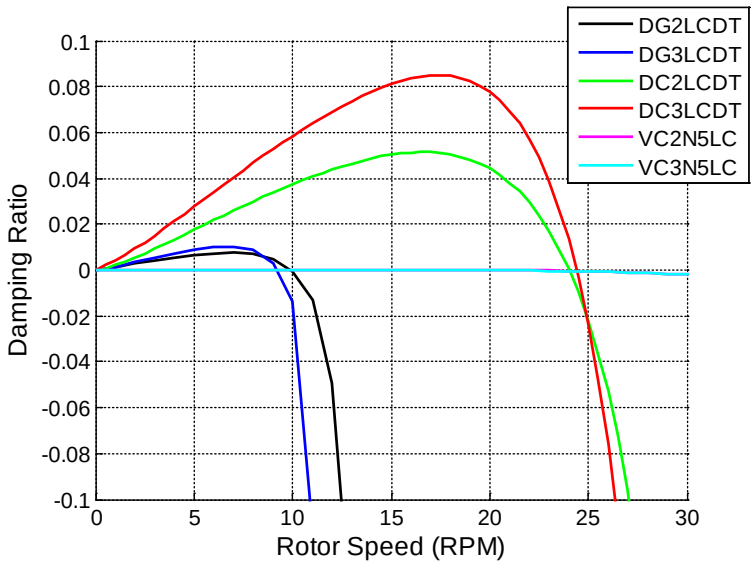

Figure 100. Damping trends of primary flutter modes for VAWT configurations.

It is notable that the glass composite Darrieus designs have much lower flutter speeds than the carbon composite designs. The higher stiffness to mass ratio of carbon composite raises the modal frequencies of a structure compared to a glass composite design. This increase in frequency tends

to alleviate flutter concerns well outside the operating range of the turbine for the carbon Darrieus configurations. In this study, the number of blades employed on a Darrieus design did not have a significant impact on the flutter speed. However, it can be noted that the magnitudes of damping in flutter modes tend to be larger for configurations with three blades.

The mode shapes of the soft flutter modes for the two- and three-bladed carbon V-VAWT configurations are presented in Figure 103 and Figure 104 respectively. The flutter mode shape for the two-bladed configuration in Figure 103 shows a coupled flap and edgewise mode with some twisting of the blades. The flutter mode shape for the three-bladed configuration in Figure 104 is primarily a tower mode, with some local blade motion. The flutter mode shapes observed for the entire VAWT configuration can be hard to compare to classical flutter mode shapes of coupled pitch/plunging for aircraft wings or HAWT blades. Indeed, the VAWT configurations have fairly significant geometrical differences and the impact of this should be explored in the future.

Although Figure 100 identifies the flutter speed of the various turbines considered in this study it is important to view these within the context of the operating speed of the turbine. Thus, a flutter margin which normalizes the flutter speed by the operating speed shown in Table 10 and Table 12 was computed as shown in Figure 105. A flutter margin below or around 1 is undesirable, indicating the flutter mode could be excited during normal operating conditions. Although none of the configurations employed in this study had flutter margins at or below unity, the glass Darrieus configurations had the lowest flutter margins below 1.5. Additional design considerations may be desirable to further increase the flutter margin of these designs. The carbon Darrieus designs performed well with flutter margins above 3. Furthermore, the V-VAWT designs had relatively large flutter margins, especially considering the very soft nature of their flutter modes which is likely to be mediated by the presence of modal damping.

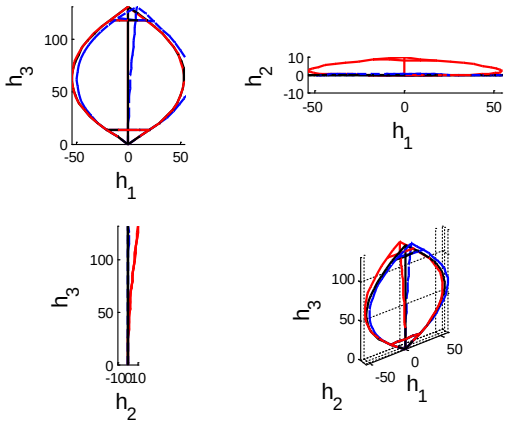

Figure 101. Flutter mode shape for DG2LCDT.

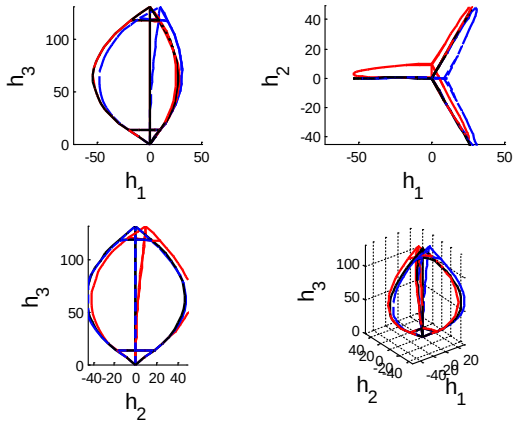

Figure 102. Flutter mode shape for DG3LCDT.

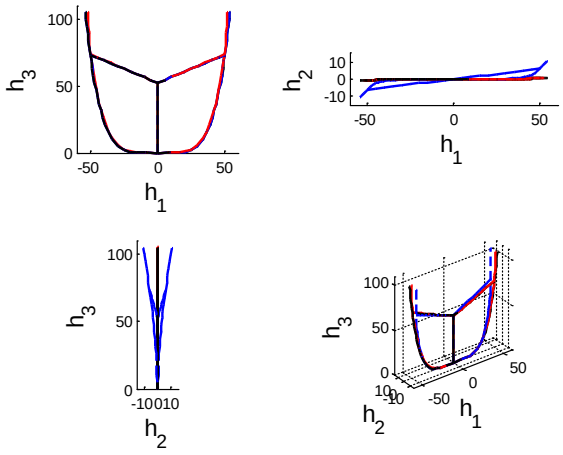

Figure 103. Flutter mode shape for VC2N5LC.

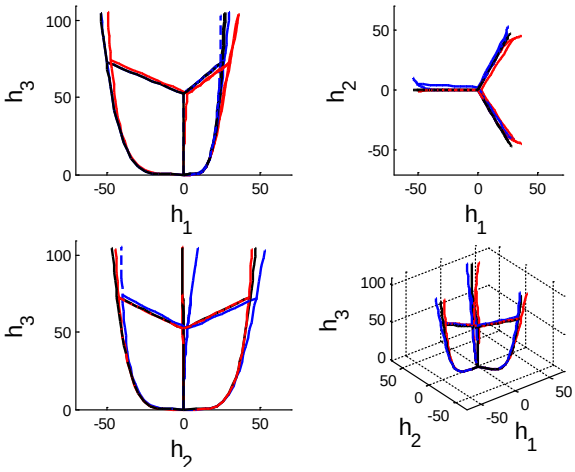

Figure 104. Flutter mode shape for VC3N5LC.

The aeroelastic stability analysis presented here is considered to be an initial design study to scope the preliminary large-scale VAWT configurations of this study for aeroelastic instabilities. This issue, until now, has been an unknown for this technology. Future analysis should seek to improve upon the aeroelastic formulation by considering the effects of inflow and wake and accounting for the actual periodicity of the aeroelastic system. Nevertheless, the current aeroelastic implementation allows for a convenient, straightforward extension of existing structural dynamics software (OWENS) that may serve as a foundation for the development of future analysis capabilities.

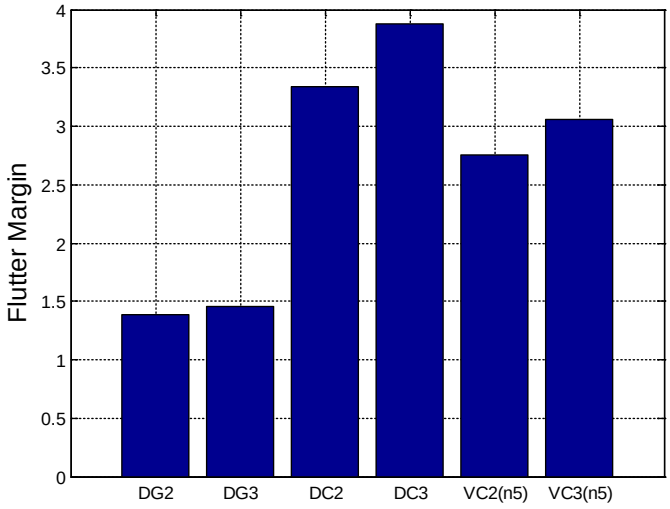

Figure 105. Flutter margins for VAWT configurations.

4.3. Coupled Rotor/Platform Structural Dynamics Impact Study

This section presents an initial design impact study for assessing the structural dynamic behavior and dynamic stability of large multi-megawatt deepwater offshore VAWTs. This is documented in greater depth in Reference (40). Understanding the modal dynamics of a system is useful for gaining insight into the fundamental behavior of a system before a large number of loading scenarios are considered. Furthermore, identifying potential instabilities at the initial design stage is critical for proactively mediating undesirable large dynamic response of a system. The analysis and understanding of very large, highly flexible VAWT structures is further complicated by the rigid body modes of a floating support structure. Previous research investigated smaller scale land-based VAWTs and identified resonance concerns (15). The support conditions or boundary conditions, however, are known to dramatically influence the modal behavior (natural frequencies and mode shapes) of the structural dynamic system (41), (42), (43). Thus, it is imperative to understand the behavior of a deepwater offshore turbine affixed to a platform (floating condition) relative to a land-based turbine (fixed condition). In addition, the presence and stability of additional rigid body modes for the floating case should be assessed along with elastic modes. Previous investigations have studied the effects of support condition on the tower modes of offshore HAWTs (44). Nevertheless, the fundamental differences between VAWT and HAWT configurations require unique design considerations and design analysis techniques.

Initial design studies to investigate the stability of floating VAWT configurations are conducted using the Offshore Wind Energy Simulation (OWENS) toolkit. Validation procedures for OWENS for VAWTs have demonstrated the ability of the tool to predict the modal response of a rotating land-based Darrieus-type VAWT (6). Herein, the OWENS toolkit is used to assess the stability of very large multi-megawatt VAWT configurations in a deepwater environment, and the influence of a floating platform configuration on the structural modes of a VAWT is investigated. The goal of this investigation was to obtain a fundamental understanding of the interplay of platform support structure and the structural modes of a rotating VAWT. Furthermore, the effect of the large rotating structure on the rigid body modes of the turbine/platform system has been analyzed. Resonance concerns for rotating structures are commonly identified by inspecting the natural frequencies of a system for coincidence with per-rev excitations. For a VAWT, the sensitivity of resonance to a particular per-rev excitation is closely tied to the number of blades employed in a configuration. Therefore, a fundamental understanding of per-rev resonance sensitivities as related to the number of blades has been developed in this work. Parametric studies are performed across various turbine configurations, including the effect of scale: from a utility scale 500 kW turbine to very large 5 MW turbines (two- and three-bladed designs), as well as a variety of support configurations including land-based, monopile, and floating configurations.

4.3.1. Description of the Rotor/Platform Model Configurations

To gain a better understanding of modal dynamics of offshore VAWTs, various VAWT configurations and support conditions were considered. The VAWT configurations considered in the study described in Reference (40) include the Sandia National Laboratories' (SNL) 34-meter VAWT (15) which was a utility scale 500 kW design that served as an experimental test bed. To explore the effect of scale, two variants of an initial 5 MW VAWT design employing two and three blades are also considered. Only the 5 MW VAWT configurations are presented herein, but the complete study is available in Reference (40). The basic specifications of these VAWT configurations are given in Table 19. Note that the 5 MW VAWT configurations have the same

height and height to diameter ratios. To maintain rotor solidity, the chord of the two-bladed design was increased by 50% relative to the three-bladed design. Initial design studies have employed an operational rotor speed between 6 and 8 RPM for these 5 MW VAWT designs. This estimated rotor speed is similar to those for other large multi-megawatt VAWT design (45).

Various support conditions were also considered for the turbine designs considered in this study. A land-based support condition was considered by simply specifying a cantilevered boundary condition at the base of the turbine. For offshore deployment, 20- and 30-meter monopile support conditions were also considered. For this initial design study, the tower properties were simply extended from the base of the turbine, and a fixed-base cantilevered boundary condition was specified at the monopile base. More detailed design studies could make use of more accurate monopile properties and base condition (44). For deepwater offshore deployment, two platform configurations were also considered. An initial spar buoy configuration designed for the 5 MW VAWT configuration was considered with physical and hydrodynamic added mass properties shown in Table 20. The ITI energy barge designed for a 5 MW HAWT (44) configuration is also considered in this support condition study. Although this platform was not designed specifically for the 5 MW VAWT configuration, the rigid body mass properties of the 5 MW VAWT and HAWT configurations are similar. This platform provides a distinctly different platform condition from the spar buoy configuration and was useful in initial design studies on support condition of this work. The last column in Table 20 provides the ratio of spar buoy to barge platform properties. Perhaps most noticeable is the increased pitch/roll moments of inertia (physical and added) as well as the significant mass center offset from the still water level (SWL) for the spar buoy platform. In this initial support condition study, translational and rotational springs were attached to the rigid body platform and stiffness values were tuned to the platform/turbine rigid body frequencies shown in Table 21. Figure 106 shows schematics for SNL 34-meter and two- and three-bladed 5 MW VAWT configurations on the 30-meter monopile support.

Table 19. Specifications for VAWT configuration

	SNL 34-meter	SNL 3 blade 5 MW	SNL 2 blade 5 MW
Rating	500 kW	5 MW	5 MW
Configuration type	Darrieus	Darrieus	Darrieus
Height (m)	42.5	132.1	132.1
Height to diameter ratio	1.25	1.22	1.22
Operating speed (RPM)	37.5	6-8	6-8
Mass (kg)	3.06×10^4	6.49×10^5	6.50×10^5
Mass center above base (m)	21.1	65.8	65.8
In-plane MOI about c.m. $(kg - m^2)$	7.28×10^6	1.20×10^9	1.30×10^9
Out-of-plane MOI about c.m. $(kg - m^2)$	5.88×10^6	1.20×10^9	1.09×10^9
Polar MOI about c.m. $(kg - m^2)$	1.43×10^6	2.11×10^8	2.23×10^8
Minimum chord (m)	0.91	1.92	2.88
Maximum chord (m)	1.22	2.57	3.86
Blade material	6063-T5 Al	Fiberglass	Fiberglass

Table 20. Mass platform specifications for platform configurations

	Spar Buoy	ITI Energy Barge	Ratio (Spar to Barge)
Mass (kg)	5.47×10^6	5.45×10^6	1.003
Mass center above still water level (m)	-68.40	0.28	-242.55
Pitch MOI about c.m. $(kg - m^2)$	2.32×10^9	7.27×10^8	3.19
Roll MOI about c.m. $(kg - m^2)$	2.32×10^9	7.27×10^8	3.19
Yaw MOI about c.m. $(kg - m^2)$	6.52×10^7	1.45×10^9	0.05
Surge added mass (kg)	6.00×10^6	7.49×10^5	8.01
Sway added mass (kg)	6.00×10^6	7.49×10^5	8.01
Heave added mass (kg)	2.26×10^5	1.86×10^7	0.01
Pitch added MOI $(kg - m^2)$	7.18×10^9	1.26×10^9	5.70
Roll added MOI $(kg - m^2)$	7.18×10^9	1.26×10^9	5.70
Yaw added MOI $(kg - m^2)$	0	1.18×10^8	0

Table 21. Platform/turbine system rigid body frequencies (Hz)

	Spar Buoy	ITI Energy Barge
Sway	0.0084	0.0076
Surge	0.0084	0.0076
Heave	0.0330	0.1283
Pitch	0.0241	0.0980
Roll	0.0241	0.0980
Yaw	0.0270	0.0198

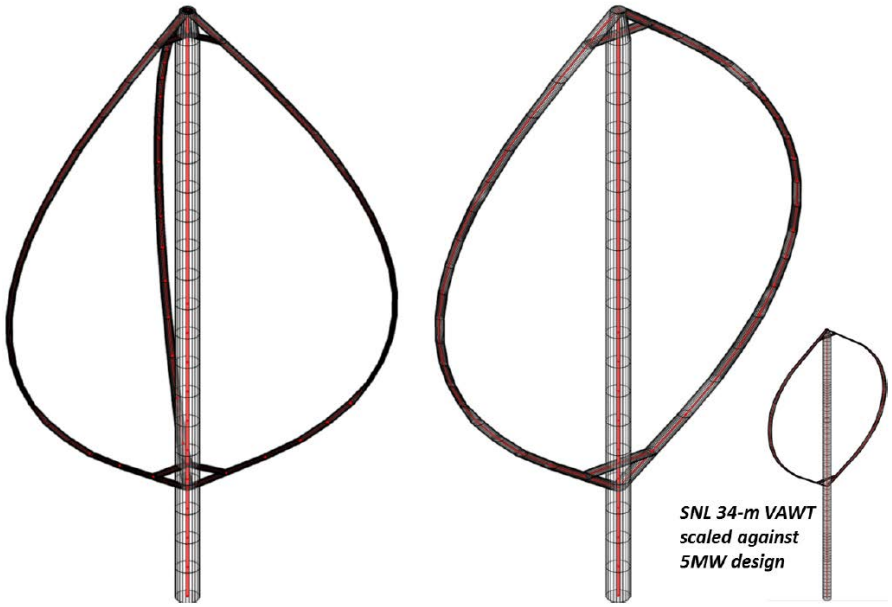

Figure 106. VAWT configurations on 30-meter monopile support.

4.3.2. Support Condition Study

Herein, a support condition study is considered for two- and three-bladed 5 MW VAWT designs with land-based, monopile, and two floating platform supports. As shown in Reference (40), two- and three-bladed VAWT designs have different tower resonance per-rev sensitivities and it is important to explore the impact of this in design studies. First, the Campbell diagrams for the land-based configurations are presented, and the effect of scale as well as number of blades is discussed. Next, the effect of support condition on tower mode resonance is discussed. Monopile and floating support conditions are considered and different platform designs are found to have a profoundly different impact on the turbine structural response. The effect of the rotating turbine on rigid body modes of a platform supported system is also investigated. As with the smaller scale VAWT support study, commonly employed "rules of thumb" are examined for applicability to very large VAWT designs with various support conditions.

4.3.3. Land-based Configuration

Before examining the effect of offshore support conditions on a large multi-megawatt VAWT design, the land-based configuration is considered. The Campbell diagrams of the two- and three-bladed 5 MW VAWT designs from 0 to 10 RPM are shown in Figure 107 and Figure 108 respectively. The three-bladed design makes mode labeling difficult, and modes are simply labeled as tower modes (T), flatwise modes (F), or edgewise modes (E) in Figure 107. Mode labeling in the two-bladed design uses the convention described previously for the SNL 34-meter VAWT (15). Comparisons of these diagrams with the SNL 34-meter VAWT (15)shows that the larger scale of the 5 MW machines results in much lower modal frequencies. These lower modal frequencies are potential causes for concern as critical per-rev crossings on the Campbell diagrams will occur at lower rotor speeds. Such issues may limit the operating speed of the turbine configurations or require innovative solutions to mediate resonance concerns. Furthermore, comparison of Figure 107 and Figure 108 show that the larger blade in the two-bladed design (with a 50% larger chord

compared to the three-bladed design) affords the opportunity to provide higher bending stiffness in the blades and elevate blade mode frequencies. This may be useful in alleviating stability concerns (resonant or aeroelastic) in the two-bladed design.

Comparison of tower modes in Figure 107 and Figure 108 shows that both two- and three-bladed designs have similar parked tower frequencies. The upper tower mode behavior with respect to rotor speed is similar between the two designs. The lower tower mode of the three-bladed design, however, interacts with lower frequency blade modes. As a rotor speed of 5 RPM is approached, the lower tower and flatwise modes begin to interplay and a "hybrid" mode develops that is a combination of tower and flatwise modes. Beyond 5 RPM the mode shapes "swap" and once again become more distinct mode shapes. This phenomenon has been termed "frequency veering" and "mode localization" (46), (47) and typically occurs when two modes have similar frequencies, common mode shape attributes, and are varying with some parameter (such as rotor speed in the current study). The combination of low frequency modes, coupled modes due to rotational effects, and frequency veering complicate the structural dynamics analysis of VAWT configurations and require more careful interpretation of modal analysis results compared to conventional VAWT configurations.

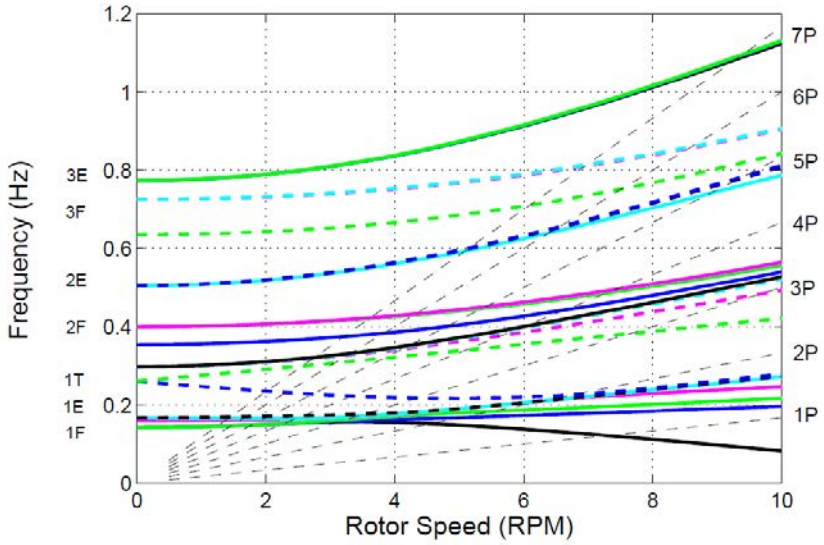

Figure 107. Campbell diagram of land-based 3-bladed SNL 5 MW VAWT.

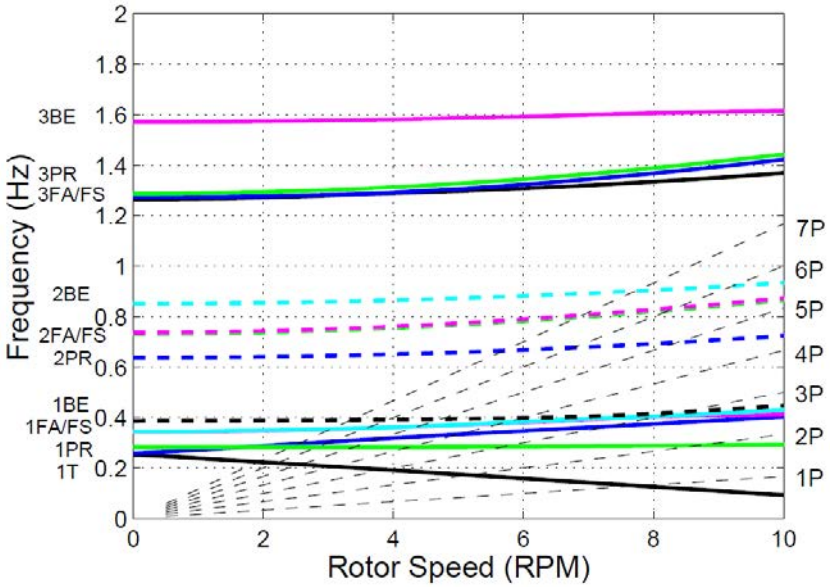

Figure 108. Campbell diagram of land-based 2-bladed SNL 5 MW VAWT.

4.3.4. Monopile Support

Both 20 and 30-meter monopile support conditions were considered for the 5 MW VAWT designs. As seen in initial studies of smaller scale VAWTs (40) blade modes were not significantly affected by support condition and the tower modes are considered herein. Figure 109 and Figure 110 show the tower mode Campbell diagrams for the two- and three-bladed 5 MW VAWTs respectively for land and monopile support conditions. Qualitatively, many of the trends from the 34-meter VAWT support condition study presented in Reference (40) are echoed in this study. The monopile serves to reduce the parked tower mode frequencies and results in critical per-rev crossings at lower rotor speeds. For the three-bladed configuration the 20 and 30-meter monopile reduce parked tower mode frequencies approximately 20 and 27% respectively relative to the land-based turbine. For the two-bladed configuration, the 20 and 30-meter monopile reduce parked tower mode frequencies approximately 24 and 33% respectively relative to the land-based turbine. Furthermore, the low frequency blade modes of the three-bladed design result in noticeable frequency veering behavior in the lower tower and flatwise modes. Mode shapes of the lower modes undergoing frequency veering were examined in an attempt to identify which of the modes was associated with a dominant tower mode. The thicker line on Figure 109 shows the mode with a dominant tower mode while thinner lines show the evolution of the modes experience frequency veering as rotor speed increases. Inspection of Figure 110 shows an absence of frequency veering phenomenon in tower modes, which can be explained by the stiffer blade of the two-bladed design resulting in higher blade mode frequencies above those of the tower modes.

Critical tower mode per-rev excitations for the two- and three-bladed configurations (as determined in Reference (40)) are denoted by red lines on the Campbell diagrams. Figure 109 shows the monopile-supported, three-bladed design has 2 per-rev crossings of the lower tower modes below a rotor speed of 4 RPM. This is a relatively significant decrease compared to the crossing around 5 RPM for the land-based support. For the upper tower mode, higher per-rev crossings occur below a rotor speed of 4 RPM as well. These lower per-rev crossings are below the estimated operating speed of 6-8 RPM for these initial turbine designs. Figure 110 shows the

monopile supported two-bladed design has 1 per-rev crossings of lower tower modes below 6 RPM, while the land-based configuration crosses the 1 per-rev excitation closer to 8 RPM. The 3 per-rev excitation crossings occur before 3 RPM for the lower tower mode and before 6 RPM for the upper tower modes of the monopile supported configurations. Thus, for each 5 MW design, the land-based support potentially has significant limitations on operating speed, and such limitations are only made more severe by the consideration of a monopile support.

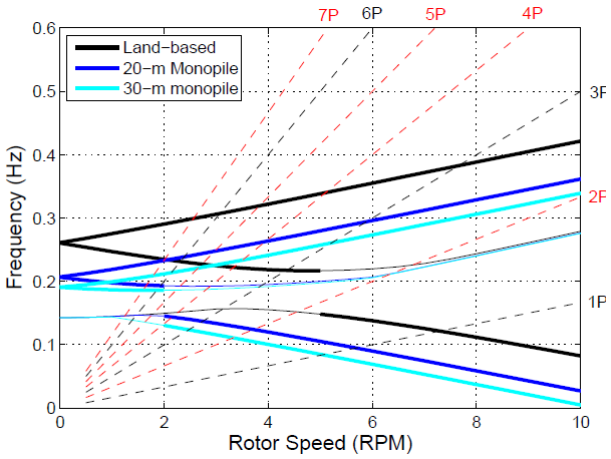

Figure 109. Tower mode Campbell diagram of 3 bladed 5 MW VAWT for land and monopile support conditions.

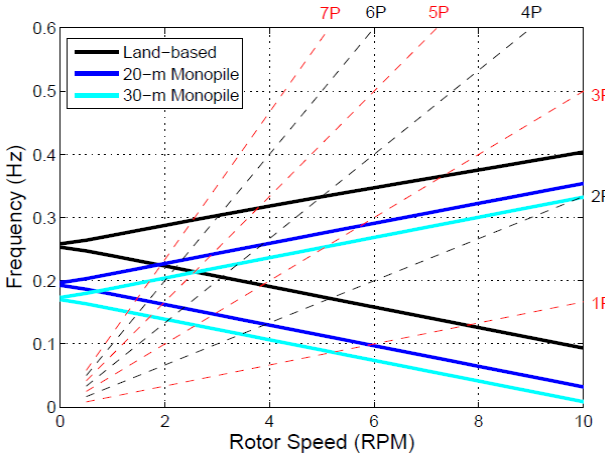

Figure 110. Tower mode Campbell diagram of 2 bladed 5 MW VAWT for land and monopile support conditions.

4.3.5. Floating Support

Floating support conditions on the 5 MW designs were also considered using the spar buoy and barge platforms described in the configurations section. As with the monopile support, blade modes were not significantly affected by the floating support and Figure 111 and Figure 112 show the tower mode Campbell diagrams for the two- and three-bladed 5 MW VAWT designs respectively with land-based and floating support condition. For the three-bladed configuration, the spar buoy and barge platform support conditions elevate tower modes approximately 5 and 94% respectively relative to the land-based support. For the two-bladed configuration, the spar buoy and barge platform support conditions elevate tower modes approximately 4 and 100% respectively relative to the land-based support. There is a striking difference on the effect of platform support on tower modes for the spar and barge supports. The last column of Table 20 compares the properties of the two platform configurations. A noticeable difference is the much larger moment of inertia (physical and added) for the spar buoy design as well as a significant mass center offset. These characteristics of the spar buoy platform result in a much higher effective moment of inertia compared to the barge platform. This results in a support condition closer to the land-based (fixed boundary condition) support than the “free” boundary condition (48) and the increase in frequency is not as pronounced. Thus, the lower effective moment of inertia associated with barge design allows for a more significant increase in tower mode frequencies.

As before, critical tower mode per-rev excitations for the two- and three-bladed configurations (as determined in Reference (40) are denoted by red lines on the Campbell diagrams. The spar buoy platform support does not result in any significant difference from a land-based configuration, with

respect to critical per-rev crossings of tower modes. The barge support, however, provides some noticeable advantage in eliminating upper tower mode critical per-rev crossings due to the increased frequency and slope of tower modes for both two- and three-bladed configurations. For the three-bladed configuration, the 2 per-rev crossing of the lower tower mode is delayed until a rotor speed of 8 RPM and a 4 per-rev crossing at a rotor speed of approximately 4.5 RPM. For the two-bladed configuration, the 1 per-rev crossing of the lower tower mode is delayed until a rotor speed of approximately 9.5 RPM and the 3 per-rev crossing is delayed until a rotor speed of approximately 5.5 RPM. The rotor speeds at these crossings are noticeably higher than the corresponding crossing in the land-based and spar buoy supported configuration.

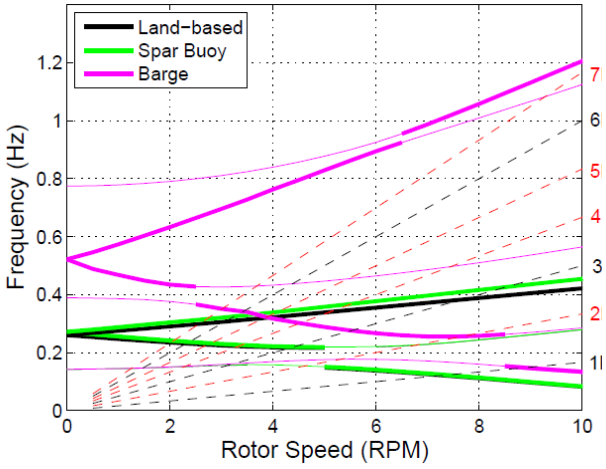

Figure 111. Tower mode Campbell diagram of 3 bladed 5 MW VAWT for land and floating support conditions.

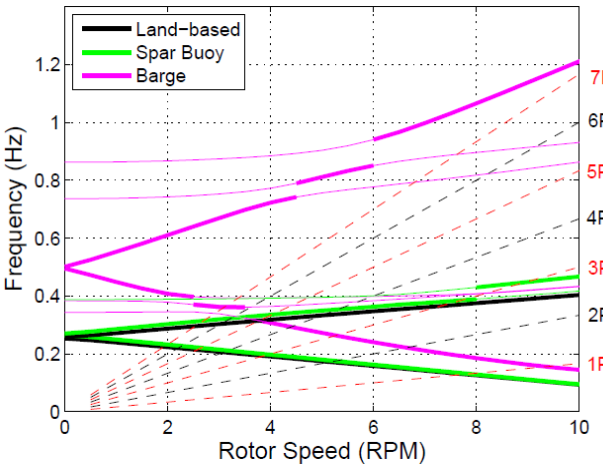

Figure 112. Tower mode Campbell diagram of 2 bladed 5 MW VAWT for land and floating support conditions.

The rigid body modes of the spar buoy and barge platform supported two-bladed 5 MW configuration are shown in Figure 113 and Figure 114 respectively. The rigid body mode trends for the platform supported three-bladed design are similar to two-bladed design and are not discussed here. As seen in the Campbell diagram in Figure 112 the spar buoy platform has minimal interaction with structural modes of the turbine, and Figure 113 shows that the structural modes of the turbine have no perceivable interaction with the rigid body modes of the spar buoy supported system. Different trends are seen for the rigid body modes of the barge platform supported configuration in Figure 114 with the rotating structure having noticeable interaction with the pitch/roll rigid body modes. Indeed, the lower moment inertia of the barge platform relative to the rotating turbine allows more interaction between rigid body modes and structural modes. Thus, while such a platform type can be employed to improve structural response of the turbine, care should be taken to ensure rigid body modes are not adversely affected. Note that since the analysis has been performed in the rotating frame, the pitch/roll modes as viewed in an inertial frame will be a combination of the “pitch/roll” modes characterized in Figure 114 transformed from the rotating frame to the inertial frame.

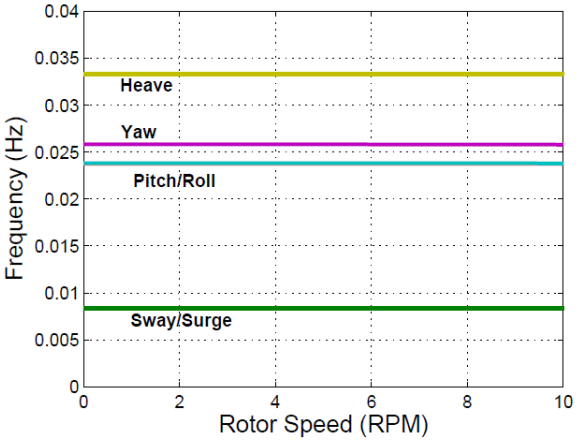

Figure 113. Rigid body mode Campbell diagram of 2 bladed 5MW VAWT on spar buoy platform.

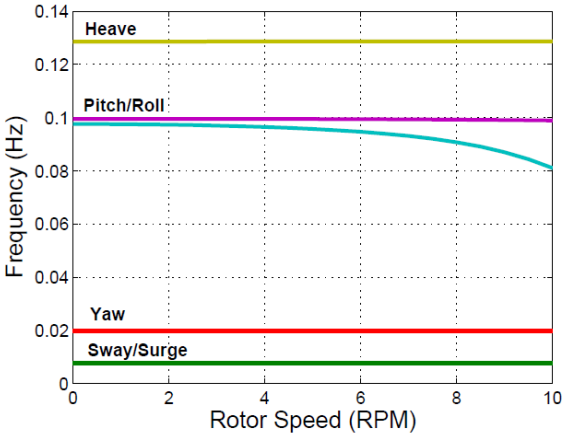

Figure 114. Rigid body mode Campbell diagram of 2 bladed 5MW VAWT on barge platform.

Figure 115 summarizes the effect of support condition on the parked tower mode frequencies of the 5 MW VAWT designs. Qualitatively, many of the trends observed in the support condition study for the SNL 34-meter VAWT presented in (40) are observed for the larger 5 MW configurations. Due to the scale of the 5 MW machine, the addition of a 20 or 30-meter monopile support has a less profound decrease in parked tower mode frequencies, but further decrease from the already low tower mode frequencies of the land-based configuration is undesirable. Similarly, the spar buoy support provides a negligible increase in parked tower mode frequencies while the barge support provides a significant increase in parked tower mode frequencies. Figure 116 and Figure 117 show the tower mode frequency slope magnitudes for the two- and three-bladed 5 MW designs. The slope is estimated using the tower mode frequencies at 0 and 10 RPM rotor speed. The tower mode slopes of the land-based, monopile supported, and spar buoy supported configurations characterized decently by the “rule of thumb” and differences are mostly due to frequency veering that results from the frequency veering interaction of low frequency modes. Furthermore, the barge platform supported configuration results in much higher tower mode frequency slopes that are not captured well by the “rule of thumb” approximation typically employed in initial design studies.

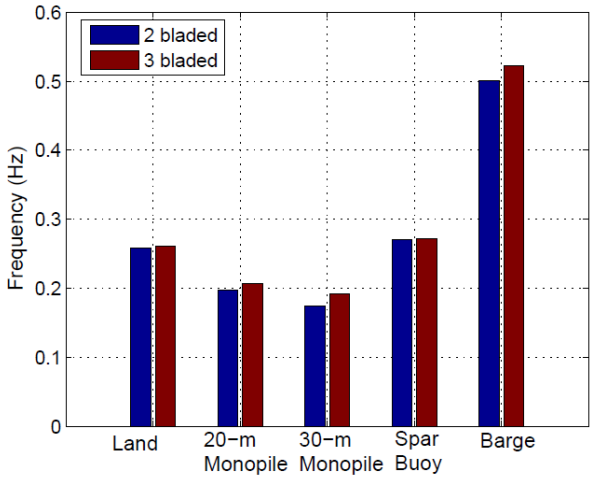

Figure 115. Parked tower mode frequencies for 2- and 3-bladed SNL 5 MW VAWT on various support conditions.

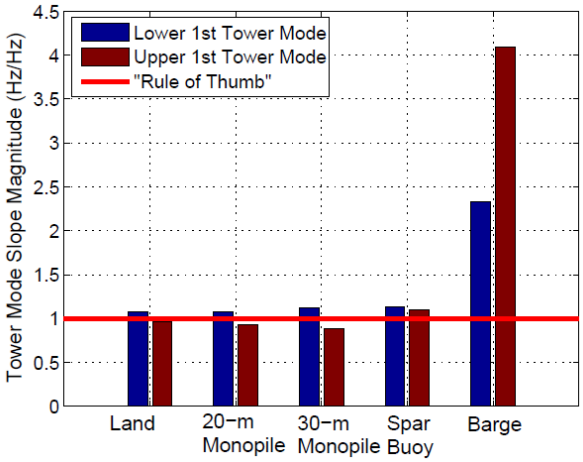

Figure 116. Tower mode slope for 3-bladed SNL 5 MW VAWT on various support conditions.

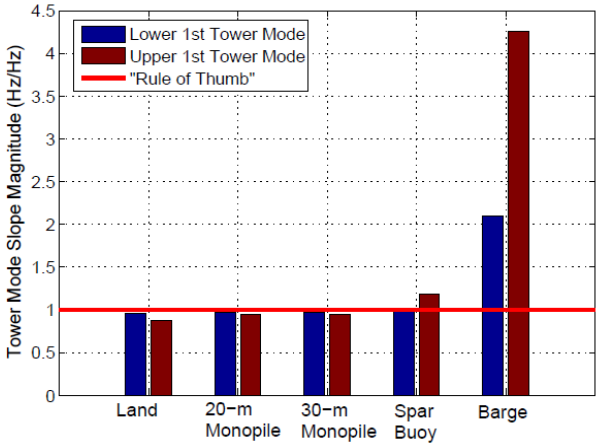

Figure 117. Tower mode slope for 2 bladed SNL 5 MW VAWT on various support conditions.

4.3.6. Conclusions of the Structural Dynamics Impact Study

This study of modal dynamics and stability in large offshore VAWTs (further documented in Reference (40)) has provided the following contributions:

- This work has developed a greater understanding of tower resonance in VAWT structures by developing an analytical expression for critical per-rev excitations related to the number of blades employed in a VAWT configuration. This greater understanding of tower mode resonance in VAWT design is an invaluable resource that may be employed by VAWT designers and analysts.

- The large scale of multi-megawatt VAWT designs results in very low frequency modes, and a noticeable interplay between the tower and blade modes was observed in the form of frequency veering. Thus, the interpretation of modal analysis results for multi-megawatt VAWT configurations requires greater care than conventional VAWT configurations.
- A support condition study was conducted for VAWTs of different scale and number of blades. Overall, results indicated that a monopile support had the detrimental effect of lowering tower mode frequencies as well as lowering rotor speeds at which resonance may occur relative to a land-based support condition.
- Investigations revealed that floating support conditions may alleviate resonance concerns, but to a varying degree depending on the platform design. This study also showed that the influence of support structure on the turbine structural modes can come at the expense of turbine modes interacting with the rigid body modes of the platform/turbine system. Thus, care should be taken to ensure rigid body modes are not adversely affected by the attached flexible turbine structure.
- Consideration of different platform designs showed that spar and barge platform designs provide a range of influence on turbine structural response, and demonstrate an opportunity to design the platform in a way to mitigate tower resonance. System-level design studies with cost modeling, however, will determine the best solutions for rotor configuration, rotor operating conditions, and platform configuration.
- Investigations revealed "rules of thumb" for estimating the evolution of a VAWT tower mode frequency with respect to rotor speed are found to be less applicable to both floating configurations and larger VAWT structures with modes undergoing "frequency veering" as rotor speed varies. Therefore, a more detailed analysis may be necessary than those previously employed for smaller scale, land-based VAWTs.

4.4. Innovative Platform Design and Balance of Station Cost Reduction

The platform design studies in Section 3.5 indicated that a VAWT has promise for reducing platform mass and cost in comparison to a comparable HAWT. A sizing study was performed using existing proven platform concepts for both HAWT and VAWT topsides with the same pitch angle and pitch period constraints applied to all topsides. However, additional opportunities to reduce platform costs could be found in innovative platform designs optimized for VAWTs. Offshore wind platforms have been typically designed within an envelope that is acceptable for HAWT rotor operation, as was the case for the concepts this platform scaling study was based on.

Unique aspects of the VAWT rotor indicate that the design envelope that has thus been applied to offshore floating platforms is not optimized. For instance, the VAWT rotor potentially exhibits increased aerodynamic efficiencies when it is moderately tilted to the incident wind, which indicates that the mean pitch angle constraint could be relaxed to a higher value for a VAWT versus a HAWT. This is just one example, but overall an innovative floating platform initiative would systematically address the necessity of these design envelope conditions for a VAWT rotor.

A few of the driving design envelope conditions for the floating platform include mean pitch (/roll) angle of the platform when subject to the designated aerodynamic load at the identified center of

pressure of the rotor. A target pitch (/roll) natural resonance period typically chosen to give the platform a stable “ground-like” base when subject to operational waves. And finally, the total water-plane area is considered with respect to the heave natural resonance period, again attempting to have a larger natural period than is typically seen in the environment so that a “ground-like” base may be achieved. An innovative floating platform initiative would systematically address the necessity of these design envelope conditions for a VAWT rotor. Since a moderate mean pitch increases aerodynamic efficiency, allowing the platform to react more to the operational environment potentially has the possibility of increasing power delivered. Further, a platform that reacts more to the operational environment will displace a smaller volume of water, and hence will require less steel to manufacture.

Finally, an innovative floating platform initiative would also consider the major categories of current offshore platforms: gravity stabilized, mooring-line stabilized, and buoyancy stabilized. Potentially, the desired platform response can be obtained through a hybrid design that capitalized on strengths of each of these major designs simultaneously. As noted above, a limitation of this platform design study was that only spar and semi-submersible type platforms were analyzed. Thus, one recommendation for future work is to consider all floating system types along with design solutions tailored to VAWTs.

4.5. Storm Survival and Load Alleviation (Novel Operating Strategies)

Aeroelastic load alleviation, both passive and active, has been explored at a conceptual level as an aerodynamic braking mechanism for VAWT rotors. This would take the form of either swept blades or laminate-induced twist-extension or twist-bend coupled blades depending on the application. Estimates of as little as 4° of twist in the equatorial region of the rotor could be enough to provide protection against overspeed in the event of an emergency. This amount of twist or greater has been proven in multiple HAWT experiments.

5. PRELIMINARY LEVELIZED COST OF ENERGY ANALYSIS

This section presents a preliminary levelized cost of energy (LCOE) analysis for deep-water offshore VAWT systems with inputs from the various design studies for the rotor structure, rotor aerodynamics (AEP), platform design, and drivetrain designs as described in the design section of this report. Details of cost modeling and assumptions are presented for balance of system, turbine capital, and operations and maintenance costs. LCOE results are presented for a subset of down selected systems that proved to be the most competitive designs within particular rotor design classes.

5.1. Deep-water Offshore VAWT System Cost Analysis

The cost of an offshore wind farm can be decomposed into three main categories (as detailed in Figure 118): balance of system costs, turbine capital costs, and operations and operations & maintenance (O&M) costs. Balance of system costs can be further decomposed to include: transportation, installation, electrical interconnection, and other costs. Other costs associated with balance of system may include permits and engineering site assessments, personnel access equipment, and surety bonds. Turbine capital cost can be further decomposed into: rotor cost, drive-train cost, support structure cost, control & monitoring system costs, and marinization cost.

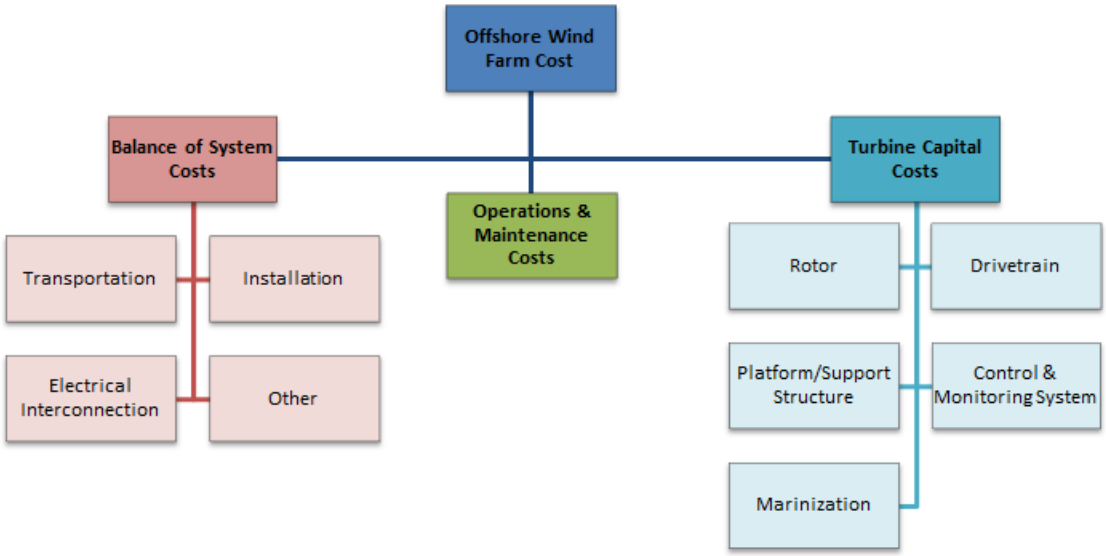

Figure 118. Offshore wind farm cost categories and sub components.

5.1.1. Balance of System Costs

Herein, a wind farm with a 300 MW rating (composed of 60 5 MW VAWTs) is considered. Machines were considered to have a 20 year service life. The balance of system costs (and breakdown) for this wind farm is shown Table 22. Where applicable, cost models from reference (49) were employed, with an inflation factor of 1.38 to adjust cost models developed in 2003. Transportation costs include transportation of the turbine/components to the port/staging area. The transportation cost value for the wind farm at hand considered the scaling relationships developed in reference (49), with a 10% reduction in transportation cost assumed for a VAWT design relative to a comparable HAWT design. Installation costs include port and staging equipment, transportation of turbine from port/staging area to site, and turbine installation. Offshore

installation costs are presented in Section 3.5 with a detailed discussion in Appendix A. The electrical interconnection costs were developed in reference (49), and no modifications were employed for the VAWT wind farm. The breakdown of "other costs" is presented in Table 23. Other costs also include a turbine-specific surety body which is 3% of the initial capital cost of the wind farm. The values of permits, engineering, site assessment, and personal access equipment were developed using methodologies in reference (49). For the deep-water, floating VAWT wind farm, scour protection was not required. This resulted in a 37% reduction "other balance of system costs" relative to a comparable shallow-water HAWT considered in reference (49).

Table 22. Balance of station cost breakdown for 300 MW deep-water VAWT wind farm

Sub-component	Cost (M USD)
Transportation	97.79
Installation	Turbine specific (see Section 3.5 /Appendix A)
Electrical Interconnection	150.70
Other	43.08

Table 23. Balance of station cost: other costs breakdown

Sub-component	Cost (M USD)
Permits, Engineering, Site Assessment	15.32
Personnel Access Equipment	4.97

5.1.2. Turbine Capital Costs

Turbine capital cost for an offshore turbine can be subdivided into the components shown in Figure 118. Costs for the rotor, drive train, and support structure (platform and mooring) are computed based on the design studies described in detail in Section 3. The rotor cost was calculated by employing the approach discussed in Section 3.2. Note that only material cost is captured in the rotor cost model. Future work should account for manufacturing costs as well. Drive-train costs are related to the operational rotor speed of the turbine and drive-train cost considerations for both three-stage and direct drive generators. Support structure (platform and mooring) results were presented in Section 3.5, with a detailed discussion in Appendix A. A control and monitoring system cost of 75,900 USD was considered using scaling laws (and inflation adjustments) from Reference (49). Finally, a marinization factor of 13.5% of the rotor cost was considered (49).

5.1.3. Operations and Maintenance Costs

Cost scaling models from reference (49) were employed to characterize levelized replacement/overhaul and operations and maintenance costs for the wind farm under consideration. It is estimated that the simpler design of a VAWT relative to a HAWT will provide a 20% reduction in O&M costs and a 33% reduction in replacement and overhaul costs. Under

these assumptions, the levelized replacement/overhaul costs are calculated as 4.69 M USD/year. Levelized O&M is related to annual energy production (AEP) which is a turbine specific parameter, and was accounted for on a turbine-by-turbine basis in the cost analysis.

5.1.4. Levelized Cost of Energy Approach

The levelized cost of energy (LCOE) is calculated using the approach described in reference (49). In this analysis, a fixed charge rate (FCR) of 8% is considered. An FCR of 8% was selected as this is the same value that was utilized in the originally proposed LCOE analysis (based on DOE guidelines).

5.1.5. Offshore VAWT System Cost Analysis Results

A number of turbine/platform/drive-train configurations were considered for economics analysis. Design choices for the rotor and platform showed the most impact on the LCOE. Furthermore, the semi-submersible platform proved to be a much more expensive design than the spar-buoy design, with noticeable increases in LCOE for the offshore VAWT system. Finally, a number of V-VAWT designs proved to be structurally insufficient under aerodynamic loading and were not plausible design concepts in their current state. Therefore, cost of energy results will be restricted to systems with a spar-buoy platform support and the following rotor concepts:

- Glass Darrieus rotor concepts (2 or 3 blade, various chord profiles)
- Carbon Darrieus rotor concepts (2 or 3 blade, various chord profiles)
- Select carbon V-VAWT designs with 50%-70% tower-to-blade strut attachments.

In total, results of cost of energy analysis are presented for 31 offshore VAWT systems in Figure 119. The plot shows the trends of LCOE versus rotor mass for these configurations. Investigations revealed that LCOE trends most noticeably with rotor mass as this is a critical parameter for both rotor cost and platform support structure costs. The effect of material choice is also evident in this figure, with carbon designs having LCOE trending with a higher slope than glass designs due to increased material cost relative to glass. Figure 118 shows that the Darrieus designs perform better from a cost perspective, while V-VAWT designs will likely require additional optimization or innovation to become cost competitive.

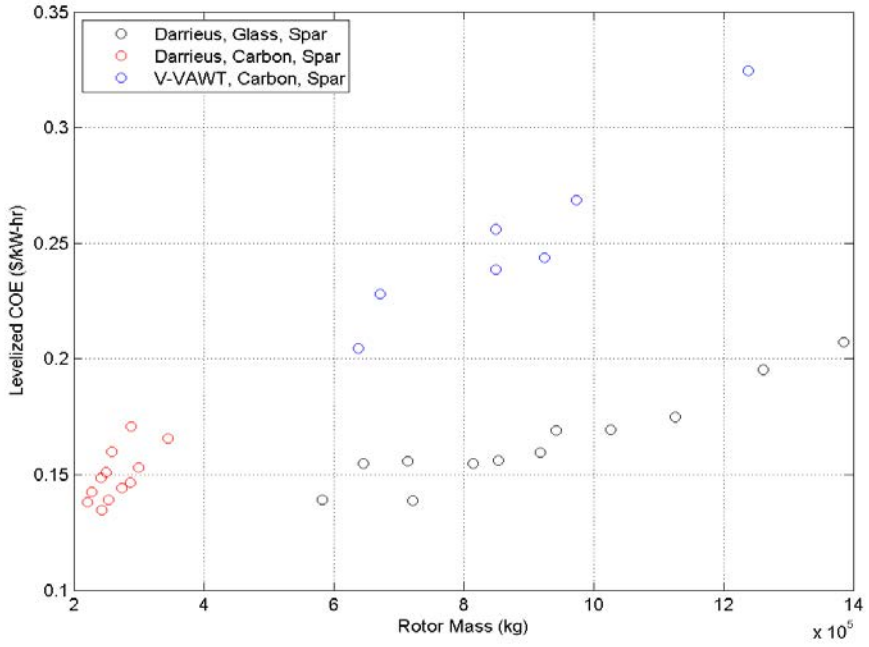

Figure 119. LCOE vs. Rotor mass.

Table 24 provides a summary of various operating and cost of energy parameters for Darrieus and V-VAWT turbines respectively. For Darrieus designs, the minimum LCOE is 0.134 USD/kW-hr, the maximum LCOE is 0.207 USD/kW-hr, and the mean LCOE is 0.157 USD/kW-hr. V-VAWT designs haven noticeably higher LCOE with minimum, maximum and mean of 0.205, 0.325, and 0.252 USD/kW-hr respectively.

Table 24. Summary of operating conditions and cost of energy analysis for the lowest LCOE turbines in each turbine class

Parameter	DC_3B_LCDT	DC_2B_LCDT	DG_3B_SCDT	DG_2B_SCDT	VC_2B_LCN5
LCOE (USD/kW-hr)	0.134	0.138	0.139	0.139	0.205
Turbine AEP (MW-hr)	20069	18443	18880	17004	18992
Rotor Speed (RPM)	6.30	7.20	7.20	8.25	7.40
Farm Initial Capital Cost (M USD)	1616	1529	1579	1421	2523
Farm Initial Capital Cost (USD/W)	5.39	5.10	5.26	4.73	8.42

Rotor Cost (M USD)	7.0	6.3	4.0	3.2	18.3
Spar Platform Cost (M USD)	5.3	5.2	8.6	7.4	7.84
Drive-train Cost (M USD)	3.7	3.2	3.2	2.8	3.1

The turbines with the lowest LCOE were examined for each class of turbine (carbon Darrieus, glass Darrieus, and carbon V-VAWT). Table 24 presents the operating conditions and cost of energy results for these select turbines. Cost of energy analysis showed that for carbon Darrieus, large chord, double tapered (two- and three-bladed) designs performed best. Analysis also showed that glass Darrieus, small chord, double tapered designs (two- and three-bladed) also performed well. Finally, out of the carbon V-VAWTs considered the large chord, 2 bladed design with n=5 power law performed best, but with a much higher LCOE than competitive Darrieus designs. Inspection of Table 24 shows the interplay of maximizing AEP while lowering initial capital costs to minimize LCOE.

Analysis of the LCOE variation shows the interplay of material choice in rotor and platform support costs, while most other costs have essentially the same breakdown. While carbon composite comes at a much higher cost (5.2 times more expensive than glass composite material) it also provides a significant reduction in rotor mass, which resulted in significant reduction in the platform/support costs that may lead to lower LCOE for the overall system.

5.2. Cost Analysis Summary and Discussion

A preliminary levelized cost of energy analysis was conducted based on the design specifications resulting from the 5 MW VAWT system design studies presented earlier. A subset of rotor/platform/drivetrain configurations was considered for detailed cost of energy analysis along with other system and project cost elements (such as electrical infrastructure, marinization, etc).

Darrieus rotor designs were found to perform better with respect to LCOE than V-VAWT rotor designs, which had significantly higher LCOE values. Competitive carbon and glass Darrieus rotor designs have predicted LCOE of 0.134 – 0.139 USD/kW-hr.

For comparison, we consider recent offshore wind LCOE studies for conventional HAWT deployment including near-term LCOE estimates and longer-term projected LCOE (50), (53) and (54). Reference (50) provides a recent offshore LCOE analysis of current HAWT technology along with cost reduction projections to the year 2030. The report presents an LCOE range for floating systems of 0.13 to 0.45 USD/kW-hr covering the entire range of offshore site conditions in all US regions. By 2022, this range is projected to be 0.095 to 0.30 USD/kW-hr and by 2027 the range is projected to be 0.08 to 0.22 USDs/kW-hr. Cost reduction projections for a site specific generic scenario (representing the approximate “average site conditions at the current BOEM wind energy areas along the East Coast”) were also provided in References (50) and [54]. The cost reduction projection in these reports shows that, for a floating HAWT wind system, a LCOE of 0.214

USD/kW-hr in the year 2015 is projected to reach 0.089 USD/kW-hr in the year 2030. Reference (54) provides a similar estimate of the current or near-term LCOE of floating offshore wind systems with a value of 0.229 USD/kW-hr for a reference floating project. Again, all of these LCOE values are projections for floating offshore wind projects.

Of course, offshore wind developers will choose to develop projects in more favorable LCOE sites. Thus, for floating VAWTs to be competitive with floating HAWTs the near-term LCOE will need to be less than the projected year 2015 value of 0.214 USD/kW-hr and in the longer term less than 0.089 USD/kW-hr, which are values that represent more favorable and more likely to be developed sites.

Based on a comparison of the above presented offshore floating VAWT LCOE and these floating offshore HAWT LCOE projects, floating VAWTs show promise to be an attractive option for floating wind. These floating VAWT LCOE estimates of 0.134 to 0.139 USD/kW-hr are competitive with current costs; however, whether floating VAWTs or floating HAWTs can reach less than 0.10 USD/kW-hr as projected in the coming decades (year 2030 and beyond) is an open question for future study.

6. CONCLUDING REMARKS

Deep-water offshore sites are an untapped opportunity to bring large-scale offshore wind energy to coastal population centers. The primary challenge has been the projected high costs for floating offshore wind systems. In this work, we investigate a new opportunity for deep-water offshore wind using large-scale vertical axis wind turbines. Owing to inherent features of the technology, there is a potential transformational opportunity to address the major cost drivers of floating wind using vertical axis wind turbines (VAWT). The focus of the work presented in this report was to evaluate the technical potential of new floating VAWT technology. Our approach to evaluating this technical potential was to perform system design studies focused on improving the understanding of technical performance while looking for cost reduction opportunities in the design space. VAWT design codes were developed in order to perform these design studies. A better understanding of the design space for floating VAWT systems was needed, therefore we started with a comprehensive design study of multiple rotor configuration options. Floating platforms and moorings were then sized and evaluated for each of the candidate rotor configurations. Preliminary LCOE estimates and LCOE ranges were produced based on the design study results for each of the major turbine and system components.

The major outcomes of these studies are a comprehensive technology assessment of VAWT performance, and preliminary LCOE estimates that demonstrate that floating VAWTs may have favorable performance and costs in comparison to conventional HAWTs in the deep-water offshore environment where floating systems are required, indicating that this new technology warrants further study.

6.1. Summary of Accomplishments and Main Findings

The major accomplishments and findings of these studies are summarized as follows:

- Challenges and opportunities for floating VAWTs have been outlined and examined.
- New design codes were developed or modified specifically for design and analysis of VAWTs.
- Design studies were performed to explore the design space of the floating VAWT system, which involved:
    - Rotor design studies of the aerodynamic characteristics of VAWTs (loads analysis and AEP trends) and structural characteristics (materials usage, rotor mass & cost),
    - Platform design studies (for semi-submersible and spar platform types) for a wide range of VAWT rotor topsides produced in the rotor design studies, and
    - A drivetrain sizing study based on rotor loads and RPM.
- An assessment of critical design load cases and applicability of existing design standards to floating VAWTs was performed.
- Novel VAWT airfoils were evaluated in rotor design studies.
- Flutter (aeroelastic instability) analysis was performed for large-scale VAWT rotors.
- Structural dynamics design guidelines were developed for VAWTs to mitigate resonance (i.e. excessive vibrations) including a study of:
    - the impact of number of blades on resonance conditions, and
    - the impact of different platform types on resonance conditions.

- And, finally, preliminary system LCOE analysis was performed with presentation of LCOE trends and CAPEX trade-offs in the design space.

6.2. Next Steps and Future Work

This report addresses the technical challenges for floating VAWTs by presenting design studies for the major floating VAWT system components (including the rotor structure, rotor AEP, and floating system). These design studies sought to explore and narrow the design space by reducing technical risk for this new technology through producing design definitions for the major components with sufficient detail to produce reasonable preliminary cost estimates. More detailed design studies should follow in future work to increase confidence and reduce uncertainty in the rotor, platform, and drivetrain costs given the limitations of the present study. Several promising directions have been identified for future investigations focused on integrated design of the major system components for optimal LCOE reduction.

Next steps should include refining the design models to reduce uncertainty in technical and economic specifications for a floating VAWT system. A focus should be placed on the platform design including investigating platform options in addition to semi-submersible and spar type platforms. A detailed analysis of the generator and entire drivetrain should be performed as the present study only considered scaling of existing drivetrain components for HAWTs. Optimization of the rotor should be considered utilizing refined cost models incorporating manufacturing and assembly costs. Further, VAWT controls should also be evaluated as there is potential for increased energy capture and loads reduction through refined control architecture. Loads reduction could, in turn, lead to reduction in rotor, drivetrain, and overall floating system design loads and, therefore, to reduced system costs.

REFERENCES

1. **Lobitz D.W., Veers, P.S., Eisler, G.R., Laino D.J.** *The Use of Twisted-Coupled Blades to Enhance the Performance of Horizontal Axis Wind Turbines.* 2001. Sandia Technical Report SAND01-1303.

2. **Ashwill, T. D.** *Sweep-Twist Adaptive Rotor Blade: Final Project Report.* 2009.

3. **Simão Ferreira, C. J.** The near wake of the VAWT: 2D and 3D views of the VAWT aerodynamics. *PhD Thesis.* Delft, The Netherlands : Delft University of Technology, 2009.

4. **Jonkman, J. and Buhl, M.** *FAST User's Guide.* Golden, CO : National Renewable Energy Laboratory, 2005.

5. **Berg, J. and Resor, B.** *Numerical Manufacturing and Design Tool (NuMAD v2.0) for Wind Turbine Blades: User's Guide.* Albuquerque, NM : Sandia National Laboratories, 2012.

6. **Owens, B.** *Theoretical Developments and Practical Aspects of Dynamci Systems in Wind Energy Applications.* College Station, tX : Ph.D. Dissertation, Texas A&M University, 2013.

7. **Schaub, H. and Junkins, J.** *Analtyical Mechanics of Space Systems.* Reston, VA : American Institute of Aeronoatuics and Astronautics, 2003.

8. **Reddy, J.N.** *An Introduction to Nonlinear Finite Element Analysis.* New York NY : Oxford University Press, 2004.

9. **Cook, R.D.** *Concepts and Applications of ?inite Element Analysis.* New York, NY : John Wiley & Sons, 1981.

10. *A Method of Computation for Structural Dynamics.* **Newmark, N.** 1959, ASCE Journal of the Engineering Mechanics Division, pp. 67-94.

11. *The New Modularization Framework for the FAST Wind Turbine CAE Tool.* **Jonkman, J.** Grapevine, TX : AIAA, 2013. Proceedings of the 51st AIAA Aerosciences Meeting. pp. 1-26.

12. *Mixed Methods for Time Integration.* **Belytchko, T., Yen, H. and and Mullen, R.** 1979, Computer Methods in Applied Mechanics and Engineering, pp. 259-275.

13. *Algorithms for Strong Coupling Procedures.* **Matthies, H., Newkamp, R. and and Steindorf, J.** 2006, Computer Methods in Applied Mechanics and Engineering, pp. 2028-2049.

14. *The Development of CACTUS, a Wind and Marine Turbine Performance Simulation Code.* **Murray, J. C. and Barone, M.** 2011. AIAA 2011-147, 49th AIAA Aerospace Sciences Meeting.

15. **Sutherland, H.J., Berg, D.E. and Ashwill, T.D.** *A Retrospective of VAWT Tetchnology.* Albuquerque, NM : Sandia National Laboratories, 2012.

16. **Cottet, G. and Koumoutsakos, P.** *Vortex Methods: Theory and Practice.* s.l. : Cambridge University Press, 2000.

17. **Daeninck, G.** *Developments in Hybrid Approaches: vortex method with known separation location, vortex method with near-wall Eulerian solver RANS-LES coupling.* s.l. : Ph.D. Thesis, Universite Catholique de Louvain, 2006.

18. *Modified interpolation kernels for treating diffusion and remeshing in vortex methods.* **Wee, D. and Ghoniem, A.** 2006, Journal of Computational Physics, Vol. 213, pp. 239-263.

19. **The FEniCS Project.** Autoamted Solution of Differential Equations. *FEniCS Project.* [Online] March 23, 2014. [Cited: March 23, 2014.] http://www.fenicsproject.org.

20. **Alvez, M.** *Numerical Simulatin of the Dynamics of Point Absorber Wave Energy Converters using Frquency and Time Domain Approaches.* Lisboa, Portugal : Universidade Tecnica De Lisboa, Instituto Superior Tecnico, 2011.

21. **Jonkman, J.** *Dynamics Modeling and Loads Analysis of an Offshore Floating Wind Turbine.* Golden, CO : National Renewable Energy Laboratory, 2007.

22. **WAMIT, Inc.** WMAIT (Version 6.4) [Software]. 2011.

23. **Det Norske Veritas.** Position Mooring. *Offshore Standard DNV-OS-E301.* 2008.

24. **Berg, J.** *Extreme Ocean Wave Conditions for Northern California Wave Energy Conversion Device.* Albuquerque, NM : Sandia National Laboratories, 2011.

25. **Viselli, A., et al.** *Gulf of Maine Extreme Wave and Wind Design Parameters for Offshore Wind Turbines.* 2013.

26. **Tegen, S.** *2011 Cost of Wiond Energy Review.* Golden, CO : National Renewable Energy Laboratory, 2013.

27. **Arapogianni, A.** *Deep Water - The nexst step for offshore wind energy.* s.l. : European Wind Energy Association, 2013.

28. **Jonkman, J.** *Definition of a 5-MW Referece Wind Turbine for Offshore System Development.* Golden, CO : National Renewable Energy Laboratory, 2009.

29. —. *Definition of the floating system for Phase IV of OC3.* Golden, CO : National Renewable Energy Laboratory, 2010.

30. **Paquette, J.** *Personal communication.* November 21, 2013.

31. *WindFloat: A floating foundation for offshore wind turbines.* **Roddier, D., et al.** 2010, Journal of Renewable and Sustainable Energy.

32. *Hywind Demo - Technip Experience with Offshore Wind.* **Crome, T.** Bergen, Norway : Underwater Technology Conference, 2010. Underwater Technology Conference.

33. *Derivation of an objective function for the aerodynamic optimization of aerofoils for vertical axis wind turbines.* **Simao Ferreira, C. and Geurts, B.** 2013, Submitted to Wind Energy.

34. *Experimental investigation of an optimized airfoil for vertical axis wind turbines.* **Ragni, D., Simaeo Ferreira, C. and Correale, G.** 2014, Submitted to Wind Energy.

35. *Aeroelastic Stability Predictions for a MW-sized Blade.* **Lobitz, D.** 2004, Wind Energy, Vol. 7, pp. 211-224.

36. *Impact of Modleing Approach on Flutter Predictions for Very Large Wind Turbine Blade Designs.* **Owens, B., et al.** Phoenix, AZ : American Helicopter Society, 2013. Proceedings of the American Helicopter Society (AHS) 69th Annual Forum.

37. *Aeroelastic Instability of Very Large Wind Turbine Blades.* **Resor, B., Owens, B. and Griffith, D.** Copenhagen, Denmark : European Wind Energy Association, 2012. Proceedings of the European Wind Energy Conference Annual Event.

38. *Aeroelastic Instability Problems for Wind Turbines.* **Hansen, M.** 2007, Wind Energy, Vol. 10, pp. 551-577.

39. **Popelka, D.** *Aeroelastic stability analysis of a Darrieus wind turbine.* Albuquerque, NM : Sandia National Laboratories, 1982.

40. *Modal Dynamics and Stability of Large Multi-megawatt Deepwater Offshore Vertical-axis Wind Turbines: Initial Support STructure and Rotor Design Impact Studies.* **Owens, B., Griffith, D. and Hurtado, J.** National Harbor, MD : American Institute for Aeronautics and Astronautics, 2014. Proceedints of the 32nd ASME Wind Energy Symposium.

41. *Excitation Methods for a 60 kW Vertical Axis Wind Turbine.* **Griffith, D., Mayes, R. and Hunter, P.** Jacksonville, FL : Society for Experimental Mechanics, 2010. Proceedings of the IMAC-XXXVIII , International Modal Assurance Conference, Society for Experimental Mechanics. pp. 329-338.

42. *Structural Dynamics Analysis and Model Validation of Wind Turbine Structures.* **Griffith, D.** Palm Springs, CA : American Institute for Aeronautics and Astronautics, 2009. Proceedings of the 50th AIAA/ASME/ASCE/AHS/ASC Structures, Structural Dynamics, and Materials Conference. pp. 1-12.

43. *Support Conditions for Experimental Modal Dynamics.* **Carne, T., Griffith, D. and Casias, M.** 2007, Journal of Sound and Vibration, pp. 10-15.

44. *Modal Dynamics of Large Wind Turbines with Different Support Structures.* **Bir, G. and Jonkman, J.** Estoril, Portugal : American Society of Mechanical Engineers, 2008. Proceedings of the ASME 27th International Conference on Offshore Mechancis and Arctic Engineering. pp. 1-11.

45. *1st DeepWind 5 MW Baseline Design.* **Paulsen, U., et al.** 2012, Energy Procedia, Vol. 24, pp. 27-35.

46. *Comments on Curve Veering in Eigenvalue Problems.* **Perkins, N. and Mote, C.** 3, 1986, Journal of Sound and Vibration, Vol. 106, pp. 451-463.

47. *Mode Localization and Frequency Veering in a Non-conservative Mechanical System with Dissimilar Components.* **Natsiavas, S.** 1, 1993, Journal of Sound and Vibration, Vol. 165.

48. **Blevins, R.** *Formulas for Natural Frequency and Mdoe Shape.* Malabar, Florida : Krieger Publishing Company, 2001.

49. **Fingersh, L., Hand, M. and Laxson, A.** *Wind Turbine Design Cost and Scaling Model.* s.l. : NREL Technical Report NREL/TP-500-40566, 2006.

50. **Maples, B, et al.** *Installation, Operation, and Maintenance Strategies to Reduce the Cost of Offshore Wind Energy.* Boulder, CO : National Renewable Energy Laboratory (NREL/TP-5000-57403), 2013.

51. **White, F.** *Fluid Mechanics.* 4th. New York, New York : WCB McGraw-Hill, 1998.

52. **Smith, A.** *A Preliminary Economic Assessment of Floating Offshore Wind Technology in the United States.* Golden, CO : National Renewable Energy Laboratory, 2013.

53. **Bloomberg New Energy Finance.** Levelized Cost of Energy Update. [Online] 2012. [Cited: May 15, 2014.] http://www.bnef.com/WhitePapers/download/114.

54. *Opportunities and Challenges for a Sustainable Energy Future.* **Chu, S and Majumdar, A.** 2012, Nature, Vol. 488, pp. 294-303.

55. **Musial, W. and Ram, B.** *Large-Scale Offshore Wind Power in the United States: Assessment of Opportunities and Barriers.* 2010 : National Renewable Energy Laboratory, 2010.

56. **School of Marine Sciences, University of Maine.** *Gulf of Maine Moored Buoy Program.* [Online] [Cited: May 28, 2011.] http://gyre.umeoce.maine.edu/buoyhome.php.

57. *Experimental comparison of three floating wind turbine concepts.* **Goupee, A.Koo, B., et al.** Rio de Janeiro, Brazil : American Societry of Mechanical Engineers, 2012. Proceedings of OMAE 2012, ASME 31st International Conference on Offshore Mechanics and Arctic Engineering.

58. **Bourbon.** Bourbon Liberty 200 AHTS. *Bourbon-Online.* [Online] December 15, 2013. [Cited: December 15, 2013.] http://www.bourbon-online.com/media/liberty/liberety-200-technical-sheet-brochure.pdf.

59. *Implementation of a 2MW floating wind turbine prototype offshore Portugal.* **Cermelli, C., Roddier, D. and Weinstein, A.** Houston, TX : Offshore Technology Conference, 2012. Proceedings of the Offshore Technology Conference.

60. *Installation of the Horn Mountain Spar Using the Enhanced DCV Balder.* **Dijkhuizen, C, Coppens, T. and van der Graff, P.** Center of the Netherlands : Offshore Technology Conference, 2003. Offshore Technology Conference.

61. **Vryhof Anchors BV.** *Anchor Manual 2010 - The Guide to Anchoring.* 2010.

62. **University of Maine.** *Detailed Cost of Energy Analysis for SWF System.* Orono, ME : Advanced Structures and Composites Center, 2013.

63. **Technip.** *Technip Offshore Finland.* 2013.

64. *Modeling offshore wind installation costs on the U.S. Outer Continental Shelf.* **Kaiser, M and Snyder, B.** 2012, Renewable Energy.

65. **Barone, M.** *Personal communication.* December 19, 2013.

66. *Model tests for a floating wind turbine on three diferent floaters.* **Boo, K., et al.** Rio de Janeiro, Brazil : American Society of Mechanical Engineers, 2012. Proceedings of OMAE 2012, ASME 31st International Conference on Offshore Mechanics and Arctic Engineering.

67. **WireCo World Group: Royal Lankhorst Euronete.** Ropes for Deepwater Mooring. *Lankhorst Ropes.* [Online] November 22, 2013. [Cited: November 22, 2013.] http://www.lankhorstropes.com/files/uploads/Offshore/brochure/DWM_brochure_100dpi_April_2013.pdf.

68. **United States Department of Energy.** *20% Wind Energy by 2030.* Washington D.C. : Department of Energy, 2008.

69. **Kaiser, M. and Snyder, B.** *Offshore Wind Energy Installation and Decomissioning Cost Estimation in the U.S. Outer Continental Shelf.* s.l. : Energy Research Group, LLC, 2010.

70. **Dice Holdings Inc.** Rigzone - Offshore Rig Day Rates. *Rigzone.* [Online] December 13, 2013. [Cited: December 13, 2013.] http://www.rigzone.com/data/dayrates/.

71. **Kooijman, H., et al.** *DOWEC 6 MW Pre-Design; Aero-elastic mdoeling of the DOWEC 6 MW pre-design in PHATAS.* Petten, the Netherlands : Energy Research DOWEC, 2003.

72. **Musial, W. and Ram, B.** Large-Scale Offshore Wind Power in the United States. *NREL/TP-500-40745.* 2010.

73. **Ashwill, T. D.** Measured Data for the Sandia 34 Meter Vertical Axis Wind Turbine. *Sandia Technical Report SAND91-2228.* Albuquerque, NM : s.n., 1991.

74. **Tegen, S., et al.** *2010 Cost of Wind Energy Review.* Golden, CO : National Renewable Energy Laboratory, 2012.

75. **Jonkman, J.** *Definition of a 5-MW Reference Wind Turbine for Offshore System Development.* Golden, CO : National Renewable Energy Laboratory, 2009.

76. **Mone.**

APPENDIX A: PLATFORM AND MOORING DESIGN METHODOLOGY

Hydrodynamic Analysis of Platform Designs using WAMIT

To determine the dynamic behavior of each platform design in the design environment, a WAMIT analysis is performed on the preliminary platform for the spar and the semi-submersible. This analysis provides a baseline set of WAMIT data which can be applied to the entire range of designed platforms by taking advantage of the Froude scaled nature of each platform.

For example, original WAMIT mean drift force results can be used to determine the mean drift force of a 90% Froude scaled platform (λ=0.9) for an incident wave period of 12 seconds. First, the wave period must be scaled to account for the fact that the platform is 10% smaller than the original but the design environment is unchanged.

$$P_{new} = \sqrt{\frac{1}{\lambda}} * \ P_{orig} \tag{20}$$

where λ=0.9 is the scale factor, P_{orig} is the original period of 12 seconds and P_{new} is the scaled period. As the platform gets smaller, the new period appears larger. Another way to view this is that the wavelength of the design environment doesn't change but the characteristic length of the structure decreases, therefore the wavelength relative to the platform characteristic length appears longer. To determine scaled results from the original WAMIT baseline data, the new period is used to lookup the desired quantity and obtain the scaled WAMIT result. This value gives the transfer function, which is normalized by the characteristic length of the platform (L), density of water (ρ), gravity (g), and the square of the wave amplitude (A). Froude scaling of the platform changes the characteristic length, so to determine the force value one must multiply by the scaled characteristic length and the other scaling terms, which remain unchanged. As the WAMIT results were calculated originally with a characteristic length of L_o = 1.0, the scaled characteristic length (L) is equal to the scale factor for the Froude scaled platform.

$$TF_{new} = \frac{L}{L_o} * \rho * g * A^2 * \ TF_{orig} = \lambda * \rho * g * A^2 * \ TF_{orig} \tag{21}$$

This method is employed during the analysis to apply the WAMIT baseline data to the range of Froude scaled platform designs.

Mooring Design

Environment

The hypothetical deployment site off the coast of Maine is shown in Figure 120 along with the location and water depth of an NBDC buoy.

Data from the NDBC buoy (Figure 121) was used to estimate the extreme wave conditions at the deployment site. There is also NERACOOS buoy E01 that is located closer to the deployment site and whose data is publicly available. The wind, wave and current conditions for these cases are shown in Table 25.

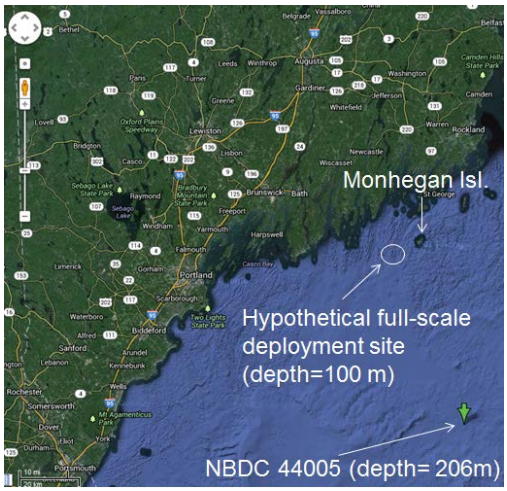

Figure 120. Deployment site off the coast of Maine and NBDC buoy used for wave characterization.

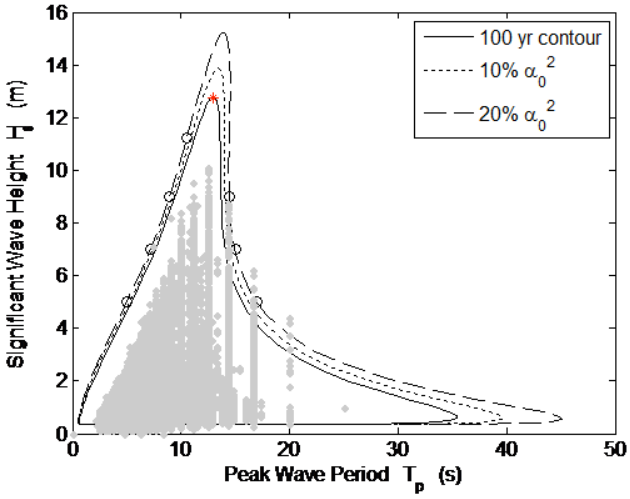

Figure 121. 100-year contour for spectral wave conditions from NBDC buoy 44005.

Table 25. Environmental conditions for 100-year storm event

Extreme Case	
Water Depth	206 m
Regular Wave Height Equivalent	24.24 m
Period	12.97 s
Wind Speed	50 m/s
Ocean Current Speed	0.88 m/s

Design Procedure

The mooring system is designed as a combined synthetic rope and chain system. The synthetic rope runs in a taut configuration from the platform connection to a clumped weight at the sea bed. A delta connection is used in the spar system to add yaw stiffness to the platform (Figure 122 inset). Chain runs along the seabed from the clumped weight to the anchor (Figure 122). Parameters to be chosen for this system are the mooring spread (line length, chain length), wire rope type (type, size, strength), chain type (size, strength), clumped weight size, and the anchor type (type, size). The method for determining design forces is based on a quasi-static approach and is detailed in the next section.

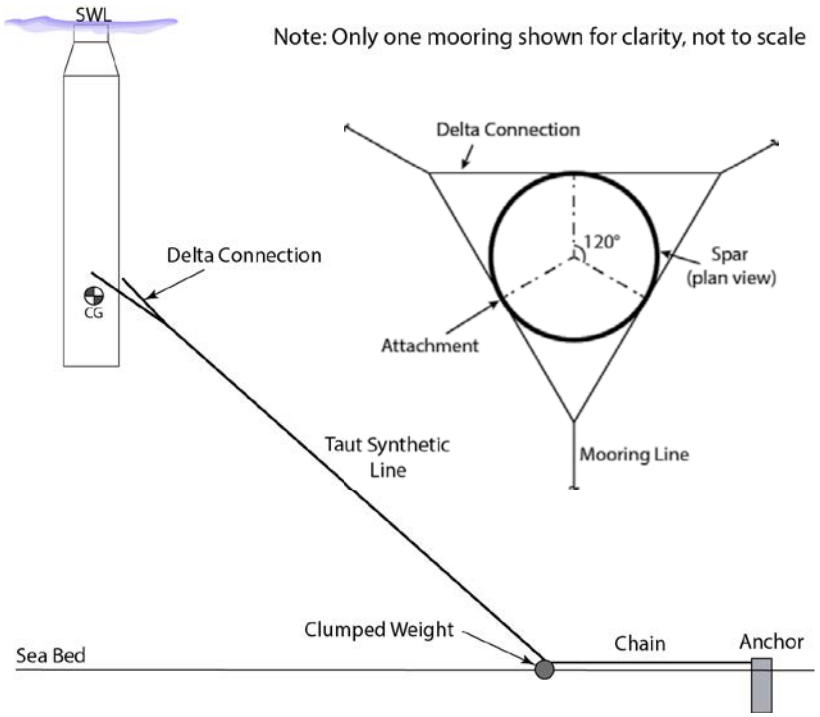

Figure 122. Mooring System with Delta Connection Detail.

Design Loads

The loads considered in this analysis can be broken down into four sections; wind loads, mean drift loads, current loads, and platform surge dynamic loading.

Wind Loads

The wind loads are provided based on drag of the topsides in an extreme event wind case. They are considered independent of the platform type or size. For all VAWT designs, the wind load is given as 3,140 kN. This value is based on a CACTUS analysis and represents the form drag of a parked VAWT and tower subject to the Gulf of Maine extreme mean wind speed of 50 m/s (25). For this study it is assumed that all VAWT designs have the same cross sectional area and drag. While this assumption is likely unrealistic for the large variety of VAWT designs considered, there was not enough data available at the time of this study to create an appropriate parameterized function. The calculated value is for what was considered the worst case VAWT design for area and drag and should be conservative. Future work will consider determining a more accurate functional relationship for the wind load based on topside size. For the HAWT, the drag loads on the turbine blades during an extreme event can be mitigated by the blade pitch mechanism. A FAST analysis of the NREL 5 MW turbine with parked and feathered blades in a 50 m/s wind yields a drag force of 90 kN. Therefore, it is chosen to use the operating thrust load of 825 kN corresponding to a wind speed of 11.4 m/s (28) as the worst case design wind load. To calculate the drag on the tower and nacelle under these conditions, the drag force is calculated using the method shown below.

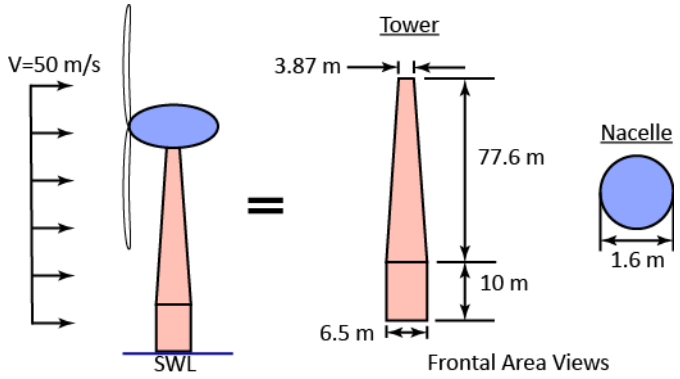

$$F_D = \frac{1}{2}\rho V^2 C_D A \text{ [57]}$$

Component	Tower	Nacelle	Rotor
Frontal Area (m^2)	467.4	8	--
C_D	0.82	1.0	--
F_D (kN)	25.5	0.53	82

Figure 123. NREL 5 MW HAWT dimensions and drag calculation. (28) (51)

For this analysis, dimensions of the tower are from (28) and the nacelle from (56). The drag coefficient of 0.82 for the tower was taken from (55) as that of a vertical cylinder with L/D = 87.6/6.5 = 13.5 and 1.0 for the nacelle is from (56). The drag force on the tower and nacelle are calculated using the formula for drag force (55), with ρ is the density of air (1.025 kg/m^3) and V is the wind speed (11.4 m/s). The thrust value on the rotor is from (28). The total wind load on the HAWT is 851.0 kN.

Mean Drift Loads

The mean drift loads are based on a WAMIT analysis and are taken from the .8 output file. The force is calculated as:

$$F_{MD} = TF * \rho * g * A^2 * \left(\frac{V}{V_0}\right) \quad (22)$$

where TF is the adjusted period dependent transfer function from WAMIT (adjusted using the method described earlier for the WAMIT analysis), ρ is the density of sea water (1025 kg/m^3), g is the acceleration due to gravity (9.80665 m/s^2), A is the wave amplitude (12.12 m) and V/V_0 is the scaling parameter relating the initial design volume V_0 to the scaled volume V. This allows the force to scale with the displacement of the platform.

Current Induced Force

The force due to the current was calculated as a function of the current velocity and the drag coefficient of a submerged cylinder. The formulation is shown below:

$$F_{CD} = \frac{1}{2} * \rho * A_{sub\,0} * C_D * Vel^2 * \left(\frac{A_{sub}}{A_{sub\,0}}\right) \quad (23)$$

Where C_D is the drag coefficient for a submerged cylinder in turbulent flow for steady current (inf KC, C_D = 1.05), Vel is the current velocity (0.88 m/s, Table 25), A_{sub} and $A_{sub\,0}$ are the submerged areas subject to the current with the subscript 0 denoting the original area and A_{sub} being the scaled area. This allows the force to scale with the frontal area of the platform.

Dynamic Induced Loads

The dynamic induced loading is due to the dynamic surge motion of the platform. For a typical floating platform, the magnitude of the dynamic surge motion is insensitive to the mooring design as the mooring system is compliant enough to have little effect on the dynamic surge motion. From

the WAMIT analysis, the dynamic surge RAO of the floating platform can be determined. Similar to the mean drift calculation, the range of periods for this study are based on Froude scaling the full scale period to account for the fact that the platform is changing size but the environment is not (hence the wavelength changes relative to the platform size). However, it can be shown that the surge RAOs for the platforms considered are a weak function of the wave period. Therefore, for the mooring analysis, the surge RAO was assumed to be constant and equal to the value for the WAMIT baseline case. A RAO value of 0.41 is used for the spar and 0.6 for the semi-submersible (31). Using the design wave amplitude of 12.12m, this yields a surge amplitude of 4.97m for the spar and 7.27m for the semi-submersible.

Total Mooring System Loads

The wind, mean drift, and current forces provide a reasonable estimation of the "steady" forces acting on the platform, termed the "static load". To this end, they are used to determine a mean surge offset of the platform in the quasi-static mooring model. Based on the design of the mooring system, the quasi-static model generates a force/displacement curve for the platform. Using this data, the mean displacement is determined through a reverse lookup of the static load on the platform. Then, the amplitude of the dynamic surge motion of the platform is added. This gives a maximum surge displacement of the platform corresponding to the mean offset plus the maximum dynamic excursion. Using the force/displacement curve again, the maximum mooring line tension can then be determined from the maximum surge displacement. A factor of safety of 1.3 is then applied to this tension to determine the design tension in the mooring line. The mooring loads over the design range are summarized in Table 26 below.

Table 26. Mooring load summary

Platform	Wind Force (kN)	Mean Drift Force (kN)	Current Force (kN)	Total Static Load (kN)	Dynamic Load (kN)	Tension (1.3 Safety Factor) (kN)
VAWT Spar	3,140	5.0-14.8	231-405	3,376-3,560	~2,870	8,280-8,521
VAWT Semi	3,140	2.1-33.7	216-334	3,390-3,478	~6,052	12,517-12,634
HAWT Spar	851	16.8	436	1,304	1,434	3,634
HAWT Semi	851	23.8	296	1,171	2,100	4,340

Example output from the quasi-static mooring analysis tool is shown in Figure 124 below. The tool computes force displacement curves based on the geometry of the mooring system and selected properties of the mooring line. The reverse lookup of the static load is performed using the "Fairlead – Horizontal Force" curve to determine the "Static Surge", which represents the amount of surge motion the system will displace when the mean load is applied. Then, the RAO surge value is added as shown by the "Dynamic Surge" on the graph. The sum of the "Static Surge" and "Dynamic Surge" is the "Max Surge". Then, using the mooring tool, the "Max Tension" can

be determined by looking up the value that corresponds to the “Max Surge” on the “Line Tension” curve.

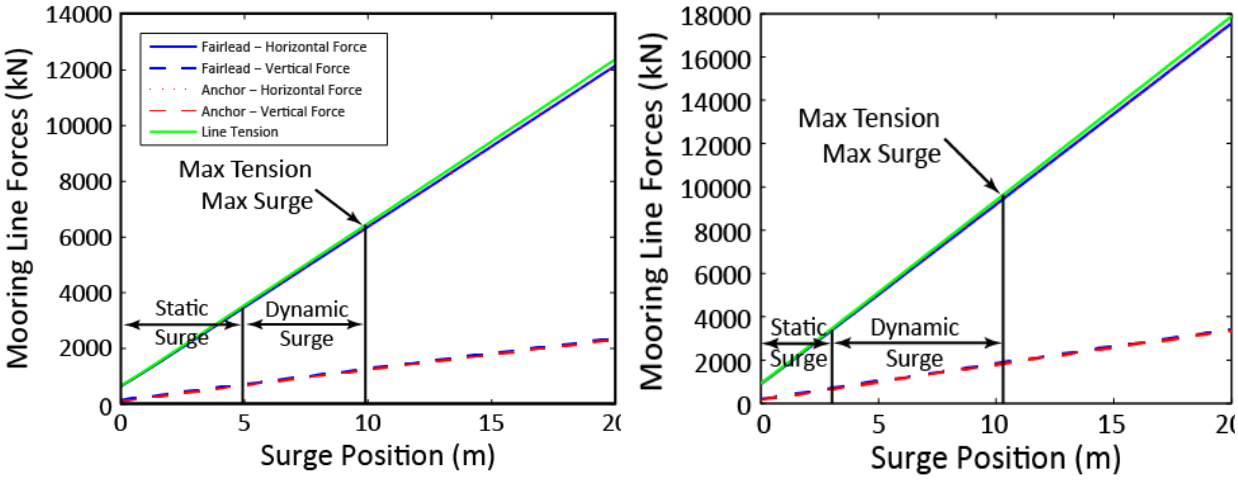

Spar Force/Displacement Graph

Semi Force/Displacement Graph

Figure 124. Quasi-Static Mooring Analysis Force-Displacement Results.

As a qualitative check on the quasi-static methods used to determine the mooring loads, the mooring loads are compared with scale model test data from the Maritime Research Institute Netherlands (MARIN) offshore test basin. The tests performed at MARIN were part of the DeepCwind test campaign which investigated the response of three floating platforms with a HAWT topside to various wind and wave conditions using 1/50th scale models (57) (58). The platforms considered were a spar based on the OC3 Hywind design, a three-columned semi-submersible, and a TLP. For the purposes of this study, comparisons with the spar and semi-submersible tests are used. Of the various load cases in the test matrix, the closest test is a white noise test with an H_s of 11.3m. The mooring system in the model test consists of three catenary lines arranged at 120° around the platform, similar to what is used in this study. During this test, a steady wind speed of 11.3 m/s generated a mean thrust on the platform of 750 kN. To compare mooring line forces, loads from the bow line are examined and shown in Table 27.

Table 27. MARIN test data

Platform	Hs (m)	Wind Force (kN)	Total Line Load (kN)
Spar	11.3 White Noise	750	3,022
Semi	11.3 White Noise	750	9,516

To compare the results from the mooring model with the MARIN test data, the safety factor of 1.3 is removed from the calculated mooring loads. Also, as the MARIN data had a considerably lower wind force and this force is almost directly taken up by the mooring system, the difference in applied wind force is also accounted for. The results are shown in Table 28.

Table 28. Comparison of mooring model and MARIN model data

	VAWT Mooring Model		MARIN Data		Comparison	
Platform	Wind Load (kN)	Total Load (kN)	Wind Load (kN)	Total Load (kN)	Total Load Delta (kN)	Wind Adjusted Delta (kN)
Spar	3,140	6,555	750	3,022	3,533	1,143
Semi	3,140	9,719	750	9,516	203	-2,187

The mooring model provides a reasonable estimate of the mooring loads, considering that the MARIN data is for a different sea state and wind speed. This comparison was used to benchmark the quasi-static mooring model and ensure reasonable results for use in this study.

Mooring Design

Based on the previous design procedure, a mooring system was developed for the two platforms. The overall configuration of the mooring system is similar for both platforms with the major difference being the size and/or strength of the individual components. The particulars for each platform are shown in the tables below.

Synthetic Rope

The synthetic rope is sized based on the maximum tension determined above. This value is compared with the minimum breaking strength of various mooring lines (59) to determine the size of line required. The results are summarized below.

Table 29. Synthetic rope requirements

Platform Type	Max Tension (kN)	Rope OD (mm)	Stiffness (MN)	Breaking Strength (kN)
Spar	8,280-8,521	177	241	8,826
Semi	12,517-12,634	208	348	12,749

Clump Weight

The mooring model also predicts the vertical force applied to the anchor. In this mooring design the vertical force is entirely resisted by a clumped weight to ensure only horizontal loads are resisted by the anchor. Through converting the vertical force to kg, the mass and volume of a concrete clumped weight can be determined. As with other loads in the mooring analysis, a safety factor of 1.3 was used on the vertical uplift load.

Table 30. Clump weight requirements

Platform Type	Max Uplift Force (kN)	Required Concrete Volume (m^3)
Spar	1,573-1,619	117-120

Semi	2,392-2,414	177-179

Chain

The chain is sized using a similar method to the synthetic line. However, instead of using the maximum tension in the line, the maximum horizontal load at the anchor is used. A safety factor of 1.3 is used for these loads as was done with the maximum tension load. The length of chain required is likely to be determined based on the topology at the installation site and will allow the anchors to be located in the best substrate. To that end, a nominal length of 100m is assumed for all platforms. Chain properties are from (60).

Table 31. Chain requirements

Platform Type	Max Horizontal Load (kN)	Chain Type	Chain OD (mm)	Breaking Strength (kN)
Spar	8,117-8,354	R4 Stud	92	8,497
Semi	12,274-12,389	R4 Stud	114	12,420

Anchor

The drag embedment anchor is sized based on the required horizontal tension in the mooring chain. Design charts from the Vryhoff Anchor Manual (61) were used to size an appropriate Stevpris Mk6 style drag embedment anchor based on the ultimate holding capacity (UHC) of the anchor. The design charts give UHC values based on the type of substrate and the mass of the anchor. The most conservative design line was used which corresponds to very soft clay or mud. Hence, the anchor mass is determined using the required UHC and the very soft clay design line. Results are shown in the table below.

Table 32. Anchor requirements

Platform Type	Max Horizontal Load (kN)	Anchor Mass (t)	Holding Capacity (kN)
Spar	8,117-8,354	21	8,483
Semi	12,274-12,389	31	12,455

DISTRIBUTION

1	MS0899	Technical Library	9536 (electronic copy)


Sandia National Laboratories